

CHARACTERIZATION OF EMECİK LIMESTONE FIGURINES FOR PROVENANCE

A THESIS SUBMITTED TO  
THE GRADUATE SCHOOL OF NATURAL AND APPLIED SCIENCES  
OF  
MIDDLE EAST TECHNICAL UNIVERSITY

BY

ÜFCADE MUŞKARA

IN PARTIAL FULFILLMENT OF THE REQUIREMENTS  
FOR  
THE DEGREE OF DOCTOR OF PHILOSOPHY  
IN  
ARCHAEOLOGY

FEBRUARY 2013



Approval of the thesis:

**CHARACTERIZATION OF EMECİK LIMESTONE FIGURINES FOR PROVENANCE**

Submitted by **ÜFTADE MUŞKARA** in partial fulfillment of the requirements for the degree of **Doctor of Philosophy in Archaeometry, Middle East Technical University** by,

Prof. Dr. Canan Özgen  
Dean, Graduate School of **Natural and Applied Sciences**

\_\_\_\_\_

Prof. Dr. Ümit Atalay  
Head of Department, **Archaeometry**

\_\_\_\_\_

Prof. Dr. O. Yavuz Ataman  
Supervisor, **Chemistry Dept., METU**

\_\_\_\_\_

Prof. Dr. Numan Tuna  
Co-Supervisor, **City Planning Dept., METU**

\_\_\_\_\_

**Examining Committee Members:**

Prof. Dr. Asuman G. Türkmenoğlu  
Geological Engineering Dept., METU

\_\_\_\_\_

Prof. Dr. O. Yavuz Ataman  
Chemistry Dept., METU

\_\_\_\_\_

Prof. Dr. Gerhard-Wilhelm Weber  
Financial Mathematics Dept., METU

\_\_\_\_\_

Prof. Dr. Nusret Ertaş  
Analytical Chemistry Dept., Gazi University

\_\_\_\_\_

Assist. Prof. Dr. Zeynep I. Kalaylıoğlu  
Statistics Dept., METU

\_\_\_\_\_

**Date: 11.02.2013**

**I hereby declare that all information in this document has been obtained and presented in accordance with academic rules and ethical conduct. I also declare that, as required by these rules and conduct, I have fully cited and referenced all material and results that are not original to this work.**

Name, Last name: Üftade MUŞKARA

Signature:

## ABSTRACT

### CHARACTERIZATION OF EMECİK LIMESTONE FIGURINES FOR PROVENANCE

Muşkara, Üftade  
Ph.D., Archaeometry Graduate Program  
Supervisor: Prof. Dr. O. Yavuz Ataman  
Co-Supervisor: Prof. Dr. Numan Tuna

February 2013, 168 pages

Archaeometry, the collaboration of different disciplines with archaeology, has revealed some facts that could change our understanding of the past. Provenance studies should be among the primary topics in interdisciplinary archaeometric research. Provenance studies, determining the source of the archaeological materials, play an important role in the understanding and reconstruction of trade connections, and social, political and religious relationships of ancient societies.

A group of limestone figurines dated to 6th century BC constitutes an interesting case since they have a high abundance in Eastern Mediterranean region. Generally, it is accepted that these figurines were of Cypriot origin. However, beside the ones made according to Cypriote style and were found in Cyprus; the extended distribution of the figurines and the varieties in their styles raised the questions on the location of production and/or the provenance.

The Sanctuary of Apollon in Emecik is situated in Datça peninsula. The amount and the variety of types found in Emecik make it reasonable to think that they were produced locally. Therefore, it is reasonable to suggest that possibly a local limestone was used.

The islands of Dodecanese are located at one of the busiest and most important cross roads of the Eastern Mediterranean and readily accessible from all directions, including Asia Minor. Geologically the Dodecanese form an extension of south Western Anatolia known as Caria enclosing Emecik where the figurines within the scope of this work. The two areas appear to have shared a common culture. Indeed, the archaeological evidence seems to agree. The overall interpretations for the results of this work would provide a wide perspective for understanding the common culture of this area.

Provenance studies of Emecik figurines were applied through the determination of trace and REE's (rare earth elements) with ICP- OES (inductively coupled plasma optical emission spectrometry) and ICP-MS (inductively coupled plasma mass spectrometry) along with mineral examinations through thin section and XRD analysis.

Various statistical approaches were applied in order to interpret the original data obtained by the determination of concentration values of REE's and major and trace elements in the samples. Bivariate analysis of the samples will be plotted. In addition, hierarchical cluster analysis and principal component analysis, PCA, were used to understand the relation between archaeological and geological samples. The resulting groups and variations as a result of these statistical analyses were shown in dendrogram plots and graphs.

According to the results of mineralogical, chemical and statistical analysis of this study, it is obvious now that there was a local production for the limestone figurines in Datça. It is even clear that the local artists tried different limestone sources in Datça perhaps in order to improve the quality of their works. Beside the locally produced figurines, it has been understood that majority of the figurines that were analyzed in this study were made from limestone material which was collected from quarries within Pachna formation in Cyprus. These figurines were either imported from Cyprus or made in Datça using limestone brought from Cyprus. The result of this study also supports the theory on the commercial relations of limestone from Cyprus through other sites in Eastern Mediterranean.

Further studies on limestone figurines should cover the discovery of new production center, *Emecik* for the figurines beside Cyprus. Figurines found at other sites in western Anatolia should be studied to reveal true nature of the extensive relation between Aegean and Mediterranean sites in Archaic Period.

**Keywords:** provenance, limestone figurines, Cyprus, rare earth elements, foraminiferal limestone, multivariate analysis

## ÖZ

### HAMMADDE KAYNAĞI KAPSAMINDA EMECİK KİREÇTAŞI HEYKELCİKLERİNİN NİTELENDİRİLMESİ

Muşkara, Üftade  
Doktora, Arkeometri Doktora Program  
Tez Yöneticisi: Prof. Dr. O. Yavuz Ataman  
Ortak Tez Yöneticisi: Prof. Dr. Numan Tuna

Şubat 2013, 168 sayfa

Farklı bilim dallarının ortak çalışmasını kapsayan Arkeometri, geçmiş algısını değiştirebilecek birçok gerçeği gün yüzüne çıkarmıştır. Heykel, mimari elemanlar gibi taş malzemeden yapılmış arkeolojik eserlerin hammadde kaynağını araştırma çalışmaları da başlıca arkeometrik incelemeler arasındadır. Bu tür kaynak araştırmaları, antik dünyanın ticaret ilişkilerinin ve ticaret yollarının, sosyal, siyasi ve dini ilişkilerin yeniden anlaşılması ve şekillendirilmesinde önemli rol oynamaktadır.

M.Ö. 6. yüzyıla tarihlenen kireçtaşından yapılmış heykelcikler, Akdeniz havzasında yaygın olarak bulunmaları yönünden dikkat çekicidir. Genel olarak bu tip heykelciklerin Kıbrıs yapımı olduğu düşünülmektedir. Ancak, Kıbrıs sanatı ekolünde yapılmış ve Kıbrıs'ta bulunmuş olanlar dışında, geniş buluntu alanı ve farklı stillerde betimlenmiş heykelciklerin bulunması yapım yeri ve/veya hammadde kökeni konusunda tartışmalara neden olmaktadır.

Emecik Apollon kutsal alanı, Datça yarımadasındadır. Emecik'te bulunan heykelciklerin farklı stilleri ve sayısı, bu heykelciklerin yerel olarak üretilmiş oldukları olasılığını kuvvetlendirmektedir. Bu nedenle, yerel bir kireçtaşı kaynağının kullanılmış olması da akla yakın bir olasılıktır.

Ege Denizi'nin güneyinde yer alan Oniki adalar, Doğu Akdeniz bölgesindeki en yoğun ve en önemli kavşak noktalarından biridir ve her yönden kolaylıkla erişilebilen bir merkezdir. Jeolojik konum itibarıyla, Oniki adalar güneybatı Anadolu'da Karya olarak bilinen ve tez çalışmasının konusunu oluşturan heykelciklerin bulunduğu Emecik'i de kapsayan bölgenin devamıdır. Tez çalışmasını sonucu ile ilgili yorumlar, bu bölgenin ortak kültür mirası ile ilgili önemli ipuçları sağlayabilecek niteliktedir.

Emecik heykelciklerinin kaynak araştırması ile ilgili çalışma kapsamında, eser element ve nadir toprak elementlerinin tayini indüktif eşleşmiş plazma-optik emisyon spektrometri (ICP-OES) ve indüktif eşleşmiş plazma-kütle spektrometri (ICP-MS) ile yapılmıştır. Bu analizlerin yanı sıra, örneklerin ince-kesitleri ve XRD analizleri yardımıyla mineralojik incelemeleri yapılmıştır.

Nadir toprak elementleri, temel ve eser elementlerin derişim değerlerinin tayini ile elde edilen verinin değerlendirilmesinde farklı istatistiksel yöntemlerden yararlanılmıştır. Çoklu değişme analizleri bu tür kaynak araştırmalarında bulunun yoğun sayısal sonucun değerlendirilmesinde ve anlamlandırılmasında yaygın olarak kullanılmaktadır. Bunlara ek olarak, temel bileşen analizi

(PCA), hiyerarşik küme çözümlemesi bu çalışmada arkeolojik ve jeolojik örneklerin karşılaştırılması ve gruplandırılması amacıyla kullanılmıştır.

Bu çalışmada elde edilen mineralojik, kimyasal ve istatistiksel incelemelerin sonuçları Datça'da yerel kireçtaşı heykelcik üretimi olduğunu ortaya çıkarmıştır. Yerel sanatçıların belki de eserlerin kalitesini arttırmak için farklı kaynaklardan aldıkları kireçtaşını denedikleri de anlaşılmıştır. Yerel olarak üretilen heykelciklerin yanı sıra, bu çalışmada incelenen heykelciklerin çoğunun Kıbrıs'taki Pakhna formasyonundaki farklı ocaklardan alınan kireçtaşı kullanılarak yapıldığı ortaya çıkmıştır. Bu heykelcikler ya Kıbrıs'tan ithal olarak gelmiş ya da Datça'da Kıbrıs kökenli bir kireçtaşı kullanılarak yapılmıştır. Aynı zamanda bu çalışmanın sonuçları, Kıbrıs kökenli kireçtaşının Doğu Akdeniz'deki ticareti ile ilgili teorileri doğrulamaktadır.

İlerde bu kireçtaşı heykelciklerle ilgili yapılacak çalışmalarda, Kıbrıs ile beraber Emecik'in de heykelciklerin üretim merkezi olduğu yönündeki bu bulguların göz önünde bulundurulması gerekmektedir. Ege ve Akdeniz havzasında Arkaik dönem yerleşimleri arasındaki yoğun ilişkilerin gerçek yapısını ortaya çıkarmak için Batı Anadolu'da diğer yerleşim merkezlerinde bulunan kireçtaşı heykelciklerin hammadde özelliklerinin çalışılması önemlidir.

**Anahtar kelimeler:** hammadde kaynağı araştırması, kireçtaşı heykelcikler, provenance, Kıbrıs, nadir toprak elementleri, foraminiferli kireçtaşı, çoklu değişme analizi

*To my son bitaneçiđim Güneş,  
and  
to my great family*

## ACKNOWLEDGMENTS

I would like to express my deep appreciation to my supervisor Prof. Dr. O. Yavuz ATAMAN for his guidance, understanding and friendship throughout this study. I would also like to thank him especially for his encouragement to study with his group in Chemistry Department, METU from the beginning and his great support for this study which requires a big collaboration from different disciplines.

I thank my co-supervisor Prof. Dr. Numan TUNA for offering me the subject of the study, selecting the figurine samples, and his excellent help, guidance and support.

I am much indebted to Prof. Dr. Asuman G. TÜRKMENOĞLU for her excellent help, guidance and support during my research. She always helped me for geological sampling, thin section analysis and mineralogical interpretation of samples. I also like to thank Prof. Dr. Sevinç ALTINER for the preliminary micropaleontologic analysis of thin sections.

I am also very grateful to Dr. Aynur HAKYEMEZ for her examination of thin sections of archaeological and geological samples, her detailed micropaleontologic study and interpretations on samples.

I wish to thank Assist. Prof. Dr. Erdal ONURHAN, Prof. Dr. Hüseyin GÖKÇEKUŞ, Prof. Dr. Osman YILMAZ, Mustafa ALKARAVLI and Dr. Mehmet Necdet for their assistance and great help for geological sampling from possible sources in Cyprus.

I am also grateful to Assoc. Prof. Dr. Sezgin BAKIRDERE not only for his enormous guidance and support for the chemical analysis in my PhD studies, but also for his warm friendship and brotherhood.

I could not find the proper words to express my gratitude to my family. My father, mother and sister, Atilla, Asuman and Hanzade MUŞKARA; they have given me all their love, support, patience and time from the very beginning. I will not be able to thank them enough. My baby boy, Sinan Güneş DOĞAN, has really been great even before he was not yet born. He worked with me as if we were a team.

I am indebted to Assist. Prof. Dr. Ali Akın AKYOL for helping me at every stage of my work for XRD analysis of geological samples which were done at Ankara University, Yer Bilimleri Uygulama ve Araştırma Merkezi and also to Assoc. Prof. Dr. Ayşen YILMAZ for XRD analysis of archaeological samples.

I would like to extend special thanks to Prof. Dr. Erkan KARAMAN, Assistant Prof. Dr. Sibel Tatar ERKUL and Fuat ERKUL for photomicrographs of thin sections which were taken at Akdeniz University.

I would like to express my endless thanks to all my group members and my friends, Yasin ARSLAN, Selin BORA, Emrah YILDIRIM, Erhan ÖZDEMİR, Merve YURTSEVER, Seval ATAMAN, Gamze KARAMAN, İlkem EVCİMEN and Başak DÜGENCİLİ for their support.

I would also like to extend special thanks to Prof. Dr. Cemal GÖNCÜOĞLU, Prof. Dr. Yaşar E. ERSOY, Dr. Rıza TUNCEL for their meaningful advices and help.

I should express my deepest thanks to Assist. Prof. Dr. Zeynep I. KALAYLIOĞLU for her help in statistical evaluation of the results. I would also like to thank M. Tuğba ERDEM and İçten TANSEL for their help in understanding SPSS.

I also wish to thank Prof. Dr. Aymelek ÖZER and Prof. Dr. Şahide DEMİRCİ for their long lasting support throughout my study at Archaeometry Graduate Program at METU.

I would like to thank my PhD examination committee members, Prof. Dr. Gerhard Wilhelm Weber and Prof. Dr. Nusret Ertaş for valuable suggestions during the defense of my PhD thesis.

## ABBREVIATIONS

C-1	Type 1 chondrite meteorite
Ce/Ce*	Ce anomaly
EC	External calibration
HCA	Hierarchical cluster analysis
HFSE	High field strength elements
HREE	Heavy rare earth elements
ICP-MS	Inductively coupled plasma-mass spectrometry
ICP-OES	Inductively coupled plasma-atomic emission spectrometry
LOI	Loss on Ignition
LREE	Light rare earth elements
MREE	Middle rare earth elements
MW	Microwave
n.d.	Not detected
NAA	Neutron activation analysis
NIST	National Institute of Standards and Technology
PAAS	Post-Archean Australian Sedimentary rocks
PCA	Principal component analysis
PIGME	Proton induced gamma ray emission
PIXE	Particle-induced X-ray emission
PPL	Plane polarized light
REE	Rare earth element
Rf	Radiofrequency
SA	Standard additions
XPL	Cross polarized light
XRF	X-ray fluorescence

## TABLE OF CONTENTS

ABSTRACT.....	v
ÖZ.....	vii
TABLE OF CONTENTS.....	xiii
LIST OF FIGURES.....	xv
LIST OF TABLES.....	xix
CHAPTERS	
1. INTRODUCTION.....	1
1.1 Limestone.....	1
1.1.1 Mineralogy of Limestone.....	3
1.1.2 Component of Limestone.....	3
1.1.3 Classification of Limestone.....	8
1.1.4 Physical Properties of Limestone.....	9
1.1.5 Chemical Properties of Limestone.....	9
1.2 Limestone Figurines from Archaic Period in Mediterranean Region.....	10
1.2.1 Cypriote Type Figurines.....	10
1.2.2 Emecik Figurines.....	15
1.2.3 Datça / Emecik Sarı Liman Excavations.....	17
1.3 Trace Elements in Geochemical Studies.....	17
1.3.1 Rare Earth Elements.....	18
1.3.2 Importance of REE in Geochemistry.....	20
1.4 Provenance Studies of Archaeological Limestone.....	22
1.4.1 Provenance Studies on Limestone Figurines of Cypriote Type.....	22
1.4.2 Provenance Studies on Archaeological Objects Made of Limestone.....	24
1.4.3 Provenance Studies on Geochemistry Using REE Analysis.....	26
2. EXPERIMENTAL.....	31
2.1 Chemicals and Reagents.....	31
2.1.1 Water and Acids.....	31
2.1.1 Standard Solutions.....	31
2.2. Instrumentation and Apparatus.....	32
2.2.1. Microwave Dissolution System.....	32
2.2.2. Inductively Coupled Plasma-Optical Emission Spectrometry.....	32
2.2.3. Inductively Coupled Plasma-Mass Spectrometry.....	33
2.3 Samples.....	34
2.3.1 Archaeological Samples.....	34
2.3.2 Geological Samples from Datça.....	43
2.3.3 Geological Samples from Cyprus.....	48
2.4 Procedures.....	52
2.4.1 Microwave Assisted Dissolution.....	52
2.4.2 Dissolution by Fusion.....	54
2.4.3 Calibrations for ICP-OES Using Standard Additions.....	54
2.4.4 Calibrations for ICP-OES Using External Calibration.....	56
2.4.5 ICP-MS Studies.....	56
2.5 Thin Section Analysis.....	58
2.6 X-ray Diffraction Analysis.....	65
3 RESULTS AND DISCUSSION.....	77
3.1 Optimization of ICP-OES Conditions.....	77
3.2 Optimization of ICP-MS Conditions.....	77
3.3 Results of Analysis of Reference Materials.....	77

3.4 Evaluation of Dissolution Procedures.....	80
3.5 Matrix Factor.....	80
3.6 Results of Chemical Analysis of Samples.....	81
3.7 Results of Thin-section Analysis.....	87
3.8 Results of XRD Analysis of Samples.....	91
3.9 REE Patterns of Figurines and Geological Samples.....	93
3.10 Multielement Diagrams of Figurines and Geological Samples.....	105
3.11 Element Ratios for Figurines and Geological Samples.....	113
3.12 Binary Diagrams of Figurines and Geological Samples.....	118
3.13 Statistical Evaluation of Chemical Analysis.....	119
3.13.1 Variable Selection for Hierarchical Cluster Analysis.....	120
3.13.2 Hierarchical Cluster Analysis.....	125
4 CONCLUSION.....	131
REFERENCES.....	137
APPENDIX A	
ANALYTICAL FIGURES OF MERIT.....	145
APPENDIX B	
RESULTS OF GEOLOGICAL AND ARCHAEOLOGICAL SAMPLES USING ICP-OES.....	147
APPENDIX C	
RESULTS OF GEOLOGICAL AND ARCHAEOLOGICAL SAMPLES USING ICP-MS.....	151
VITA.....	165

## LIST OF FIGURES

### FIGURES

Figure 1.1. Doubly-terminated, orange-tipped calcite crystal 6 cm in length from Taff's Well Quarry Mid Glamorgan, National Museum of Wales.....	2
Figure 1.2. Acicular aragonite crystals from Britannic Merthyr Colliery , Field of view 1 cm across, National Museum of Wales.....	2
Figure 1.3. Acicular Ooid sand from Abu Dhabi.....	4
Figure 1.4. Oolitic packstone to grainstone.....	4
Figure 1.5. Kolymia Limestone packstone with Lindos Limestone, (c) gastropods.....	5
Figure 1.6. Nautiloid limestone facies grainstones with abundant cephalopod .....	5
Figure 1.7. The planktonic foraminifera groups identified based on the morphology.....	6
Figure 1.8. The ecological distribution of larger and key smaller benthic and planktonic foraminifera through space and time.....	7
Figure 1.9. Dunham classification for carbonate rocks.....	9
Figure 1.10. The map of Greek Colonization.....	11
Figure 1.11. Figurine of a woman nursing.....	12
Figure 1.12. Figurine of a woman holding a flower.....	12
Figure 1.13. Figurine of Zeus Ammon.....	13
Figure 1.14. Figurine of a male.....	13
Figure 1.15. Limestone figurine of kouros.....	16
Figure 1.16. Limestone figurine of lyre player.....	16
Figure 1.17. Limestone figurine of a male sitting on a thorne.....	16
Figure 1.18. Limestone figurine of a goddess holding a lion.....	16
Figure 1.19. Periodic Table by International Union of Pure and Applied Chemistry.....	19
Figure 2.1. Typical drill hole for archaeological sampling.....	34
Figure 2.2. Plan of Emecik Sanctuary Excavation Site.....	43
Figure 2.3. Geological map of Datça peninsula, MTA 1997, enlarged area of Datça graben.....	44
Figure 2.4. Geological map of Datça peninsula, MTA 1997 1:100.000. ....	45
Figure 2.5. Geological sampling location KRC.....	47
Figure 2.6. Geological sampling location RZG.....	47
Figure 2.7. Geological sampling location AKYC.....	47
Figure 2.8. Geological sampling location AKYA.....	47
Figure 2.9. Geological sampling location AKYB.....	48
Figure 2.10. Geological zones in Cyprus.....	48
Figure 2.11. Geological map of Cyprus.....	49
Figure 2.12. Limestone quarry at Karpaz.....	51
Figure 2.13. Limestone quarry at Değirmenlik.....	51
Figure 2.14. Sample from Erdemli.....	51
Figure 2.15. Sample from Değirmenlik.....	51
Figure 2.16. Sample from Kumyalı.....	52
Figure 2.17. Sample from ancient quarry.....	52
Figure 2.18. ICP-OES calibration plot of Fe using NIST 1d Limestone, Argillaceous 1.....	54
Figure 2.19. ICP-OES calibration plot of Fe using NIST 1d Limestone, Argillaceous 2.....	54
Figure 2.20. ICP-OES calibration plot of Fe using NIST 1d Limestone, Argillaceous 1.....	55
Figure 2.21. ICP-OES calibration plot of Fe using NIST 1d Limestone, Argillaceous 2.....	55
Figure 2.22. ICP-OES calibration plot of Mg using NIST 1d Limestone, Argillaceous 1.....	55
Figure 2.23. ICP-OES calibration plot of Mg using NIST 1d Limestone, Argillaceous 2.....	55
Figure 2.24. ICP-OES calibration plot of Mg using NIST 1d Limestone, Argillaceous 1.....	55

Figure 2.25. ICP-OES calibration plot of Mg using NIST 1d Limestone, Argillaceous 2.....	55
Figure 2.26. ICP-OES calibration plot of Mn.....	56
Figure 2.27. ICP-OES calibration plot of Ba.....	56
Figure 2.28. ICP-OES calibration plot of Sr.....	56
Figure 2.29. Flow injection ICPMS signals for Y.....	57
Figure 2.30. Flow injection ICPMS signals for for Nb.....	57
Figure 2.31. Flow injection ICPMS signals for for Sm.....	58
Figure 2. 32. Flow injection ICPMS signals for La.....	58
Figure 2.33. Flow injection ICPMS signals for Ce.....	58
Figure 2.34. Thin-section photomicrograph of figurine 93. (XPL, objective x4).....	59
Figure 2.35. Thin-section photomicrograph of figurine 93. (PPL, objective x4) .....	59
Figure 2.36. Thin-section photomicrograph of figurine 2 (XPL, objective x4) .....	60
Figure 2.37. Thin-section photomicrograph of figurine 2 (PPL, objective x4) .....	60
Figure 2.38. Thin-section photomicrograph of figurine 4 (XPL, objective x4) .....	60
Figure 2.39. Thin-section photomicrograph of figurine 4 (PPL, objective x4) .....	60
Figure 2.40. Thin-section photomicrograph of figurine 38 (XPL, objective x4) .....	60
Figure 2.41. Thin-section photomicrograph of figurine 38 (PPL, objective x4) .....	60
Figure 2.42. Thin-section photomicrograph of figurine 56 (XPL, objective x4) .....	61
Figure 2.43. Thin-section photomicrograph of figurine 56 (PPL, objective x4) .....	61
Figure 2.44. Thin-section photomicrograph of figurine 84 (XPL, objective x4) .....	61
Figure 2.45. Thin-section photomicrograph of figurine 84 (PPL, objective x4) .....	61
Figure 2.46. Thin-section photomicrograph figurine 47 (XPL, objective x4) .....	61
Figure 2.46. Thin-section photomicrograph of figurine 47 (XPL, objective x4) .....	61
Figure 2.47. Thin-section photomicrograph of figurine 47 (PPL, objective x4) .....	61
Figure 2.48. Thin-section photomicrograph of figurine 37 (XPL, objective x4) .....	62
Figure 2.49. Thin-section photomicrograph of figurine 37 (PPL, objective x4) .....	62
Figure 2.50. Thin-section photomicrograph of figurine 22 (XPL, objective x4) .....	62
Figure 2.51. Thin-section photomicrograph of figurine 22 (PPL, objective x4) .....	62
Figure 2.52. Thin-section photomicrograph of AKYA, Datça (XPL, objective x4) .....	62
Figure 2.53. Thin-section photomicrograph of AKYA, Datça (PPL, objective x4) .....	62
Figure 2.54. Thin-section photomicrograph of RZG, Datça (XPL, objective x4) .....	63
Figure 2.55. Thin-section photomicrograph of RZG, Datça (PPL, objective x4) .....	63
Figure 2.56. Thin-section photomicrograph of KRC, Datça (XPL, objective x4) .....	63
Figure 2.57. Thin-section photomicrograph of KRC, Datça (PPL, objective x4) .....	63
Figure 2.58. Thin-section photomicrograph of AKYB, Datça (XPL, objective x4) .....	63
Figure 2.59. Thin-section photomicrograph of AKYB, Datça (PPL, objective x4) .....	63
Figure 2.60. Thin-section photomicrograph of AKYC, Datça (XPL, objective x4) .....	64
Figure 2.61. Thin-section photomicrograph of AKYC, Datça (PPL, objective x4) .....	64
Figure 2.62. Thin-section photomicrograph of figurine 56 (XPL, objective x4) .....	64
Figure 2.63. Thin-section photomicrograph of figurine 56 (PPL, objective x4) .....	64
Figure 2.64. Thin-section photomicrograph of figurine 47 (XPL, objective x4) .....	64
Figure 2.65. Thin-section photomicrograph of figurine 47 (PPL, objective x4) .....	64
Figure 2.66. XRD plot for NIST 1d.....	65
Figure 2.67. XRD plot for figurine 4.....	65
Figure 2.68. XRD plot for figurine 22.....	66
Figure 2.69. XRD plot for figurine 23.....	66
Figure 2.70. XRD plot for figurine 24.....	66
Figure 2.71. XRD plot for figurine 28.....	67
Figure 2.72. XRD plot for for archaeological sample 30.....	67
Figure 2.73. XRD plot for figurine 31.....	67
Figure 2.74. XRD plot for figurine 32.....	68
Figure 2.75. XRD plot for figurine 34.....	68
Figure 2.76. XRD plot for figurine 37.....	68
Figure 2.77. XRD plot for figurine 38.....	69

Figure 2.78. XRD plot for figurine 40.....	69
Figure 2.79. XRD plot for figurine 41.....	69
Figure 2.80. XRD plot for figurine 44.....	70
Figure 2.81. XRD plot for figurine 46.....	70
Figure 2.82. XRD plot for figurine 47.....	70
Figure 2.83. XRD plot for figurine 51.....	71
Figure 2.84. XRD plot for figurine 52.....	71
Figure 2.85. XRD plot for figurine 55.....	71
Figure 2.86. XRD plot for figurine 58.....	72
Figure 2.87. XRD plot for figurine 61.....	72
Figure 2.88. XRD plot for figurine 62.....	72
Figure 2.89. XRD plot for figurine 63.....	73
Figure 2.90. XRD plot for figurine 64.....	73
Figure 2.91. XRD plot for figurine 65.....	73
Figure 2.92. XRD plot for figurine 69.....	74
Figure 2.93. XRD plot for figurine 74.....	74
Figure 2.94. XRD plot for figurine 75.....	74
Figure 2.95. XRD plot for figurine 80.....	75
Figure 2.96. XRD plot for figurine 81.....	75
Figure 2.97. XRD plot for figurine 84.....	75
Figure 2.98. XRD plot for figurine 92.....	76
Figure 2.99. XRD plot for figurine 94.....	76
Figure 2.100. XRD plot for figurine 95.....	76
Figure 3.1. The REE patterns of ST.06.I12.d5.c12 (2), ST.02.8B.19A.13 (40), ST.02.K9c.27b.1 (65), ST.02.I8b.23.9 (80), ST.02.I8b.28.B3 (92), ST.00.K8C.16.152 (95), and K1, K2.....	94
Figure 3.2. The REE patterns of ST.02.I8B.19.b6 (34), ST.02.I8b.11.b9 (35), ST.02.I8b.25.12 (45), ST.02.I8b.19.A12 (84), ST.99.I9b.2.17 (88), ST.01.I8.B.10.26 (89) .....	94
Figure 3.3. The REE patterns of ST.02.I8b.28.A2 (36), ST.02.I8B.19.6 (41), ST.02.I8b.21.17 (44), ST.02.I8b.23.11 (61), ST.02.I8b.28A.2 (62), ST.02.I8b.15.17 (72), ST.02.K9c.27a.11 (77), ST.99.K8C.9.22 (94) .....	95
Figure 3.4. The REE patterns of ST.02.I8b.16A.16 (33), ST.02.K9c.27A.13 (56), ST.02.I8b (74), ST.00.K8C.16.148 (86) .....	95
Figure 3.5. The REE patterns of ST.06.I12.d3.9 (17), ST.02.I8b.16A.11 (24), ST.02.I8B.16.A.15 (37), ST.02.I8b.28.6.3 (47), ST.02.I8b.28.8 (48), ST.00.D8.A.5.25 (93) .....	96
Figure 3.6. The REE patterns of ST.06.H12.a2A.23 (9), ST.06.I12d.6A.11 (12), ST.06.I12.d5.B11 (16), ST.02.K9c.26.4 (59), ST.02.I8b.14.30 (71) .....	96
Figure 3.7. The REE patterns of ST.06.I12.d7.43 (7), ST.06.I12.d5.A11 (8), ST.02.I8b.16A.11 (26), ST.02.I8b.14.20 (58), ST.02.K9.c27.A12 (69), ST.99.I9B.4 (91) .....	97
Figure 3.8. The REE patterns of ST.02.I8b.28A.11 (32), ST.02.I8b.19.2 (50), ST.02.I8b.14.17 (53), ST.01.G11.D1 (63), ST.02.I8b.16A.17 (73) .....	97
Figure 3.9. The REE patterns of ST.06.I12.d5A.12 (18), ST.02.I8b.19.2 (49), ST.02.K9c.27A.3 (67), ST.02.K9.c28.14 (68), ST.99.I9b.4.65 (87) .....	98
Figure 3.10. The REE patterns of ST.06.I12.d6A.14 (10), ST.02.I8b.16.20 (39), ST.02.I8b.22.2 (46), ST.02.I8b.23.9 (81), ST.00.K8.C.16.151 (90) .....	98
Figure 3.11. The REE patterns of ST.02.I8b.16A.11 (23), ST.02.I8b.25.11 (31), ST.02.I8b.18.7 (52), ST.02.I8b.11b.10 (57), ST.02.I8b.28.3 (75) .....	99
Figure 3.12. The REE patterns of ST.06.H12.a3.16 (4), ST.02.I8b.11.c26 (28), ST.02.I8b.16A.16 (33), ST.02.I8b.28.A3 (43), ST.02.K9c.28.6 (54), ST.02.K9c.27.4 (55), ST.02.K9.c27.A12 (69) .....	99
Figure 3.13. The REE patterns of ST.06.I12.d8.19 (1), ST.02.I8b.16A.11 (24), ST.02.I8B.16.A.15 (37), ST.02.I8b.28.6.3 (47), ST.02.I8b.28.8 (48), ST.00.K8C.16.148 (86) .....	100
Figure 3.14. The REE patterns of ST.06.I12.d3.9 (17), ST.06.I12.d5.17 (19), ST.02.I8B.11c.29 (38), ST.02.K9c.27A.13 (56), ST.02.I8b.28.A9 (70), ST.00.D8.A.5.25 (93) .....	100
Figure 3.15. The REE patterns of ST.06.I12.d6.B (5), ST.06.H12.d5.15 (6), ST.06.H12.a5.22	

(11), ST.06.H12.a3.17 (14), ST.06.I12.d7.44 (20) .....	101
Figure 3.16. The REE patterns of ST.06.I12.d7.45 (15), ST.02.I8b.18.3 (22), ST.02.I8b.16A.11 (27), ST.02.K9c.28.7.4 (42) .....	101
Figure 3.17. The REE patterns of geological samples from Datça.....	102
Figure 3.18. The REE patterns of the figurines that were made from local limestone.....	102
Figure 3.19. The REE patterns of ST.02.K9c.28B1 (30), AKYA, AKYB.....	103
Figure 3.20. The REE patterns of ST.02.I8b.28A.2 (64), AKYC.....	103
Figure 3.21. The REE patterns of ST.06.I12.d8.21 (3), KRC.....	104
Figure 3.22. The REE patterns of ST.02.I8b.19.A.12 (85), RZG.....	104
Figure 3.23. The multi-element diagrams of ST.06.I12.d5.c12 (2), ST.02.K9c.27b.1 (65), ST.02.I8b.23.9 (80), ST.02.I8b.28.B3 (92), ST.00.K8C.16.152 (95).....	106
Figure 3.24. The multi-element diagrams of ST.02.I8b.28.A2 (36), ST.02.I8B.19.6 (41), ST.02.I8b.21.17 (44), ST.02.I8b.23.11 (61), ST.02.I8b.28A.2 (62), ST.02.I8b.15.17 (72), ST.02.K9c.27a.11 (77), ST.99.K8C.9.22 (94) .....	107
Figure 3.25. The multi-element diagrams of ST.02.I8B.19.b6 (34), ST.02.I8b.11.b9 (35), ST.02.I8b.25.12 (45), ST.02.I8b.19.A12 (84), ST.01.I8.B.10.26 (89).....	107
Figure 3.26. The multi-element diagrams of ST.02.I8b.16A.16 (33), ST.02.K9c.27A.13 (56), ST.02.I8b (74), ST.00.K8C.16.148 (86) .....	108
Figure 3.27. The multi-element diagrams of ST.06.I12.d3.9 (17), ST.02.I8b.16A.11 (24), ST.02.I8B.16.A.15 (37), ST.02.I8b.28.6.3 (47), ST.00.D8.A.5.25 (93) .....	108
Figure 3.28. The multi-element diagrams of ST.06.H12.a3.16 (4), ST.02.I8b.11.c26 (28), ST.02.I8b.16A.16 (33), ST.02.I8b.28.A3 (43), ST.02.K9c.28.6 (54), ST.02.K9c.27.4 (55), ST.02.K9.c27.A12 (69) .....	109
Figure 3.29. The multi-element diagrams of ST.06.H12.a2A.23 (9), ST.06.I12d.6A.11 (12), ST.06.I12.d5.B11 (16), ST.02.K9c.26.4 (59), ST.02.I8b.14.30 (71) .....	109
Figure 3.30. The multi-element diagrams of ST.06.I12.d7.43 (7), ST.06.I12.d5.A11 (8), ST.02.I8b.16A.11 (26), ST.02.I8b.14.20 (58), ST.02.K9.c27.A12 (69), ST.99.I9B.4 (91)..	110
Figure 3.31. The multi-element diagrams of ST.02.I8b.28A.11 (32), ST.02.I8b.19.2 (50), ST.02.I8b.14.17 (53), ST.01.G11.D1 (63), ST.02.I8b.28.A9 (70), ST.02.I8b.16A.17 (73)..	110
Figure 3.32. The multi-element diagrams of ST.06.I12.d5A.12 (18), ST.02.I8b.19.2 (49), ST.02.K9c.27A.3 (67), ST.02.K9.c28.14 (68), ST.99.I9b.4.65 (87) .....	111
Figure 3.33. The multi-element diagrams of ST.06.I12.d6A.14 (10), ST.02.I8b.16.20 (39), ST.02.I8b.22.2 (46), ST.02.I8b.23.9 (81), ST.00.K8.C.16.151 (90) .....	111
Figure 3.34. The multi-element diagrams of ST.02.I8b.16A.11 (23), ST.02.I8b.25.11 (31), ST.02.I8b.18.7 (52), ST.02.I8b.11b.10 (57), ST.02.I8b.28.3 (75) .....	112
Figure 3.35. The multi-element diagrams of ST.06.I12.d7.45 (15), ST.02.I8b.18.3 (22), ST.02.I8b.16A.11 (27), ST.02.K9c.28.7.4 (42) .....	112
Figure 3.36. The multi-element diagrams of geological samples from Datça.....	113
Figure 3.37. $\Sigma$ REE ( $\mu\text{g}/\text{kg}$ ) vs Ce anomaly binary plot for all the samples.....	118
Figure 3.38. $(\text{La}/\text{Sm})_n$ vs $\text{Sm}_n$ binary plot for all the samples.....	119
Figure 3.39. Scatter plots of five principal components scores.....	125
Figure 3.40. Dendrogram of archaeological and geological samples by Euclidean distance....	127

## LIST OF TABLES

### TABLES

Table 1.1. The Rare Earth Elements.....	39
Table 2.1. Acids used in all experiments.....	51
Table 2.2. Standard solutions used in experiments.....	51
Table 2.3 Plasma Conditions for ICP – OES, Leeman DRE.....	52
Table 2.4. ICP-MS, Thermo X series 2 plasma operation parameters. ....	53
Table 2.5. The Nomenclature of Archaeological Samples. ....	54
Table 2.6. Geological Sampling Points in Datça peninsula.....	66
Table 2.7. Geological Sampling Points in Cyprus.....	71
Table 2.8. Microwave Program 1.....	71
Table 2.9. Microwave Program 2.....	71
Table 2.10. Some information about the measured isotopes.....	75
Table 2.11. The list of figurines that were analyzed through thin-sections.....	77
Table 3.1. Plasma Conditions for ICP – OES, Leeman DRE.....	95
Table 3.2. Results for NIST 1d Argillaceous.....	96
Table 3.3. Results for NIST 1d Argillaceous.....	96
Table 3.4. Results for NIST 1d Argillaceous external calibration.....	97
Table 3.5. Results for NCS DC 73306 carbonate rock.....	97
Table 3.6. Matrix factor for each element.....	99
Table 3.7. Results of Geological and Archaeological Samples using ICP-OES.....	99
Table 3.8. Results of geological and archaeological samples using ICP-MS for Cr, Y, Nb, La, Ce, Nd and Sm.....	101
Table 3.9. Results of geological and archaeological samples using ICP-MS for Eu, Gd, Ho, Er, Yb, Lu and Hf.....	103
Table 3.10. Samples examined by thin-section analysis.....	105
Table 3.11. The list of figurines, names, descriptions and mineral inclusions.....	109
Table 3.12. PAAS values of the elements.....	111
Table 3.13. C1 values of the elements.....	123
Table 3.14. REE fractionations, Ce anomaly and $\Sigma$ REE of samples.....	131
Table 3.15. Communalities for PCA.....	138
Table 3.16. Initial Eigenvalues of the PCA.....	139
Table 3.17. Extraction Sums of Squared Loadings and Rotation Sums of Squared Loadings..	140
Table 3.18. Rotated Component Matrix.....	140
Table 3.19. Component Score Coefficient Matrix.....	141
Table 4.1. The groups for Emecik limestone figurines.....	151



## CHAPTER 1

### INTRODUCTION

Characterization and determination of the source of archaeological materials play an important role in understanding and reconstruction of technology of ancient civilizations, trade connections, and social, political and religious relationships of ancient societies. Since 1960's, instrumental methods of analytical chemistry have been used for archaeological provenance studies of various artifacts, such as lithic, ceramic, glass and metal, although obsidian was the first and most widely analyzed material [1].

The class of limestone statuettes, widespread over the Mediterranean area during Orientalizing and Archaic periods, has long been controversial [2].

One of these sanctuaries where limestone statuettes were found is attributed to Apollo and is located in Emecik, which is 15 km east of Old Cnidus in Datça peninsula. Limestone figurine fragments of a great number and variety of types made it reasonable to think that they were produced locally. It was also suggested that possibly a local limestone was used [3].

This study involves the characterization of limestone figurines found at Emecik, investigation on whether they all have the same origin or have different sources, and possibility of using a local source.

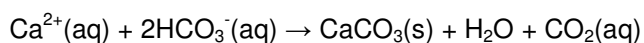
#### 1.1 Limestone

Emecik figurines are supposed to be made of *limestone* [3]. Limestone is essentially composed of calcium carbonate mineral  $\text{CaCO}_3$ . This mineral is one of the most common species among the chemically precipitated sedimentary rocks [4]. Biological and biochemical processes are dominant in the formation of carbonate sediments; however inorganic precipitation of  $\text{CaCO}_3$  from seawater also takes place [5]. After the formation, chemical and physical processes of diagenesis can considerably change the limestone.

Organisms with carbonate skeletons occur throughout seas and oceans; therefore carbonate sediments can develop anywhere. Limestones can also form in lakes and soils. However, there are several factors that control limestone deposition such as temperature, salinity, water depth and siliciclastic input [5]. The input of siliciclastic material is the overriding control on limestone deposition. Many carbonate producing organisms cannot tolerate the influx of large quantities of terrigenous mud.

##### 1.1.1 Mineralogy of Limestone

Although the calcium carbonate mineral may be precipitated directly from seawater, limestone is the result of organic precipitation. Many living organisms extract  $\text{CaCO}_3$  from water to build hard protected shells. After the death of organisms, the hard calcareous parts accumulate on the sea floor. When marine life is abundant, shells of great thickness and other hard parts may build up, which, when consolidated, become limestone. Precipitation of calcium carbonate can be shown by the following reaction equation [6]:



After the precipitation and deposition of calcium carbonate, it hardens into limestone through the growth of crystals and has two principal forms, calcite and aragonite. Trigonal calcite  $\text{CaCO}_3$  and its orthorhombic polymorph aragonite  $\text{CaCO}_3$  are the common minerals in modern sediments. Several cations can substitute in varying amounts for  $\text{Ca}^{2+}$  in the crystal structures [7];  $\text{Mg}^{2+}$ ,  $\text{Fe}^{2+}$  and  $\text{Mn}^{2+}$  are more readily accepted in the hexagonal calcite structure, and  $\text{Sr}^{2+}$  and  $\text{Ba}^{2+}$  by the aragonite structure.

Deposition of calcite is of either high-magnesium or low-magnesium calcite [8]. Aragonite is unstable at surface temperatures and pressures and changes to calcite in time. If the  $\text{MgCO}_3$  content of calcite is greater than 4 % by weight, it is called *high magnesium calcite*, while if it is less than 4 % the calcite is called *low magnesium calcite*.

High-magnesium calcite is more soluble in water than low-magnesium calcite; eventually, in time this mineral is converted into low-magnesium calcite [8]. The appearances of calcite and aragonite minerals are given in Figure 1.1 and 1.2, respectively.



**Figure 1.1.** Doubly-terminated, orange-tipped calcite crystal 6 cm in length from Taff's Well Quarry Mid Glamorgan. National Museum of Wales.



**Figure 1.2.** Acicular aragonite crystals from Britannic Merthyr Colliery, Field of view 1 cm across, National Museum of Wales

On the other hand, dolostone, quite similar to limestone, is also a sedimentary carbonate rock composed largely or entirely of the mineral dolomite  $\text{CaMg}(\text{CO}_3)_2$  [9]. Limestone is recognized by the bubbly evolution of  $\text{CO}_2$  gas when a few drops of dilute  $\text{HCl}$  are dropped on it; however dolomite does not react visibly with dilute  $\text{HCl}$  unless the mineral is powdered. Carbonate rocks are normally quite free of impurities, which total less than 5 % of an average limestone and consist of clay minerals and fine-grained quartz [9]. Impurities could be introduced at any stage of deposition of the sediment [10], such as the transfer of water-borne suspended materials, mainly clay and silt, and dissolved elements,  $\text{Mg}$ ,  $\text{Si}$ ,  $\text{F}$ ,  $\text{Pb}$ ,  $\text{Fe}$  and other heavy metals, into faults, then these elements may have migrated from fault into the deposition through cracks and pores in limestone.

Diagenesis is the conversion of sediments into rock by organic, physical and chemical processes [10]. Six main processes have been identified for limestone: microbial micritization, cementation, neomorphism, dissolution, compaction and dolomitization [11]:

In Microbial micritization, the bore-holes made by organisms in carbonate deposits become filled with a calcium carbonate structure called micrite.

Cementation results from the passage of water, which is super-saturated with respect to calcite, through porous limestone deposits, leading to the growth of calcite crystals in pores and thus binding together the components of the deposit.

Neomorphism involves recrystallization. Aragonite progressively recrystallizes over time to produce very low-magnesium calcite. Calcite recrystallizes into larger crystallites, so the magnesium in high-magnesium calcite slowly dissolves and leaves low-magnesium deposits.

Dissolution generally occurs when unsaturated ground waters flow through deposits.

Compaction occurs during the burial process and is a combination of physical effects, such as dissolution/recrystallization under high pressure. Dolomitization results in the formation of the double carbonate  $\text{CaCO}_3 \cdot \text{MgCO}_3$ . The mechanisms of dolomitization are not well understood, but involve passage of seawater through the pores of limestone over long periods [10]. The dissolved magnesium is able to replace calcium ions in the crystal lattice, because dolomite is more stable than calcite.

### **1.1.2 Components of Limestone**

Limestone has a variety in composition but the components can be divided into four groups: non skeletal grains, skeletal grains, micrite and cement.

Non skeletal grains are classified as ooids and pisoids, peloids, aggregates and intraclasts. Modern ooids are spherical-sub spherical grains, consisting of one or more regular concentric lamellae around a nucleus, usually a carbonate particle or quartz grain [5].

The carbonate sediment composed of ooids is called as oolite. Ooids and pisoids can form in shallow waters of seas, as well as lagoons. Structures resembling ooids are also known in calcareous soils. Ooids are spherical particles with concentric laminae coating a nucleus. Modern marine ooids consist of aragonite or High-Mg calcite [7]. Pisoids are carbonate or non carbonate grains resembling ooids in structure however they are different in origin, environment, and internal structure and often have a larger size.

Peloids are spherical, ellipsoidal, or angular grains, composed of microcrystalline carbonate, but with no internal structure [5]. Most peloids are of faecal origin and can be referred to as pellets. Organisms such as gastropods that are snails and slugs, crustaceans and polychaetes that are a class of ringed worms marine produce vast amount of pellets. Faecal pellets have regular shapes and are rich in organic matter. The definition of pellets is commonly lost as a result of diagenetic processes, and limestones may show flocculent or clotted texture. The term also covers the micritized bioclastic grains formed by alteration of skeletal fragments. The appearances of ooids and peloids are given in Figure 1.3. and 1.4., respectively.



**Figure 1.3.** Ooid sand from Abu Dhabi (Persian Gulf) [12]

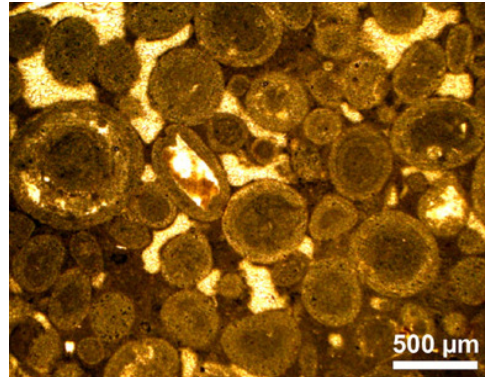


**Figure 1.4.** Oolitic packstone to grainstone. Ooids show concentric laminations. Nuclei are peloids, Northern Tunisia [13]

Aggregates consist of several carbonate particles cemented together by microcrystalline cement or bound by organic matter [5]. Intraclasts are fragments of lithified or partly lithified sediments. A common type of intraclast in carbonate sediments is a micritic flake or chip.

The skeletal components of limestone are a reflection of the distribution of carbonate bearing invertebrates through time and space [5]. Environmental factors such as depth, temperature, salinity, substrate and turbulence, control the distribution and development of organisms in the various carbonate environments. Skeletal grains are the most valuable grain types in determining the age of the limestone samples [7]. The type and composition of skeletal grains are highly sensitive to the depositional environment and offer significant proxies for paleoenvironmental conditions on the formation of limestone. The diagenesis of limestone is also reflected in the diagenesis of fossils. The original mineralogy of most calcareous fossils are known so fossil diagenesis is very helpful in understanding the diagenetic processes of the stone.

Mollusca are of the main contributors of skeletal grains in limestone [5]. They are a large phylum of invertebrate animals such as bivalves, gastropods and cephalopods. The bivalves are the common skeletal grains especially since Tertiary Period. The majority of bivalve shells are composed of aragonite; some are of mixed mineralogy and others such as oysters and scallops are calcite. Bivalve shells consist of several layers of specific internal microstructure.

Gastropods are very common in shallow marine environments [5]. They also occur in vast numbers in saline waters like tidal flats. Most gastropods are benthic creatures. The majority of them have shells of aragonite with similar internal microstructures to bivalves. The internal structure of a gastropod fossil is also rarely seen because the original aragonite is mostly dissolved and the voids are filled by calcite cement. Gastropod fossils can be easily recognized under the optical microscope; however, the plane of the section is also important. They can resemble foraminifers, but foraminifers are usually much smaller and composed of dark micritic calcite. The appearances of gastropod skeletal grains are given in Figure 1.5.

Cephalopods are relatively common in Paleozoic and Mesozoic limestones [5]. They are more common in pelagic deposits. The shells of nautiloid and ammonoid, which were squid like creatures living inside of an external shell, of the cephalopods were of aragonite originally, so in limestones they are typically composed of calcite spar with little internal structure. The appearances of ooids and peloids are given in Figure 1.6.

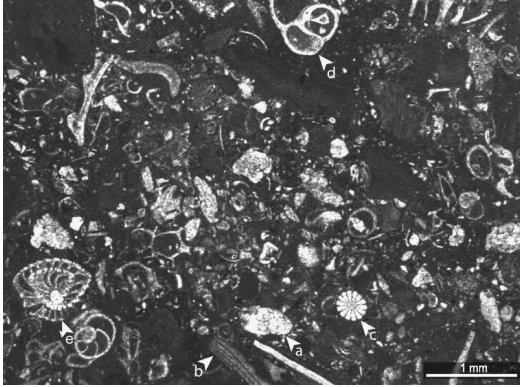


**Figure 1.5.** Kolymbia Limestone packstone with Lindos Limestone, (c) gastropods [14]

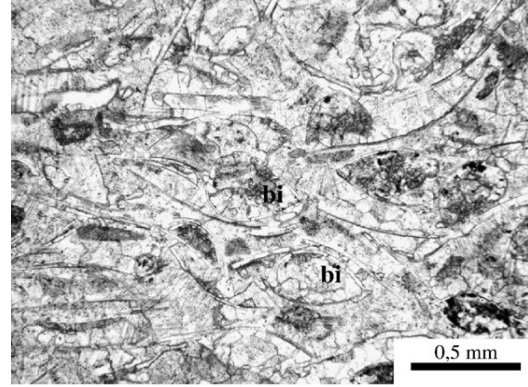


**Figure 1.6.** Nautiloid limestone facies grainstones with abundant cephalopod and bivalve debris [15]

Foraminifera are dominantly marine protozoa, mostly of microscopic size [5]. They are characterized by having tests with web-like filaments [16]. The filaments are either granular, branched and fused or pencil-shaped and pointed emerging from the cell body. These organisms have existed in oceans for more than 500 million years. Both living and fossil foraminifera have many different shapes and sizes, and occur in many different environments, from shore to the deep sea. Their elaborate, solid calcite tests are made of a series of chambers. The evolution of their shell structures is the basis of their usefulness [16].

The simple forms of foraminifera appeared approximately 500 million years ago. They became abundant and developed with complicated test structure by the Late Paleozoic, 360 to 286 million years ago [16]. By the Cenozoic era, 65 million years ago to today, they provide a model of evolutionary diversity. Because of this well recorded evolution, foraminifera are widely used in many disciplines such as palaeoenvironmental, palaeobiological and palaeoceanographic interpretation and analysis.

Foraminifers are divided into two groups, namely planktonic and benthic foraminifers. Many species of foraminifers are planktonic and have a worldwide occurrence in broad latitudinal and temperature belts [16]. In each interval of morphological diversification since the Early Cretaceous, planktonic foraminiferal assemblages were consisted of species with globigerinid form of generally small size [17]. Planktonic foraminifers dominate some pelagic deposits and some Cretaceous and Tertiary chalks and marls [5]. Benthic foraminifers are common in warm, shallow seas, living within and on the sediment, and encrusting hard substrates. The planktonic foraminifer groups are given in Figure 1.7.

Foraminifers are composed of low or high Mg-calcite and rarely aragonite [5]. Although they have many different shapes, in section many common forms are circular to sub-circular with chambers. The test wall is dark and micro-granular in many thin-walled foraminifera endothyraclids and miliolids, but light-coloured and fibrous in larger thicker species such as rotaliids, nummulitids, and orbitolinids. The ecological distribution of foraminifera is given in Figure 1.8.

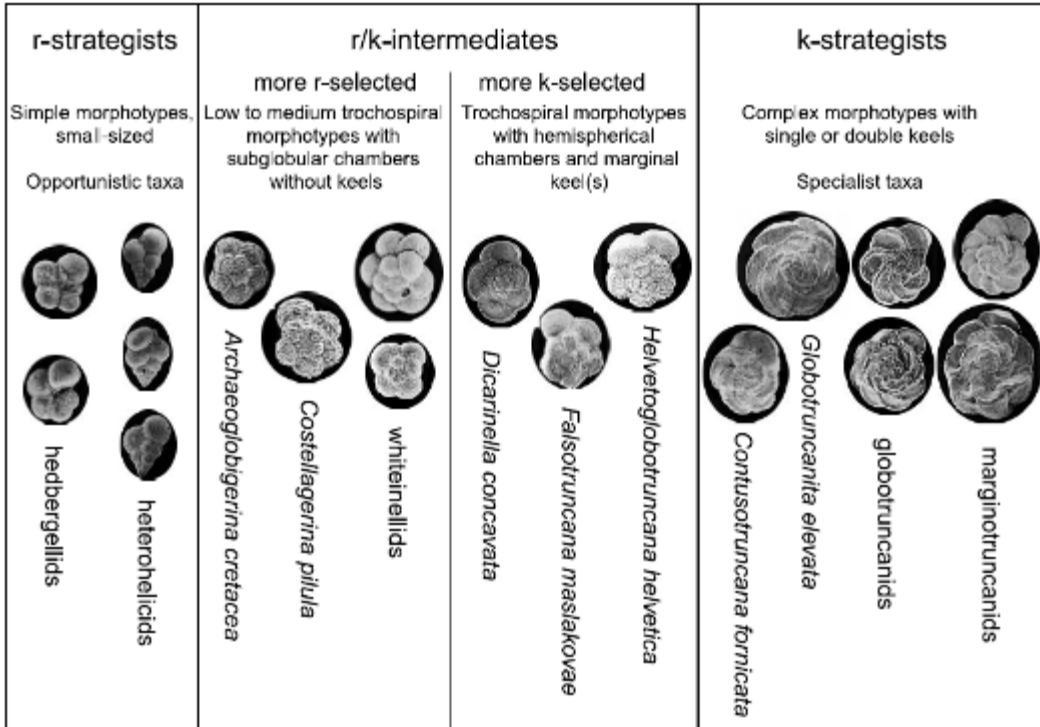


**Figure 1.7.**The planktonic foraminifera groups identified based on the morphology [18].

Foraminifers have been known and studied for centuries. They were first mentioned by Herodotus who noted that the limestone of the Egyptian pyramids contains the larger benthic foraminifera which is Nummulites. The name derived from a hybrid of Latin and Greek terms means “bearing pores or holes” as the surfaces of most foraminifera shells are covered with microscopic holes [16].

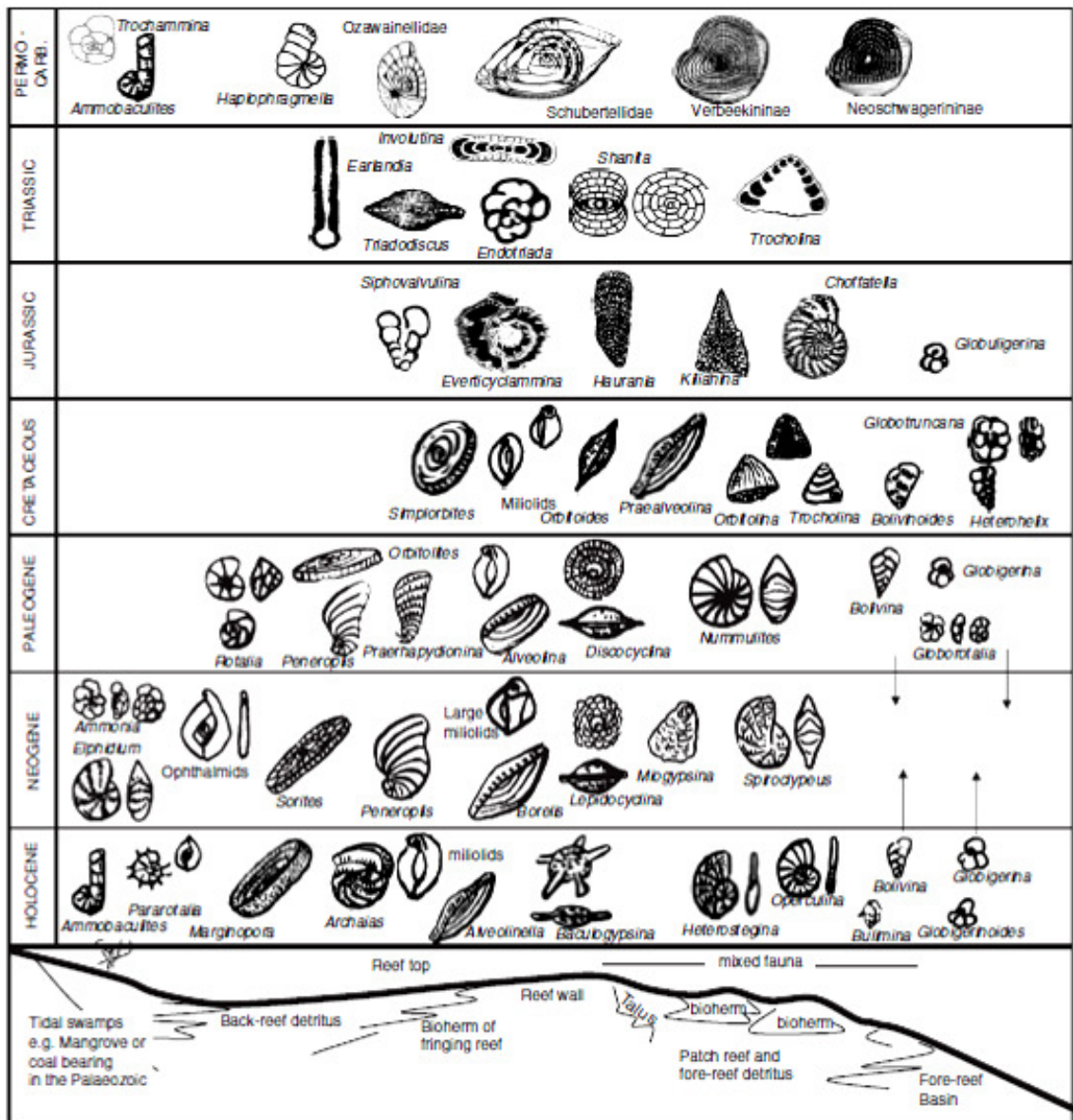


**Figure 1.8.** The ecological distribution of larger and key smaller benthic and planktonic foraminifera through space and time [16].

There are many other organisms that have calcareous skeletons but contributed in only a minor way to limestone formation. Sponges are such organisms. Spicules of sponges could be composed of silica or calcite minerals. The importance of spicules is as a source of silica for the formation of chert nodules in limestone and silicification [5]. The ostracods are locally important in Tertiary limestones. They live in shallow depths in marine, brackish and freshwater environments. Ostracods have small, thin bivalve shells, smooth or ornamented, composed of calcite with radial-fibrous structure. Calciferes are simple spherical objects composed of calcite, in some cases with a micrite wall [5]. It is been suggested that they could be a form of alga or foraminifera. They occur in many Paleozoic limestones.

Many grainy limestones have a fine, usually dark matrix and many others are composed entirely of fine grained carbonate [5]. This material is called micrite, which is microcrystalline calcite. Studies have shown that the micrite is not homogenous but has areas of finer or coarser crystals. Micrite is susceptible to diagenetic alteration. Carbonate muds are accumulating in many modern environments, from tidal flats and shallow lagoons to deep-sea floor. There are many sources of carbonate mud. Some of the processes are bioerosion, where organisms such as sponges attack carbonate grains; mechanical breakdown of skeletal grains by waves and currents; biochemical precipitation through microbial photosynthesis and decomposition.

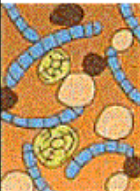
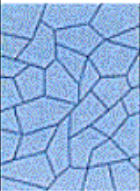
### 1.1.3 Classification of Limestones

Limestone takes many forms and according to these forms it is classified as biosparites, micrites, reef limestones, algal limestones, travertine and tufa [10]. However, there are also many other ways of classifying limestone, which have been developed to describe the nature of the deposit. These classifications may be based on:

- *the average grain size* [19],
- *micro-structure* [11],
- *texture* [11]
- *principal impurities*, e.g., carbonaceous, ferruginous, argillaceous, or clayey, phosphatic [11] carbonate content, e.g., ultra-high calcium, high-calcium, high purity carbonate, calcitic, magnesian, dolomitic, high magnesium dolomite.

Any classification may have a generic or a genetic base [20]. A generic classification simply involves defining certain properties and allocating a name to them. A genetic classification is one in which the basis for the classification uses some fundamental property relating directly to the origin of the item being classified. The classifications that are widely used are based on the textural maturity, where the fabric is believed to relate to the energy level during the depositions of the limestone.

Durham classification for carbonate rocks based on texture and grain size is given in Fig.1.9. This classification is the simplest and most widely used. The classification of Durham is based on the rock or sediment fabric, and the presence of any biological binding [20]. However, in study this classification is not followed, only the petrographical identification is given.

Mudstone	Wackestone	Packstone	Grainstone	Boundstone	Crystalline
					
Less than 10% grains	More than 10% grains	Grain-supported	Lacks mud and is grain-supported	Original components were bound together	Depositional texture not recognizable
Mud-supported					
Contains mud, clay and fine silt-size carbonate					
Original components were not bound together					
Depositional texture recognizable					

**Figure 1.9.** Dunham classification for carbonate rocks [21].

#### 1.1.4 Physical Properties of Limestone

The color of limestone usually reflects the levels and the nature of the impurities present [10]. White deposits are generally of high purity; various shades of grey and dark hues indicate carbonaceous material or iron sulfide; yellow, cream and red hues are indicative of iron and manganese [10].

The texture of limestone varies widely. All limestones are crystalline with grain sizes ranging from less than 4  $\mu\text{m}$  to about 1000  $\mu\text{m}$ . The distribution of grain sizes affects the texture and ranges from mudstone to grainstone [10].

Crystal structures of calcite and aragonite are rhombic or hexagonal, while dolomite is trigonal [14]. At a wavelength of 590 nm calcite has ordinary and extraordinary refractive indices of 1.658 and 1.486, respectively [22].

The specific gravities of the crystalline forms of calcium carbonate and dolomite at 20°C are calcite 2.71, aragonite 2.93 and dolomite 2.87 [22].

The porosity of limestones is generally in the range 0.1 to 30 % and of dolostones 1 to 10% by volume [10].

The hardness of limestones generally is in the range 2 to 4 Mohs [10].

The bulk density of a limestone with an apparent density of 2.7  $\text{g}/\text{cm}^3$  is 1.40 -1.45 $\text{g}/\text{cm}^3$  [10].

#### 1.1.5 Chemical Properties of Limestone

The solubility of aragonite is 0.0015 g/L, and of calcite is 0.0014 g/L under ambient conditions and calcite is metastable with respect to dolomite [22]. When limestone reacts with acids,  $\text{CO}_2$  is released [10]:

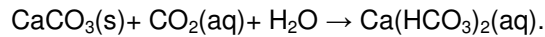


where M shows  $\text{Ca}^{2+}$  or  $\text{Mg}^{2+}$ .

It also releases  $\text{CO}_2$  on heating and form calcium oxide, usually known as burnt or quick lime

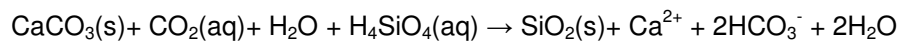


Calcium carbonate reacts with water that is saturated with carbon dioxide and forms the soluble calcium bicarbonate [10]



This is the reaction that is the reason of the formation of caverns and the temporary hard water. Limestone is alkaline with the pH values of 8 to 9 depending on the temperature.

Silicification process most likely occurs at low pH, low temperature environments in this process accumulation of silica in pores takes place [10]. Silicification reaction can be shown as follow:



## **1.2 Limestone Figurines from Archaic Period in Mediterranean Region**

### **1.2.1 Cypriote Type Figurines**

The type of limestone figurines classified as Cypriot, was popular during the Orientalizing (last quarter of 7th century B.C.) and Archaic periods (middle of 6th century B.C.) [2, 23]. Figurines were found not only in all sites in the Island, but also in various sites in Aegean region, Egypt, and Syro-Palestinian sanctuaries. Map of Mediterranean basin is given in Figure 1.10.

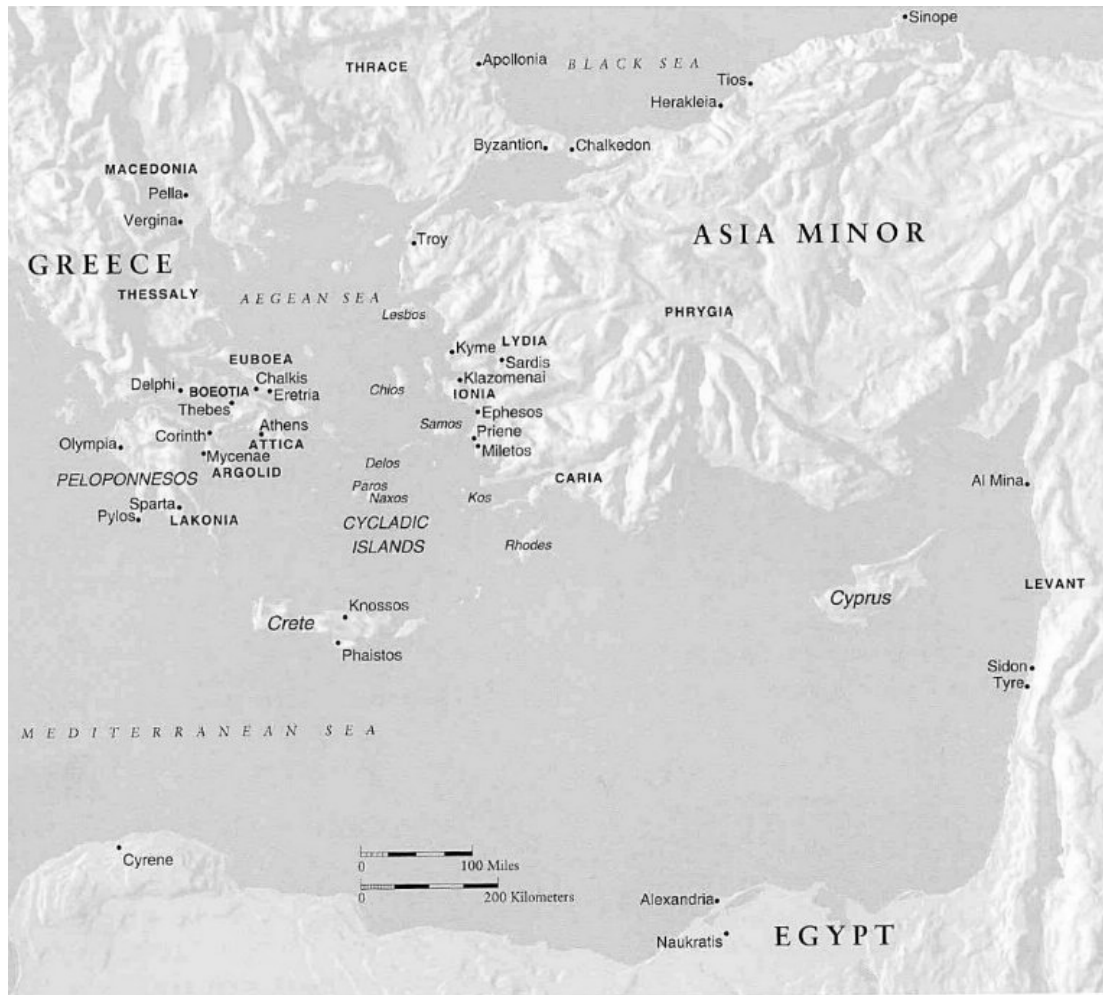


**Figure 1.10.** The map of Greek Colonization, [http:// http://creefest.ca/ud/ut-map-of-ancient-mediterranean/index.phtml](http://creefest.ca/ud/ut-map-of-ancient-mediterranean/index.phtml)

The size of the figurines is generally 10-20 cm; however larger pieces of 40-70 cm, have also been found [23]. Pictures of some figurines found in Mediterranean are given in Fig.1.11-14. The Cypriot type figurines present a wide variety of typology including human and animal figures, mythological or imaginary hybrid creatures, and compositions [25]. The other figurines found in Aegean region and Naucratis has same typology with minor differences, although iconographic divergence exists between Cypriot figurines and the others.



**Figure 1.11.** Figurine of a woman nursing, Cypriot, 15.6 x 10.2 x 5.1 cm, Metropolitan Museum of Art



**Figure 1.12.** Figurine of a woman holding a flower, Cypriot, 14.9 x 7.3 x 3.2 cm, Metropolitan Museum of Art

Although very few figurine types can be claimed as exclusive to just one class, Cypriot, Aegean or Naucratis, there is a certain difference in the preference of types within each class, which results in distinct basic repertoires and fixed popular types for each class [25]. Generally, it is just variation in style or iconography resulting in converting a type to a version exclusive only to one class; however the same type also occurs in the other classes. Because of this, it is reasonable to say that Cypriot type figurines were like Greek pottery during Geometric or Archaic periods that were found all over the Mediterranean and inspired the artists outside Greece. In that case, there were many local productions other than Attica imitating Attic vases which were in modern worlds very trendy.



**Figure 1.13.** Figurine of Zeus Ammon, Cypriot 9.5 x 4.4 x 4.4 cm, Metropolitan Museum of Art



**Figure 1.14.** Figurines of a male, Cypriot, 73 x 27.3 x 14 cm, Metropolitan Museum of Art

The limestone figurines of all types can be broadly classified into five groups according to the typology [25]. These are:

*Standing human figures;*

This group includes both male and female figures. While male figures are represented either naked or draped, female figures are always draped.

*Enthroned human figures;*

This group also includes both male and female figures. They appear in all types; however they are not very common in Aegean class. The human figure is shown seated on a throne that is generally with armrests. No version of the enthroned type belongs to Aegean iconography. The drapery and throne style of figurines are closer to Cypriote iconography.

*Animal figures;*

The Aegean class includes a variety of non-human figures. Animal figurines are mostly lions, ram or bull figurines appear rarely. Bird figurines are almost exclusively confined to birds of prey. Fantastic creatures present a larger variety in the Aegean class. Sphinx is the commonest one, but there are also sirens, griffins.

*Group compositions;*

This type of figurines is rare. The most observed scene in this type is the banquet.

*A small group of rare productions consisting of ritual vessels.*

The extended distribution of the figurines and the varieties in their styles raised the questions on the origins of them and this has been an argumentative issue for archaeologists. The period when the development in the monumental Greek sculpture took place corresponds to the time that the early figurines are dated and some archaeologists studying especially on Greek

sculptural art even considers the figurines as the miniature Greek kouroi, male statues [24]. The initiation of this art in Greece has Egyptian origins, since during the middle of 7th century B.C. Greeks were in closely contact with Egyptians, especially when according to Herodotus Greek military forces were in Egypt in Psammetichos I time. However, it developed its own Greek style within time [24].

These figurines range from purely Cypriote to a mix styled that includes Ionian, Aegean, and Egyptian elements [25]. Scholars have tried to group the figurines according to their styles as Aegean [25] or mixed Cypro - Aegean [2] and this kind of distinctions are generally accepted. However, the places of production are a more controversial issue. Discovery at most find-sites of both Cypriot pieces and others that are made in a mixed Cypriot – Aegean style has raised questions about the origin of the mixed style ones [26]. Some see them as products of Aegean craftsmen, responding a demand already created by the success of Cypriot exports [27]; while others attribute the whole corpus to Cypriot craftsmen, adapting native style to meet the tastes of Aegean culture [2, 23, 25, 28].

The latter theory explains the variations in style and iconography as they were made in Cyprus for the desire of different Aegean markets, although the mix styled figurines have been found in Cyprus rarely [27]. This is in contrast with contemporary Cypriot terracotta figurines that were also exported but avoid foreign elements [25]. Meantime, detailed stylistic analysis of the material from Cnidus or Miletus strongly suggested the possibility of one or more production centers other than Cyprus [25].

One of the earliest opposing views for Cypriot origin for the figurines was by Pryce [29]. He argued that the limestone figurines from Naucratis and Rhodes were made in local workshops. His determination based on iconography and style also included his observations on the material used for production. He described the figurines from Camiros, Rhodes were made from a light grey limestone and small in size.

Another opinion on the behalf of local productions was offered by Richter who made an intensive study on Archaic sculpture [24]. Later Boardman suggested early examples from Naucratis were clearly not of Cypriote type, but produced by East Aegean artists inspired by generally dull but many products of Cypriote workshops [30].

Hermay has been the most vigorous advocate of a local Aegean production [31]. She worked on a group of limestone figurines found at Cnidus. He demonstrated a sharp stylistic distinction between the figurines found in and outside Cyprus. As he was using the term Cypro-Ionian, he underlined the importance of Salamis in the creation and diffusion of certain Cypro-Ionian series. Regarding the figurines found at Cnidus, he suggested that at least a part of them was made locally. Meantime, Rhodes was probably another major production site.

For the figurines found at Aphrodite sanctuary at Kalabak Tepe in Miletus, a mixed Cypro-Aegean style was proposed by Senff [32]. He emphasized Ionian character of the style of the sculpture that is in contrast with the plank-like Cypriote figurines.

More recently, stylistic and iconographical differences between the figurines from Emecik and Cypriote figurines were mentioned once again by Tuna and proposed a local production center based on stylistic and material analysis [33].

It was proposed previously that distinctive mineral features found in some limestone of Cypro-Aegean class of Archaic statuette would seem to be consistent with a Cypriot origin of the limestone [25]. This, taken together with the Cypriot style of many pieces found outside Cyprus, would argue in favor of the suggestion that the entire class of Archaic limestone statuettes is of Cypriot manufacture. They are likely to have been made on Cyprus and exported from there to

other sites, or possibly, purchased by visiting traders and carried them to sanctuaries as far apart as Byblos and the Cnidian promontory [2].

Determining the date of limestone figurines in Aegean region has been very difficult since only a few of them have been excavated from well-dated contexts [25]. The first systematic search on the dating problems of the figurines of Cypriote type was accomplished by Sørensen [26]. She assigned relative dates to the figurines stylistically on the basis of the finds from Cyprus. Absolute dates, then, have been fixed by studying the other findings from more reliable contexts at Samos, Chios and Naucratis.

For the Aegean class of limestone figurines, stylistic analysis with Cypriote or Greek sculpture was useful [25]. On the other hand epigraphic evidences were also helpful in assigning dates to the figurines. For instance, an inscription on a fragmentary figurine from Cnidos provided information on its date when compared with an inscription of the Cnidian treasury at Delphi, which was completed before 540 B.C., when Cnidos was conquered by Persians.

The general idea for dating the Cypriote type figurines is then fixed to rather short period of time between last quarter of the 7<sup>th</sup> century and middle of the 6<sup>th</sup> century B.C.

### 1.2.2 Emecik Figurines

The figurines that have been found in numerous amounts in Emecik are of a style, which is definitely different from what is defined as Cypriot [3, 34-36]. The types of Emecik figurines, the distribution of the similar types in Mediterranean region and possible dating were studied in a recent work by Berges [27]. However, this work include only a small part of the all findings; besides the stratigraphy and the context where the figurines are found are not mentioned in this work, for the dating they are evaluated stylistically and compared with the other figurines previously found around the Mediterranean. Some of these figurines are now in museums and some are in the storeroom of the Emecik excavation complex.

Although their original places or situations are not known since they are mostly from filling debris of south terrace wall, they are dated before the time when this wall was constructed e.g. before the last quarter of 6th century B.C. [3, 34-36].

The limestone was described in Berges' work as very white, although varieties such as light grey, which are somehow harder, or brownish, and soft, even too soft to be carved for bigger statues [27]. They were made by a sharp chisel and cut marks can be seen. Some of these figurines also have inscriptions on them and some bears traces of paintings.

The types of Emecik figurines are given below [27],

*Kouroi*, male figurines, fragments including head, body, leg and base, picture of a kouros is given in Fig.1.15;

*Praying (priest ?) and offering figurines*, fragments including head, body;

*A musician*, including flute or lyre playing, picture of this type of figurine is given Fig.1.16;

*Male figures sitting on a throne*, resembles the type were found in Didyma, showing a man having a self-confidence, probably representation a local person, picture of this type of figurine is given in Fig.1.17;



**Figure 1.15.** Limestone figurine of kouros [27]



**Figure 1.16.** Limestone figurine of lyre player [27]



**Figure 1.17.** Limestone figurine of a male sitting on a throne [27]



**Figure 1.18.** Limestone figurine of a goddess holding a lion [27]

*Goddess with a ram sitting on a throne*, representing which god is not clear, could be Zeus Ammon or Baal Hamon. This type may have connections to Egyptian or Near East iconography; beside it could be also related with Apollon cult because of the ram figure. Same type of figurines was found in Milet, Samos, Ialysos, Lindos in Rhodes, and Salamis in Cyprus.

*Goddess holding (catching?) a lion*, probably representation of a goddess, has iconographical connection to Near East, North Syria and also to East Greek, Same type of figurines was found in Samos, Lindos, Kamiros in Rhodes, Salamis in Cyprus, and Naucratis in Egypt. Picture of such figurine type is given in Fig.1.18.

*Lion figurines*, representing in sitting position, They are related to Apollon cult and have Egypt and North Syria origins. Although they have found sporadically in Cyprus and Naucratis, the main distribution of them was within the Dodecanese region, Chios, Samos, Milet, Lindos, Kamiros, Ialysos.

*Falcon figurines*, one has an inscription on it and it is probably related to an Oracle, therefore it can be assumed that there was an Oracle in Emecik sanctuary. Same type has been found in Samos, Ialysos, Kamiros and Lindos.

*Bull and ram figurines* related to Apollon cult, have also been found in Emecik, while terracotta figurines of bull type have been obtained numerously in Emecik.

### 1.2.3 Datça / Emecik Sarı Liman Excavations

The Archaic sanctuary in Emecik is located to 15 km east of Old Knidos, Burgaz in Datça peninsula from where Rhodes is approximately 18 km away. The area is in the mountain region, Kocadag Mountain is in the north and southern part rises over Sarı Liman Bay, however it is not clear that what the coast line was in ancient times [27]. Because of these topographical features, the area was a proper place to be used as a harbor. The surface of the area is about 100 m and 80 m, and 32-45 m above the sea level. [37].

The site has been excavated since 1998 by the supervision of Tuna [34]. The sanctuary is situated on a terrace; the southern wall bordering the sanctuary is by the Datça-Marmaris highway. The excavations are focused on upper terrace, Hellenistic structure and lower Terrace [34]. An Early Byzantine Church was unearthed in 1998 excavation period on upper terrace. The length of church is 20.3 m, width is 14 m and was built mainly with reused materials [3].

The other preserved monumental structure is of Hellenistic and it is understood to be a Doric temple, which has a peripteral plan with a krepidoma of 6 by 11 column stylobate and three krepis [34].

The lower terrace, considered as to be the central area during the Archaic Period, has given important stratigraphical information for the development of sanctuary. The south wall of sanctuary bordered the lower terrace. The figurines that were sampled for this study have been found in that area together with other imported votive objects, such as terracotta figurines. All these objects were found in filling layers of either artificial or natural. Therefore it is impossible to follow a regular chronology and stratigraphy. Based on these findings, such as votive figurines with ram, bull or lion representation, it is indicated that Emecik sanctuary was related to Apollon [33].

According to the results of excavations the sanctuary was abandoned after Late Archaic Period (6th century B.C.) by the 4th century on cultic activities revived but in local sense until Late Classical Period (4th century B.C.) and as the church at upper terrace shows that it was used through Byzantine times. In the northwest of sanctuary, there is also a cult cave and a spring that defined the location of sanctuary [3].

### 1.3 Trace Elements in Geochemical Studies

Trace element in geochemical studies can be defined as an element that is present in a rock in concentrations of less than 0.1 wt %. They generally substitute for major elements in the rock forming minerals. Trace elements are often studied in groups. The deviations from group behavior or systematic changes in behavior within the group are used as an indicator of diagenetic processes [38].

The compatible and incompatible terms for trace elements describe their behavior in magmatic system [38]. When the Earth's mantle was melted, trace elements display a preference either for the molten phase or the solid phase. Trace elements preferring the solid, mineral, phase are called as *compatible* and the other preferring melt phase are called *incompatible elements*. The

reason the term used incompatible is that these elements will leave the solid matrix at the first available opportunity.

Sometimes incompatible elements are grouped according to their charge/size ratio [38]. This property is described as field strength meaning the electrostatic charge per unit surface area of cation. This property is also described as the ionic potential of an element. Small highly charged cations are known as high field strength elements, HFSE and large cations of small charge are known as large ion lithophile elements, LILE. Elements with the same ionic charge and size are expected to behave similarly.

HFSE are rare earth element, Sc, Y, Th, U, Pb, Zr, Hf, Ti, Nb and Ta [38]. LILE include Cs, Rb, K and Ba. Sr, divalent Eu and divalent Pb could be included in LILE. Meantime, Zr and Hf, and Nb and Ta pairs are very similar in size and charge.

Trace element mobility is controlled by the mineralogical changes that occur during alteration and the nature of the fluid phase [38]. In general the elements that belongs to LILE group are mobile, whereas the elements of HFSE group are immobile. In addition to this, Mn, Zn and Cu tend to be mobile, while Co, Ni, V and Cr are immobile.

Regarding the provenance study of a sedimentary rock, rare earth elements, Th, Sc, Cr and Co are important [38]. The concentrations of these elements in sea are very low, and element ratios are unaffected by diagenesis. Therefore, they are kept in the terrigenous component of the sediment and reflect the origin of it. However, other elements such as Fe, Mn, and Pb are more soluble [38]. Cs, Rb and Ba are fixed during weathering but Sr is leached. Meantime, some immobile elements like Zr, Hf and Sn could be distributed according to grain size and controlled by the concentrations of heavy minerals.

### **1.3.1 Rare Earth Elements**

In the periodic table f-block elements are composed of two series of metal: the lanthanoids, the 14 elements that follow La, and actinoids, the 14 elements that follow Ac [38]. Periodic table is given in Fig.1.19. Sc, Y, La and lanthanoids are together called the rare earth elements (REE) [39-41], although the true rare earths are the elements occurring in periodic table between atomic numbers of 58-71 [41]. In the elements in this part of the periodic table, 58-71, as the charge on the nucleus increases, the balancing electron fill in the inner incomplete 4f subshells [40]. This subshell can hold 14 electrons and 4f electrons are well screened by the completed 5s5p subshells, they play almost no part in the valency forces, although they play very important role in some physical properties such as magnetism and spectra [41]. Outer shell electrons screened 4f electrons are held tightly by the nucleus and atomic radii do not increase [41]. In fact, in the series of elements in which 4f subshell is filled, atomic radii decrease and this phenomenon is called lanthanoids contraction [41]. All the elements, between 58-71, have three electrons in their valency shells in aqueous media and because the outermost electrons of an atom are responsible for most physical and chemical properties, these elements closely resemble each other in this media. The fact that IIIA group in periodic table has elements, which also have 3 electrons in the valency shells, makes these elements closely resemble the elements in the range of 58-71, and moreover Y and La are almost always found associated with these true rare earths [40].



For this reason they are also frequently referred as rare earth elements [40]. The descriptive classification of rare earths is established according to their atomic numbers: light rare earth elements (LREE) comprise La to Eu, middle rare earth elements (MREE) Sm to Ho, and heavy rare earth elements (HREE) Gd to Lu [39]. Due to their electronic configuration, they are stable in earth and used in most of the provenance studies [42, 43].

The REEs have very similar chemical and physical properties [38]. This similarity arises from the fact that they all form stable 3+ ions of similar size. Such differences as there are in chemical behavior are a result of the small but constant decrease in ionic size with increasing atomic number [38]. These small changes in ionic size and this behavior are the reasons that REE become fractionated relative to each other during some petrological processes. This leads to the preferential uptake by some minerals of HREE relative to the LREE, or vice versa. The ionic radius for eight fold coordination for each REE is given in Table 1.1.

A small number of the REE also exist in oxidation states other than 3+, but only ions of geological importance are Ce and Eu [38]. Ce occurs in tetravalent form under oxidizing conditions, while  $\text{Eu}^{3+}$  may be reduced to  $\text{Eu}^{2+}$  can lead to extensive fractionation of Ce and Eu relative to the other REE. Therefore, a plot of such normalized concentrations against atomic number should produce a smooth graph; Ce and Eu are the exceptions [44]. Useful information includes the slope of the graph, any changes in slope and the magnitude, and direction of the Ce “anomaly” and Eu “anomaly”. Information on the complete REE group may not be essential to define the graph, but is certainly useful.

**Table 1.1.** The Rare Earth Elements

Atomic Number	Name	Symbol	Ionic radius for eight fold coordination
57	Lanthanum	La	$\text{La}^{3+}$ 1.160
58	Cerium	Ce	$\text{Ce}^{3+}$ 1.143
59	Praesodymium	Pr	$\text{Pr}^{3+}$ 1.126
60	Neodymium	Nd	$\text{Nd}^{3+}$ 1.109
61	Promethium	Pm	Not naturally occurring
62	Samarium	Sm	$\text{Sm}^{3+}$ 1.079
63	Europium	Eu	$\text{Eu}^{3+}$ 1.066
64	Gadolinium	Gd	$\text{Gd}^{3+}$ 1.066
65	Terbium	Tb	$\text{Tb}^{3+}$ 1.040
66	Dysprosium	Dy	$\text{Dy}^{3+}$ 1.027
67	Holmium	Ho	$\text{Ho}^{3+}$ 1.015
68	Erbium	Er	$\text{Er}^{3+}$ 1.004
69	Thulium	Tm	$\text{Tm}^{3+}$ 0.994
70	Ytterbium	Yb	$\text{Yb}^{3+}$ 0.985
71	Lutetium	Lu	$\text{Lu}^{3+}$ 0.977
39	Yttrium	Y	$\text{Y}^{3+}$ 1.019

### 1.3.2 Importance of REE in Geochemistry

REE value of a sample could be found by its REE pattern. This pattern is a graph that shows normalized REE values versus atomic numbers in logarithmic scale. Normalized values are found by dividing the concentration of a REE in the sample to its value in either a meteoric stone, such as chondrite, upper crust or shale values and the value is shown with a subscript

such as  $Yb_{cn}$ . Concentrations at individual points on the normalization graph are connected to each other with a straight line [38].

Chondritic meteorites were chosen for normalization because they are considered to be relatively unfractionated samples of solar system dating from the original nucleosynthesis [52]. However, the concentrations of the REE in the solar system are variable because of the different stabilities of the atomic nuclei. REE with even atomic numbers are more stable, therefore more abundant than REE with odd atomic numbers producing a zig-zag pattern on a composition-abundance diagram. This pattern of abundances is also found in natural samples. Chondritic normalization therefore has two important functions [38]; it eliminates the abundance differences between odd and even atomic number elements and it allows any fractionation of the REE group relative to chondrite to be identified [38].

The REE pattern is related directly to the chemical composition of the stone. The constant relation of the REE pattern and the type of stone is a result of the atomic structure of REE.

This pattern is an important tool for understanding the geochemical processes and also to detect anomalous data that could be due to natural processes, anthropogenic contamination, in field or laboratory, or analytical error [45].

Generally, the plotted position of Eu or Ce lie off the general trend defined by the other elements on the REE diagram [38]. If the position of Eu or Ce is above the trend, the anomaly is described as positive. If their positions are below the trend than the anomaly is called as negative.

According to generally accepted theory, Eu and Ce are the only REEs that show potential variations as a function of oxidation – reduction conditions in natural sedimentary/oceanic environments [46]. Meantime, variations in Ce anomalies can result many factors such as lithology and diagenesis, and Fe-organic-rich colloids from river sources [47]. In oxic conditions, Ce is less readily dissolved in seawater, so that oxic seawater is more depleted with respect to Ce, whereas oxic sediments are more enhanced with respect to Ce [46]. Accordingly, organisms extracting phosphate from oxic seawater show a negative Ce anomaly, whereas Fe-oxide-rich oxic sediments, such as red clay, have a positive Ce anomaly. Conversely, in suboxic seawater Ce-containing sediments are mobilized so that Ce is released into the water column resulting in a less negative to a positive anomaly in seawater. Therefore in anoxic sediments, Ce is depleted and the sediments show a negative anomaly.

Calculation of the Ce anomaly which is also expressed as  $Ce/Ce^*$  is based on the assumption of a linear decline in REE concentrations with an increase of atomic number when the elements are normalized [46]. This assumption is based on an empirical observation of such a pattern in certain sedimentary rocks. According to the order of REE, ideally the Ce anomaly would be calculated as normalized Ce values that plot above or below the straight line extrapolation between La and Pr. This results in an anomaly of  $\log[2Ce_{cn}/(La_{cn} + Pr_{cn})]$ . However, for analytical reasons, Pr and Pm are rarely reported. Thus, Ce anomaly is calculated with respect to Nd that is  $3Ce_{cn}/(2La_{cn} + Nd_{cn})$  [48]. In this study, this calculation was used.

It is been observed that the concentration of many elements in fined-grained sedimentary rocks in continental platforms is similar which is a result of repeated cycles of erosion [52]. So, REE concentrations in sedimentary rocks are generally normalized to an average sedimentary standard, but this is not a universal rule [38]. Some researches prefer to normalize the concentration results of sedimentary rocks using chondrite values. The sedimentary standards meantime include North American Shale Composite, NASC, European shale, post Archaean average Australian sedimentary rock, PAAS.

## **1.4 Provenance Studies and Characterization of Raw Material of Archaeological Limestone**

The widespread use of limestone both for sculptural and architectural purposes requires that a suitable means be established for assessing provenance [49]. As the literature showed many researches and publications have been made for provenance of various archaeological objects and materials. These works are especially concentrated on archaeometric investigations of marble, obsidian and ceramic findings. Still, there are not as many provenance studies on limestone like the others mentioned. Limestone, including dolomite, forms 10-15% of all sedimentary rocks [49]. In most cases, the limestone used as building material or to make sculpture and other small objects was obtained from a local quarry, so there would be no need for a provenance study. In addition to this, apart from some valuable stone material, such as marble, the trade of limestone was not commonly made in ancient times.

The distribution of trace elements and stable isotopic ratios in limestone are controlled by the kind and amounts of aluminosilicate minerals, largely clay minerals; the carbonate, calcite, aragonite or dolomite minerals; and diagenetically formed sulfides, carbonates, and oxides of iron [50]. All these factors are controlled by the original environment of deposition, amount and kind of impurities in limestone, and diagenetic processes of limestone after formation. Different trace element content and stable isotopic ratios in limestone are a result of the contribution of each factor. Since these factors could be very different for every limestone formation, great variations are to be expected in samples with varying amounts of clay minerals, carbonate, or diagenetic cement [49].

Meantime, one of the important issues is using the terms *sourcing* or *provenance*. These terms imply that whatever is determined would be considered as certified source provenance that is not probabilistic at all, confidently determined [51]. As Shackley underlined, actually these studies can be best described as characterization of archaeological materials using various methods and investigate to fit the results to a known source of production.

### **1.4.1 Provenance Studies on Limestone Figurines of Cypriote Type**

The generally accepted assumption is that most of the figurines that have been found in Mediterranean region are of Cypriot origin, if not all. This assumption is insufficient to answer some important questions such as the wide distribution and more important the varieties in style. Although the figurines found outside of Cyprus are stylistically quite different from Cypriot figurines, distinguishing stylistic classes based on the locations where they are found is very difficult since they all bear mixing elements of North Syrian, Cypriot, and East Greek art. Besides, archaeologists faced the case that how it is possible if all the figurines were made in Cyprus the mix style ones have been found only rarely in the Island. Then, they started to work with other scientists of different disciplines in order to search for the provenance of the limestone, raw material. The aims of these studies were to locate different ateliers other than Cyprus or prove that they were actually made in Cyprus to be exported to Aegean markets. However, a limited number of provenance studies on this area have been done so far. The researches include microscopic examinations with optical microscopy; chemical analysis, X-ray Fluorescence spectrometry (XRF), Electron Paramagnetic Resonance spectrometry (EPR), of archaeological samples and/or geological samples taken from quarries [25, 27, 32].

The first attempt of a scientific analysis for the origin of the figurines was made by the National Museum in Copenhagen [52]. According to petrographic analysis of the three figurines in this Museum, the material used was the same, and it is been suggested that the raw material was from Cyprus. However, no geological sample from Cyprus was studied in order to compare.

Another study was made on the figurines found at Miletus using XRF [25]. Seven figurines were analyzed and the results indicate that these figurines were made from the same type limestone. The origin of the limestone, however, is still unknown.

A study by I. Jenkins was on the origins of the figurines on the basis of the material used for production [2]. Although the study was undertaken only using macroscopic observations of limestone and its treatment, Jenkins concluded that figurines he studied were made from limestone from Cyprus, identifying Idalion area as the main quarry area.

Two works by the same group are on the provenance of some Cypriot type figurines found in Cyprus and other figurines found at Aegean sites [23, 25].

In one study the characteristics of the material used in the sampled figurines were investigated using optical microscopy and EPR [25]. They also compared the results with those of quarries in Cyprus, Samos, Rhodes, and Naucratis using optical microscopy and EPR [25].

The archaeological samples that were studied include 14 figurines from Samos, 22 figurines from Rhodes and 3 from Cyprus. They also studied some architectural fragments in order to compare them. Microscopic examination of the archaeological samples reveals a basic consistency in the texture which shows often porous and chalky with large amounts of nanofossils character and color, from creamy white to light buff-yellowish, of the limestone used. According to the researchers the archaeological samples demonstrate characteristics that are most closely related to those from Cypriote quarries. The geological samples from Cyprus are characterized as fine-grained creamy white chalks with abundant foraminiferal remains. Actually these remains are imparting pocked marked appearance as Jenkins described [2]. According to their description the foraminifera are planktonic, mostly globigerinids [25].

As it could be expected the chemical composition of the Cypriot samples are in accordance with the Cypriot geological samples, while, with some exceptions, the figurines from Samos are also similar to the Cypriot samples. The figurine from Egypt is found to be made either by Samian or Egyptian limestone but not Cypriot. All of the figurines from Rhodes, with one exception are also in accordance with Cypriot samples. So they concluded that the figurines they were examined were made from Cypriot limestone [25].

The work by Polikreti's group is the more systematic research using EPR for investigation the provenance of figurines called Aegean class from Samos and Rhodes [23]. They also included two figurines of Cypriote class from Cyprus in order to compare them. They collected geological samples from quarries in Cyprus, Samos, Rhodes, and Naucratis thought to be the most probable production centers for figurines as taking into consideration of archaeological evidences. According to their results, limestone samples from Rhodes and Naucratis are physically insufficient for carving, chemical composition of samples from Samos are not similar to those of statuettes examined, On the other hand, properties of all sampled statuettes were matched the limestone of a specific geological formation in Cyprus which is called Lympia-Kossi chalk of Pachna formation.

The recent work by Berges, includes also XRF analysis of ten fragments of figurines and a Doric column fragment from Emecik, seven fragments of figurines from Milet, besides the geological samples from Cyprus, from a crop between Kızlan and Emecik, and also from different places around Emecik [27]. According to the results the author concluded that the chemical composition of the figurines both from Emecik and Milet including the column fragment from Emecik do not show much variation, therefore the raw material of them should be from the same quarry [27]. According to the interpretations in this work, based on the concentration values of the elements, the composition of the geological samples from Datça peninsula, however, is completely different therefore; Datça could not be the geological source. Meantime, the geological samples

from Cyprus are in accordance with the figurines both from Emecik and Milet, though the variations are present because of the heterogeneity of the stone matrix. Then the author concluded that the figurines were made from the Cypriot limestone.

#### **1.4.2 Provenance Studies on Archaeological Objects Made of Limestone**

Many different techniques have been used to determine the material characteristics and provenance of archaeological limestone. With the general improvements in technology, instrumental techniques in archaeological geochemistry have similarly improved. In general for the provenance studies of lithic objects almost all instrumental and empirical techniques have been used, including density, magnetism, atomic absorption, PIXE–PIGME, ICP-MS [51].

While some of these techniques could be applied to other raw materials, the use of stable isotope analysis of carbon, oxygen, and other light elements for provenance studies is mainly limited to limestone, marble, and other carbonate containing lithic materials [1]. Cathodoluminescence and electron paramagnetic resonance have also been used in marble provenance studies with some success [1].

An extensive study, Brookhaven Limestone Database Project, was carried on by the International Center of Medieval Art on the provenance of limestone sculptures and monument especially within France [50, 53-58]. In this project, Neutron Activation Analysis (NAA) was used in compositional characterization of limestone. According to their studies, limestone sources tend to be characterized by rare earth elements, alkali and transition elements [50]. Their studies showed that compositional analysis differentiates among limestones from the regions they have been worked on [53].

In order to determine the geographic origin of an archaeological object based on the composition of its stone, discrete compositional groups to which a sample of unknown origin can be compared must be defined [54]. In this study, since the samples vary widely in composition, discrete groups were distinguished by plotting the concentrations of selected pairs of elements for each quarry samples such as chromic oxide versus manganese oxide.

On the study for the analysis of “*Caen Stone*”, high degree of bivariate correlation was observed [50]. The logarithms of the concentrations are used to calculate ‘principal components’ in multidimensional Mahalanobis space. Principal components, which resemble canonical functions, are linear combinations of log concentrations chosen to account for the maximum variance by the smallest possible number of variables. The distance of an individual sample from the group centroid in Mahalanobis space is also closely related to its probability of membership in that group [50].

According to the authors the advantages of such multidimensional space are [54, 56]:

- It incorporates all the useful concentration information for each sample;
- Fewer combinations are needed to be plotted;
- Clearer distinctions among groups can be obtained.

Third alternative method, canonical functions, on the other hand [56]:

- Maximizes the differences among most groups;
- Permits statistical analysis with fewer samples per group.

Although difference was small among the samples of limestones from proximate quarries, distinction among them was still possible by linear discriminant analysis [50]. Distinction depended on 15 variables chosen to maximize differences among the groups. These variables

were Sr, La, Mn, Na, Lu, Fe, Ce, Cr, Sm, K, Ba, Hf, Sc, Yb and Eu in the order of their importance.

In this study, they also mentioned that information on the minerals and microorganisms that formed the calcareous mud can be obtained from petrographic observations [50]. However, petrography is limited to localizing stone in larger regions. Because, differences in microscopic structures are generally related to depositional process subsequent diagenesis rather than to geographical location. On the other hand, compositional analysis of samples reveals data to distinguish among stone sources in a relatively small area within a specific geological formation [50].

In another work by the same group, the composition of limestone samples taken from Romanesque arch at The Cloisters Museum and from a portal at Notre-Dame d'Aiguevives was analyzed [57]. Determination of Na, K, Cs, Cr, Fe, Ce, Sm, Yb, Lu, Zr, Hf indicated that stone for both portals came from the same limestone formation.

Another study on the “Elemental Characterization of Medieval Limestone Sculpture from Parisian and Burgundian Sources” was one of the earliest works by the same group [58]. They have studied the compositional patterns of limestone from quarries at Paris and limestone material used in the production of Romanesque sculpture from Paris basin and Burgundy. Correlation diagrams of concentration values for different locations indicated that limestone from Paris region is completely different from the limestone of Burgundian Romanesque sculpture. The difference is more obvious in the REE concentrations as could be seen in a plot of europium oxide versus cerium oxide.

The search on “A Provenance Study of French Limestones Based on Variable Selection from Compositional Profiles” was about the applications of multivariate analysis and variable selection techniques that could be used in archaeological provenance studies [59]. Using the same technique as Brookhaven Limestone Database Project, Na, K, Rb, Cs, Ba, Sc, La, Ce, Eu, Lu, Hf, Th, Ta, Cr, Mn, Fe, Co, Sb, U, Zr, Ca, As, Sm, Yb, Sr and Nd were determined to constitute the compositional profile. In this study, however, the researchers aimed to improve the statistical tools to process NAA data. In doing so, they have applied stepwise linear discrimination to discriminate limestone samples from different quarries across the north of France. Then hierarchical classification approach was followed in order to specify the sources of origin to the narrowest units.

De Vito's group studied on limestones used for two monuments dated to 4th – 3rd centuries B.C. and 1st century B.C. – 1st century AD., in Italy and limestone samples as the possible geological raw materials [60]. In this work Atomic Absorption Spectrometry, AAS, isotopic analyses were used for the determination of major, minor and trace elements, of totally 12 elements; C and O isotopic compositions and microscopy for petrographic characterization of the samples were included. Na, Mn, Fe and Sr were selected because of their significance in carbonate sedimentation and diagenesis; Li, K and Rb were selected since they are considered diagnostic in carbonate sedimentation; Ni, Co, Zn and Cu, since they are widely used to obtain paleo-environmental information. Ternary plots for Li-Rb-Pb and Pb-Co-Ni are shown and the authors concluded that Pb-Co-Ni could not discriminate between samples.

Marinoni's group studied black limestone samples used in architecture obtained from three quarries in Italy in order to provide a characterization and determination of provenance [61]. Samples were separated into organic and inorganic fractions. Inorganic fractions were characterized in terms of textural features by optical microscopy, mineralogical features by XRD analysis, chemical compositions by AAS, and C and O isotopic ratios. Fe, Mn, Cd, Co, Cu, Zn and Sr, which substitute Ca in calcite-like structures, were determined as well as Na. Binary diagrams, Fe/Mn, Co/Zn, Sr/Zn and Cd/Na, were used to mark compositional differences.

In another work by Bello and Matin [62], limestone material, which was used in the construction of Cathedral of Seville, Spain, and samples from six different quarries, were examined. Flame Emission Spectroscopy (FES) and AAS were used to determine fourteen trace elements, Rb, Cs, Sr, Ti, Cr, Mo, Mn, Ni, Cu, Zn, Cd, Sn, Pb, Sb,  $\text{SiO}_2/\text{CaO}$  ratio characterized eight different groups from Cathedral stones. Two groups among them were chosen to identify their geological sources by enrichment diagrams of trace elements (EDTE). EDTE results, confirmed by cluster analyses, were found useful for provenance determination.

Harell studied on twenty-three ancient Egyptian limestone quarries in the Nile Valley to obtain provenance indicators that differs each [63]. Si, Al, Ca, Mg, Na, K, Fe, Ti and P were determined using XRF method and examined using thin-section petrography in totally twenty-eight samples. According to the results, geological formations could be identified by petrography and XRF analyses.  $\text{CaO}/[\text{CaO} + \text{MgO}]$  vs.  $\text{SiO}_2/\text{Al}_2\text{O}_3$  plot were applicable to narrow the possibilities of two or three formations and then petrographic parameters will identified the most likely source within the quarries.

Another study for obtaining provenance indicators of limestone in Greece was done by Wenner and Herz [49]. The authors worked on samples from monuments and quarries in two regions and isotope analysis as well as petrographic observations appeared to be useful for discriminating the different sources and determination the provenance of the archaeological samples. Moreover there are geological researches on limestone and other sediments for provenance and diagenesis of the rocks especially based on their rare earth elements (REE) compositions.

There are two studies on archaeological lime mortars by Sanjurjo-Sánchez's [64] and Ortega's [65] groups. Sanjurjo-Sánchez have aimed to contribute technological and provenance inferences, and evaluate possible correlations with the various identified stages along historical periods of construction [64]. The descriptive and multivariate statistical analyses showed that among the chemical elements studied, the best discriminates are the less mobile in surface environments (K, Sc, Ga, Rb, Cs, REE, Hf, Ta and Th). These elements can be used to differentiate the original materials of mortars particularly related with the aggregate.

Ortega's group has studied to establish accurately the chemical constitution of the binders, to show eventual differences between them, and to correlate such differences with cultural changes at the archaeological site [65]. According to their results, geochemical analysis makes possible a comparison of mortars of different epochs and allows reconstructing mortar technology and helps to identify the provenance of the applied raw material. Mortar compositional groups were thus established by quantitative pattern-recognition analysis of principal component scores of the elements that have geological significance (Li, V, Cr, Co, Zn, Rb, Sr, Y, Zr, Ba,  $\Sigma\text{REE}$ , Hf, Pb, Th, U) and insoluble residue content. The principal components analysis (PCA) method is typically employed to reduce the dimensionality of the data.

### **1.4.3. Provenance Studies on Geological Limestone Using REE Analysis**

There are studies on provenance of geological samples using rare earth element analysis since 1980's. Since this study is generally focused on the determination of REE in archaeological and geological samples for provenance analysis of figurines from Emeçik, the studies using REE contents of limestone for geological studies are summarized here.

According to two early works using REE concentrations for characterization of geological samples by Date and Hutchison [44] and Jawis [66] the value of REE concentrations in geochemistry is a function of the close chemical similarity of the group, and the gradual change in ionic radius for their cations in octahedral co-ordination. The distribution of REE in nature corresponds to the Oddo - Harkins rule; i.e., a plot of concentration against atomic number

shows striking differences in abundance between neighboring REE with odd and even atomic numbers. Therefore, concentrations of REE are often reported relative to levels in chondritic meteorites, which may be taken as reasonable base-line concentrations for any method developed for their determination.

Armstrong-Altrin's group worked on the "Geochemistry of Upper Miocene Kudankulam Limestones, Southern India" [67]. According to them and to previous studies dominant factors influencing the REE contents of carbonate rocks are:

- (1) the amount of terrigenous input;
- (2) variations in the oxygen level in the water column; and
- (3) biogenic sedimentation

Meantime, the distribution of REE, particularly the Ce anomaly, in marine sediments and carbonate rocks has considered being an excellent indicator of depositional environments such as widespread marine anoxia, oceanic palaeo-redox conditions, proximity to source area, surface productivity variations, lithology, and diagenesis. The predominance of a negative Eu anomaly in the Kudankulam limestones may reveal that the terrigenous part of these samples was probably derived from felsic source rocks [67].

In this study, shale normalized (s) REE patterns and La/Sc, La/Th, Th/Sc, and (La/Yb)<sub>s</sub> ratios together with negative Eu anomalies were interpreted. According to the results terrigenous sediments present in the Kudankulam limestones were mainly derived from felsic source rocks. In these limestones, the (La/Yb)<sub>s</sub> ratio is higher than the average values of terrigenous sediments. All but one Kudankulam limestone sample exhibits negative Ce anomalies. Variations in (La/Yb)<sub>s</sub> ratios and Ce anomalies may have resulted from differences in detrital sediments and diagenetic effects.

In their work on "Characteristics of Rare Earth Element Abundances in Shallow Marine Continental Platform Carbonates of Late Neoproterozoic Successions from India", Mazumdar's group has aimed to classify the REE abundance patterns into groups based on chondrite normalized elemental ratios and curvatures of the abundance patterns [46]. The results showed that (Y/Ho) and (Y/Dy) concentration ratios have been shown to reflect a combined effect of Y fractionation relative to neighboring trivalent REEs during carbonate precipitation from seawater and influence of continental contributions with chondritic ratios. The contrasting behavior of Y has been related to its different electronic configuration which determines its complexation behavior and partition coefficient [46]. The absence of Ce anomaly and distinct positive anomalies in some cases reflect post-depositional Ce mobilization during early diagenesis [46]. Variations in LREE and HREE abundance patterns as well as the scatter in chondrite normalized elemental ratios have been explained as a result of variable contaminations with continental material and early diagenetic process in the carbonate sediments. HREE remobilization and fractionation during dissolution/re-precipitation process involving early mineralogical stabilization has been attributed to high stability of HREE(CO<sub>3</sub>)<sub>2</sub> – complexes in the solution flushing the carbonate sediment during meteoric water diagenesis [46]. Variations in LREE have been linked to contribution of LREE enriched particulates during carbonate recrystallization and also to mobilization of silicate hosted REEs during formation of authigenic clay mineral phases [46].

In another work by Madhavaraju's group, Mural Formation in Mexico has been determined to provide information on depositional conditions and provenance [47]. In the results, they have concluded that the large variations in terrigenous percentage, high Al<sub>2</sub>O<sub>3</sub> and ΣREE contents, high La<sub>n</sub>/Yb<sub>n</sub> ratios, low Y/Ho ratios and non-seawater-like REE patterns suggest that the observed variations in ΣREE contents are mainly controlled by the amount of detrital sediments in the limestones of the Mural Formation. The limestones of the Mural Formation were deposited under both coastal and open shelf environments, and they exhibit non-seawater-like REE+Y

patterns [47]. The presence of terrigenous materials in these carbonates as contaminants effectively masks the seawater signature due to their high concentration of the REE [47]. The La/Sc, La/Co, Th/Sc, Th/Cr, Th/Co and Cr/Th ratios suggest that the terrigenous materials present in the limestones were mainly derived from a nearby exposed basement of intermediate to felsic igneous rocks [47].

Cullers worked on shales and limestones in Pueblo, Colorado, USA for the provenance, the redox conditions and the metamorphism of the rocks [69]. Major and some trace elements concentration including REE were determined using AAS and NAA. In order to realize which elements are incorporated into carbonate phase, samples were also treated with HCl to obtain acid insoluble residue, non-carbonate phase of the stone. According to plots of element oxides vs. % residue, CaO vs. % residue, SiO<sub>2</sub>, Al<sub>2</sub>O<sub>3</sub>, Fe<sub>2</sub>O<sub>3</sub>, MgO, Na<sub>2</sub>O, K<sub>2</sub>O, TiO<sub>2</sub> and Sm, Eu, Tb, Yb, Lu, Ta, Sc, Th, Cr, Hf, Cs and Rb are incorporated into residue while La and Ce are held in silicate minerals included in the insoluble residue with a lesser amount existed in calcite and Sr, in contrast, included in the calcite. The Th/Co, Th/Sc, Th/Cr, La/Co, La/Sc, La/Cr, La/Lu ratios and Eu/Eu\* that are characteristics of the provenance of terrigenous sedimentary rocks and Ce/Ce\* that is used to interpret the redox conditions of the seawater at the time the REE were incorporated into marine sediment.

Another study on the provenance of playa sediments in India, REE, major and trace elements were determined using ICP-MS and XRF, mineralogical investigations were carried out using XRD [70]. The detrital-rich samples show enriched values of SiO<sub>2</sub>, Al<sub>2</sub>O<sub>3</sub>, K<sub>2</sub>O, TiO<sub>2</sub>, Fe<sub>2</sub>O<sub>3</sub>, Zn, Rb, Cr, Ni, Ba and Zr. Similarly, the samples containing calcite and dolomite have higher abundances of Cu, Sr, CaO, MgO. Meantime, Y and Th showed a strong positive correlation and Rb, Ba, TiO<sub>2</sub> show signification correlation with all REE and total REE (TREE). Zr influences only LREE while CaO, MgO and SR show negative correlations with REE. REE patterns, fractionation of LREE (La/Sm)<sub>n</sub>, HREE (Gd/Yb)<sub>n</sub>, TREE (La/Yb)<sub>n</sub> and Eu anomaly indicated different groups.

Bellance's group studied the REE distribution in limestone / marlstone couplet in Southern Alps for investigation REE sensitivity to environmental changes [71]. REE and As, Cd, Mo, Sb, Th, Y and U were determined by ICP – MS. TREE content of the limestone shows a strong negative correlations with CaO. Limestone exhibit seawater-like REE pattern and both Ce anomaly and La/Yb fall in the range of average seawater and these indicate calcite uptaking REE from seawater in which it is formed. The correlation between Eu anomaly and other major or trace elements is not apparent. Therefore it could be concluded that no single mineral is responsible for the anomaly.

Bolhar's group investigated the chemical characterization of metasomatic sediments in Greenland evaluating major elements, first transition elements (Sc, V, Cr, Co, Ni), high field strength elements (HFSE, the element of large ionic valences and are not readily incorporated into lattice of common rock forming silicate minerals: Zr, Hf, Nb, Ta, Y), strongly lithophile elements (that are having large ionic radius: U, Rb, Sr, Ba) [72]. In the study, REE contents were determined by ICP-OES and ICP-MS. SiO<sub>2</sub>/Al<sub>2</sub>O<sub>3</sub> vs K<sub>2</sub>O/Na<sub>2</sub>O, Ni vs. Cr, Zr vs. Hf, Nb vs. Ta, Y/Ho vs. Nb/Ta, Th vs. U plots and for REE (La/Sm)<sub>cn</sub>, (La/Yb)<sub>cn</sub> and (Gd/Yb)<sub>cn</sub> and Eu/Eu\* values were interpreted for the lithological makeup of the source stone, post depositional element mobilization and subaerial weathering.

In addition, the studies by Igarashi were on the REE determination in limestone geological reference material Ls-1 by ICP-MS [73], by Ionov on trace element distribution including REE of calcite – dolomite carbonatites in South Africa in order to investigate the factors that affect the composition [74], by Halicz on the REE determination in fresh water and comparison of REE pattern of water with that of the associated rocks [45].

When these studies are considered it can be understood that limestone has some chemical characteristics that help to interpret the origins of the rock. An ancient rock that began as a sediment with average of 50% or more porosity may have less than 10% porosity today [9]. This required either introduction of calcium carbonate approximately equal to the original solid volume of the rock or a loss of one-half of the original volume of the rock by compaction. There is abundant evidence that most carbonate rocks have undergone relatively little compaction. Thus, introduction of calcium carbonate from an outside source is required. The source of this calcium carbonate and its means of transportation and deposition within the rock should be one of the main problems of limestone diagenesis.

The distinction between dolostone and limestone is one of the main issues of the carbonate rocks. Dolostone could be best described as the rock composed largely or entirely of mineral dolomite  $\text{CaMg}(\text{CO}_3)_2$  [10]. Dolomite forms in two ways: the origin of dolomite on the surface of the earth and the origin of dolomite in sedimentary rocks [43]. In both cases, pre-existing  $\text{CaCO}_3$  react with solutions, resulting in the formation of dolomite. In this reaction, metastable  $\text{CaCO}_3$ , which forms in place of stable dolomite, is changed into dolomite by diagenetic solutions, which generally abundant in Mg. Different amounts of dolomite are thus formed from a definite amount of  $\text{CaCO}_3$  depending on the anion contents of the medium [71].

The amounts of most of the minor elements in limestones are extremely variable among the samples and the differences are due largely to liquid or solid inclusions among calcite or aragonite crystals rather than to structural or interstitial substitutions of the minor elements for calcium ions [10]. In the diagenetic process of limestone, a decrease in strontium contents of limestones with increasing age has been noted and this decrease results from conversion of aragonite to calcite [10]. Moreover, the distinction between aragonite and calcite appears in the contents of some other elements: in aragonitic shells the abundance of Mg and Mn decrease with time, Ba and Fe increase, in calcitic shells Mg decreases, however other elements remain unchanged [10].

Above mentioned studies show that while REE are related to silicates within the rock matrix like some other trace elements such as Ti, Al, K, Na, Ba and so on, within REE La and Ce are also related to the carbonate fraction of the rock matrix [69]. There are also other studies that relate the REE patterns of the water reflected underlying water-rock interactions [45].

Although limestone is not as homogenous as igneous rocks such as obsidian [76, 77] since it is a sedimentary rock, some chemical characteristics, especially REE contents, are found to be discriminating the provenance of the limestone.

Studies on the geochemistry and provenance marble are also related to limestone and could be helpful in the same manner. A research on the "Petrographical and geochemical investigation of the Triassic marbles associated with Menderes massif metamorphics, Kavaklıdere, Muğla, SW Turkey" by Afyon Kocatepe University and Dumlupınar University revealed the petrographical and geochemical characteristics of the samples using mineralogy, major, trace and REE analyses [78]. They mentioned that the abundance of Sr has been recognized as a powerful tool to evaluate the degree of secondary alteration of marbles and limestones. Due to the similarity of ionic radius and valence with calcium, Sr replaces Ca in carbonates during diagenesis. The high Sr concentration in the samples, therefore, indicates that the original limestone did not undergo diagenetic exchange. The Sr/Ca ratio in seawater, the sedimentation environment, and biogenic factors affecting strontium separation in biogenic carbonates control the Sr/Ca ratio in marine carbonate rocks. Meantime elements such as K, Na, Rb, and Sr are known to be mobilized during sedimentation and metamorphism. Since elements such as Th, Sc, and Y are least affected during these processes, they give more reliable information on the source properties [78].

Another study is on the “Provenance of the Marbles from Naxos based on Microstructural and Geochemical Characterization” [79]. Microstructural analysis coupled with geochemical analysis, cathodoluminescence, and isotopic analyses provide information on the provenance of samples. Major, trace, and REE were determined using LA-ICP-MS on thin sections. According to their results of chemical analysis samples share similar characteristics, which is primarily the result of crystallographic controls on trace element contents. Among them, Ce and U show variable oxygen fugacity conditions during calcite growth, since they have multiple oxidation states. In this case, Ce and U show significant variations between samples from a single location so that these criteria could not be used for provenance discrimination.

An interesting study entitled “Probably counterfeit in Roman Imperial Age: Pattern recognition helps diagnostic performed with inductive coupled plasma spectrometry and thermogravimetry analysis of a torso and a head of a Roman Age marble statue” is about the investigation the raw materials of head and torso of a Roman sculpture [80]. Out of 22 elements, 8 of them, elements Ca, Mg, K, Al, Fe, Sr, Mn along with LOI are selected for PCA. As a result, they obtained a separation of Italian marbles cluster from marbles of other countries and recognize the different provenience of the body and head.

*These could be summarized as follows:*

Total REE concentration, beside the degree of fractionation of a REE pattern, LREE and HREE fractionations, found by  $La_{cn}/Lu_{cn}$ , or  $La_{cn}/Yb_{cn}$ ,  $La_{cn}/Sm_{cn}$  and  $Gd_{cn}/Yb_{cn}$  respectively, Th/Sc, Th/Cr and Eu/Ce, ratios, Eu anomaly,  $Eu/Eu^*$  and Ce anomaly,  $Ce/Ce^*$  are used to discriminate different types of stone [38, 43, 70, 81].

The expression of degree of fractionation of a REE pattern can be plotted against either  $Ce_{cn}$  or  $Yb_{cn}$  on a bivariate graph [38]. This graph is a measure of the degree of REE fractionation with changing REE content. Similar diagrams could be constructed as following:

To measure the degree of LREE fractionation  $(La/Sm)_{cn}$  vs  $Sm_{cn}$ ;  
HREE fractionation  $(Gd/Yb)_{cn}$  vs  $Yb_{cn}$ .

The effects of LREE/HREE fractionation in modern and ancient marine systems can be represented by examining the Er/Nd ratios [71]. REE fractionations indicated by variations in Er/Nd ratios are controlled by changes in the redox conditions of sediments and of the overlying water column.

In the meantime, Mn is also highly sensitive to environment redox conditions [82]. The  $Mn^*$  parameter was used by Bellenca as a palaeochemical indicator of the redox conditions of depositional environments [71]. Low Eh conditions generally support the production of reduced, soluble forms ( $Mn^{2+}$ ) that migrate to an oxic zone where re-oxidized manganese can precipitate.

## CHAPTER 2

### EXPERIMENTAL

#### 2.1 Chemicals and Reagents

##### 2.1.1 Water and Acids

Deionized water obtained from a Millipore Milli-Q 18 MΩ cm (Molsheim, France) system and the acids listed in Table 2.1 were used in all procedures. In order to obtain high purity acids, PTFE subboiled acid distillation system by Berghof (Eningen, Germany) was used.

**Table 2.1.** Acids used in all experiments.

Acid	Producer and properties
HF	Merck, extra pure, 40% (w/w)
HCl	Merck, analysis grade, 36% (w/w)
HNO <sub>3</sub>	Merck, analysis grade, 65% (w/w)

##### 2.1.2 Standard Solutions

Aqueous standard solutions used in experiments are shown in Table 2.2.

**Table 2.2.** Standard solutions used in experiments

Standard	Concentration	Producer
Ti	1000 mg/L (in dilute HNO <sub>3</sub> )	Ultra Scientific
Mn	1000 mg/L (in dilute HNO <sub>3</sub> )	Merck
Fe	1000 mg/L (in dilute HNO <sub>3</sub> )	Merck
Mg	1000 mg/L (in dilute HNO <sub>3</sub> )	Merck
Sr	1005 mg/L (in dilute HCl)	Aldrich
Ba	1005 mg/L (in dilute HCl)	Aldrich
Cr	1000 mg/L (in dilute HNO <sub>3</sub> )	Ultra Scientific
Y	1000 mg/L (in dilute HNO <sub>3</sub> )	Ultra Scientific
Nb	1000 mg/L (in dilute HNO <sub>3</sub> )	Ultra Scientific
La	1000 mg/L (in dilute HNO <sub>3</sub> )	Ultra Scientific
Ce	1000 mg/L (in dilute HNO <sub>3</sub> )	Ultra Scientific
Nd	1000 mg/L (in dilute HNO <sub>3</sub> )	Ultra Scientific
Sm	1000 mg/L (in dilute HNO <sub>3</sub> )	Ultra Scientific
Eu	1000 mg/L (in dilute HNO <sub>3</sub> )	Ultra Scientific
Gd	1000 mg/L (in dilute HNO <sub>3</sub> )	Ultra Scientific
Ho	1000 mg/L (in dilute HNO <sub>3</sub> )	Ultra Scientific
Er	1000 mg/L (in dilute HNO <sub>3</sub> )	Ultra Scientific

<b>Table 2.2. continued</b>		
<b>Yb</b>	1000 mg/L (in dilute HNO <sub>3</sub> )	Ultra Scientific
<b>Lu</b>	1000 mg/L (in dilute HNO <sub>3</sub> )	Ultra Scientific
<b>Hf</b>	1000 mg/L (in dilute HNO <sub>3</sub> )	Ultra Scientific

The dissolution procedures developed were performed using certificated reference materials SRM 1d, Limestone, argillaceous sample produced by National Institute of Standards and Technology, and NCS DC 73306, Rock Reference Material produced by China National Analysis Center

Durapore Membrane Filter, with 0.45 µm pore size, manufactured by Millipore was used in the filtration of the samples.

## **2.2 Instrumentation and Apparatus**

### **2.2.1 Microwave Dissolution System**

Milestone Ethos PLUS microwave dissolution system was used in the closed system dissolution procedures. The system has a maximum power of 1000 W controlled by a temperature probe.

Simultaneously, 10 vessels made of polytetrafluoroethylene (PTFE) can be placed in the heating chamber. In this study, PTFE vessels were used since acid mixtures including HF for the dissolution by microwave oven affects the glass. All dilutions were performed using polypropylene volumetric flasks.

At the end of each working period, vessels were cleaned in 10% HNO<sub>3</sub> by heating on a hot plate for about 30 min. The volumetric flasks were immersed in 10% HNO<sub>3</sub> at least for a night. All vessels were rinsed using deionized water before each use.

### **2.2.2 Inductively Coupled Plasma-Optical Emission Spectrometry, ICP-OES**

Leeman DRE ICP-OES instrument was used for the determination of Mg, Fe, Ba, Sr, and Mn in figurine samples. The instrument includes a photomultiplier tube (PMT) as detector and allows the use of sequential multi-element analysis. An axial plasma torch was used. Burgener 17 2002 Meinhard type nebulizer was used in sample introduction system of ICP-OES. The operating parameters of the instrument throughout the study are given in Table 2.3. The wavelengths selected for Mg, Fe, Ba, Sr, and Mn are 279.553, 259.94, 445.403, 407.771, and 257.553 nm respectively.

**Table 2.3** Plasma Conditions for ICP – OES, Leeman DRE

Rf Power	1.1 kW
Nebulizer Gas	50 psi
Auxiliary Gas	0.5 L/min
Coolant Gas	18 L/min
Solution Flow Rate	1.2 L/min

### 2.2.3. Inductively Coupled Plasma-Mass Spectrometry, ICP-MS

Thermo X SERIES 2 ICP-MS instrument was used for the determination of Cr, Y, Nb, Hf and rare earth elements, REE, La, Ce, Nd, Sm, Eu, Gd, Ho, Er, Yb, Lu. Instrument has quadrupole mass analyzer and protective ion extraction and infinity II ion optics, based upon a hexapole design with chicane ion deflector, provides the lowest background specification of quadrupole ICP-MS. The instrument has the simultaneous analog/PC detector with real time multichannel analyzer electronics. The quadrupole analyzer is pumped by a novel split flow turbo pump backed by a single rotary. Peltier cooling system was used to improve the S/N ratio by cooling the spray chamber.

ICP-MS is finding increasing acceptance in geochemical applications particularly for the determination of REEs which are easily determined by ICP-MS as they are at the middle to high portion of the mass range and have few interferences from polyatomic plasma species [83]. Cerium very readily forms an oxide and Ba, meantime is most prone to formation of doubly charged species, so these elements are used for monitoring the probability of oxide and doubly charged ion formation. In general, the upper limits of 3% for CeO/Ce, and BaO/Ba are generally accepted [84, 85]. In this study CeO/Ce ratio was lower than 0.5% and BaO/Ba ratio was 0.5%, while spray chamber is kept at 3°C for avoiding oxidation of elements. All measurements were repeated three times.

ICP - MS instrument was operated in peak hopping mode, 110 sweeps and acquisition time was 27 seconds. The tune conditions of the ICP-MS instrument are given Table 2.4.

**Table 2.4.** ICP-MS, Thermo X series plasma operation parameters.

<b>Extraction voltage, V</b>	-82.0	<b>Horizontal voltage, V</b>	63
<b>Lens 1 voltage, V</b>	-200	<b>Vertical voltage, V</b>	619
<b>Lens 2 voltage, V</b>	-26.7	<b>DA voltage, V</b>	-30.6
<b>Focus voltage, V</b>	16.3	<b>Argon Flow Rate to Cool Torch Cool, L/min</b>	13.0
<b>D 1 voltage, V</b>	-43.1	<b>Argon Flow Rate in Nebulizer, L/min</b>	0.90
<b>D 2 voltage, V</b>	-166	<b>Sampling Depth, relative units</b>	40
<b>Pole Bias voltage, V</b>	0.3	<b>Standard resolution, amu</b>	125
<b>Hexapole Bias voltage, V</b>	- 0.8	<b>High resolution, amu</b>	125
<b>Nebuliser, L/min</b>	0.83	<b>Analogue Detector, W</b>	2050
<b>Lens 3 voltage, V</b>	-197.6	<b>PC detector, W</b>	3249
<b>Forward power, W</b>	1400	<b>Sample uptake, L/min</b>	1 L/min

## 2.3 Samples

### 2.3.1 Archaeological Sampling

Archaeological sampling was done especially from the recently found figurines excavated at Emeçik in 2006 and other figurines which were found in 2002 and were not sampled in previous studies. Chemical analysis requires at least a one-gram sample of powdered limestone to insure the homogeneity of the powder and produce a valid compositional profile of the sample. The powdered samples were taken by a drill with vanadium tips preferably from points on the figurine where a previous break existed, ensuring negligible damage to the object. An example for drill sampling is given in Figure 2.1. For thin-section analysis small flakes were also taken from some of the figurines.



**Figure 2.1.** Typical drill hole for archaeological sampling

The sample nomenclature is given in Table 2.5.

**Table 2.5.** The Nomenclature of Archaeological Samples

Sampling Order	Sample Name	Name	Description	Figures
1	1	ST.06.I12.d8.19	Male votary (priest?) body fragment	
2	2	ST.06.I12.d5.c12	Fragment	
3	3	ST.06.I12.d8.21	Miniature woman	

<b>Table 2.5. continued</b>				
4	4	ST.06.H12.a3.16	Bird of prey (falcon)	
5	5	ST.06.I12.d6.B	Leg fragment	
6	6	ST.06.H12.d5.15	Fragment	
7	7	ST.06.I12.d7.43	Leg fragment	
8	8	ST.06.I12.d5.A11	Leg fragment	
9	9	ST.06.H12.a2A.23	Body fragment	
10	10	ST.06.I12.d6A.14	Leg fragment	
11	11	ST.06.H12.a5.22	Body fragment	
12	12	ST.06.I12d.6A.11	Male votary (priest?) body fragment	
13	14	ST.06.H12.a3.17	Leg fragment	
14	15	ST.06.I12.d7.45	Bird of prey (falcon)	
15	16	ST.06.I12.d5.B11	Lion fragment	

<b>Table 2.5. continued</b>				
16	17	ST.06.I12.d3.9	Kouros body and legs fragment	
17	18	ST.06.I12.d5A.12	Lion paw fragment	
18	19	ST.06.I12.d5.17	Lion	
19	20	ST.06.I12.d7.44	Drapery fragment	
20	22	ST.02.I8b.18.3	Lion figurine	
21	23	ST.02.I8b.16A.11	Fragment	
22	24	ST.02.I8b.16A.11	Fragment	
23	26	ST.02.I8b.16A.11	Fragment	
24	27	ST.02.I8b.16A.11	Fragment	

Table 2.5. continued				
25	28	ST.02.I8b.11.c26	Standing male votary figurine fragment carrying goat, red paint used for details	
26	30	ST.02.K9c.28B1	Ornamented stone (base?)	
27	31	ST.02.I8b.25.11	Kouros feet and base	
28	32	ST.02.I8b.28A.11	Kouros head and body	
29	33	ST.02.I8b.16A.16	Kouros body and legs fragment)	
30	34	ST.02.I8B.19.b6	Body fragment	
31	35	ST.02.I8b.11.b9	Body fragment	
32	36	ST.02.I8b.28.A2	Body fragment	

Table 2.5. continued				
33	37	ST.02.I8B.16.A.15	Lion fragment	
34	38	ST.02.I8B.11c.29	Fragment	
35	39	ST.02.I8b.16.20	Leg fragment	
36	40	ST.02.8B.19A.13	Male votary (priest?) body fragment	
37	41	ST.02.I8B.19.6	Leg fragment	
38	42	ST.02.K9c.28.7.4	Kouros feet and base fragment	
39	43	ST.02.I8b.28.A3	Leg fragment	
40	44	ST.02.I8b.21.17	Lion	
41	45	ST.02.I8b.25.12	Lion	
42	46	ST.02.I8b.22.2	Fragment	
43	47	ST.02.I8b.28.6.3	Leg fragment	

Table 2.5. continued				
44	48	ST.02.I8b.28.8	Kouros feet and base fragment	
45	49	ST.02.I8b.19.2	Leg fragments	
46	50	ST.02.I8b.19.2	Leg fragment	
47	52	ST.02.I8b.18.7	Kouros body fragment	
48	53	ST.02.I8b.14.17	Lion fragment – plaster?	
49	54	ST.02.K9c.28.6	Leg fragment	
50	55	ST.02.K9c.27.4	Leg fragment	
51	56	ST.02.K9c.27A.13	Body fragment	
52	57	ST.02.I8b.11b.10	Kouros feet and base fragment	
53	58	ST.02.I8b.14.20	Male votary (priest?) body fragment, the figurine is wearing chiton and himation over it, red paint used for details	
54	59	ST.02.K9c.26.4	Bird pounces	

Table 2.5. continued				
55	60	ST.02.I8b.20.2	Body fragment	
56	61	ST.02.I8b.23.11	Lion fragment	
57	62	ST.02.I8b.28A.2	Small fragments	
58	63	ST.01.G11.D1	Leg ? fragment	
59	64	ST.02.I8b.28A.2	Small fragments	
60	65	ST.02.K9c.27b.1	Leg fragment	
61	66	ST.02.I8b.21.20	Lion fragment	
62	67	ST.02.K9c.27A.3	Standing male votary figurine fragment carrying goat	
63	68	ST.02.K9.c28.14	Body fragment	
64	69	ST.02.K9.c27.A12	Bird	

<b>Table 2.5. continued</b>				
65	70	ST.02.I8b.28.A9	Standing male votary figurine fragment carrying goat	
66	71	ST.02.I8b.14.30	Bird pounces	
67	72	ST.02.I8b.15.17	Fragment	
68	73	ST.02.I8b.16A.17	Bird of prey (falcon) tail fragment mounted on a rectangular plinth	
69	74	ST.02.I8b	Body fragment	
70	75	ST.02.I8b.28.3	Lion fragment	
71	77	ST.02.K9c.27a.11	Lion fragment	
72	80	ST.02.I8b.23.9	Leg fragment	
73	81	ST.02.I8b.23.9	Fragment	
74	84	ST.02.I8b.19.A12	Fragment	
75	85	ST.02.18b.19.A.12	Architectural fragment	
76	86	ST.00.K8C.16.148	Body fragment	
77	87	ST.99.I9b.4.65	Leg fragment	
78	88	ST.99.I9b.2.17	Leg fragment	
79	89	ST.01.I8.B.10.26	Body fragment	
80	90	ST.00.K8.C.16.151	Fragment	
81	91	ST.99.I9B.4	Carbonate stone	
82	92	ST.02.I8b.28.B3	Fragment	
83	93	ST.00.D8.A.5.25	Body fragment	
84	94	ST.99.K8C.9.22	Leg fragment	
85	95	ST.00.K8C.16.152	Body fragment	

The sampled figurines were obtained from 7 trenches in the lower terrace and 2 trenches in the upper terrace. The locations of these trenches are marked in the plan given in Figure 2.2.

The trenches encoded as 06 I12d and 06 H12a are dated to early 6<sup>th</sup> century BC. 02 I8b is dated to the first half of 6<sup>th</sup> century BC, while 02 K9c is dated to the second half of 6<sup>th</sup> century BC. The figurines from other trenches are probably from bothroi used as fill material for the restructuring of terraces during the Late Archaic period [86].

The samples from different trenches represent the time period when the figurines are dated, from late 7<sup>th</sup> century to middle of 6<sup>th</sup> century B.C.

There is a total of 85 sample figurines. They include 49 body or leg fragments, 4 priest body fragments, 12 lion fragments and more complete lion figurines, 7 bird fragments, 3 goat carrying male figurines, 4 kouros feet and base fragments, 1 miniature female figurine, 1 drapery fragment, 1 kouros head and body fragment, 1 ornamented stone fragment, 1 carbonate stone fragment and 1 architectural fragment. Architectural fragment was also sampled in order to compare the results, since it is safe to assume that a limestone architectural element has been made out of a local stone. Pocked marked appearance as Jenkins described are also seen on the most of Emeçik figurines [2, 28].

In this study, the archaeological sample number is increased in order to get a wider perspective on the material characteristics of limestone figurines for provenance. Including as much variety as possible among the findings in Emeçik is important, since Datça has been left out as the only probable production site along with Cyprus [25]. Doing so, the sampling strategy was to include various types of figurines that were found at Emeçik as much as possible. The figurines findings from different trenches were also taken into consideration. Meantime, different dates for the figurines were another important aspect in sampling. Although figurine fragments were also sampled, badly deteriorated figurines were not subject to sampling. The reason for this is that the deterioration process under the burial conditions may have altered the mineral and chemical structure of the figurines. Moreover, the visual differences on figurines such as the color were considered to be important. Therefore, during the sampling stage of this research, visually and typologically different groups of figurines from various trenches at excavation site were tried to be represented by sampling. This sampling method is appropriate with statistical point of view in order to ensure homogeneity.

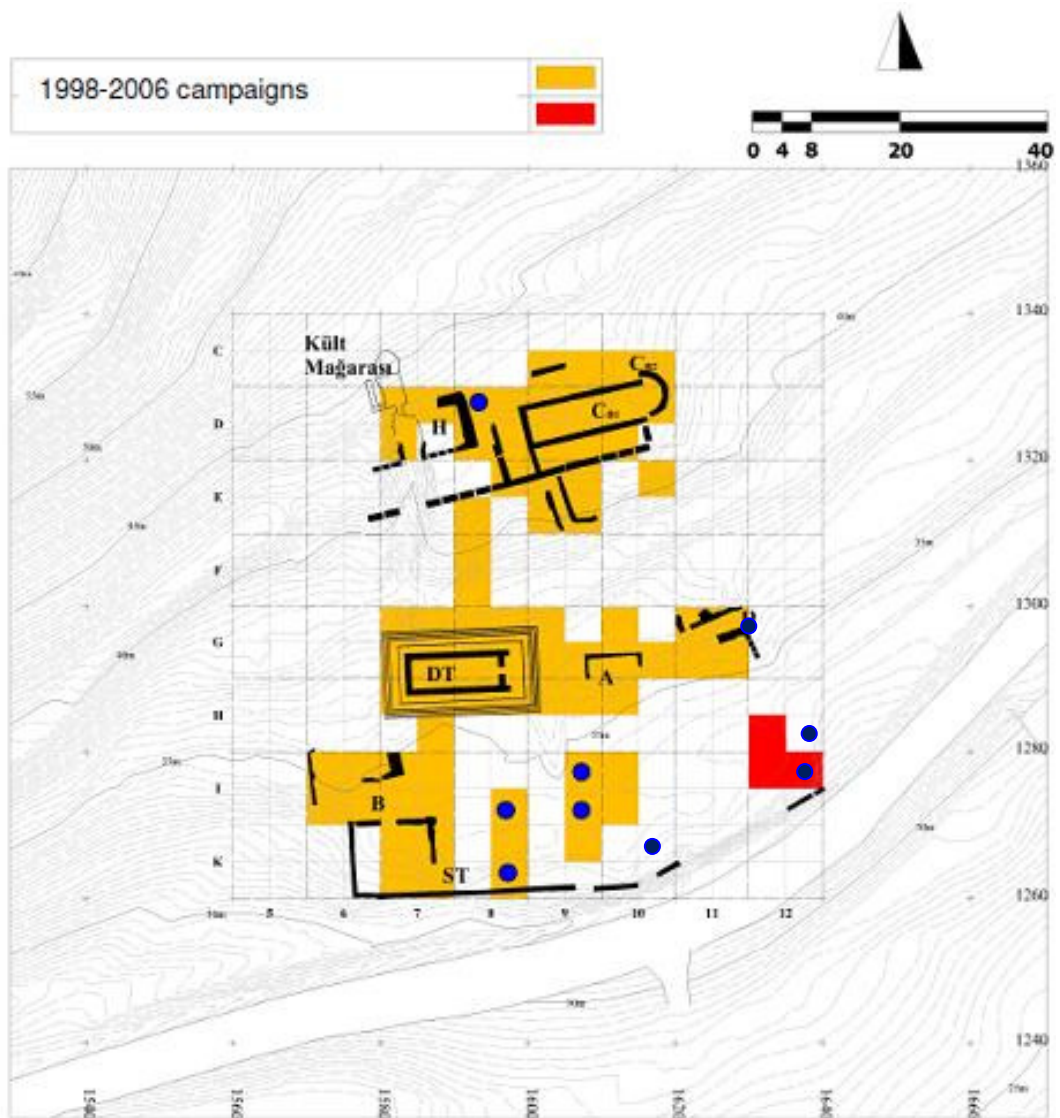


**Figure 2.2.** Plan of Emecik Sanctuary Excavation Site. Blue dots are indicating the sampling trenches

### 2.3.2 Geological Samples from Datça

Provenance studies are based on understanding the compositions of archaeological material, various geological sources and comparison of the results. The first detailed geological work on the Datça peninsula is that of Phillipson in 1915 [87]. Since then, various studies were undertaken in different times on the geomorphological structure of Datça [88, 89]. The tectonic and geological maps of Datça peninsula are given in Figure 2.3. and 2.4.



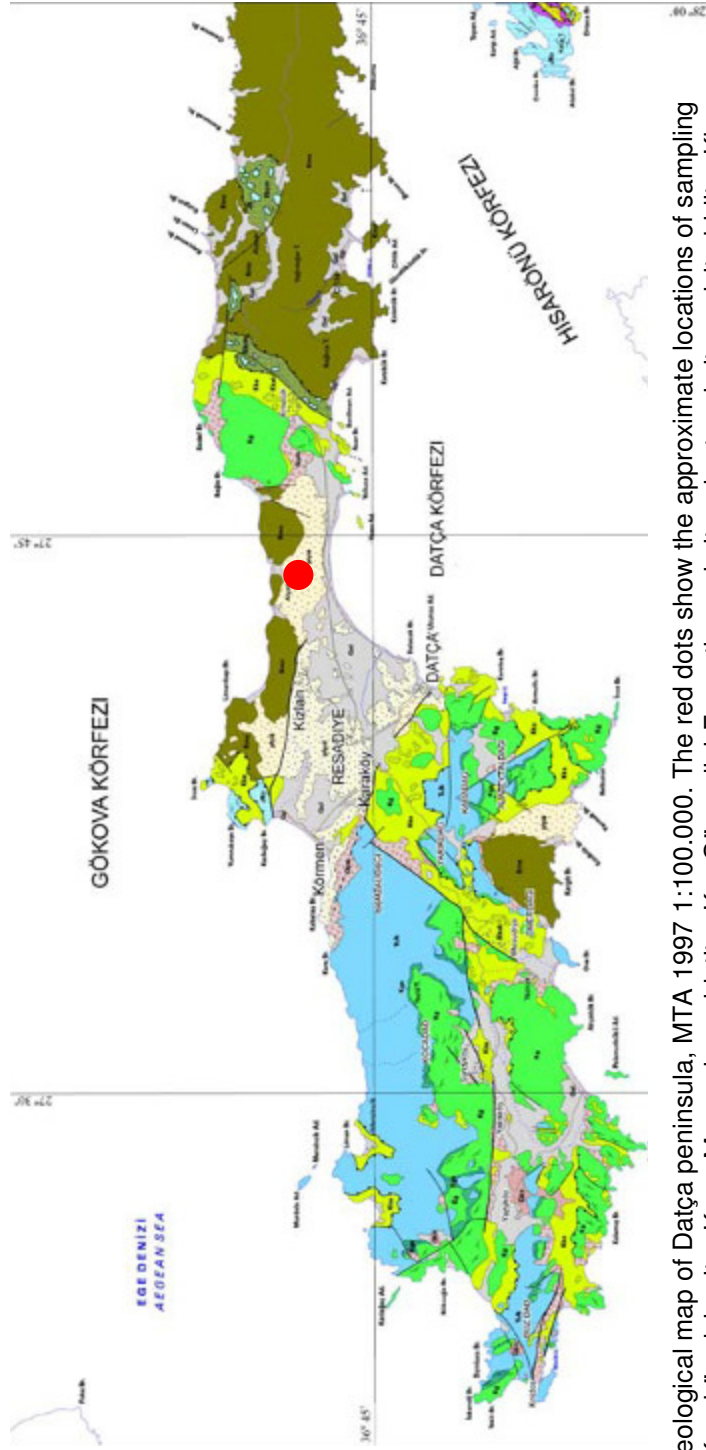


**Figure 2.4.** Geological map of Datça peninsula, MTA 1997 1:100,000. The red dots show the approximate locations of sampling areas. TRJk: Kayaköy dolomite; Kmo: Marmaris peridotite; Kg: Göçgediği Formation: micrite, cherty micrite, calciturbidite; Kka: Karaböğürtlen formation: sandstone, claystone, siltstone etc.; Kkak: limestone member: cherty limestone, calciturbidite; plyk: Yıldırımli continental formation; plyd: Yıldırımli marine formation; Qp: beach deposits; Qym: slope deposits; Qal: alluvium

characterized by the conglomerate-sandstone-marly-claystone alternation with tuff intercalation [89].

Facies change into oolitic limestone in the north of Kızlan. As described, this marble limestone is white colored, containing cherty, and ophiolite inclusions. Researches also indicated fossil inclusions either marine or continental [89].

These deposits in Datça peninsula were first dated to Pliocene and described as marine sediments by Phillipson [87]. Both lithological evidence and the examination of fossils show that a transgression occurred first in this area mentioned above; the deposition of marine strata over terrestrial strata and then it was followed by a sudden regression [87].

A recent study on the pelecypoda and gastropoda fossil remains from late Pliocene is important, since investigation of the tests remains has led to reconsidering the age of this formation [93]. According to this study, some of the marine remains are

*Ostrea lamellosa*, *Cerastoderma (C.) edule*, *Cerastoderma (C.) edule var. umbonata*, *Abra (A.) tenuis*, *Venus gaina*, *Cabula (V.) gibba*, *Bittium reticulatum*, *Theridium (T.) vulgatum*, *Chama (C.) gryphoides*, *Cerastoderma (C.) edule*, *Cerastoderma (C.) edule var. umbonata*, *Abra (A.) tenuis*, *Venus gallina*, *Corbula (V.) gibba*, *Trunculariopsis trunculus*,

Some of the freshwater remains are

*Melanopsis cf. bergeroni*, *Theodoxus doricus depressus*, *Theodoxus doricus fuchsi*, *Viviparus brevis trochlearis*, *Hydrobia denizliensis*, *Hydrobia tanerae*, *Lithoglyphus acutus decipiens*, *Melanopsis gorceixi proteus*, *Melanopsis delessei*, *Melanopsis gorceixi heldreichi*, *Melanopsis vandevelde*, *Melanopsis orientalis*, *Melanopsis inexpectata*, *Melanoides tuberculata dadiana*, *Unio pseudatavus*, *Modiolus sp.*,

Pelecypoda and gastropoda fauna of Datça peninsula indicated that the Datça peninsula was a lagoon-river environment that was connected to shallow marine in late Pliocene, instead of late Pliocene marine environment as previous researches had mentioned [92, 93].

Above information is in particular important for this project since it supports the idea that the raw material of the figurines could be originated from Datça and systematic investigation for the geological source was carried out around the peninsula.

Each sampling was marked with global positioning system device, GPS, Magellan Explorist 500. Using Magellan software Magellan MapSend Lite and Vantage Point points were put on the map.

Based on survey in the area the possible geological sources are appointed in Kızlan, around recently constructed windmills. The names, longitudes and latitudes of the points along with the altitudes for each sampling point are given in Table 2.6. The photographs of the formations are also given in Figures 5-9.

**Table 2.6.** Geological Sampling Points in Datça peninsula

Name	Comment	Longitude	Latitude	Altitude
NKT022	RZG1	27°42.815'E	36°46.746'N	44 m
NKT024	AKYA	27°42.821'E	36°46.688'N	28 m
NKT025	AKYB	27°43.279'E	36°46.531'N	44 m
NKT026	KRC	27°41.537'E	36°45.898'N	28 m
NKT027	AKYC	27°41.513'E	36°45.651'N	27 m
NKT028	RZG2	27°43.822'E	36°46.658'N	83 m



**Figure 2.5.** Geological sampling location KRC



**Figure 2.6.** Geological sampling location RZG



**Figure 2.7.** Geological sampling location AKYC  
AKYA



**Figure 2.8.** Geological sampling location AKYA



**Figure 2.9.** Geological sampling location AKYB

### 2.3.3 Geological Samples from Cyprus

There are ancient quarries in Cyprus mentioned in literature and located near the archaeological sites [25]. However, most of them are dated to either Classical to Hellenistic or Roman periods while the raw material from a few Archaic quarries are known to have different properties.

Cyprus is divided into four geological zones [94]:

- The Pentadaktylos (Kyrenia) Zone
- The Troodos Zone or Troodos Ophiolite
- Mamonia Zone or Complex
- The zone of the autochthonous sedimentary rocks

The map of Cyprus with these geological zones and geological map of Cyprus are given in Figure 2.10. and Figure 2.11.

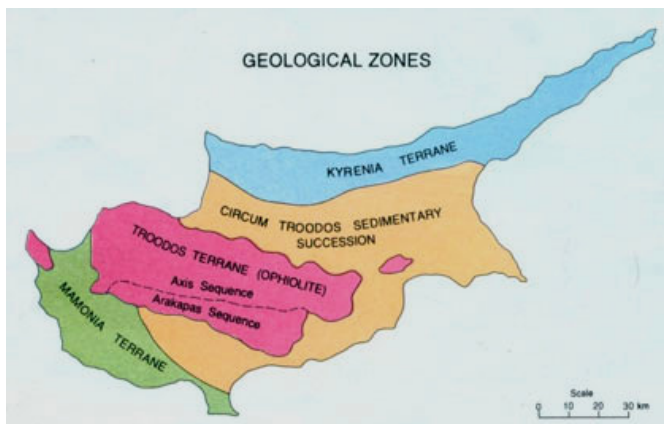


**Figure 2.10.** Geological zones in Cyprus [95]

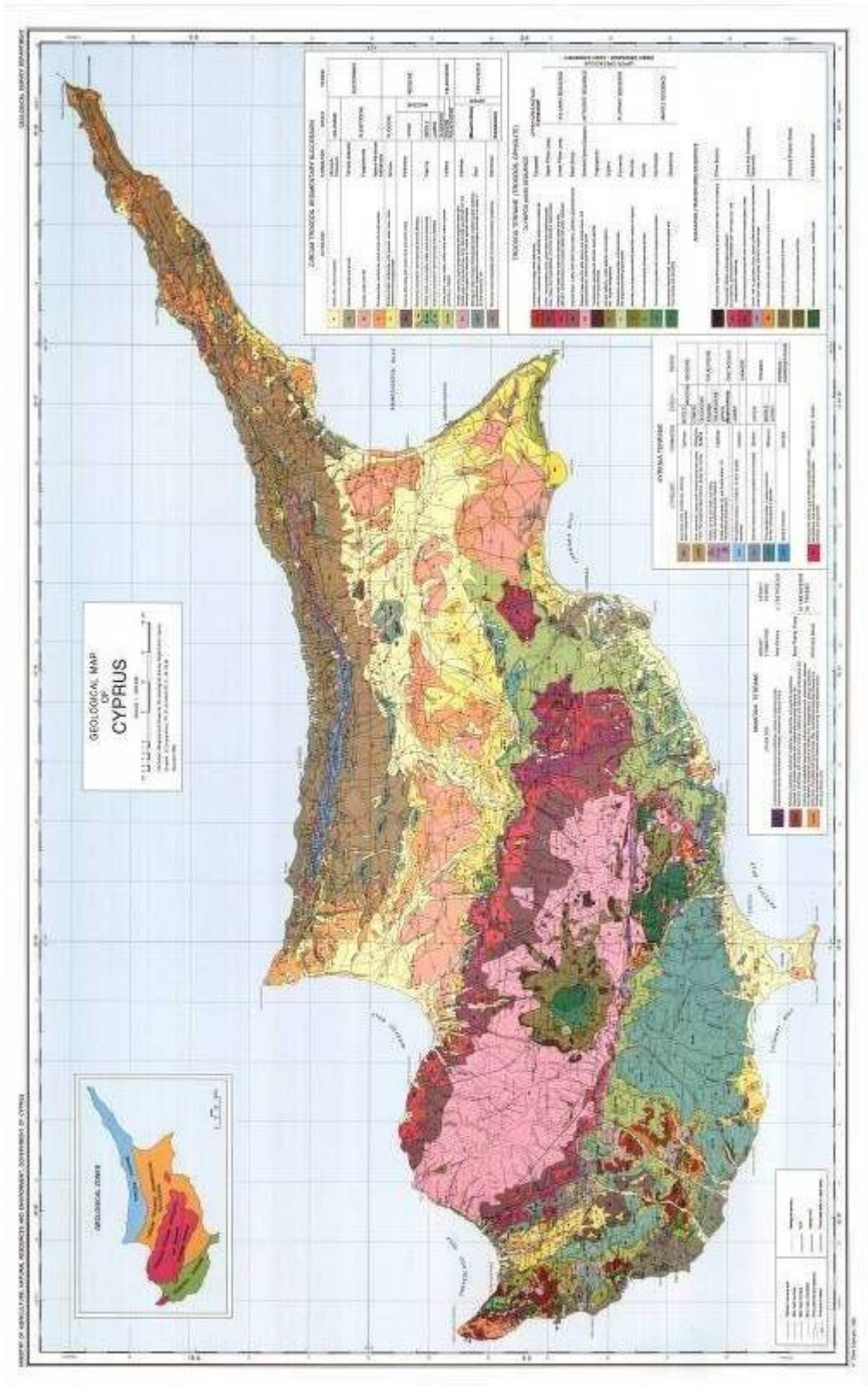


Figure 2.11. Geological map of Cyprus [97]

The Pentadaktylos (Kyrenia) Zone (Beşparmak Dağları) is the northern zone of Cyprus and is considered to be the southernmost portion of Tauro-Diranide Alpine Orogenic Zone [96]. The base of the Zone is mostly composed of massive and recrystallized limestone, dolostone and marble which are dated to Permian-Carboniferous to Lower Cretaceous periods. The base then is followed by sedimentary rocks of Upper Cretaceous to Middle Miocene age [97]. There are three main geological formations in the Zone namely Dhikomo, Sykhari and Hilarion Formations forming the main carbonate masses of the Pentadaktylos Zone [98, 99]. The Dhikomo formation is consisted of thinly bedded limestones with layers of grey and green phyllites [98]. The Sykhari formation is consisted of massive bedded dolostones. The Hilarion formation is composed of medium bedded limestones. Continuous outcrops of limestones exist in the central part of the Zone. These formations are thrust southwards over the younger marine sediments. These younger sediments are known as the Lapithos, Kalogrea-Ardana and Kythrea (Değirmenlik) formations. The Lapithos formation is of Campanian to Eocene age and is consisted of pelagic marls and chalks [101]. Kalogrea-Ardana Flysch of Upper Eocene age is overlain by Kythrea formation. Kythrea formation is composed of thick layers of sandstones, siltstones and marls of mid-Miocene age. On the south, the formation crosses with Pakhna chalks and marls.

The Troodos Zone or Troodos Ophiolite dominates the central part of the island and forms the geological core of Cyprus [97]. The zone is dated to Upper Cretaceous and was formed on the Tethys sea floor. Tethys is the ocean that occupied the general area of what is now Alpine-Himalayan orogenic belt [102]. It consists of plutonic rocks, intrusive rocks, volcanic rocks and chemical rocks [97].

The Mamonia Zone or Complex that is located in the south of Cyprus constitutes a diverse and structurally complex assemblage of igneous, sedimentary and metamorphic rocks of Middle Triassic to Upper Cretaceous age [97]. The Zone, which is considered to be allochthonous in relation to the overlying autochthonous carbonate successions and the Troodos rocks, were placed over and adjacent the Troodos Zone during the Maistrichian [96].

The zone of the autochthonous sedimentary rocks covers the area between the Pentadaktylos and Troodos Zones as well as the southern part of island [101]. The rocks are of from the Upper Cretaceous through to Pleistocene. It consists of bentonitic clays, volcanoclastics, mélange, marls, chalks, cherts, limestone, calcarenites, evaporates and clastic sediments. From the Upper Cretaceous marine sedimentation formed in the island of Cyprus in a sea which became shallower [103]. The sedimentation in the Zone began with the deposition of the Kannaviou formation, followed by the deposition of Moni and Kathikas formations. Carbonate sedimentation in the Zone first occurred around Paleocene with the deposition of Lefkara formation [104]. Lefkara formation includes pelagic marls and chalks with characteristic white color and sometimes with cherts.

The Lefkara formation is followed by Pakhna formation of Miocene [100]. It consists of mainly yellowish marls and chalks. Pakhna formation differs from Lefkara formation for its color, the presence of calcarenitic layers and the occasional development of conglomerates.

In Cyprus, geological samples were taken roughly from the quarries at Erdemli, Değirmenlik and Karpaz peninsula, because these names are mentioned in various publications as possible production centers [2, 25, 28].

The names, longitudes and latitudes of the points along with the altitudes for each sampling point are given in Table 2.7. The photographs of some of the sampling formations and samples are given in Figures 12-17.



**Figure 2.12.** Limestone quarry at Karpaz



**Figure 2.13.** Limestone quarry at Değirmenlik



**Figure 2.14.** Sample from Erdemli



**Figure 2.15.** Sample from Değirmenlik



**Figure 2.16.** Sample from Kumyalı



**Figure 2.17.** Sample from ancient quarry

**Table 2.7.** Geological Sampling Points in Cyprus

Name	Description	Longitude	Latitude
K1	Erdemli quarry, Cyprus	33° 61.713'E	35° 07.105'N
K2	Değirmenlik quarry, Cyprus	33° 46.912'E	35° 26.948'N
K3-1	Kumyalı quarry, Cyprus	34° 16.758'E	35° 44.134'N
K3-2	Kumyalı , Cyprus	34° 17.299'E	35° 44.043'N
K3-3	Kumyalı, ancient quarry, Cyprus	34° 16.901'E	35 ° 44.137'N

## 2.4 Procedures

### 2.4.1 Microwave Assisted Dissolution

Portions of the unweathered geological samples were broken into small fragments with a steel pestle. A randomly selected split was then ground in an agate mortar then sieved until the grain size was > 120 mesh. Archaeological fragments meantime, sampled using a drill with vanadium tips. Although they were powdered, they were sifted once again in order to obtain homogeneity.

In the digestion procedure, 150 mg powdered sample, was mixed with two different acid mixtures:

- A) 2.0 mL 65% HNO<sub>3</sub>, 2.0 mL 40% HF and 2.0 mL 37% HCl
- B) 1.0 mL 65% HNO<sub>3</sub>, 4.0 mL 40% HF and 1.0 mL 37% HCl

as was suggested in various related studies [105]. This mixture was placed in a PTFE vessel. The microwave heating of samples have been carried out up to 120°C and 140°C separately for each acid mixture. The microwave program 1 and microwave program 2 are shown in Table 2.8. and 2.9. Two replicate samples were studied. When the program was completed, solutions in

PTFE vessels were kept at room temperature overnight and then evaporated to dryness on hot plate at 80 °C in order to drive out excess HF. Dried mass was dissolved with 3.0 mL 65% HNO<sub>3</sub>, and evaporated to dryness once more. The residue was dissolved with 2.0 mL 65% HNO<sub>3</sub> and transferred into PTFE containers. After filtration through a PTFE, 45 µm millipore membrane filter, samples were diluted to 50 mL with 1.0% HNO<sub>3</sub>. Blank was prepared in the same way as samples.

**Table 2.8.** Microwave Program 1

Period, min	Temperature, °C
5	100 ↑
5	100 →
5	120 ↑
15	120 →

**Table 2.9.** Microwave Program 2

Period, min	Temperature, °C
5	120 ↑
10	120 →
5	140 ↑
10	140 →

To check up the success of the digestion and standard addition processes, reference materials, NIST 1d Limestone, Argillaceous, and NCS DC 73306 carbonate rock were studied at first. It was found that standard addition after digestion method gave more accurate results for some of the elements. Therefore, this approach was used for all the experiments where standard additions are used.

### 2.4.2 Dissolution by Fusion

Two reflux materials,  $\text{LiBO}_2$  and  $\text{Li}_2\text{B}_4\text{O}_7$ , were used for dissolution by fusion. Three replicate measurements were performed: 0.200 g of powdered sample was weighed and placed in the crucible. 1 g of  $\text{LiBO}_2$  - $\text{Li}_2\text{B}_4\text{O}_7$  mixture (4:1) was added to the crucible and solid material was mixed carefully with a PTFE rod. The same procedure was followed for the blank solution.

The crucibles were heated in a muffle furnace at 1050 °C for 1 hour. The fused glass was cooled and transferred into a PTFE beaker. The beaker was placed on magnetic stirrer after adding about 50 mL water and 1.5 mL concentrated  $\text{HNO}_3$ . The crucible was rinsed with 5 mL of 20 %  $\text{HNO}_3$  and the contents were poured into the beaker. The beaker was covered with a watch glass and the contents were stirred until all the melt dissolved. After filtration through a membrane filter under vacuum the solution was diluted to 100 ml or 250 ml in a plastic volumetric flask with  $\text{HNO}_3$  of about 1% final concentration.

### 2.4.3 Calibrations for ICP-OES Using Standard Additions

External calibration and standard addition methods were used for the determination of Mg and Fe to find the best method. Standard addition was applied both before and after microwave digestion. A four-point standard additions was applied to two replicates of standard reference materials, NIST 1d Limestone, Argillaceous and NCS DC 73306 carbonate rock samples. More accurate results were obtained by standard addition *before digestion* since sample preparation process involves evaporation stages that may result in partial evaporation of some elements. Standards were applied not one by one but as a mixture which contains all the analyte elements in different concentrations. The results are shown on Figures 2.18-2.25.

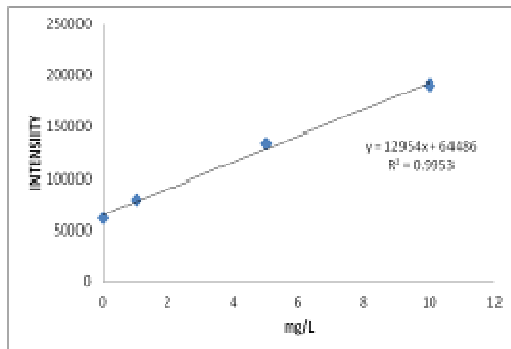


**Figure 2.18.** ICP-OES calibration plot of Fe using NIST 1d Limestone, Argillaceous (Replicate 1). Standard additions after digestion

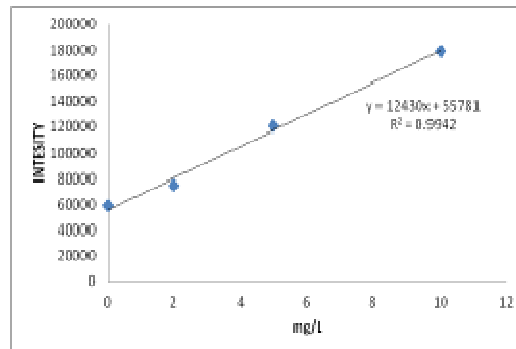


**Figure 2.19.** ICP-OES calibration plot of Fe using NIST 1d Limestone, Argillaceous (Replicate 2). Standard additions after digestion

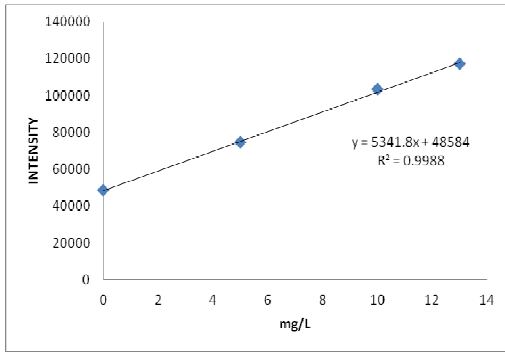


**Figure 2.20.** ICP-OES calibration plot of Fe using NIST 1d Limestone, Argillaceous (Replicate 1). Standard additions before digestion

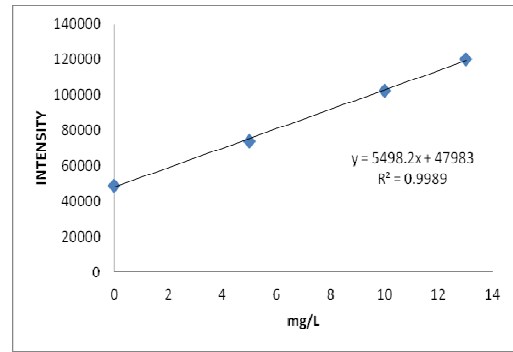


**Figure 2.21.** ICP-OES calibration plot of Fe using NIST 1d Limestone, Argillaceous (Replicate 2). Standard additions before digestion

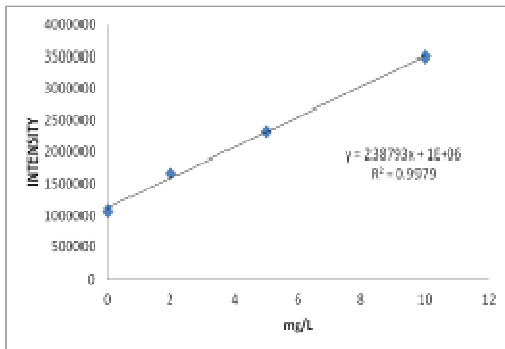


**Figure 2.22.** ICP-OES calibration plot of Mg using NIST 1d Limestone, Argillaceous (Replicate 1). Standard additions after digestion

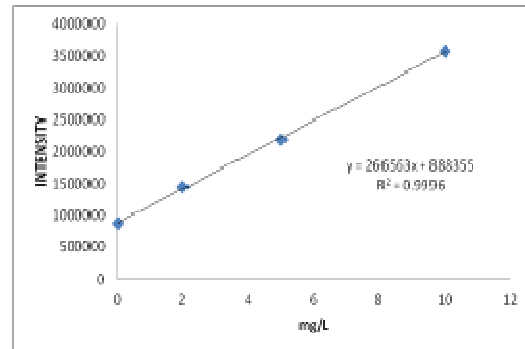


**Figure 2.23.** ICP-OES calibration plot of Mg using NIST 1d Limestone, Argillaceous (Replicate 2). Standard additions after digestion.

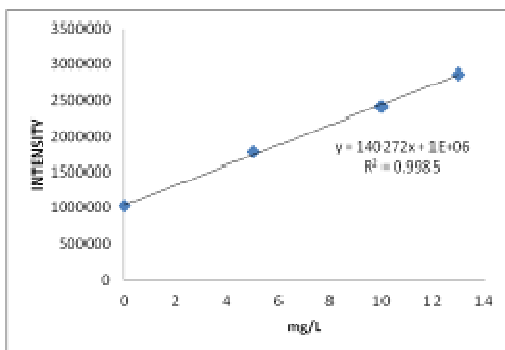


**Figure 2.24.** ICP-OES calibration plot of Mg using NIST 1d Limestone, Argillaceous (Replicate 1). Standard additions before digestion

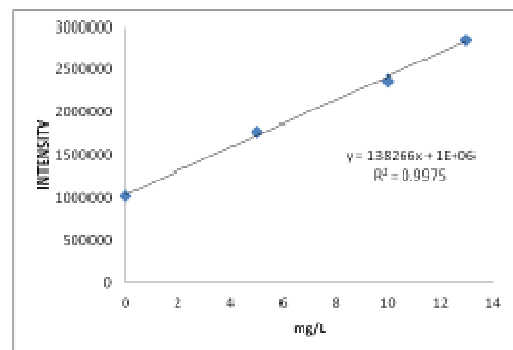


**Figure 2.25.** ICP-OES calibration plot of Mg using NIST 1d Limestone, Argillaceous (Replicate 2). Standard additions before digestion

#### 2.4.4 Calibrations for ICP-OES Using External Calibration

Mn, Sr, and Ba were determined by using ICP-OES and external calibration. The measurements were quantified by external calibration. After obtaining accurate results for three replicates of standard reference materials, NIST 1d Limestone, method was applied to real samples. Calibration plots and found values are shown in Figures 2.26-2.28.

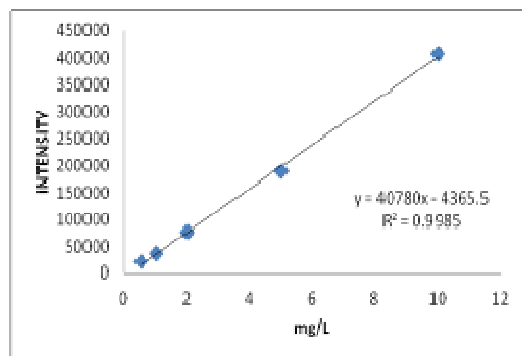


Figure 2.26. ICP-OES calibration plot of Mn

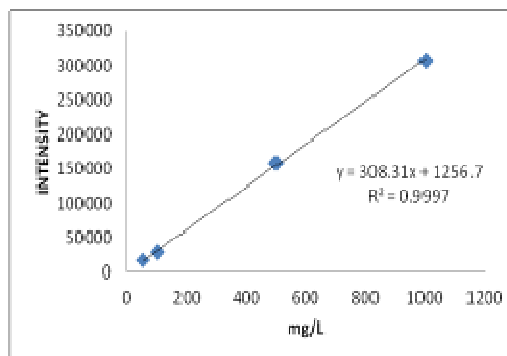


Figure 2.27. ICP-OES calibration plot of Ba

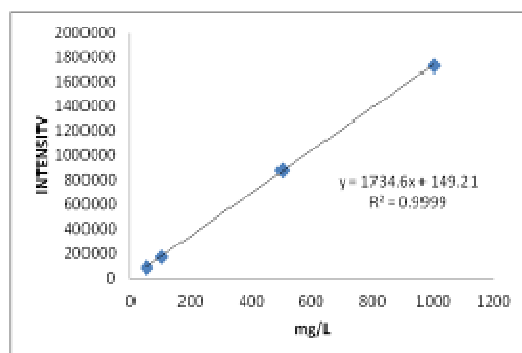


Figure 2.28. ICP-OES calibration plot of Sr

#### 2.4.5 ICP-MS Analyses

ICP-MS was used in the analysis of samples for Cr, Y, Nb, Hf and rare earth elements, REE, La, Ce, Nd, Sm, Eu, Gd, Ho, Er, Yb, Lu. Due to low concentration of above mentioned elements and high concentration of Ca limestone, standard addition method was applied and gave appropriate results for the determination of these elements.

In this study CeO/Ce ratio was lower than 0.5% and BaO/Ba ratio was 0.5%, while spray chamber was kept at 3 °C for avoiding oxidation of elements. All measurements were repeated three times. Measured isotopes are shown Table 2.10.

**Table 2.10.** Some information about the measured isotopes

Element	Nominal Mass (m/z)	Abundance (%)
Cr	52	83.76
Y	89	100.00
Nb	93	100.00
Hf	178	27.23
La	139	99.91
Ce	140	88.48
Nd	146	17.26
Sm	149	13.84
Eu	151	47.77
Gd	157	15.68
Ho	165	100.00
Er	166	33.41
Yb	174	31.84
Lu	175	97.40

The accuracy of digestion method and instrument parameters were tested using standard reference material NCS DC 73306 carbonate rock. In order to have minimized sample consumption and a minimum contamination of especially the MS parts, flow injection (FI) was used. It is known that one of the factors that affects the lifetime of cones is the sample volume injected. Therefore, 1.00 mL of the sample volume was selected to inject to the system. Flow injection ICPMS signals for Y, Nb, Sm, La, Ce are given in Figures 2.29-2.33.

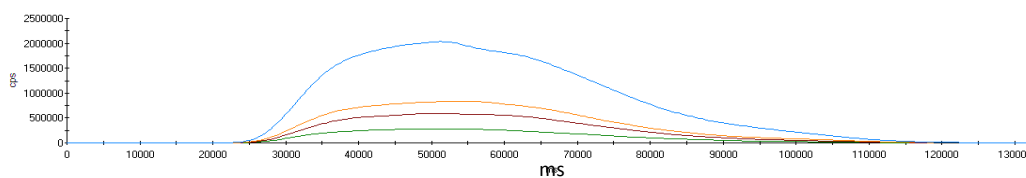


**Figure 2.29.** Flow injection ICPMS signals for Y

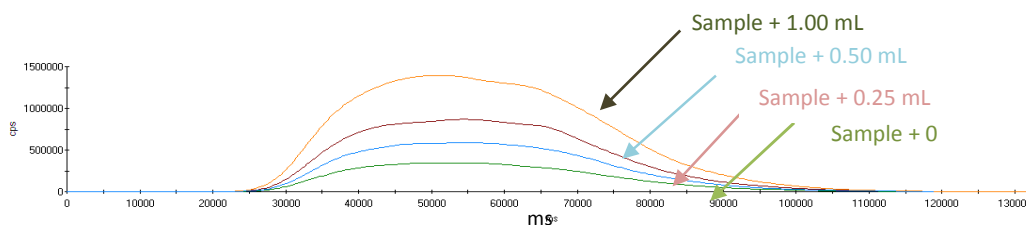


**Figure 2.30.** Flow injection ICPMS signals for Nb

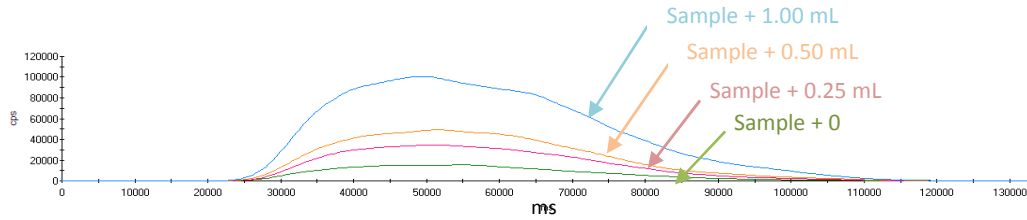


**Figure 2.31.** Flow injection ICPMS signals for for Sm

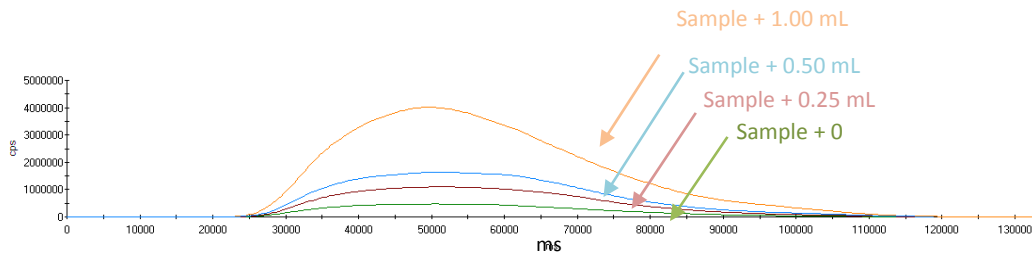


**Figure 2. 32.** Flow injection ICPMS signals for La

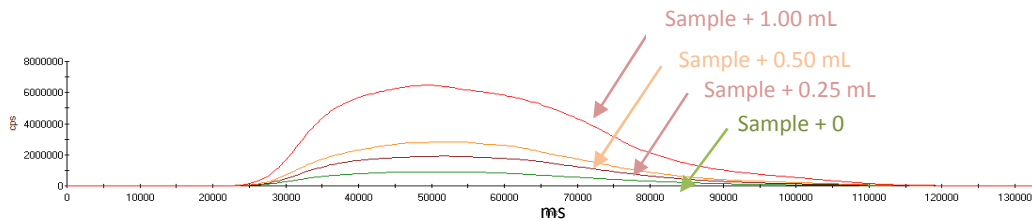


**Figure 2.33.** Flow injection ICPMS signals for Ce

The following formulas were used to calculate LOD and LOQ values:

$$\text{LOD} = 3 \times \text{Standard Deviation} / \text{Slope}$$

$$\text{LOQ} = 10 \times \text{Standard Deviation} / \text{Slope}$$

The analytical figures of merits for this study for each element determined by ICP-OES and ICP-MS are given in Appendix A.

## 2.5 Thin Section Analysis

In order to investigate mineralogy and the texture of figurines, some of the figurine samples and geological samples were prepared and observed using an optical microscope. Thin sections of samples were prepared by the Thin Section Laboratory of the Geological Engineering Department in METU and the photographs of the sample were taken at the Geological

Engineering Department in Akdeniz University. The list of the figurines that were sampled is given in Table 2.11. The photomicrographs of the samples are given in Figures 2.34-2.65.

**Table 2.11.** The list of figurines that were analyzed through thin-sections

No	Name	Description
2	ST.06.I12.d5.c12	Body fragment
3	ST.06.I12.d8.21	Minature female figurine fragment
4	ST.06.H12.a3.16	Falcon fragment
22	ST.02.I8b.18.4	Lion figurine
30	ST.02.K9c.28B1	Ornamented stone
37	ST.02.I8B.16.A.15	Lion figurine
38	ST.02.I8B.11c.29	Fragment
47	ST.02.I8b.28.63	Fragment
56	ST.02.K9c.27A.13	Body fragment
84	ST.02.I8b.19.A12(B)	Fragment
85	ST.02.I8b.19.A12	Architectural fragment
93	ST.00.D8.A.V	Body fragment

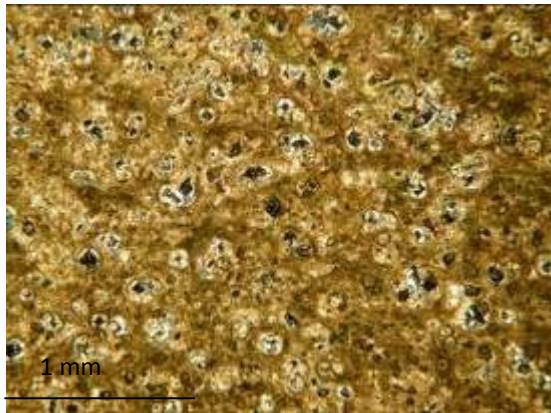


**Figure 2.34.** Thin-section photomicrograph of figurine 93 (XPL, objective x4)

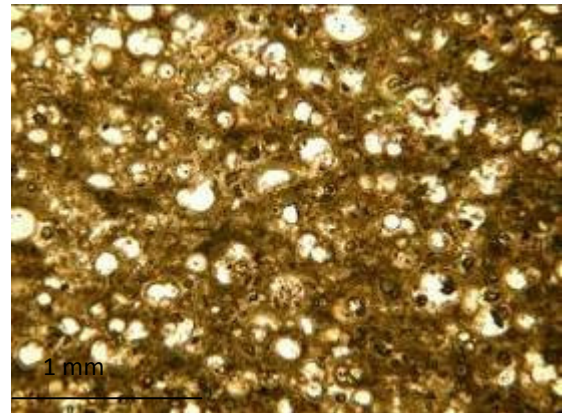


**Figure 2.35.** Thin-section photomicrograph of figurine 93 (PPL, objective x4)

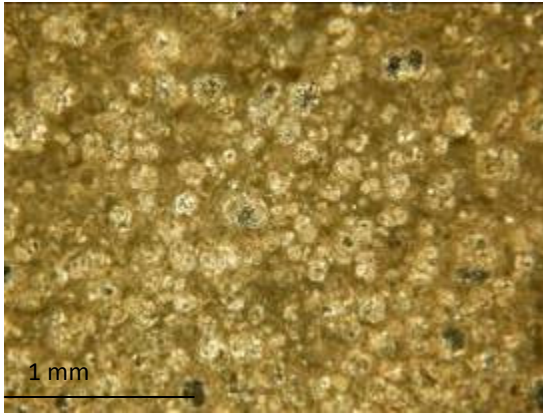


**Figure 2.36.** Thin-section photomicrograph of figure 2 (XPL, objective x4)

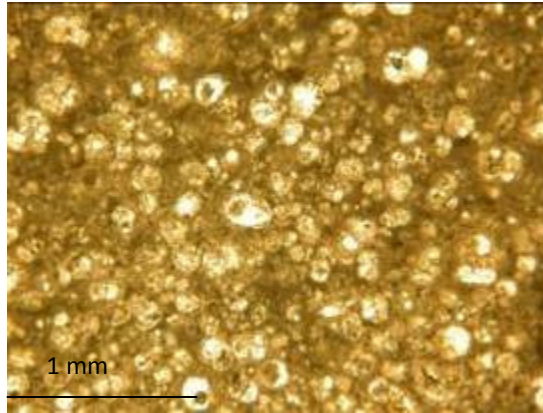


**Figure 2.37.** Thin-section photomicrograph of figure 2 (PPL, objective x4)

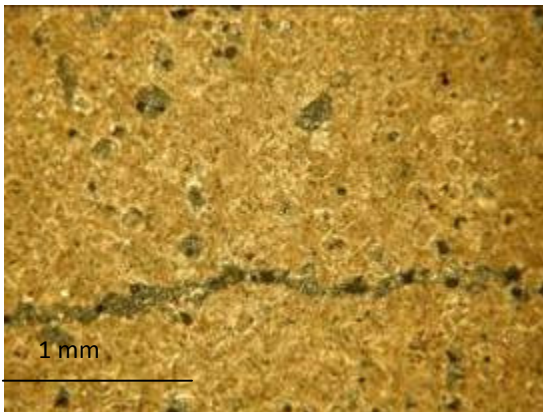


**Figure 2.38.** Thin-section photomicrograph of figure 4 (XPL, objective x4)

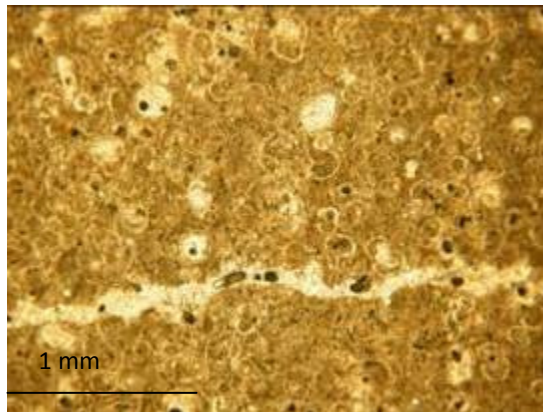


**Figure 2.39.** Thin-section photomicrograph of figure 4 (PPL, objective x4)

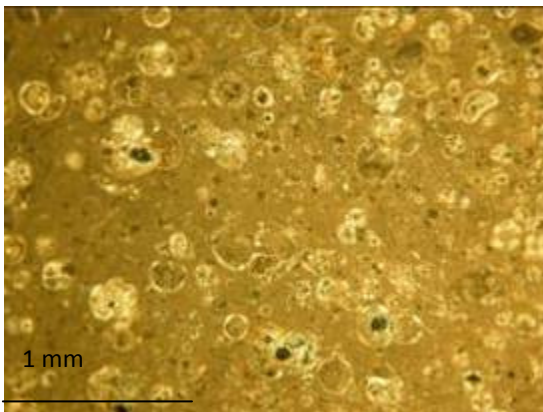


**Figure 2.40.** Thin-section photomicrograph of figure 38 (XPL, objective x4)

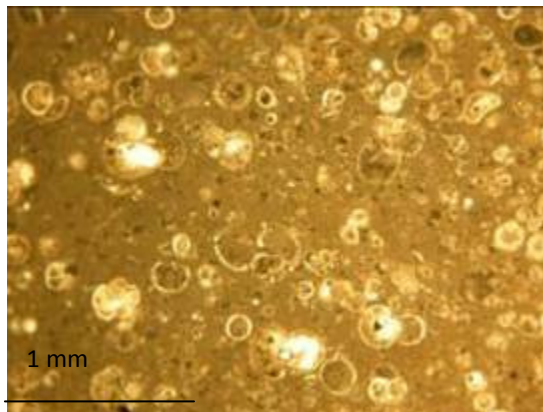


**Figure 2.41.** Thin-section photomicrograph of figure 38 (PPL, objective x4)

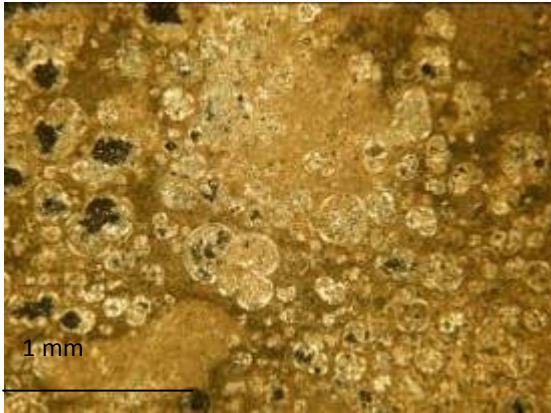


**Figure 2.42.** Thin-section photomicrograph of figurine 56 (XPL, objective x4)

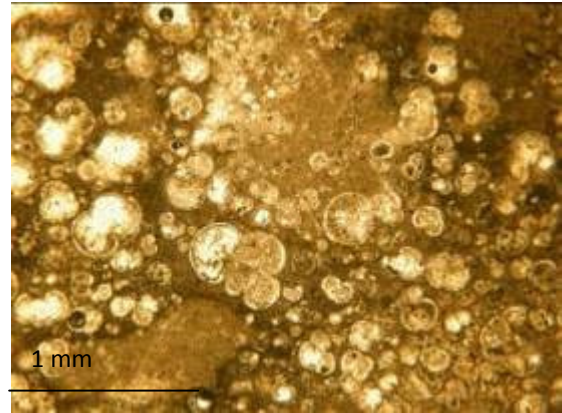


**Figure 2.43.** Thin-section photomicrograph of figurine 56 (PPL, objective x4)

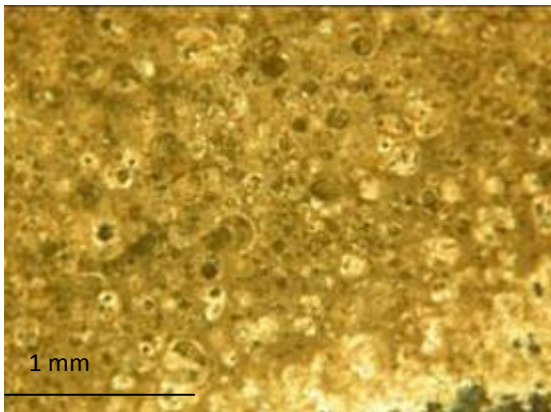


**Figure 2.44.** Thin-section photomicrograph of figurine 84 (XPL, objective x4)

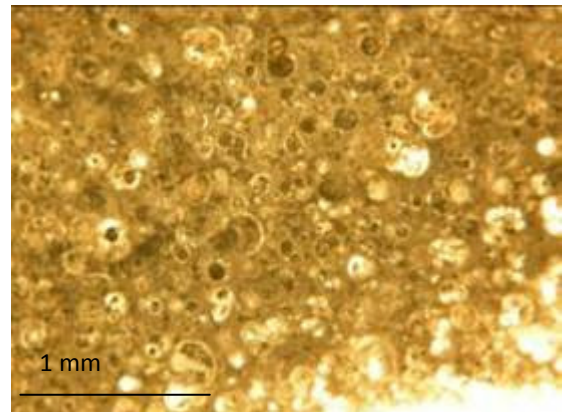


**Figure 2.45.** Thin-section photomicrograph of figurine 84 (PPL, objective x4)

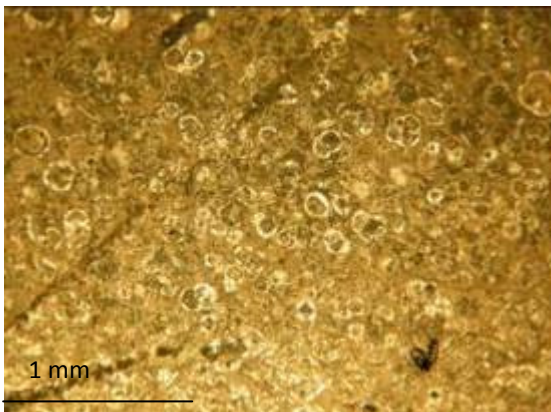


**Figure 2.46.** Thin-section photomicrograph of figurine 47 (XPL, objective x4)

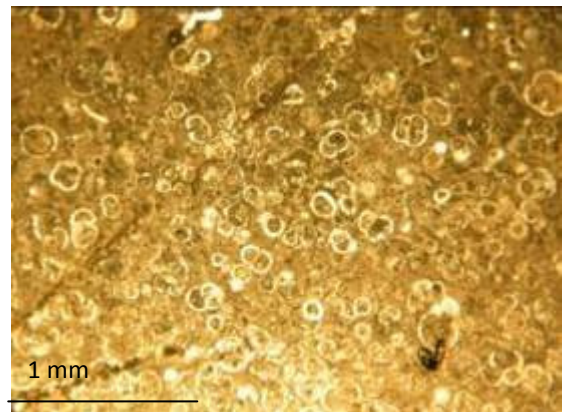


**Figure 2.47.** Thin-section photomicrograph of figurine 47 (PPL, objective x4)

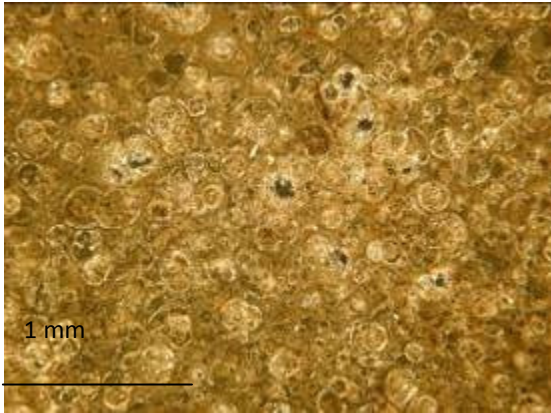


**Figure 2.48.** Thin-section photomicrograph of figurine 37 (XPL, objective x4)

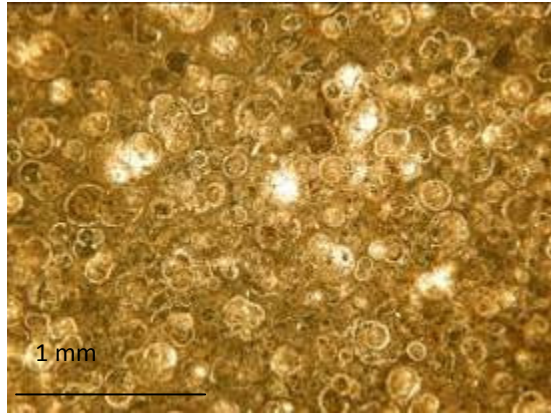


**Figure 2.49.** Thin-section photomicrograph of figurine 37 (PPL, objective x4)

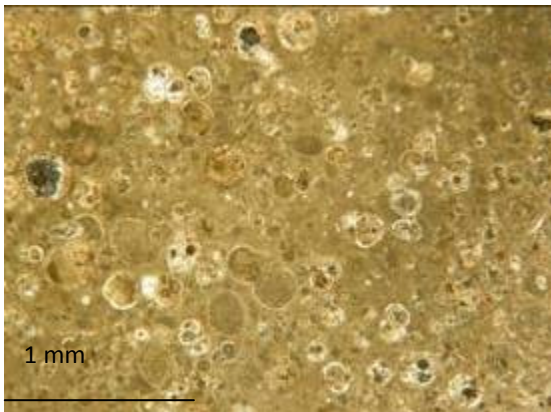


**Figure 2.50.** Thin-section photomicrograph of figurine 22 (XPL, objective x4)

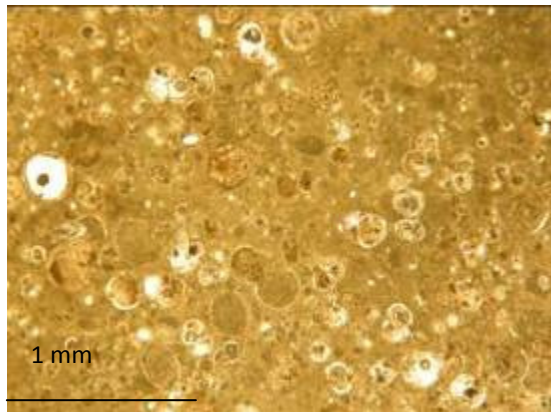


**Figure 2.51.** Thin-section photomicrograph of figurine 22 (PPL, objective x4)

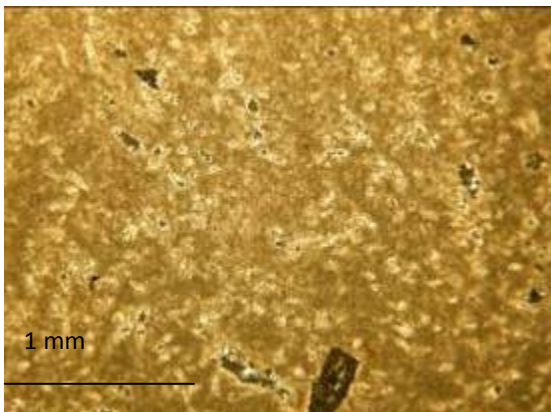


**Figure 2.52.** Thin-section photomicrograph of AKYA, Datça (XPL, objective x4)

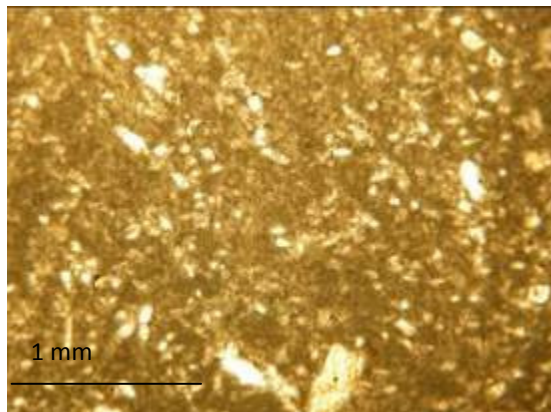


**Figure 2.53.** Thin-section photomicrograph of AKYA, Datça (PPL, objective x4)

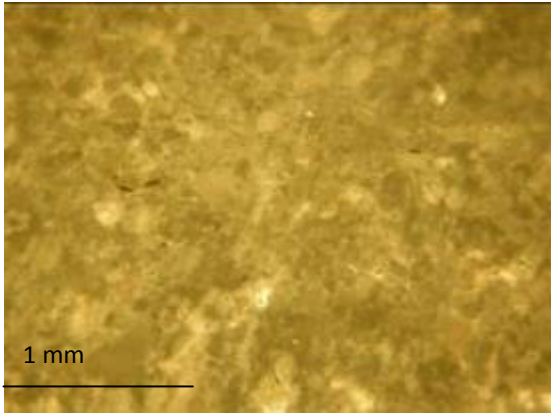


**Figure 2.54.** Thin-section photomicrograph of RZG, Datça (XPL, objective x4)

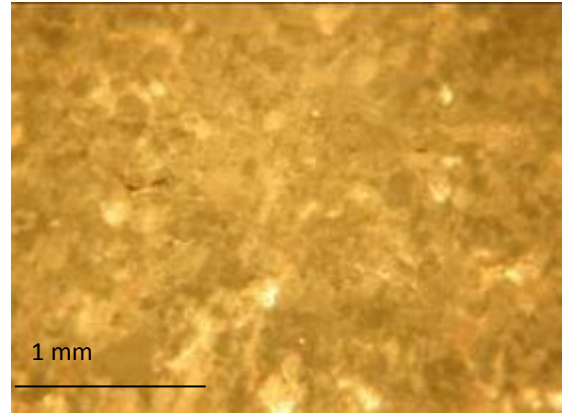


**Figure 2.55.** Thin-section photomicrograph of RZG, Datça (PPL, objective x4)

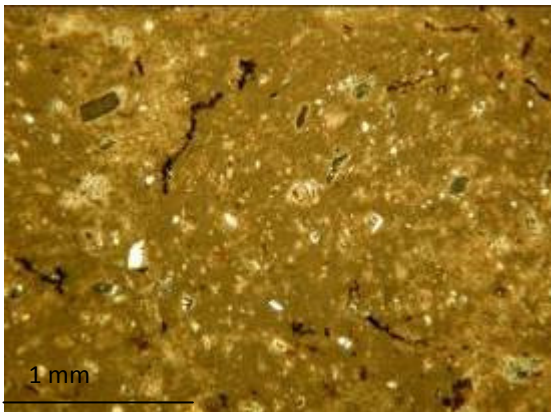


**Figure 2.56.** Thin-section photomicrograph of KRC, Datça (XPL, objective x4)

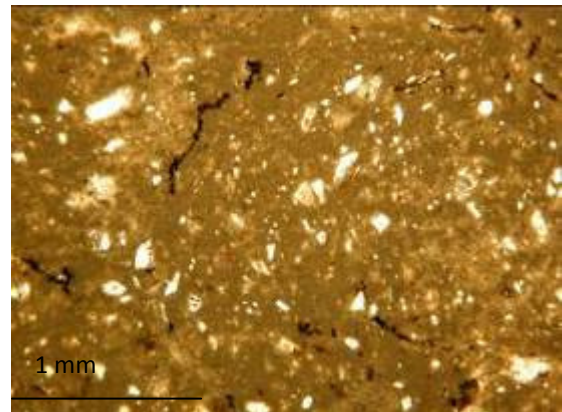


**Figure 2.57.** Thin-section photomicrograph of KRC, Datça (PPL, objective x4)

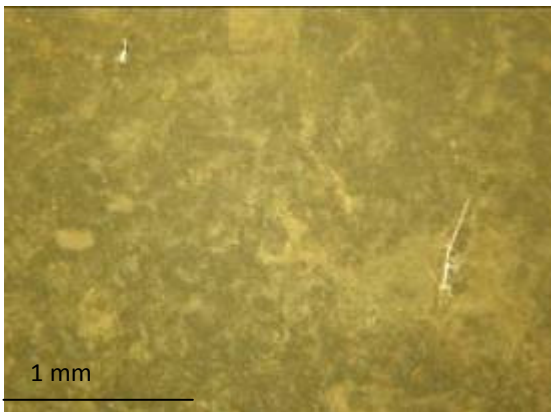


**Figure 2.58.** Thin-section photomicrograph of AKYB, Datça (XPL, objective x4)

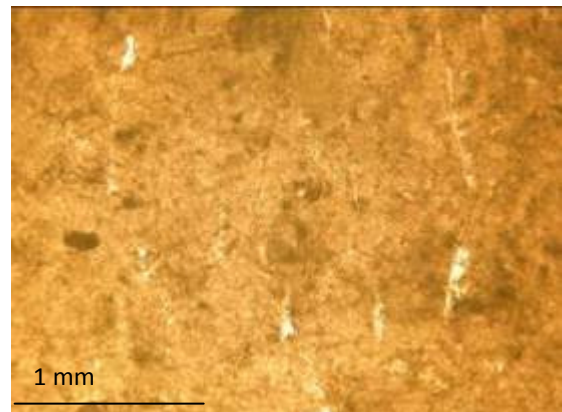


**Figure 2.59.** Thin-section photomicrograph of AKYB, Datça (PPL, objective x4)

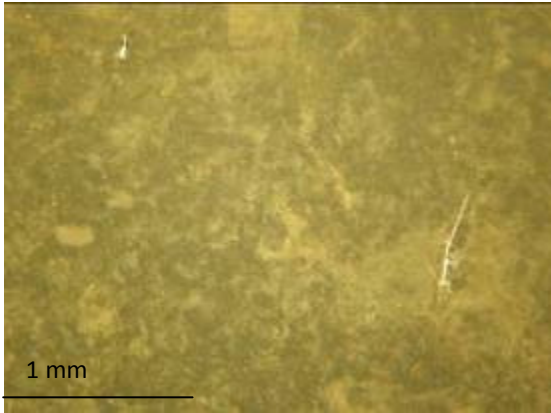


**Figure 2.60.** Thin-section photomicrograph of AKYC, Datça (XPL, objective x4)

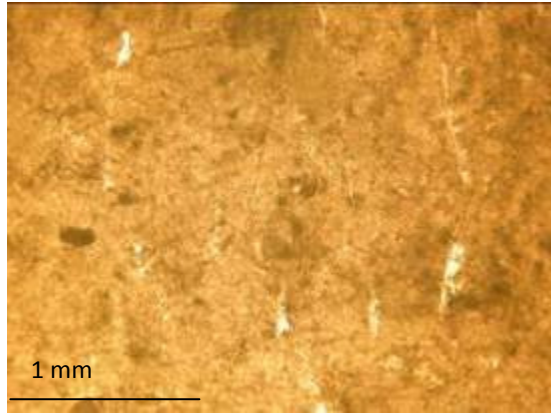


**Figure 2.61.** Thin-section photomicrograph of AKYC, Datça (PPL, objective x4)

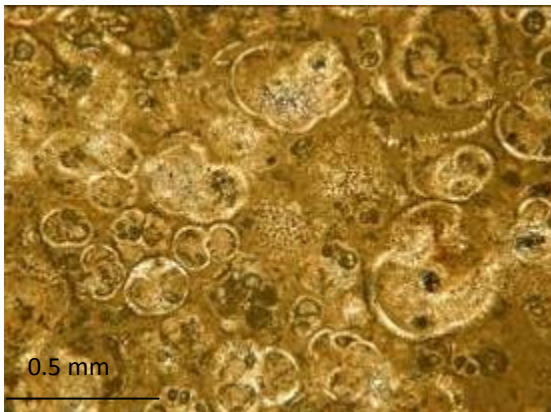


**Figure 2.62.** Thin-section photomicrograph of figurine 56 (XPL, objective x4)

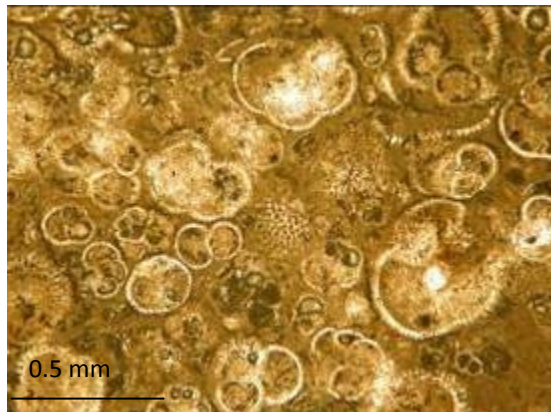


**Figure 2.63.** Thin-section photomicrograph of figurine 56 (PPL, objective x4)

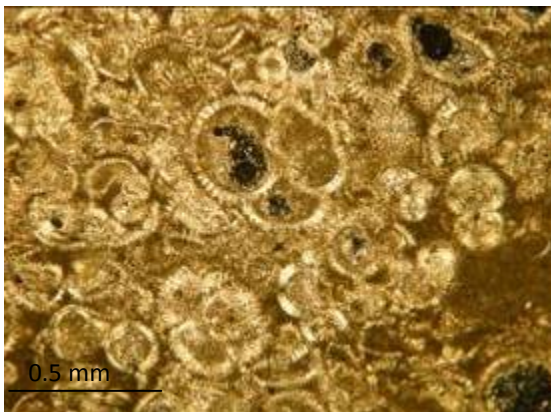


**Figure 2.64.** Thin-section photomicrograph of figurine 47 (XPL, objective x4)

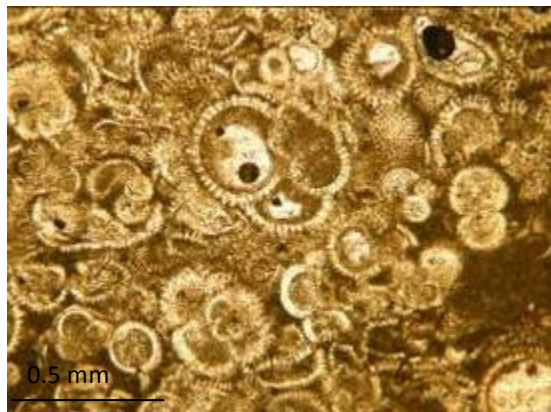


**Figure 2.65.** Thin-section photomicrograph of figurine 47 (PPL, objective x4)

## 2.6. X-ray Diffraction Analysis

In order to identify the mineral contents, geological samples some of the figurines were analyzed by X-Ray Diffraction (XRD). XRD traces of figurine samples were obtained at the Chemistry Department in METU by using Rigaku instrument operated at 40 kV /4 mA using CuK $\alpha$  radiation. XRD traces of some of the samples are given in Figures 2.66-2.100.

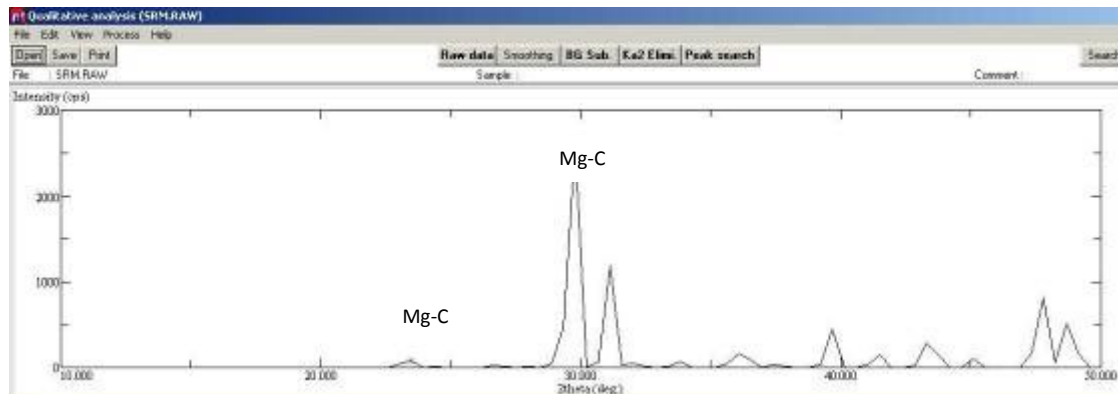


**Figure 2.66.** XRD plot for NIST 1d. Indicated signals correspond to d values of 3.78 and 2.99

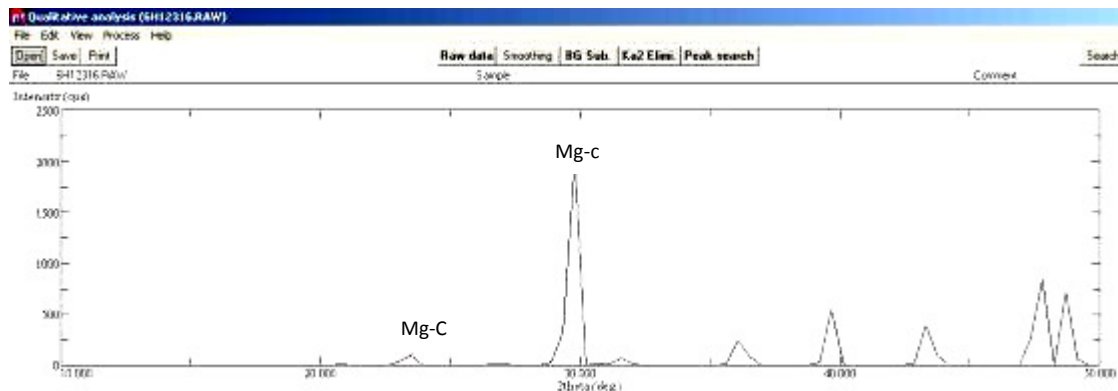


**Figure 2.67.** XRD plot for for figurine 4. Indicated signals correspond to d values of 3.78 and 2.99

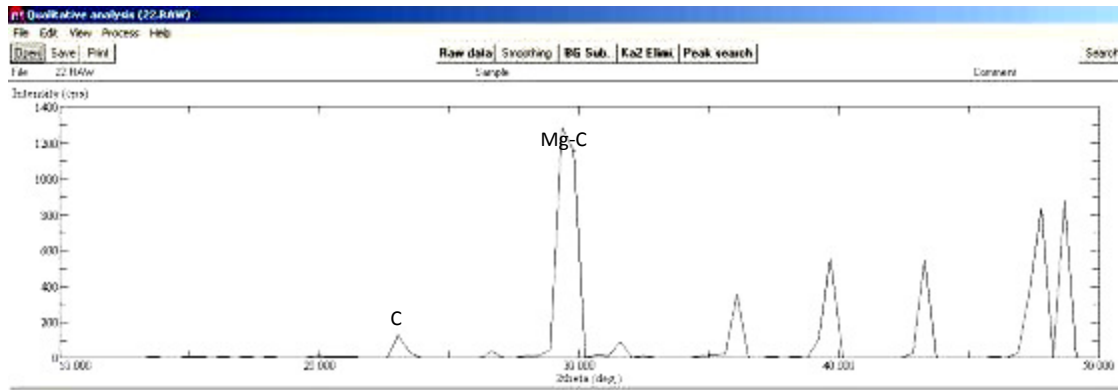


**Figure 2.68.** XRD plot for figurine 22. Indicated signals correspond to d values of 3.86, 2.99

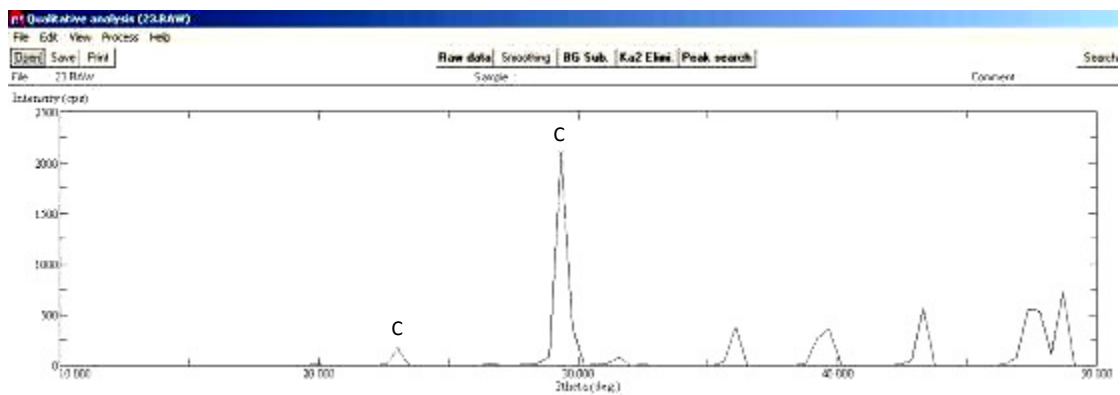


**Figure 2.69.** XRD plot for figurine 23. Indicated signals correspond to d values of 3.86, 3.04

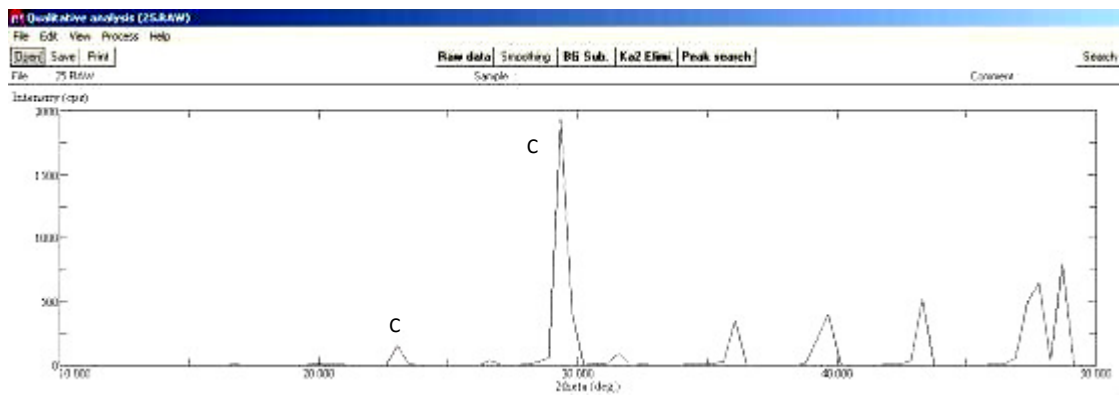


**Figure 2.70.** XRD plot for figurine 24. Indicated signals correspond to d values of 3.86, 3.04

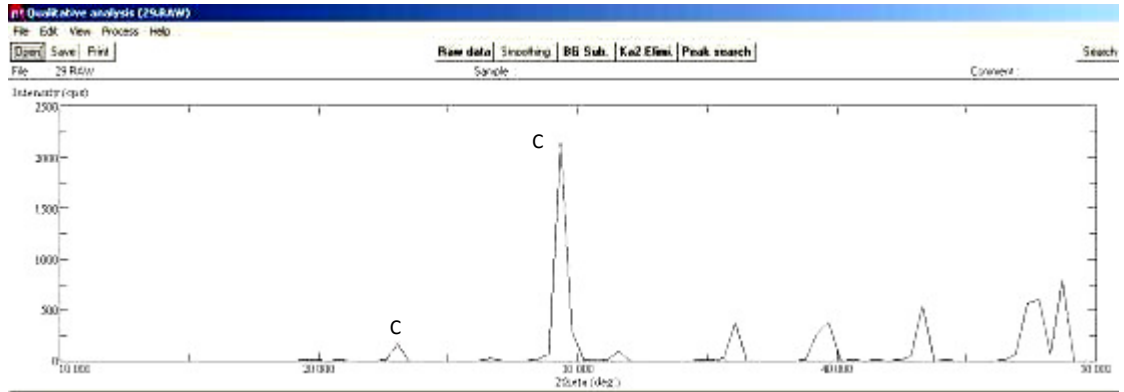


**Figure 2.71.** XRD plot for figurine 28. Indicated signals correspond to d values of 3.86, 3.04

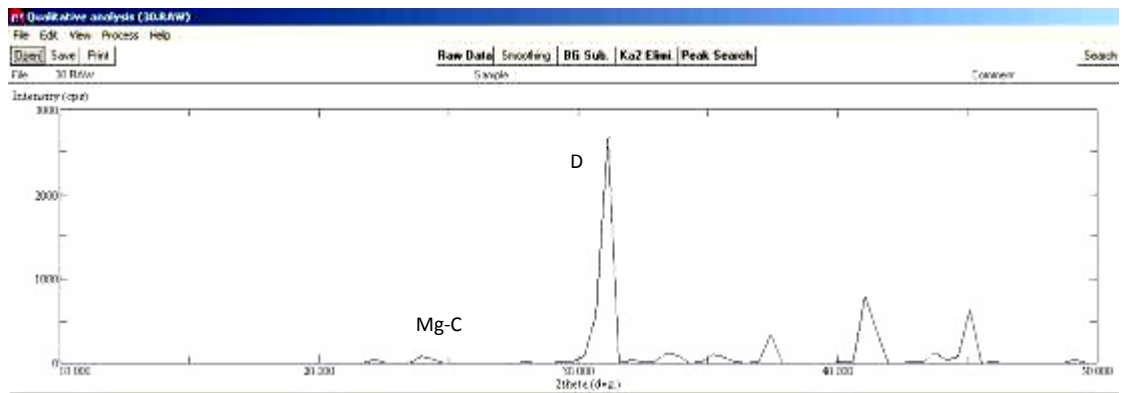


**Figure 2.72.** XRD plot for archaeological sample 30. Indicated signals correspond to d values of 3.78 and 2.88

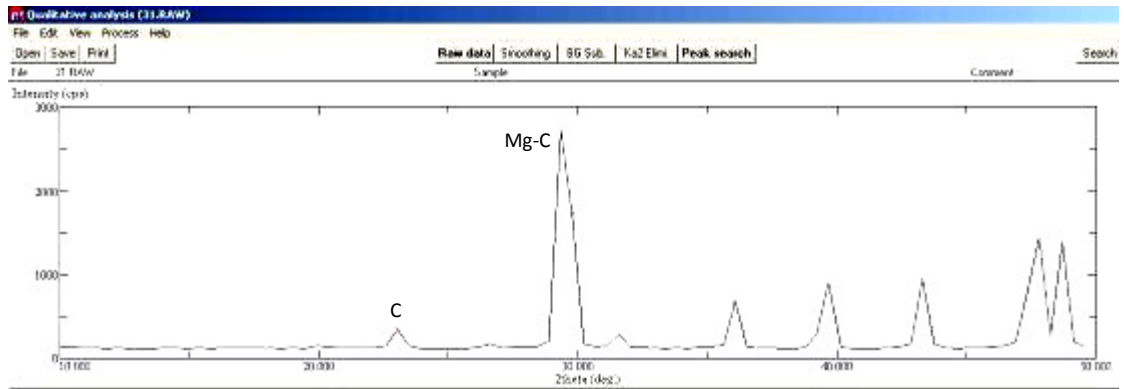


**Figure 2.73.** XRD plot for figurine 31. Indicated signals correspond to d values of 3.86, 2.99

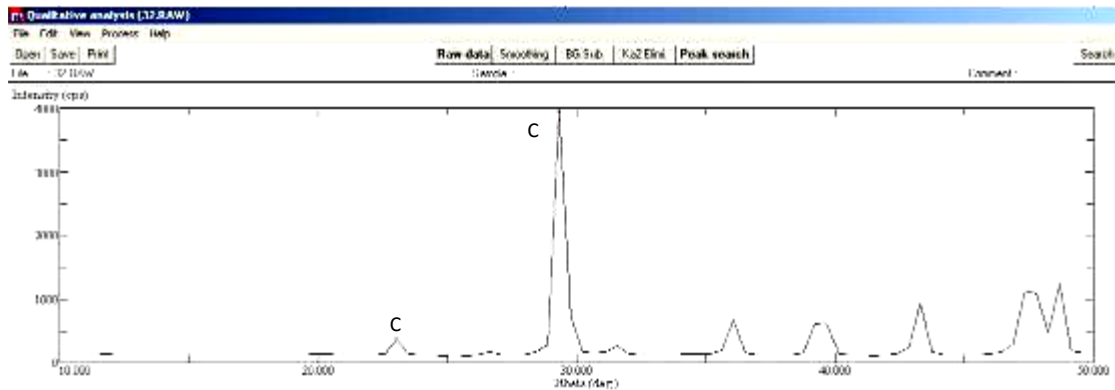


**Figure 2.74.** XRD plot for figurine 32. Indicated signals correspond to d values of d values 3.86, 3.04

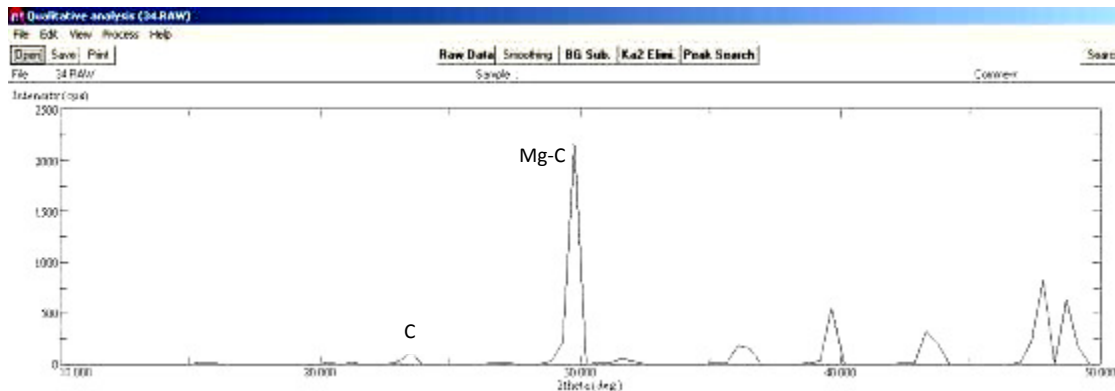


**Figure 2.75.** XRD plot for figurine 34. Indicated signals correspond to d values of 3.85 and 2.99

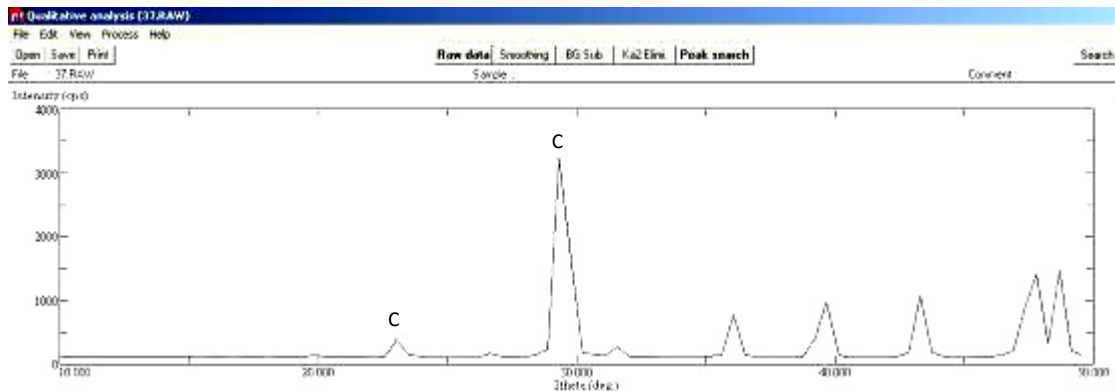


**Figure 2.76.** XRD plot for figurine 37. Indicated signals correspond to d values of 3.86, 3.04

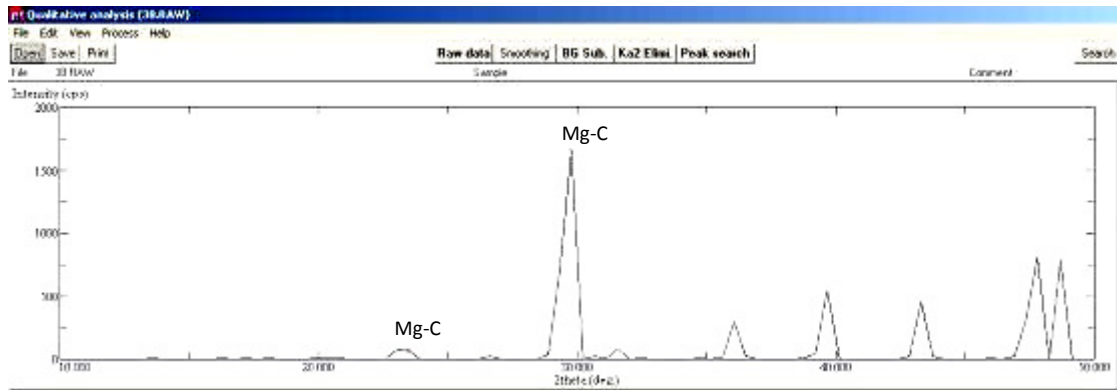


**Figure 2.77.** XRD plot for figurine 38. Indicated signals correspond to d values of d values 3.78, 2.99

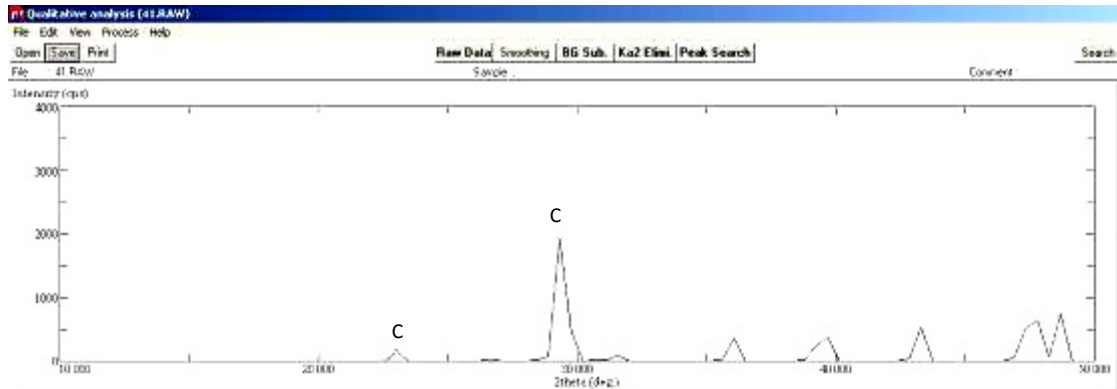


**Figure 2.78.** XRD plot for figurine 40. Indicated signals correspond to d values of 3.86, 3.04

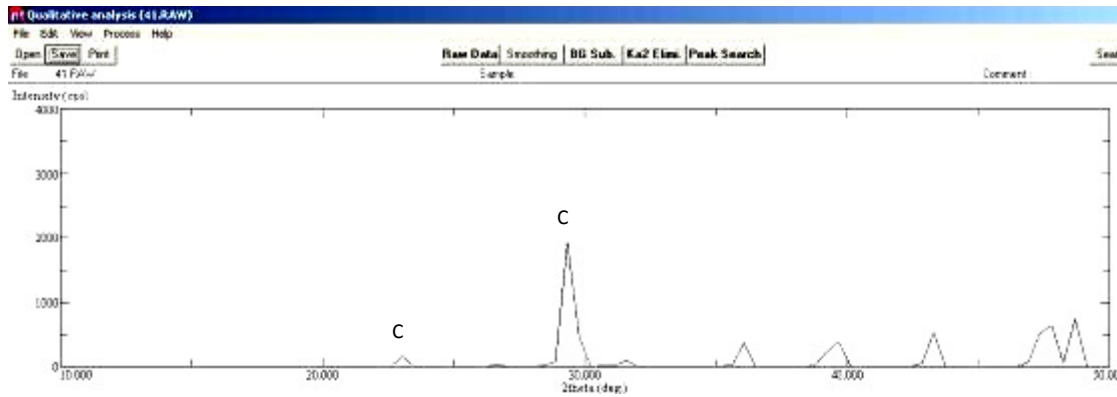


**Figure 2.79.** XRD plot for figurine 41. Indicated signals correspond to d values of 3.86 and 3.04

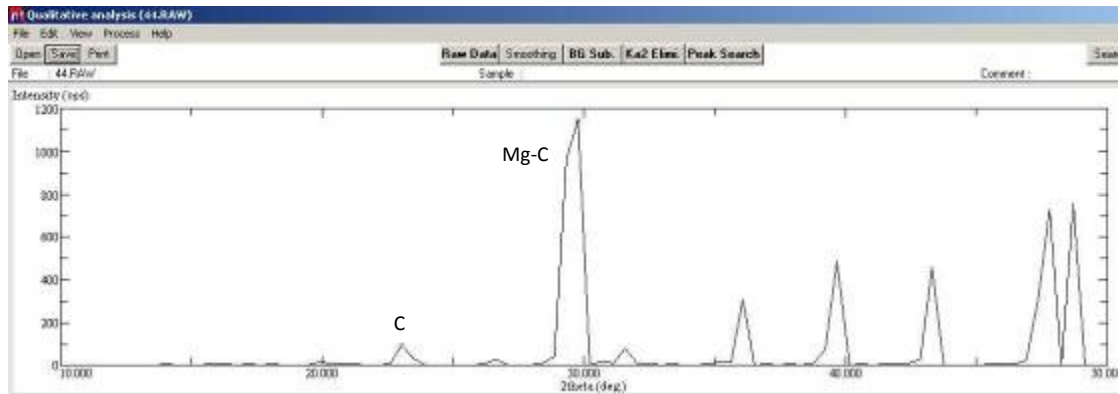


Figure 2.80. XRD plot for figurine 44. Indicated signals correspond to d values of 3.86 and 2.99

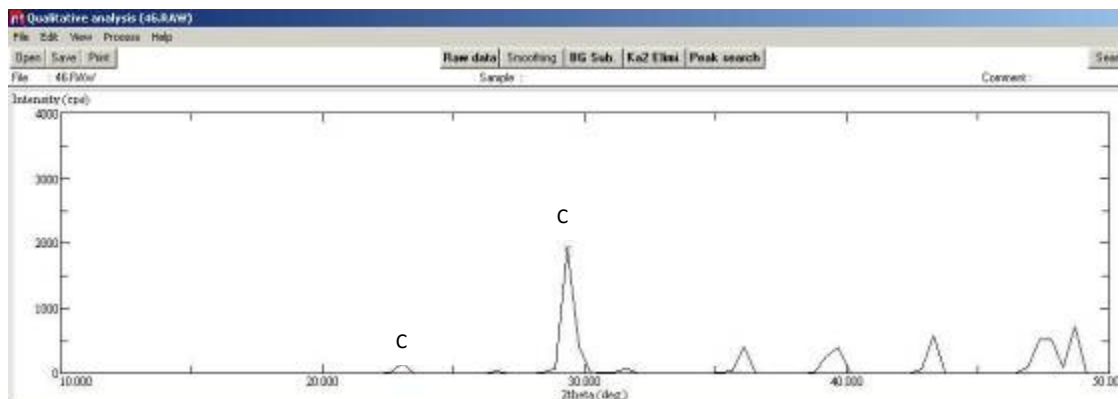


Figure 2.81. XRD plot for figurine 46. Indicated signals correspond to d values of 3.86 and 3.04

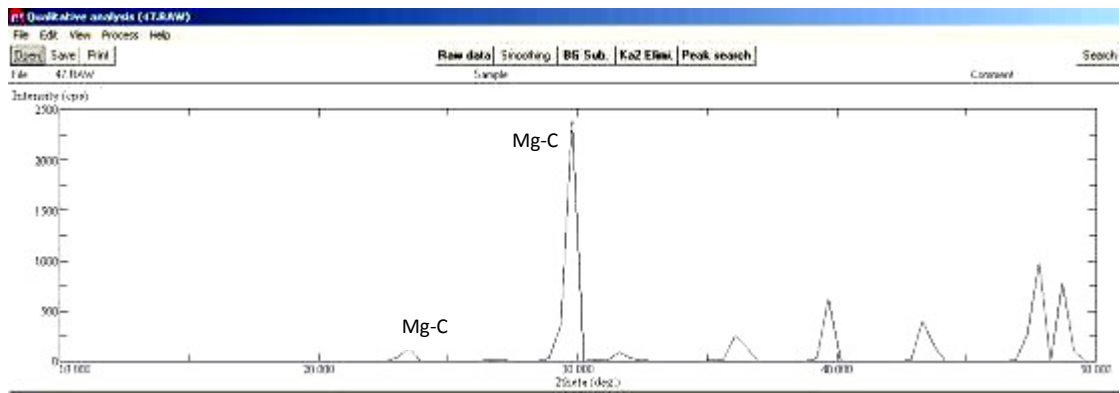


Figure 2.82. XRD plot for figurine 47. Indicated signals correspond to d values of 3.78, 2.99

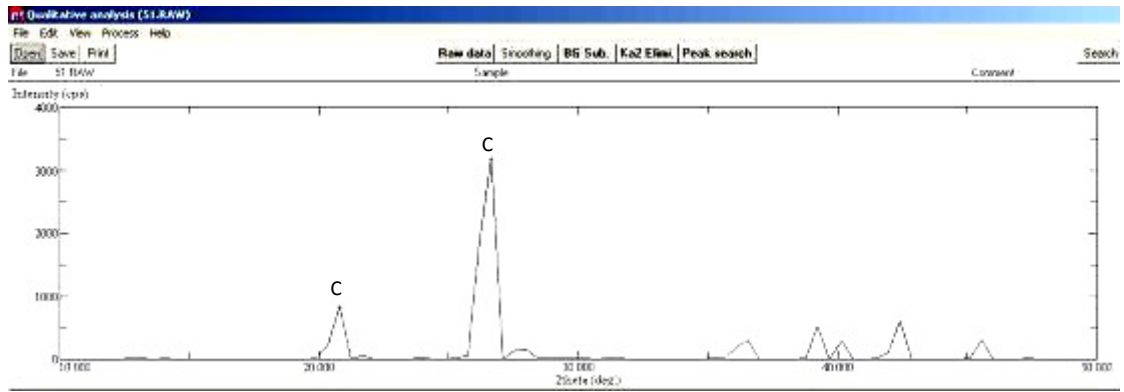


Figure 2.83. XRD plot for figurine 51. Indicated signals correspond to d values of 3.86 and 3.34

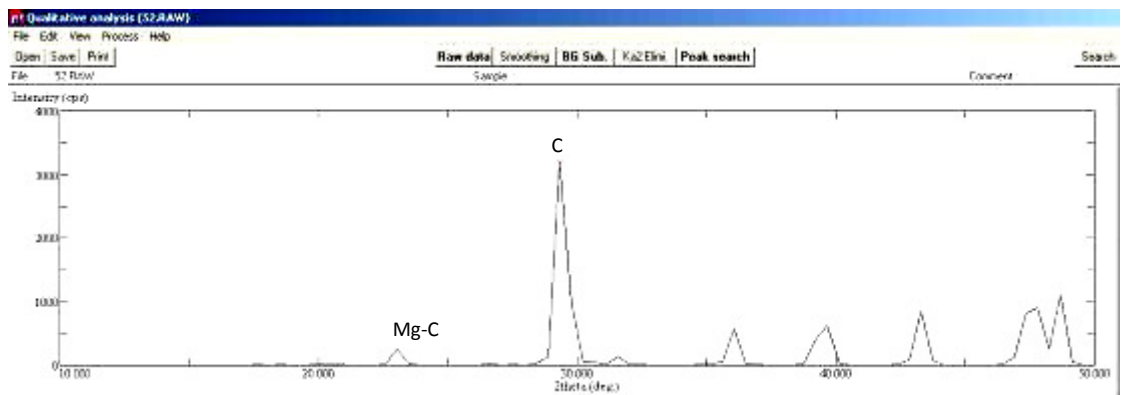


Figure 2.84. XRD plot for figurine 52. Indicated signals correspond to d values of 3.78 and 3.04

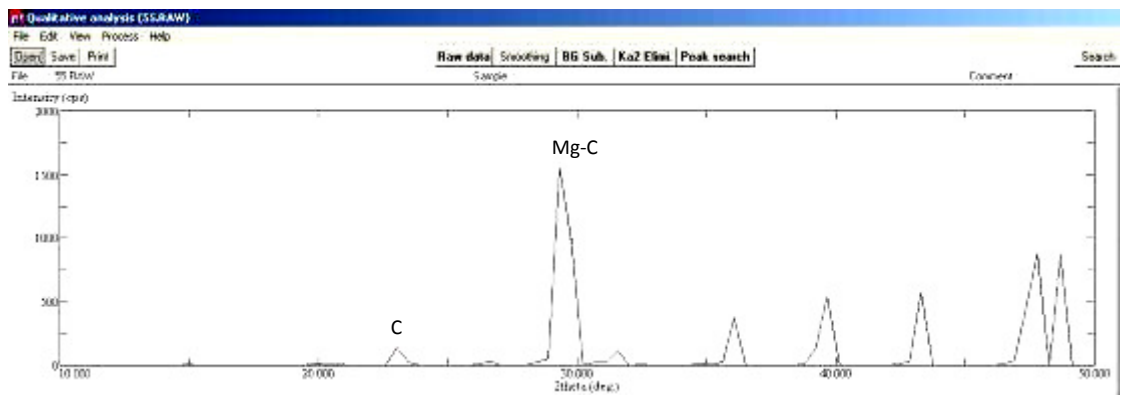
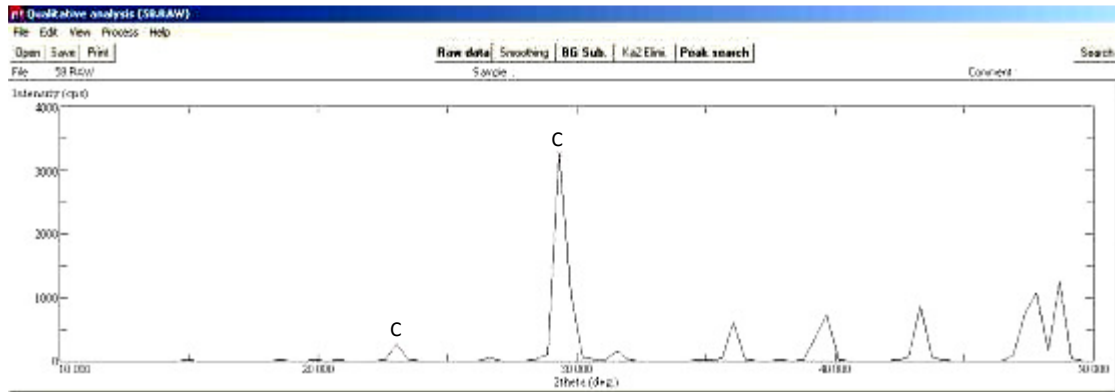
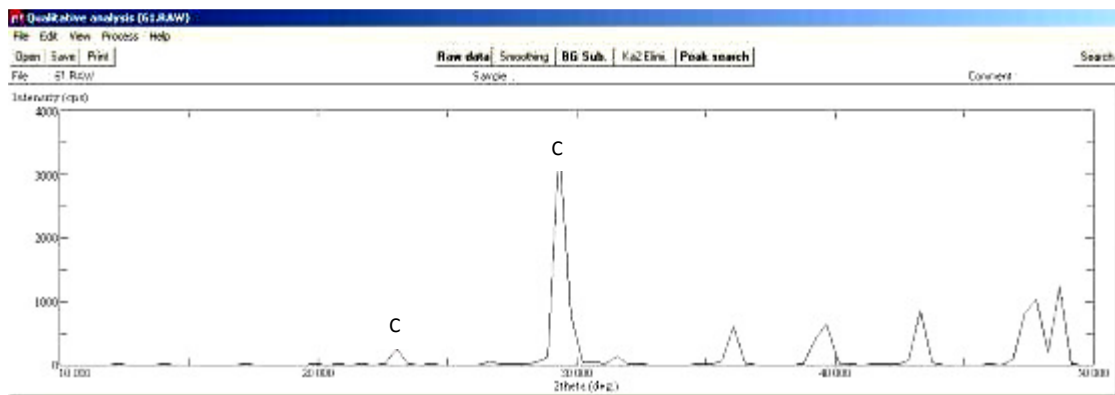


Figure 2.85. XRD plot for figurine 55. Indicated signals correspond to d values of 3.86, 2.99



**Figure 2.86.** XRD plot for figurine 58. Indicated signals correspond to d values of 3.86, 3.04



**Figure 2.87.** XRD plot for figurine 61. Indicated signals correspond to d values of 3.86, 3.04

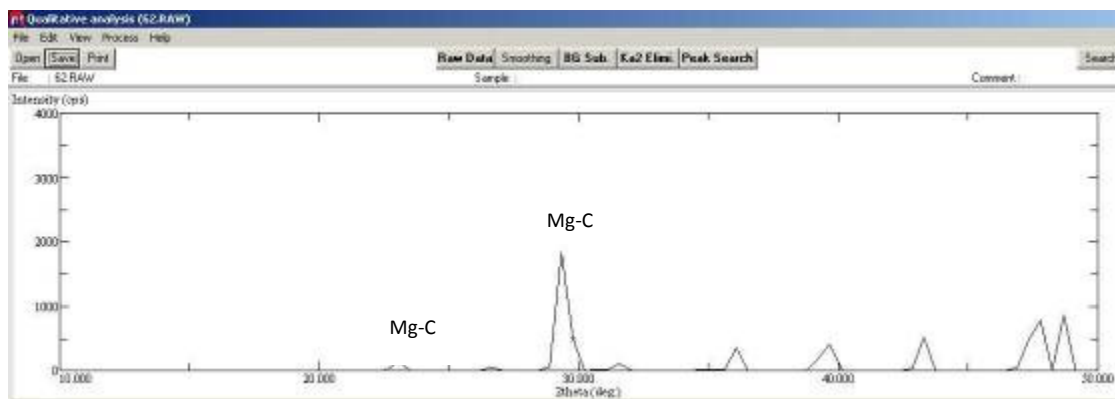


**Figure 2.88.** XRD plot for figurine 62. Indicated signals correspond to d values of 3.93 and 2.99

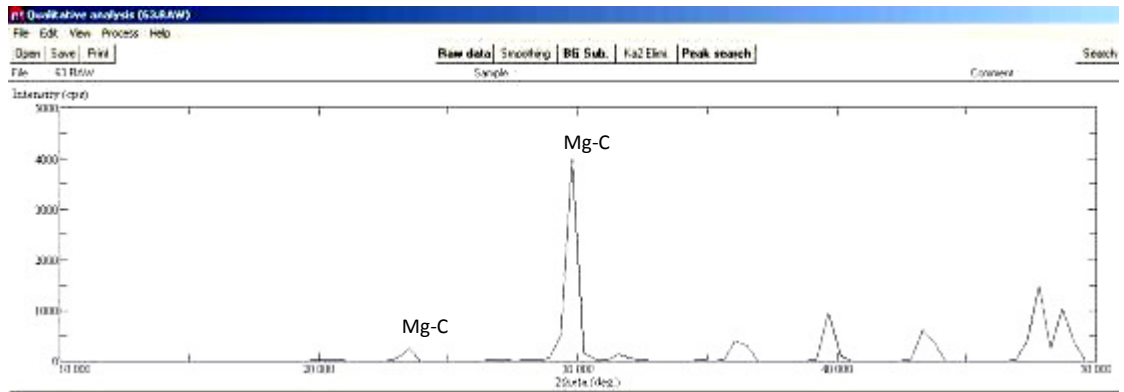


**Figure 2.89.** XRD plot for figurine 63. Indicated signals correspond to d values of 3.78, 2.99, and 2.08

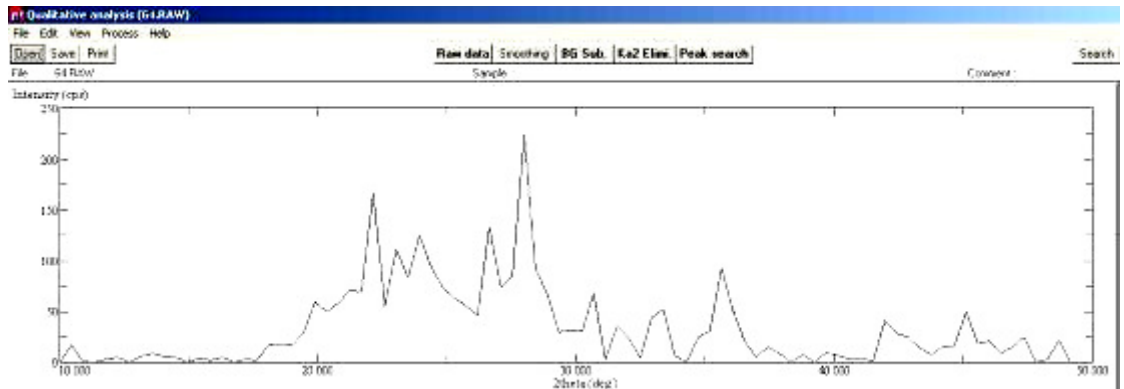


**Figure 2.90.** XRD plot for figurine 64. Indicated signals correspond to d values 2.18

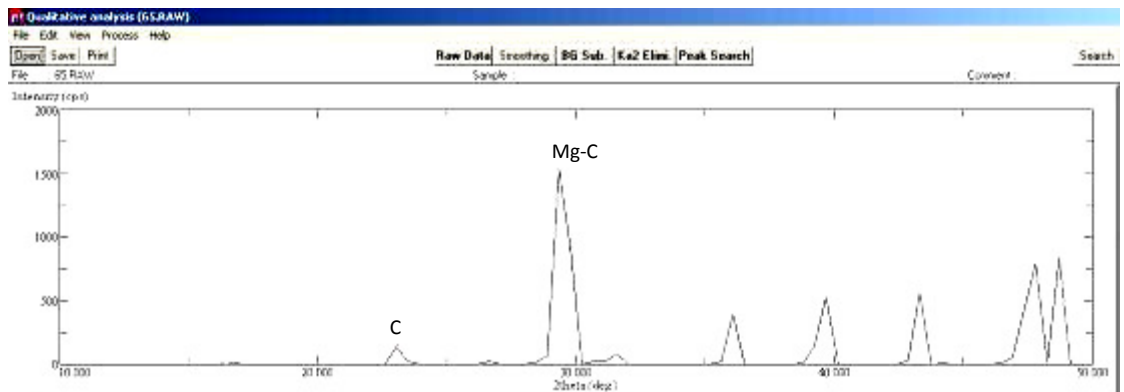


**Figure 2.91.** XRD plot for figurine 65. Indicated signals correspond to d values of 3.86 and 2.99

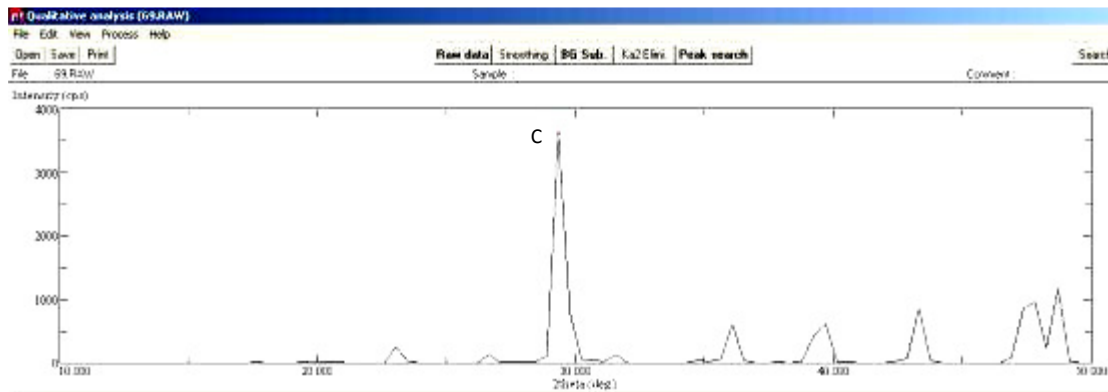


Figure 2.92. XRD plot for figurine 69. Indicated signals correspond to d values of 3.04

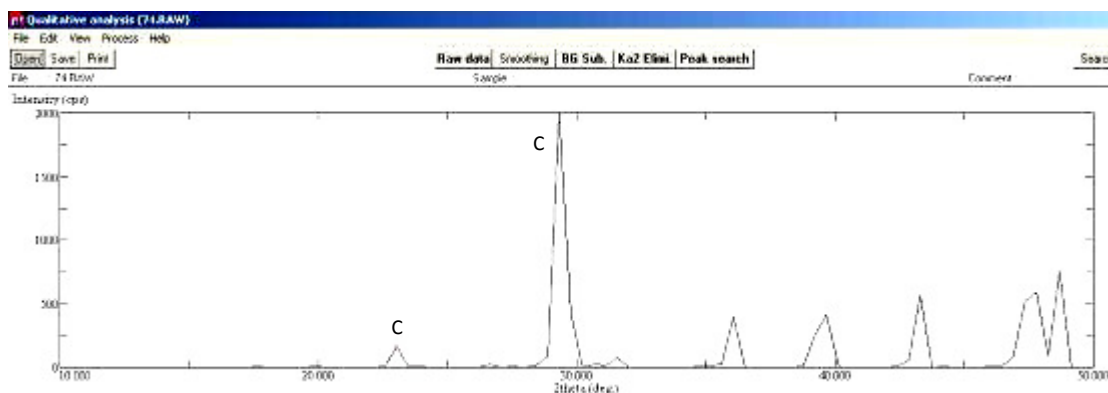


Figure 2.93. XRD plot for figurine 74. Indicated signals correspond to d values of 3.86, 3.04

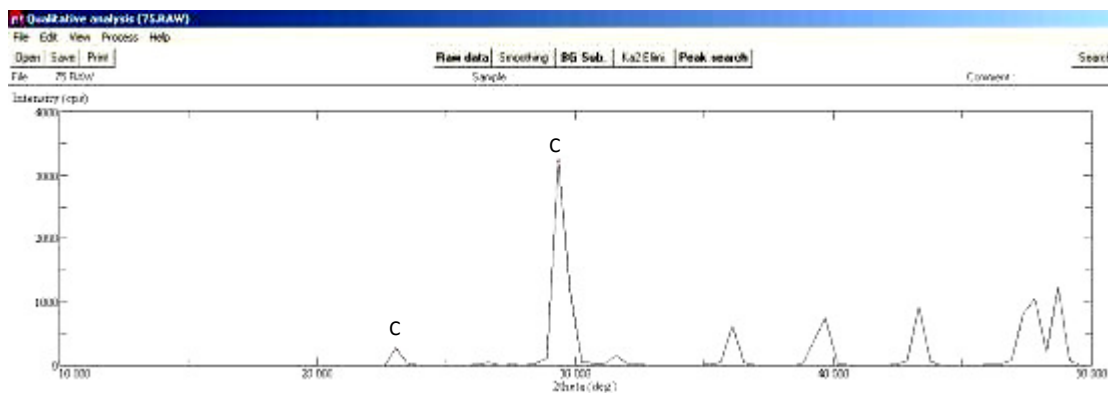
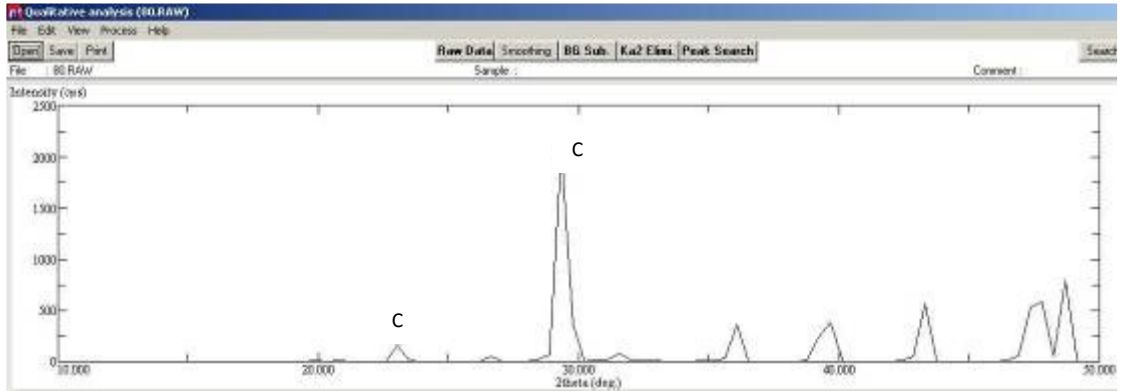
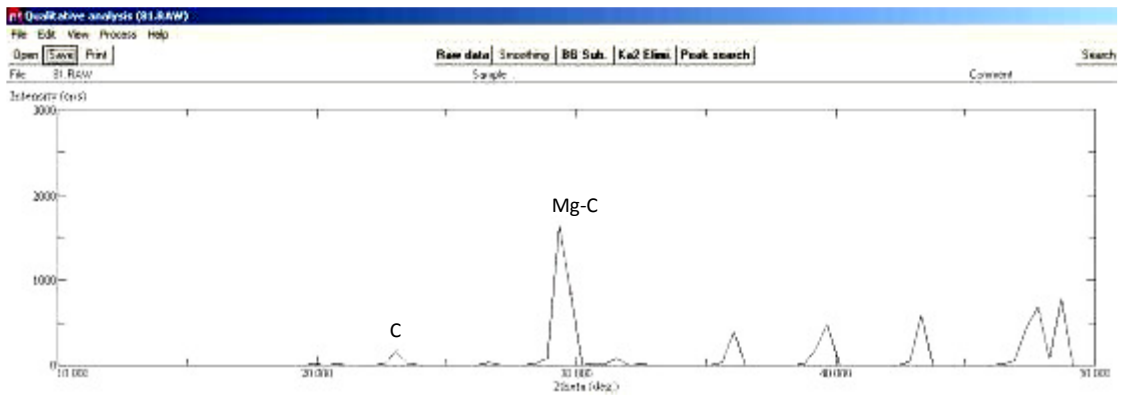


Figure 2.94. XRD plot for figurine 75. Indicated signals correspond to d values of 3.86, 3.04



**Figure 2.95.** XRD plot for figurine 80. Indicated signals correspond to d values of 3.86 and 3.04



**Figure 2.96.** XRD plot for figurine 81. Indicated signals correspond to d values of 3.86, and 2.99

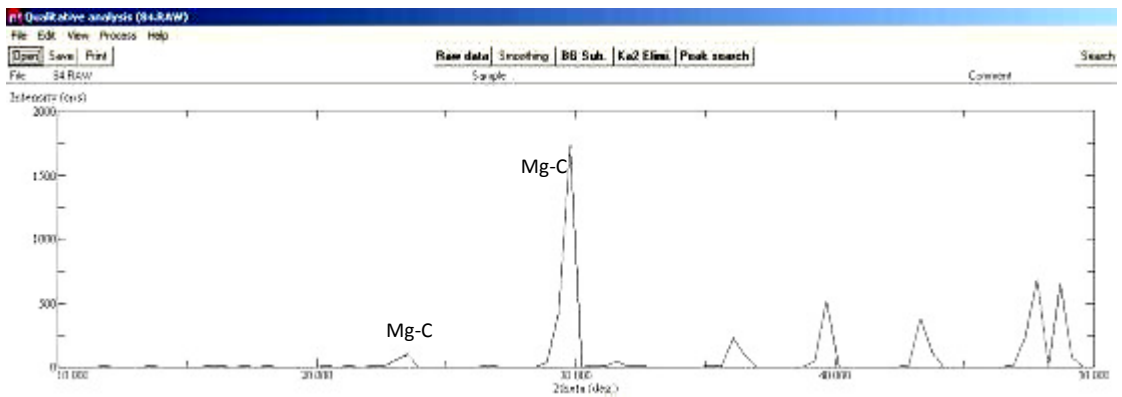


**Figure 2.97.** XRD plot for figurine 84. Indicated signals correspond to d values of 3.78 and 2.99

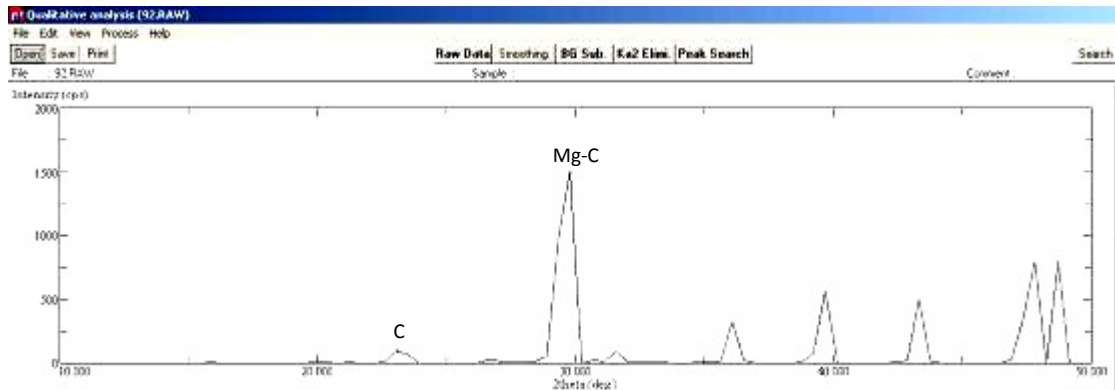


Figure 2.98. XRD plot for figurine 92. Indicated signals correspond to d values of 3.86 and 2.99

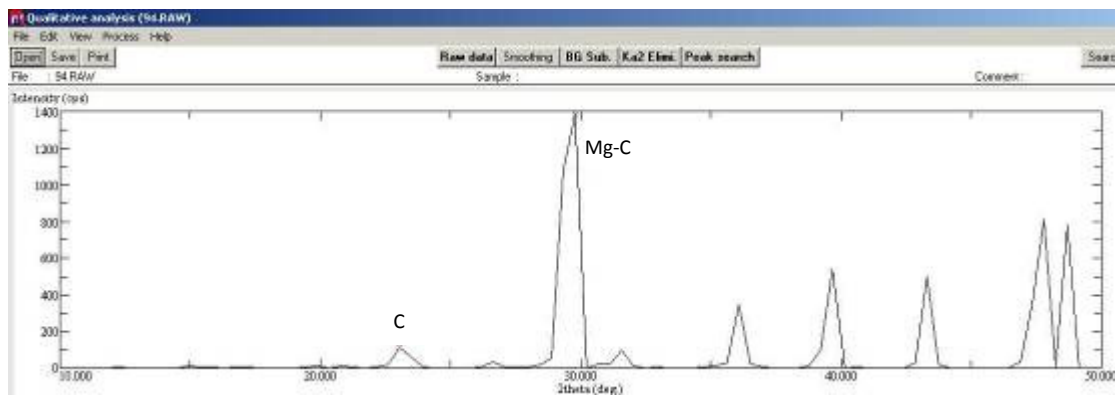


Figure 2.99. XRD plot for figurine 94. Indicated signals correspond to d values of 3.86 and 2.99

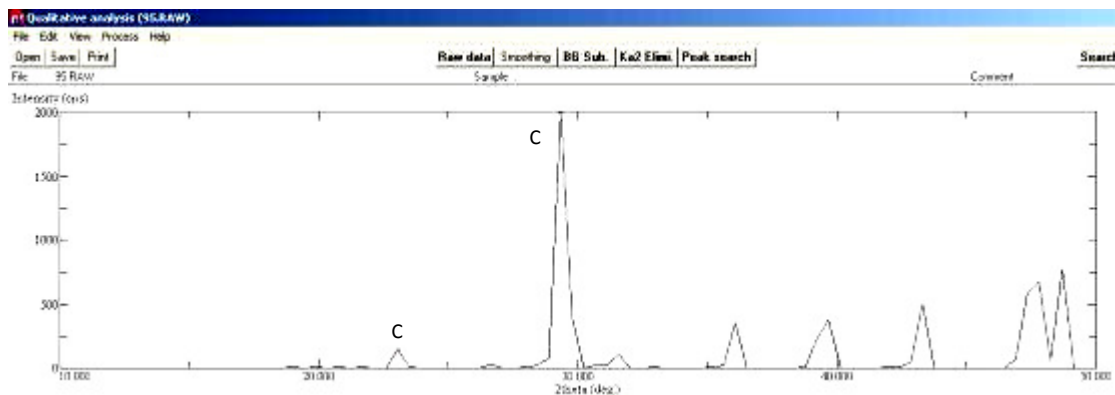


Figure 2.100. XRD plot for figurine 95. Indicated signals correspond to d values of 3.86, 3.04

## CHAPTER 3

### RESULTS AND DISCUSSION

#### 3.1 Optimization of ICP-OES Conditions

Optimizations were done for Rf power, coolant gas flow rate, and pump rate since these parameters are the most effective ones for ICP – OES analysis. Optimum values given in manual of instrument are used for other parameters such as auxiliary gas flow and nebulizer flow rate. RF power of 1.1 Kw was kept during the analyses to maintain the long term stability, robustness, of plasma. The operating parameters of the instrument throughout the study are given in Table 3.1.

**Table 3.1.** Plasma Conditions for ICP – OES, Leeman DRE

Rf Power	1.1 kW
Nebulizer Gas	50 Psi
Auxiliary Gas	0.5 L/min
Coolant Gas	18 L/min
Pump Rate	1.2 L/min

#### 3.2 Optimization of ICP-MS Conditions

ICP-MS conditions were optimized in order to improve the sensitivity of ICP-MS for Cr, Y, REEs and Hf determination. For this aim, a mixture containing 100.0 ng/mL standard solution of each of these elements prepared from their standard solutions was used. In the optimization procedure, one parameter was optimized while others were kept constant. In the first part of optimization, estimated parameters were selected and then optimizations were repeated until finding the best results. Sensitivity of system was checked before measurements. In the case of any significant reduction in the sensitivity, ICP-MS parameters were re-optimized. Any reduction of sensitivity higher than 30% warranted a new optimization; for smaller variations recalibration was used. Baseline of the Cr, Y, REEs and Hf varied in the case of changing in ICP-MS parameters. Throughout the all studies, cones of ICP-MS system were periodically cleaned to eliminate clogging possibility.

#### 3.3 Results of Analysis of Reference Materials

Results of external calibration (EC) using acid mixture 1 and MW program A along with standard addition methods (SA) using different acid mixtures and microwave heating programs for NIST 1d Argillaceous standard reference material are given in Table 3.2 and Table 3.3. Acid mixture B and microwave program 2 is considered to be better Table 3.3. Then standard addition before microwave digestion was applied to this combination. The results of obtained by this method and results obtained by fusion method are also given in Table 3.3.

**Table 3.2.** Results for NIST 1d Argillaceous using ICP-OES and external calibration and standard addition calibration.

mean ± standard deviation, w/w %				
Constituent	Found, acid mixture A, microwave program, EC	Found, acid mixture A, microwave program 1, SA	Found, acid mixture B, microwave program 1, SA	Certified Value
MgO	0.164±0.008	0.337±0.012	0.276±0.008	0.301± 0.010
Fe <sub>2</sub> O <sub>3</sub>	0.244±0.019	0.3067±0.0072	0.3180±0.0085	0.3191± 0.0068

**Table 3.3.** Results for NIST 1d Argillaceous using ICP-OES and standard addition calibration.

mean ± standard deviation, w/w %				
Constituent	Found, acid mixture B, microwave program 2, SA after digestion	Found, acid mixture B, microwave program 2 standard addition before microwave digestion	Found, Fusion, SA before fusion	Certified Value
MgO	0.270±0.008	0.306±0.005	0.299 ± 0.006	0.301± 0.010
Fe <sub>2</sub> O <sub>3</sub>	0.3124±0.0079	0.3137±0.0091	0.3211± 0.0041	0.3191± 0.0068

Mn, Sr, and Ba were determined by direct reading using ICP-OES. The measurements were quantified by external calibration. Results for NIST 1d Argillaceous, using acid mixture B and microwave program 2 are given in Table 3.4.

**Table 3.4.** Results for NIST 1d Argillaceous using ICP-OES and external calibration

mean $\pm$ standard deviation, w/w %		
Constituent	Found	Certified Value
<b>SrO</b>	0.0296 $\pm$ 0.0010	0.0303 $\pm$ 0.0010
<b>BaO</b>	0.0028 $\pm$ 0.0002	0.0033 $\pm$ 0.0011
<b>Mn</b>	0.0207 $\pm$ 0.0007	0.0209 $\pm$ 0.0005

Cr, Y, Nb, Hf and REEs were determined by ICP-MS. The accuracy of digestion method and instrument parameters were tested using standard reference material NCS DC 73306 carbonate rock. The results for NCS DC 73306 are given in Table 3.5.

**Table 3.5.** Results for NCS DC 73306 carbonate rock by ICP-MS and standard additions calibration

mean $\pm$ standard deviation, mg/kg		
Constituent	Results found, standard addition before microwave digestion	Certified Value
Cr	26.16 $\pm$ 3.17	32 $\pm$ 8
Y	8.23 $\pm$ 2.04	9.1 $\pm$ 2.5
Nb	7.10 $\pm$ 0.44	6.6 $\pm$ 2.4
Hf	1.75 $\pm$ 0.05	1.8 $\pm$ 0.3
La	12.03 $\pm$ 1.15	15 $\pm$ 5
Ce	25.56 $\pm$ 0.4	25 $\pm$ 4
Nd	12.87 $\pm$ 0.53	12.0 $\pm$ 1.4
Sm	2.4 $\pm$ 0.09	2.4 $\pm$ 0.3

Table 3.5 continued		
Eu	0.49±0.09	0.51±0.07
Gd	2.08±0.42	1.9±0.2
Er	1.28±0.1	(1.1)
Ho	0.38±0.01	0.33±0.06
Yb	1.06±0.05	0.90±0.16
Lu	0.10±0.01	0.14±0.04

### 3.4 Evaluation of Different Dissolution Procedures

Although fusion with lithium metaborate-lithium tetraborate is generally found to be the most suitable method for obsidian samples, this dissolution technique has considerable disadvantages especially in ICP-MS applications. One of them is the possible contamination from flux material that would be used in large amounts and from the crucibles. Other one is the level of the total dissolved solids in the final solution should be around 0.1-0.2 % for ICP-MS in order to keep the nebulizer or cones clean and minimize the signal drift, whereas using fusion dissolution technique would increase dissolved solids in the solution [68]. Because of that fusion technique requires further dilution which would restrict the number of elements to be determined. Therefore the most efficient dissolution of carbonate rock by acid mixture and microwave heating was aimed in this thesis. However, both dissolution methods were performed for SRM's in order to make comparisons. It was found that the results for fusion and microwave digestion methods were close as given in Table 3.3.

For microwave digestion, external calibration and standard addition methods were applied in order to compare. By using different acid mixtures and microwave programs, most appropriate dissolution procedure is decided as acid mixture B using microwave program 2 with standard addition method as given in Tables 3.2. and 3.3. The results of standard addition method were also improved by applying this method before microwave digestion as given in Table 3.3.

### 3.5 Matrix Factor

In order to analyze the real samples, a different approach was applied for practical reasons. Geological samples were collected from 10 different locations. From each location, 5 samples were taken in average. In other words, there are too many geological samples; therefore, there are problems in application of standard additions. The amounts of solid samples for archaeological samples were very limited and not sufficient for many cases to apply 4-point standard addition method.

Since the standard reference materials NIST 1d and NCS DC 73306 carbonate rock have similar matrices with the real samples, the difference in the results found by both direct reading and standard addition method for each element was determined as a correction factor; this was called *matrix factor*. For instance, when La was determined in NCS DC 73306 by external calibration, the result was 5.73 mg/kg. The La concentration in the same standard reference material was found 12.03 mg/kg using standard additions calibration. So, the correct result for La concentration is 2.1 times of the result found by direct reading. Regarding to the real samples, it

is safe to assume that 2.1 could be used as the *matrix factor* for the La result obtained from external calibration. Therefore, all the samples were analyzed by direct reading and the results were corrected using correction factors given in Table 3.6.

**Table 3.6.** Matrix factor the elements for which standard additions calibration was used.

<b>Cr</b>	<b>Y</b>	<b>Nb</b>	<b>Hf</b>	<b>La</b>	<b>Ce</b>	<b>Nd</b>	<b>Sm</b>
4.3	2.8	1.5	1.2	2.1	2.3	2.3	2.0
<b>Eu</b>	<b>Gd</b>	<b>Ho</b>	<b>Er</b>	<b>Yb</b>	<b>Lu</b>	<b>Mg</b>	<b>Fe</b>
2.5	2.0	3.3	2.0	2.2	2.3	1.5	1.5

### 3.6 Results for Chemical Analysis of Samples

Eighty-five figurine samples and ten different geological samples were dissolved in microwave oven according to above-mentioned procedures Chapter 2.4 and all were analyzed with ICP-OES for Mg, Fe, Ba, Sr, Mn and with ICP-MS for Cr, Y, Nb, Hf and REEs. Results by direct reading and corrected results for major and trace elements of geological samples and some of the figurines are given in Table 3.7. Corrected results for Cr, Nb, REE and Hf of geological samples and some of the figurines are given in Tables 3.8. and 3.9. The rest of the results for the element determined by ICP-OES and ICP-MS are given in Appendix B and C.

**Table 3.7.** Results of geological and some archaeological samples using ICP-OES. Mg, Fe by standard additions and Mn, Sr, Ba by external calibration

<b>Constituent</b>					
<b>Samples</b>	<b>MgO %</b>	<b>Fe<sub>2</sub>O<sub>3</sub> %</b>	<b>Mn mg/kg</b>	<b>Sr mg/kg</b>	<b>Ba mg/kg</b>
<b>AKYA (n=6)</b>	3.32±0.11	0.57±0.06	715±31	200±23	6.91±0.36
<b>AKYB (n=7)</b>	3.46±0.12	0.30±0.04	399±27	257±27	11.5±1.01
<b>AKYC (n=8)</b>	3.24±0.17	0.30±0.04	271±25	247±25	17.4±1.24
<b>KRC (n=6)</b>	4.55±0.26	2.06±0.09	864±7	158±20	33.9±4.04
<b>RZG(n=4)</b>	10.32±0.94	3.59±0.10	711±37	203±27	62.8±1.31
<b>K1 (n=3)</b>	0.60±0.02	0.57±0.01	97.9±1.60	628±31	467±2.34
<b>K2(n=3)</b>	0.84±0.04	1.63±0.04	171±4.48	915±76	671±3.43

**Table 3.7 continued**

<b>Samples</b>	<b>MgO %</b>	<b>Fe<sub>2</sub>O<sub>3</sub> %</b>	<b>Mn mg/kg</b>	<b>Sr mg/kg</b>	<b>Ba mg/kg</b>
<b>K3-1(n=2)</b>	0.68±0.03	0.28±0.01	102±3.27	442±22	57.8±1.14
<b>K3-2(n=2)</b>	1.04±0.05	0.33±0.02	151±4.01	442±22	66.6±1.58
<b>K3-3(n=2)</b>	0.73±0.05	0.17±0.02	96±1.10	342±15	45.1±1.32
<b>1</b>	0.57±0.03	0.45±0.02	126±4.52	476±33.4	20.2±1.62
<b>2</b>	0.45±0.02	0.48±0.03	285±14.2	517±36.2	29.4±1.76
<b>3</b>	3.90±0.20	2.45±0.09	120±2.40	155±4.65	78.7±4.72
<b>4</b>	0.69±0.02	0.71±0.04	275±13.8	711±49.8	37.3±2.24
<b>5</b>	0.33±0.02	0.62±0.03	300±6.00	548±38.3	39.4±3.16
<b>6</b>	0.52±0.02	0.70±0.03	174±3.49	591±41.2	27.6±2.20
<b>7</b>	0.54±0.03	1.07±0.06	492±14.8	635±44.5	39.2±1.49
<b>8</b>	0.52±0.03	0.32±0.02	172±3.44	599±17.9	34.6±2.07
<b>9</b>	0.60±0.03	0.50±0.03	213±4.27	675±13.5	23.3±1.87
<b>10</b>	0.49±0.03	1.80±0.10	192±5.77	794±55.6	33.5±1.27
<b>11</b>	0.53±0.03	0.50±0.03	219±4.37	845±16.9	33.4±2.67
<b>12</b>	0.37±0.02	0.83±0.05	226±6.78	411±28.8	93.8±3.57
<b>14</b>	0.58±0.03	0.86±0.04	190±3.80	629±18.9	77.6±4.66
<b>15</b>	0.48±0.03	1.22±0.06	305±6.10	430±12.9	101±6.03
<b>16</b>	0.30±0.02	0.28±0.02	197±5.90	350±24.5	23.6±0.90
<b>17</b>	0.25±0.01	0.23±0.02	331±9.92	428±29.9	114±4.35
<b>18</b>	0.47±0.02	1.00±0.04	253±5.06	354±24.8	36.7±2.94
<b>19</b>	0.48±0.03	0.47±0.03	204±4.08	488±14.6	44.6±2.67
<b>20</b>	0.38±0.03	0.29±0.02	299±5.98	540±16.2	31.2±1.87

Table 3.7 continued

Samples	MgO %	Fe <sub>2</sub> O <sub>3</sub> %	Mn mg/kg	Sr mg/kg	Ba mg/kg
22	0.63±0.02	0.65±0.04	353±17.7	632±44.2	28.6±1.72
23	0.77±0.03	0.64±0.03	171±3.42	811±16.2	21.2±1.69
30	2.50±0.12	0.10±0.01	199±5.97	487±34.1	30.2±1.15

Table 3.8. Results of geological and archaeological samples using ICP-MS for Cr, Y, Nb, La, Ce, Nd and Sm. Results are corrected by matrix factor

Samples	Constituent mg/kg						
	Cr	Y	Nb	La	Ce	Nd	Sm
AKYA (n=6)	344±25	0.67±0.14	0.54±0.09	0.55±0.06	0.99±0.15	1.13±0.23	n.d.
AKYB (n=7)	173±32	1.60±0.34	1.65±0.32	2.60±0.29	3.78±0.58	4.06±0.73	n.d.
AKYC (n=8)	140±21	1.15±0.11	1.28±0.20	2.14±0.38	3.81±0.39	2.26±0.44	n.d.
KRC (n=6)	785±73	5.71±0.64	3.12±0.36	6.47±0.76	11.9±0.78	7.35±0.77	1.26±0.17
RZG(n=4)	593±17	7.56±0.70	3.51±0.30	12.1±0.44	21.5±0.58	11.9±0.47	2.15±0.04
K1 (n=3)	45.4±1.09	19.1±1.44	2.53±0.29	8.93±0.12	10.6±0.78	9.42±0.68	1.69±0.16
K2(n=3)	93.4±5.76	31.9±2.64	5.70±0.12	16.3±0.67	23.5±1.95	16.7±1.44	3.12±0.28
K3-1 (n=2)	26.5±0.43	14.5±0.87	0.85±0.01	7.50±0.15	10.1±0.46	8.01±0.38	1.41±0.03
K3-2 (n=2)	43.6±1.26	20.9±1.07	1.03±0.05	10.4±0.30	14.4±0.68	10.5±1.11	1.95±0.25
K3-3 (n=2)	15.6±0.54	13.1±0.98	0.54±0.01	6.39±0.16	7.18±0.22	6.87±0.45	1.15±0.10
1	141±15	6.81±0.35	1.15±0.01	4.33±0.16	3.61±0.41	4.28±0.26	1.14±0.06
2	28.8±3.16	5.42±0.11	1.20±0.09	3.73±0.27	1.59±0.01	3.47±0.20	n.d.
3	88.3±5.03	4.59±0.33	4.00±0.26	5.97±0.07	13.42±0.22	8.21±0.66	1.44±0.11
4	57.5±3.28	15.5±1.12	3.36±0.22	10.20±0.12	7.40±0.12	12.29±0.98	2.12±0.17
5	41.6±5.25	43.6±3.53	2.92±0.15	20.16±0.92	20.04±1.63	17.59±1.23	5.12±0.41

**Table 3.8  
continue**

<b>Samples</b>	<b>Cr</b>	<b>Y</b>	<b>Nb</b>	<b>La</b>	<b>Ce</b>	<b>Nd</b>	<b>Sm</b>
<b>6</b>	26.7±3.37	35.0±2.83	2.55±0.13	12.27±0.56	14.18±1.15	13.53±0.95	3.80±0.30
<b>7</b>	37.6±4.12	13.2±0.27	2.10±0.15	11.30±0.83	12.15±0.06	9.60±0.57	2.19±0.22
<b>8</b>	36.8±4.65	24.8±2.01	2.08±0.10	10.14±0.46	10.87±0.88	9.88±0.69	2.45±0.20
<b>9</b>		12.2±0.88	3.06±0.20	12.72±0.15	14.29±0.23	10.37±0.83	1.89±0.15
<b>10</b>	51.6±5.65	17.2±0.35	2.91±0.22	12.63±0.93	10.87±0.06	11.84±0.70	2.61±0.26
<b>11</b>		26.9±1.94	4.23±0.27	15.88±0.18	15.45±0.25	15.92±1.27	2.72±0.22
<b>12</b>	18.9±2.07	14.3±0.29	2.48±0.18	9.76±0.72	11.32±0.06	7.73±0.46	1.75±0.17
<b>14</b>	32.8±3.59	27.8±1.44	3.11±0.03	17.99±0.69	11.30±1.29	16.96±1.02	3.76±0.19
<b>15</b>	23.6±1.35	13.2±0.95	4.11±0.27	9.48±0.11	9.95±0.16	9.19±0.74	5.38±0.43
<b>16</b>	13.8±0.79	9.12±0.66	1.85±0.12	5.91±0.07	7.30±0.12	7.14±0.57	1.34±0.11
<b>17</b>	21.6±2.73	2.90±0.23	1.31±0.07	3.25±0.15	2.29±0.19	2.87±0.20	n.d.
<b>18</b>	43.1±5.44	14.9±1.20	2.22±0.11	9.59±0.44	9.04±0.73	9.01±0.63	2.42±0.19
<b>19</b>	22.4±1.28	4.71±0.34	1.48±0.10	6.96±0.08	5.93±0.10	10.12±0.81	1.46±0.12
<b>20</b>	21.5±1.23	24.5±1.76	2.80±0.18	14.56±0.17	13.99±0.23	15.17±1.21	2.99±0.24
<b>22</b>	30.4±1.73	4.42±0.32	3.40±0.22	5.15±0.06	4.97±0.08	4.64±0.37	3.05±0.24
<b>23</b>	28.0±1.60	14.1±1.01	2.03±0.13	8.32±0.10	9.09±0.15	9.83±0.79	2.11±0.17
<b>24</b>	68.9±7.55	8.29±0.43	2.91±0.03	3.87±0.15	3.23±0.37	7.01±0.42	1.32±0.07
<b>26</b>	53.3±3.04	19.7±1.42	2.71±0.18	10.33±0.12	12.20±0.20	12.51±1.00	2.27±0.18
<b>27</b>	27.5±1.57	17.8±1.29	4.18±0.27	9.08±0.10	10.34±0.17	9.55±0.76	4.86±0.39
<b>28</b>	45.9±5.80	6.76±0.55	1.69±0.09	4.57±0.21	3.41±0.28	4.15±0.29	n.d.
<b>30</b>	33.7±3.69	1.24±0.06	0.92±0.01	1.43±0.05	1.59±0.18	1.48±0.09	n.d.
<b>31</b>	41.2±5.18	5.60±0.45	2.59±0.13	4.93±0.22	5.57±0.45	4.19±0.29	1.29±0.10

<b>Table 3.8 continue</b>							
<b>Samples</b>	<b>Cr</b>	<b>Y</b>	<b>Nb</b>	<b>La</b>	<b>Ce</b>	<b>Nd</b>	<b>Sm</b>
<b>32</b>	36.1±2.06	10.2±0.73	2.22±0.14	7.92±0.09	8.13±0.13	9.21±0.74	1.99±0.16
<b>33</b>	37.7±4.13	11.6±0.60	2.01±0.02	7.01±0.27	5.75±0.66	7.12±0.43	1.66±0.08
<b>34</b>	26.2±2.87	3.16±0.06	1.54±0.11	3.25±0.24	1.09±0.01	3.07±0.18	0.71±0.07
<b>35</b>	33.2±3.63	5.56±0.11	1.27±0.09	4.42±0.32	2.04±0.01	3.90±0.23	1.08±0.11
<b>36</b>	46.5±5.09	6.79±0.14	3.48±0.26	6.99±0.51	4.18±0.02	5.88±0.35	1.42±0.14
<b>37</b>	40.9±2.33	6.62±0.48	2.28±0.15	5.89±0.07	4.98±0.08	7.86±0.63	1.47±0.12

**Table 3.9.** Results of geological and archaeological samples using ICP-MS for Eu, Gd, Ho, Er, Yb, Lu and Hf. Results are corrected by matrix factor

<b>Samples</b>	<b>Constituent mg/kg</b>						
	<b>Eu</b>	<b>Gd</b>	<b>Ho</b>	<b>Er</b>	<b>Yb</b>	<b>Lu</b>	<b>Hf</b>
<b>AKYA (n=6)</b>	n.d.	n.d.	n.d.	n.d.	n.d.	n.d.	0.89±0.14
<b>AKYB (n=7)</b>	n.d.	n.d.	n.d.	n.d.	n.d.	n.d.	1.71±.16
<b>AKYC (n=8)</b>	n.d.	0.63±0.11	n.d.	0.54±0.06	n.d.	n.d.	0.80±0.13
<b>KRC (n=6)</b>	n.d.	1.52±0.18	n.d.	0.46±0.07	0.82±0.06	n.d.	1.38±0.14
<b>RZG (n=4)</b>	n.d.	2.68±0.23	n.d.	1.05±0.20	1.09±0.01	n.d.	1.41±0.17
<b>K1 (n=3)</b>	0.68±0.04	2.04±0.18	n.d.	1.63±0.22	1.40±0.14	n.d.	0.41±0.05
<b>K2(n=3)</b>	1.27±0.11	3.80±0.29	1.19±0.08	2.39±0.20	2.28±0.16	n.d.	0.63±0.07
<b>K3-1 (n=2)</b>	n.d.	1.76±0.02	n.d.	1.16±0.17	0.84±0.04	n.d.	0.29±0.02
<b>K3-2 (n=2)</b>	0.61±0.04	2.45±0.22	0.77±0.05	1.51±0.15	1.16±0.16	n.d.	n.d.
<b>K3-3 (n=2)</b>	n.d.	1.43±0.11	n.d.	1.20±0.08	0.72±0.04	n.d.	0.38±0.03
<b>1</b>	n.d.	1.13±0.02	n.d.	n.d.	n.d.	n.d.	n.d.

**Table 3.9  
continue**

<b>Samples</b>	<b>Eu</b>	<b>Gd</b>	<b>Ho</b>	<b>Er</b>	<b>Yb</b>	<b>Lu</b>	<b>Hf</b>
<b>2</b>	n.d.	0.80±0.10	n.d.	0.45±0.06	n.d.	n.d.	0.25±0.03
<b>3</b>	n.d.	1.91±0.07	n.d.	n.d.	n.d.	n.d.	1.28±0.10
<b>4</b>	n.d.	2.82±0.10	n.d.	0.72±0.11	1.43±0.04	n.d.	n.d.
<b>5</b>	1.31±0.10	5.35±0.06	1.45±0.05	1.49±0.22	2.37±0.06	n.d.	0.48±0.04
<b>6</b>	n.d.	4.18±0.04	n.d.	1.16±0.17	1.64±0.04	n.d.	n.d.
<b>7</b>	n.d.	2.57±0.31	n.d.	1.02±0.15	1.29±0.03	n.d.	n.d.
<b>8</b>	n.d.	3.04±0.03	n.d.	0.60±0.09	1.41±0.04	n.d.	n.d.
<b>9</b>	n.d.	2.50±0.09	n.d.	n.d.	n.d.	n.d.	1.67±0.13
<b>10</b>	n.d.	2.82±0.34	n.d.	1.30±0.19	1.79±0.05	n.d.	n.d.
<b>11</b>	n.d.	3.75±0.13	2.00±0.07	1.27±0.19	1.88±0.05	n.d.	0.82±0.07
<b>12</b>	n.d.	2.49±0.30	n.d.	0.80±0.12	1.27±0.03	n.d.	2.83±0.34
<b>14</b>	1.36±0.11	4.68±0.07	1.88±0.07	1.89±0.28	2.24±0.06	n.d.	n.d.
<b>15</b>	n.d.	7.44±0.29	n.d.		n.d.	n.d.	n.d.
<b>16</b>	n.d.	1.57±0.05	n.d.	0.38±0.05	0.81±0.02	n.d.	n.d.
<b>17</b>	n.d.	n.d.	n.d.	n.d.	n.d.	n.d.	n.d.
<b>18</b>	0.68±0.05	2.59±0.03	0.79±0.03	1.05±0.15	0.94±0.03	n.d.	1.25±0.10
<b>19</b>	n.d.	3.23±0.11	n.d.		n.d.	n.d.	n.d.
<b>20</b>	1.50±0.10	4.00±0.14	n.d.	0.98±0.14	2.03±0.05	n.d.	n.d.
<b>22</b>	n.d.	4.80±0.17	n.d.		n.d.	n.d.	n.d.
<b>23</b>	n.d.	2.16±0.07	n.d.	0.74±0.11	1.61±0.04	n.d.	0.79±0.06
<b>24</b>	n.d.	1.67±0.02	n.d.	0.63±0.09	n.d.	n.d.	n.d.
<b>26</b>	n.d.	3.21±0.11	n.d.	0.90±0.13	2.13±0.06	n.d.	n.d.

<b>Table 3.9 continue</b>							
<b>Samples</b>	Eu	Gd	Ho	Er	Yb	Lu	Hf
<b>27</b>	n.d.	7.78±0.27	n.d.		n.d.	n.d.	n.d.
<b>28</b>	n.d.	1.14±0.01	n.d.	n.d.	n.d.	n.d.	n.d.
<b>30</b>	n.d.	n.d.	n.d.	n.d.	n.d.	n.d.	0.44±0.05
<b>31</b>	n.d.	1.26±0.02	n.d.	0.20±0.03	n.d.	n.d.	n.d.
<b>32</b>	n.d.	2.36±0.08	n.d.	n.d.	n.d.	n.d.	n.d.
<b>33</b>	n.d.	1.68±0.02	n.d.	0.97±0.14	n.d.	n.d.	0.72±0.09
<b>34</b>	n.d.	0.66±0.08	n.d.	n.d.	n.d.	n.d.	0.27±0.03
<b>35</b>	n.d.	1.09±0.13	n.d.	n.d.	n.d.	n.d.	n.d.

### 3.7 Results of Thin-section Analysis

Since sedimentary rocks commonly contain a great number of microfossil, such as foraminifera, microfossils within a sample of rock can be used to match the sample to a source rock having the same fossil evidence. Therefore, micropaleontologic analysis can be a useful method for the investigation of raw material provenance in archaeology. A case study discussing the contribution of micropaleontology and biostratigraphy to an archaeological research was presented by Zambetakis-Lekkas and Elefanti [106].

In this micropaleontologic study, archaeological and geological samples were analyzed by means of micropaleontologic characteristics (fossil composition) in order to investigate whether archaeological samples were made of the quarry samples from Datça or Cyprus. Thin sections of twelve figurine samples obtained from Emecik were analyzed. Ten and five quarry samples collected from Datça and Cyprus, respectively, were used as the comparison materials. Faunal composition of all samples was analyzed by a thin section technique which is extensively used in paleontological examinations. Samples examined by thin-section analysis are given in Table 3.10.

**Table 3.10.** Samples examined by thin-section analysis.

<b>No</b>	<b>Name</b>	<b>Description</b>
<b>2</b>	ST.06.I12.d5.c12	Body fragment
<b>3</b>	ST.06.I12.d8.21	Minature female figurine fragment
<b>4</b>	ST.06.H12.a3.16	Falcon fragment
<b>22</b>	ST.02.I8b.18.4	Lion figurine
<b>30</b>	ST.02.K9c.28B1	Ornamented stone
<b>37</b>	ST.02.I8B.16.A.15	Lion figurine

<b>Table 3.10. continued</b>		
<b>38</b>	ST.02.I8B.11c.29	Fragment
<b>47</b>	ST.02.I8b.28.63	Fragment
<b>56</b>	ST.02.K9c.27A.13	Body fragment
<b>84</b>	ST.02.I8b.19.A12(B)	Fragment
<b>85</b>	ST.02.I8b.19.A12	Architectural fragment
<b>93</b>	ST.00.D8.A.V	Body fragment

According to the micropaleontologic study by Dr. Aynur Hakyemez, nine archaeological samples and two rock samples from Cyprus (K1 and K2) are rich in planktonic foraminifera. Nine figurines are namely the figurines 2, 4, 22, 34, 38, 47, 56, 84, and figurine 93. Planktonic foraminifera are the marine unicellular shell-bearing protozoa, float passively in sea water. Planktonic foraminifera are one of the most diagnostic fossil groups for the dating of the geological formations formed from the late Jurassic in the geologic record.

Archaeological samples contain abundant and well preserved planktonic foraminifera (*Globoquadrina* spp., *Globigerina* spp., *Globigerinoides* spp., *Praeorbulina* spp.) and are characterized by a very fine grained, homogeneous texture. K1 and K2 samples from Cyprus include almost the same planktonic foraminiferal assemblages as well. However, both abundance and size of the specimens in K1 and K2 are much greater than those of the archaeological samples. Although the two groups of samples are similar in planktonic foraminiferal assemblages and general texture the presence of only two reference samples from Cyprus makes it difficult to have a reliable correlation.

Identified planktonic foraminiferal assemblages in archaeological and geological samples (Cyprus) represent an interval (late Burdigalian-Langhian) within the Miocene time of the geologic time scale. This time interval corresponds to the MMi 4 Zone (*Praeorbulina glomerosa* s.l Zone) which spans approximately 16.0-14.5 m.y. [107].

A rich planktonic foraminiferal content and very fine grained homogeneous texture of the examined samples are consistent with chalk lithology, a type of limestone which constitutes widely distributed Lefkara and Pakhna formations represented by a thick chalk succession in Southern Cyprus. Miocene planktonic foraminiferal assemblages of these formations are reported in detail from the restricted outcrops in the Gürpınar and Yiğitler regions in Northern Cyprus [108]. K1 geological sample was collected from the Erdemli quarry which is located near Yiğitler. The Lefkara and Pakhna formations in this region are represented mainly by fine grained, homogeneous, porous, creamy white colored, large amount of planktonic foraminifera bearing chalks. An Early-Middle Miocene age spanning the late Burdigalian-Langhian time interval, which refers to as the Datça archaeological samples, was assigned to the Lefkara and Pakhna formations by analyzing planktonic foraminifera [108].

On the other hand the faunal composition of samples K3-1, K3-2, K3-3 are quite different from those of the samples K1 and K2. They are dominated by miliolid, textularid, rotalid specimens and *Elphidium* sp. of benthic foraminifera (marine unicellular protozoa, sea bottom dwellers) associated with red algae, gastropoda and only a few globigerinid specimens of planktonic foraminifera.

In addition, Datça geological samples are not fossiliferous except for the sample KRC. This sample contains only rare bivalve and ostracoda shells but it is barren of planktonic or benthic foraminifera. Meantime, figurines 3, 30 and 85 are also not fossiliferous just like the geological samples from Datça.

As a conclusion, based on the micropaleontologic analysis, it is clear that neither the Datça rock samples nor the three rock samples from Cyprus (K3-1, K3-2, K3-3) represent the material of Datça statuette samples. With regard to the other two Cyprus geological samples (K1 and K2), they show a similarity in planktonic foraminiferal content and general texture with the archaeological samples. By considering the micropaleontologic analysis of sample K1 together with the biostratigraphical study of Hakyemez and Toker [108] and personal communication with A. Hakyemez [109] it is possible to say that K1 sample from Erdemli quarry can represent the origin of raw material of Datça archaeological samples. Although almost the same fauna except for *Paragloborotalia* sp. and *Orbulina?* sp. is included in the K2 sample insufficient micropaleontological and geological data is a limiting factor for a reliable correlation between archaeological samples and K2 quarry sample at the present time.

In the following paragraphs, planktonic foraminiferal species identified in the samples are listed:

#### **Figurine 2**

Globigerinid specimens

#### **Figurine 3**

Not fossiliferous

#### **Figurine 4**

*Globigerina praebulloides* s.l. Blow

*Globigerinoides* sp., *Globigerina* sp.

#### **Figurine 22**

*Praeorbulina glomerosa curva* (Blow)

*Globigerinoides trilobus* (Reuss)

*Dentoglobigerina altispira altispira* (Cushman ve Jarvis)

*Globigerinoides* cf. *subquadratus* Brönnimann

*Globoquadrina baroemoenensis* (LeRoy)

*Praeorbulina* cf. *glomerosa glomerosa* (Blow)

*Praeorbulina* cf. *sicana* (de Stefani)

*Globigerina praebulloides* s.l. Blow

#### **Figurine 30**

Not fossiliferous

#### **Figurine 37**

*Praeorbulina sicana* (de Stefani)

*Globoquadrina* sp.

*Globoquadrina* cf. *venezuelana* (Hedberg)

*Globigerinoides subquadratus* Brönnimann

*Globoquadrina baroemouensis* (LeRoy)

*Globigerina praebulloides* s.l. Blow

*Globigerina ciperoensis* Bolli

**Figurine 38**

*Globigerinoides bisphericus* Todd

*Globoquadrina baroemouensis* (LeRoy)

*Globoquadrina dehiscens* (Chapman, Parr ve Collins)

*Globigerina praebulloides* s.l. Blow

*Globigerina ciperoensis* Bolli

*Globigerina praebulloides occlusa* Blow ve Banner

*Globigerina praebulloides praebulloides* Blow

*Globigerinoides subquadratus* Brönnimann

*Globigerinoides* cf. *sacculifer* (Brady)

*Globigerinoides* cf. *quadrilobatus* (d'Orbigny)

*Globigerinoides altiapertura* Bolli

**Figurine 47**

*Globigerinoides trilobus* (Reuss)

*Globigerinoides bisphericus* Todd

*Globoquadrina dehiscens* (Chapman, Parr ve Collins)

*Globigerina praebulloides* s.l. Blow

*Globigerina ciperoensis* Bolli

**Figurine 56**

*Globigerina praebulloides* s.l. Blow

*Globigerinoides sacculifer* (Brady)

*Globigerinoides subquadratus* Brönnimann

*Globigerinoides trilobus* (Reuss)

*Globigerinoides bisphericus* Todd

*Praeorbulina?* sp.

**Figurine 84**

*Globigerina* sp., *Globigerinoides* sp.

**Figurine 93**

*Globigerinoides trilobus* (Reuss)

*Globoquadrina baroemoenensis* (LeRoy)

*Globigerinoides* sp., *Globoquadrina* sp.

**K1**

*Globoquadrina baroemoenensis* (LeRoy)

*Praeorbulina* cf. *glomerosa glomerosa* (Blow)

*Globoquadrina dehiscens* (Chapman, Parr ve Collins)

*Globigerinoides trilobus* (Reuss)

*Globigerinoides bisphericus* Todd

*Praeorbulina glomerosa curva* (Blow)

*Globigerinoides altiapertura* Bolli

*Globigerina praebulloides praebulloides* Blow

**K2**

*Globigerinoides bisphericus* Todd

*Globigerinoides trilobus* (Reuss)

*Praeorbulina* cf. *glomerosa glomerosa* (Blow)

*Globoquadrina dehiscens* (Chapman, Parr ve Collins)

*Paragloborotalia* sp.

*Globigerinoides quadrilobatus* (d'Orbigny)

*Praeorbulina* cf. *sicana* (de Stefani)

*Orbulina?* sp.

**3.8 Results of X-ray Diffraction Analyses of Samples**

Thirty-one figurine samples and all the geological samples were subjected to XRD analysis. The list of figurines that were investigated for their mineral compositions through XRD analysis along with their names, descriptions and mineral inclusions are given in Table 3.11.

**Table 3.11.** The list of figurines, names, descriptions and mineral inclusions

<b>Figurine No</b>	<b>Name</b>	<b>Description</b>	<b>d values</b>	<b>Minerals</b>
4	ST.06.H12.a3.16	Bird of prey (falcon)	3.78, 2.99	Mg-Calcite
22	ST.02.I8b.18.3	Lion figurine	3.86, 2.99,	Calcite, Mg-Calcite
23	ST.02.I8b.16A.11	Fragment	3.86, 3.04	Calcite
24	ST.02.I8b.16A.11	Fragment	3.86, 3.04	Calcite
28	ST.02.I8b.11.c26	Standing male votary figurine	3.86, 3.04	Calcite
30	ST.02.K9c.28B1	Ornamented stone	3.78, 2.88	Mg-Calcite, Dolomite
31	ST.02.I8b.25.11	Kouros feet&base	3.86, 2.99	Calcite, Mg-Calcite,
32	ST.02.I8b.28A.11	Kouros head&body	3.86, 3.04	Calcite
34	ST.02.I8B.19.b6	Body fragment	3.86, 2.99	Calcite, Mg-Calcite,
37	ST.02.I8B.16.A.15	Lion fragment	3.86, 3.04,	Calcite
38	ST.02.I8B.11c.29	Fragment	3.78, 2.99	Mg-Calcite,
40	ST.02.8B.19A.13	Male votary (priest?) body fragment	3.86, 3.04	Calcite
41	ST.02.I8B.19.6	Leg fragment	3.86, 3.04	Calcite
44	ST.02.I8b.21.17	Lion	3.86, 2.99	Calcite, Mg-Calcite,
46	ST.02.I8b.22.2	Fragment	3.86 and 3.04	Calcite
47	ST.02.I8b.28.6.3	Leg fragment	3.78, 2.99	Mg-Calcite
52	ST.02.I8b.18.7	Kouros body fragment	3.78, 3.04	Calcite, Mg-Calcite
55	ST.02.K9c.27.4	Leg fragment	3.86, 2.99	Calcite, Mg-Calcite
58	ST.02.I8b.14.20	Male votary	3.86, 3.04	Calcite
61	ST.02.I8b.23.11	Lion fragment	3.86, 3.04	Calcite
62	ST.02.I8b.28A.2	Small fragments	3.93, 2.99	Mg-Calcite
63	ST.01.G11.D1	Leg ? fragment	3.78, 2.99, 2.08	Mg-Calcite,
64	ST.02.I8b.28A.2	Small fragments	2.18	Dolomite
65	ST.02.K9c.27b.1	Leg fragment	3.86, 2.99	Calcite, Mg-Calcite,
69	ST.02.K9.c27.A12	Bird	3.04	Calcite
74	ST.02.I8b	Body fragment	3.86, 3.04	Calcite
75	ST.02.I8b.28.3	Lion fragment	3.86, 3.04	Calcite
80	ST.02.I8b.23.9	Leg fragment	3.86, 3.04	Calcite
81	ST.02.I8b.23.9	Fragment	3.86, 2.99	Calcite, Mg-Calcite
84	ST.02.I8b.19.A12	Fragment	3.78, 2.99	Mg-Calcite
92	ST.02.I8b.28.B3	Fragment	3.86, 2.99	Calcite, Mg-Calcite
94	ST.99.K8C.9.22	Leg fragment	3.86, 2.99	Calcite, Mg-Calcite
95	ST.00.K8C.16.152	Body fragment	3.86, 3.04	Calcite

In XRD analysis of the figurine samples, Mg-calcite appeared to be the major mineral in most of the figurines. Meantime, calcite appeared to be the major mineral in the rest of the figurines. Dolomite is the major mineral in figurines 30 and 64.

It has been understood through thin-sections of the figurines majority of the figurines were made using foraminiferal limestone. Since foraminifera are composed of low or high Mg-calcite, it is expected to obtain such a mineral composition. However, in XRD analysis the same archaeological sample ST.02.K9c.28B1, ornamented fragment as in thin-section analysis and also ST.02.18b.28A.2, small fragments are discriminated based on their mineralogical characteristics. In these archaeological samples dolomite appeared to be the major mineral. Mg content of these two archaeological samples is much higher when compared to other archaeological samples.

### 3.9 REE Patterns of Figurines and Geological Samples

REE patterns of the samples were constructed by using ratio of sample values to Post-Archaeon average Australian sedimentary rock values for each REE [111]. PAAS values of the elements are given in Table 3.12.

Chemical sediments such as limestone are most likely to reflect the composition of the seawater from which they precipitated. The most important reason contributing to the REE content of clastic sediment is its provenance. It is because the REEs are insoluble and present in very low concentrations in sea, therefore the REE content in sediment are mainly transported from the source and reflect its chemistry. After primary evaluation of the REE patterns of the figurines and geological samples, it appears that regarding to Ce anomaly, enrichment of REEs and total REE concentration of the samples 3 groups are formed for the figurines. Geological samples are also in accordance with these groups. REE patterns for indicated samples are given in Figures 3.1 to 3.22. It should be noted that in some occasions the analyte concentrations are too low to be detected, such as Eu, Ho, Yb, causing interruptions in the pattern drawn.

**Table 3.12.** PAAS values of the elements [111]

Element	mg/kg
La	38.200
Ce	79.600
Nd	33.900
Sm	5.550
Eu	1.080
Gd	4.660
Y	27.000
Ho	0.991
Er	2.850
Yb	2.820

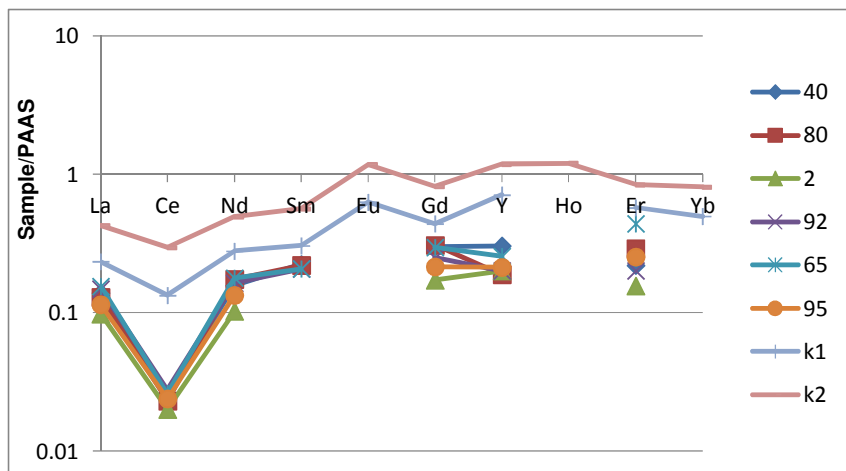


**Figure 3.1.** The REE patterns of ST.06.I12.d5.c12 (2), ST.02.8B.19A.13 (40), ST.02.K9c.27b.1 (65), ST.02.I8b.23.9 (80), ST.02.I8b.28.B3 (92), ST.00.K8C.16.152 (95), and K1, K2

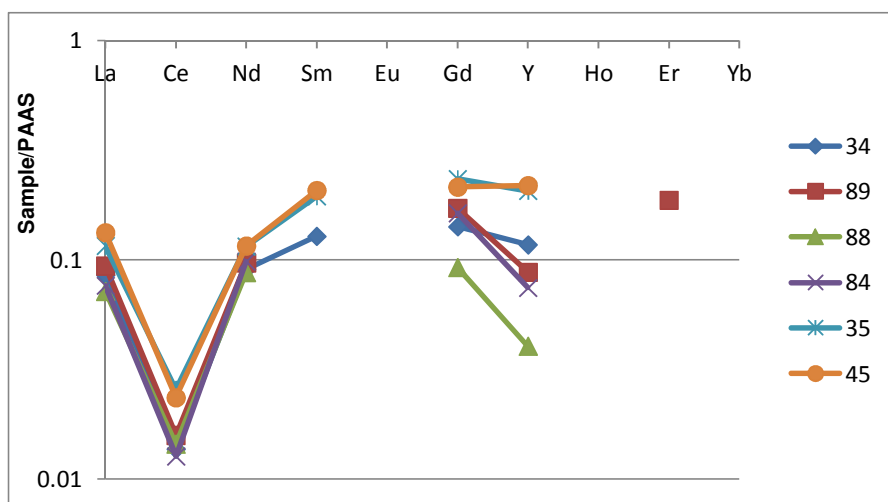


**Figure 3.2.** The REE patterns of ST.02.I8B.19.b6 (34), ST.02.I8b.11.b9 (35), ST.02.I8b.25.12 (45), ST.02.I8b.19.A12 (84), ST.99.I9b.2.17 (88), ST.01.I8.B.10.26 (89)

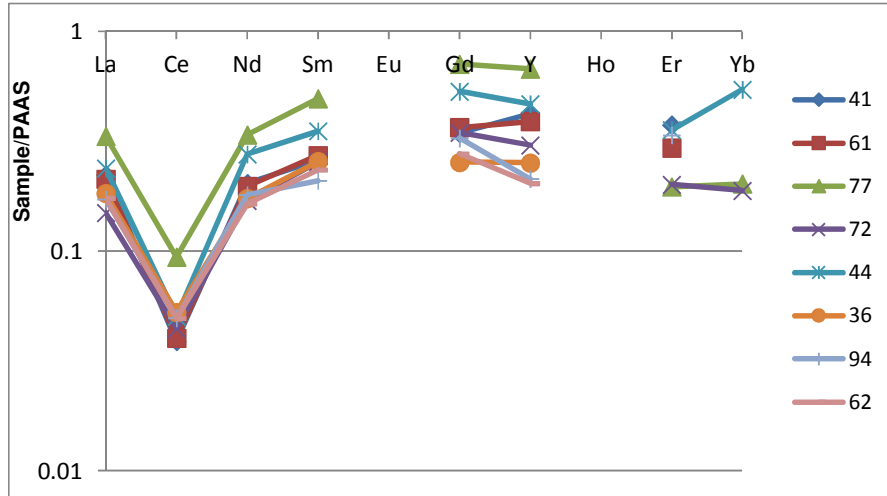


**Figure 3.3.** The REE patterns of ST.02.I8b.28.A2 (36), ST.02.I8B.19.6 (41), ST.02.I8b.21.17 (44), ST.02.I8b.23.11 (61), ST.02.I8b.28A.2 (62), ST.02.I8b.15.17 (72), ST.02.K9c.27a.11 (77), ST.99.K8C.9.22 (94)

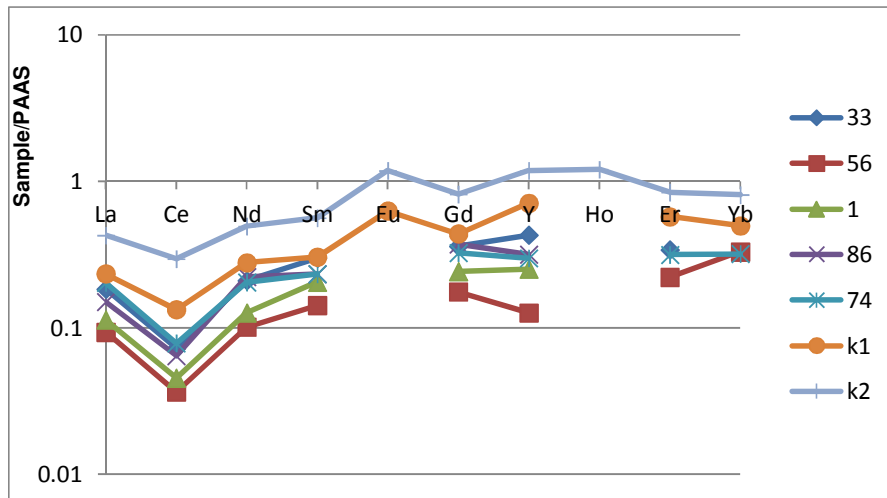


**Figure 3.4.** The REE patterns of ST.02.I8b.16A.16 (33), ST.02.K9c.27A.13 (56), ST.02.I8b (74), ST.00.K8C.16.148 (86)

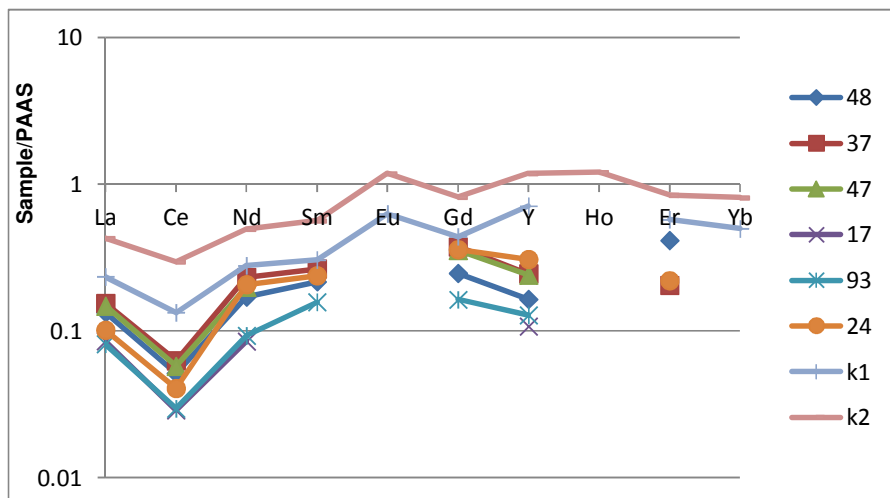


**Figure 3.5.** The REE patterns of ST.06.I12.d3.9 (17), ST.02.I8b.16A.11 (24), ST.02.I8B.16.A.15 (37), ST.02.I8b.28.6.3 (47), ST.02.I8b.28.8 (48), ST.00.D8.A.5.25 (93)

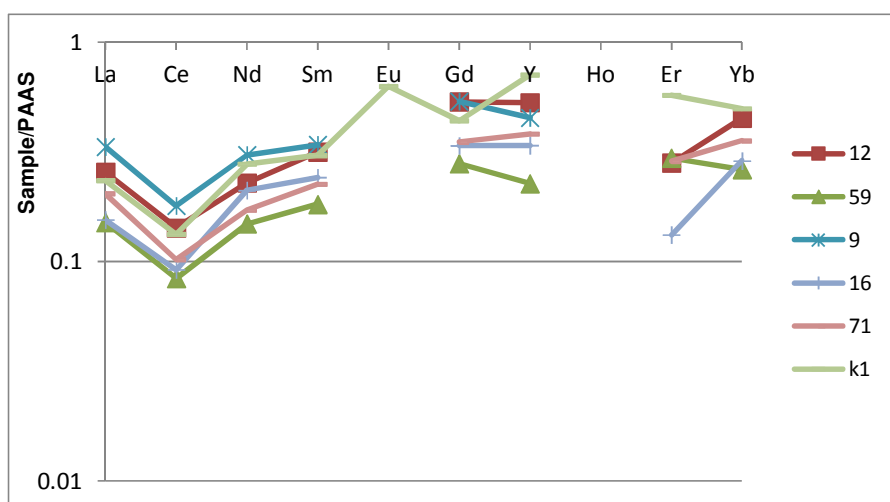


**Figure 3.6.** The REE patterns of ST.06.H12.a2A.23 (9), ST.06.I12d.6A.11 (12), ST.06.I12.d5.B11 (16), ST.02.K9c.26.4 (59), ST.02.I8b.14.30 (71)

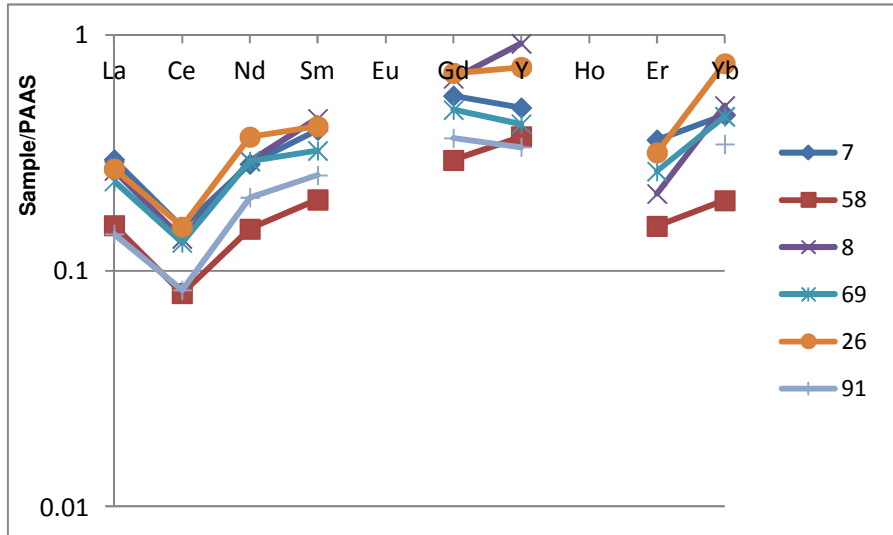


**Figure 3.7.** The REE patterns of ST.06.I12.d7.43 (7), ST.06.I12.d5.A11 (8), ST.02.I8b.16A.11 (26), ST.02.I8b.14.20 (58), ST.02.K9.c27.A12 (69), ST.99.I9B.4 (91)

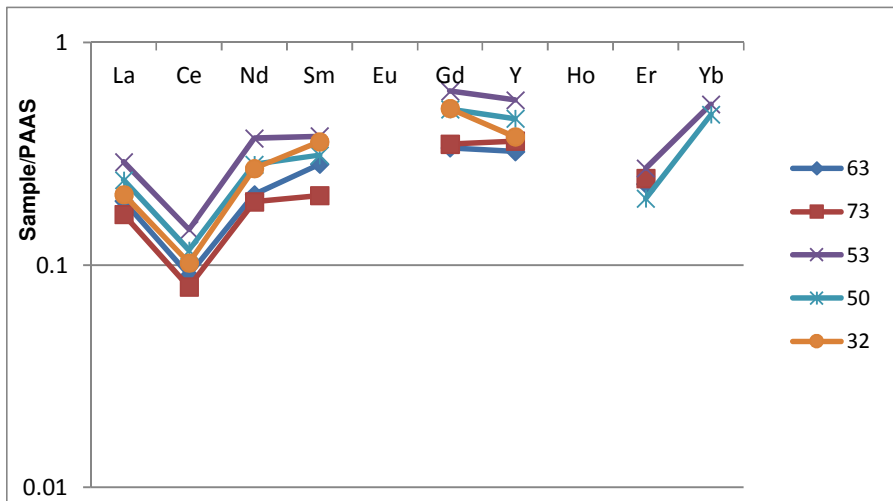


**Figure 3.8.** The REE patterns of ST.02.I8b.28A.11 (32), ST.02.I8b.19.2 (50), ST.02.I8b.14.17 (53), ST.01.G11.D1 (63), ST.02.I8b.16A.17 (73)

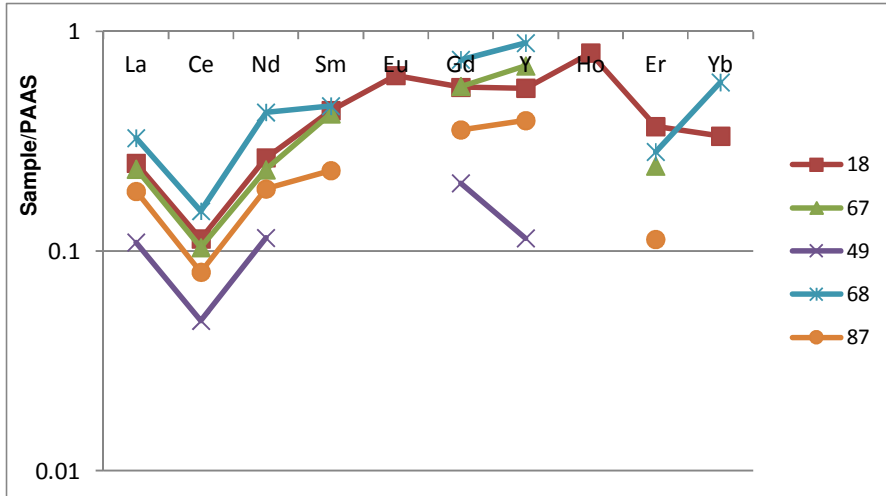


**Figure 3.9.** The REE patterns of ST.06.I12.d5A.12 (18), ST.02.I8b.19.2 (49), ST.02.K9c.27A.3 (67), ST.02.K9.c28.14 (68), ST.99.I9b.4.65 (87)

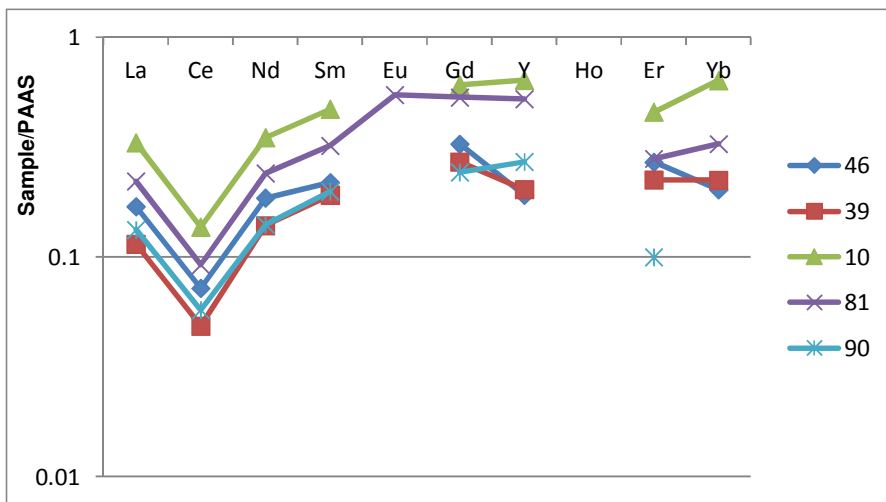


**Figure 3.10.** The REE patterns of ST.06.I12.d6A.14 (10), ST.02.I8b.16.20 (39), ST.02.I8b.22.2 (46), ST.02.I8b.23.9 (81), ST.00.K8.C.16.151 (90)

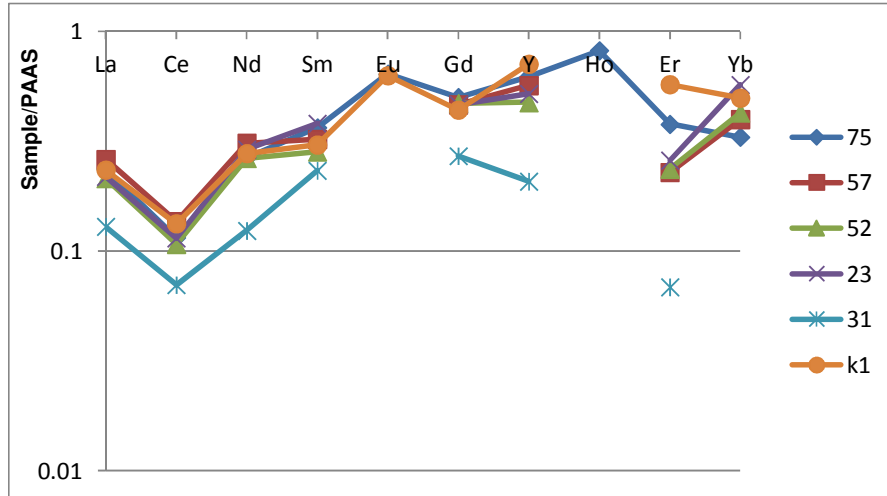


**Figure 3.11.** The REE patterns of ST.02.I8b.16A.11 (23), ST.02.I8b.25.11 (31), ST.02.I8b.18.7 (52), ST.02.I8b.11b.10 (57), ST.02.I8b.28.3 (75)

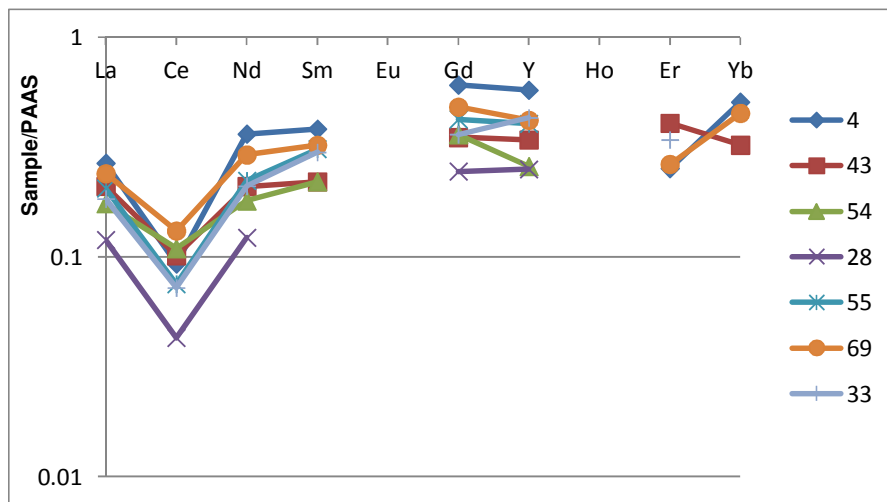


**Figure 3.12.** The REE patterns of ST.06.H12.a3.16 (4), ST.02.I8b.11.c26 (28), ST.02.I8b.16A.16 (33), ST.02.I8b.28.A3 (43), ST.02.K9c.28.6 (54), ST.02.K9c.27.4 (55), ST.02.K9.c27.A12 (69)

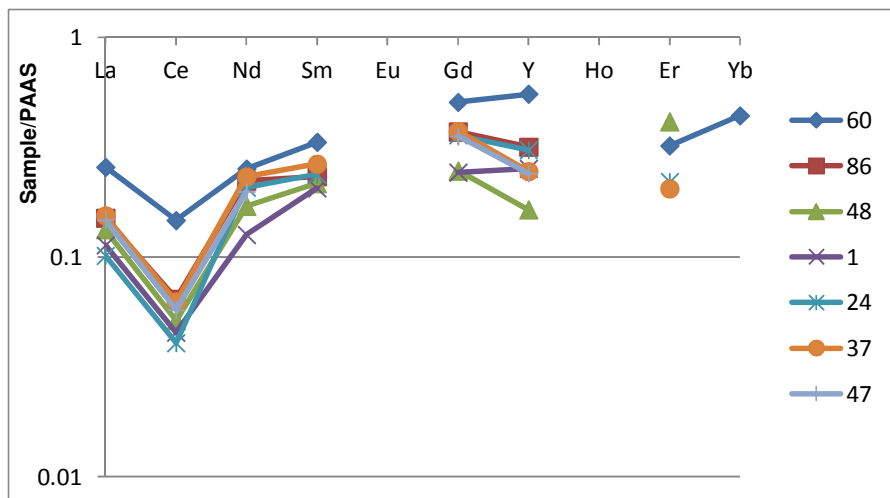


**Figure 3.13.** The REE patterns of ST.06.I12.d8.19 (1), ST.02.I8b.16A.11 (24), ST.02.I8B.16.A.15 (37), ST.02.I8b.28.6.3 (47), ST.02.I8b.28.8 (48), ST.00.K8C.16.148 (86)

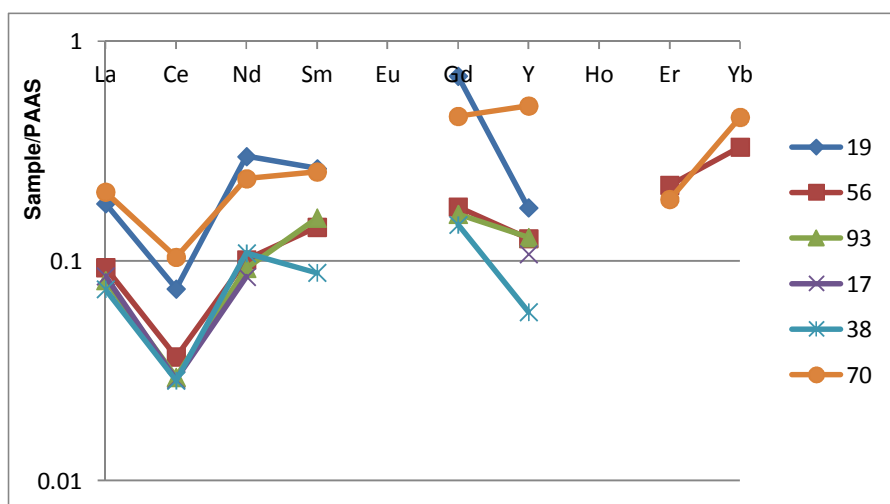


**Figure 3.14.** The REE patterns of ST.06.I12.d3.9 (17), ST.06.I12.d5.17 (19), ST.02.I8B.11c.29 (38), ST.02.K9c.27A.13 (56), ST.02.I8b.28.A9 (70), ST.00.D8.A.5.25 (93)

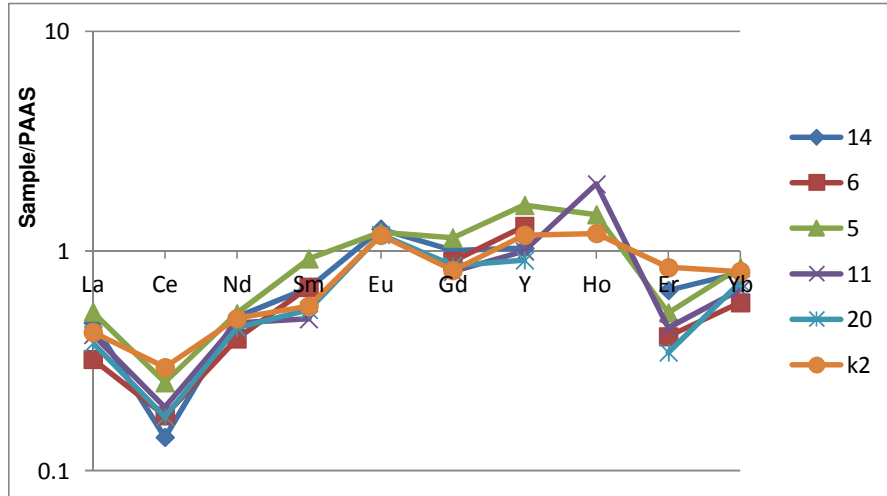


**Figure 3.15.** The REE patterns of ST.06.I12.d6.B (5), ST.06.H12.d5.15 (6), ST.06.H12.a5.22 (11), ST.06.H12.a3.17 (14), ST.06.I12.d7.44 (20)

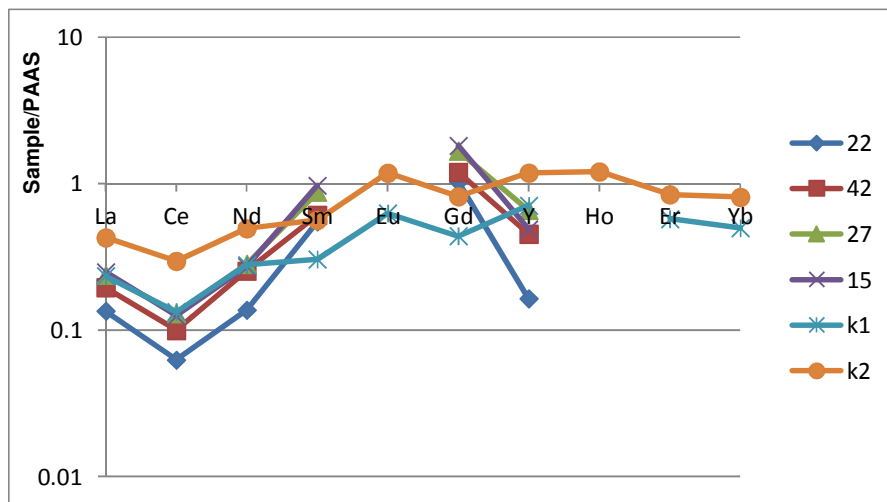


**Figure 3.16.** The REE patterns of ST.06.I12.d7.45 (15), ST.02.I8b.18.3 (22), ST.02.I8b.16A.11 (27), ST.02.K9c.28.7.4 (42)

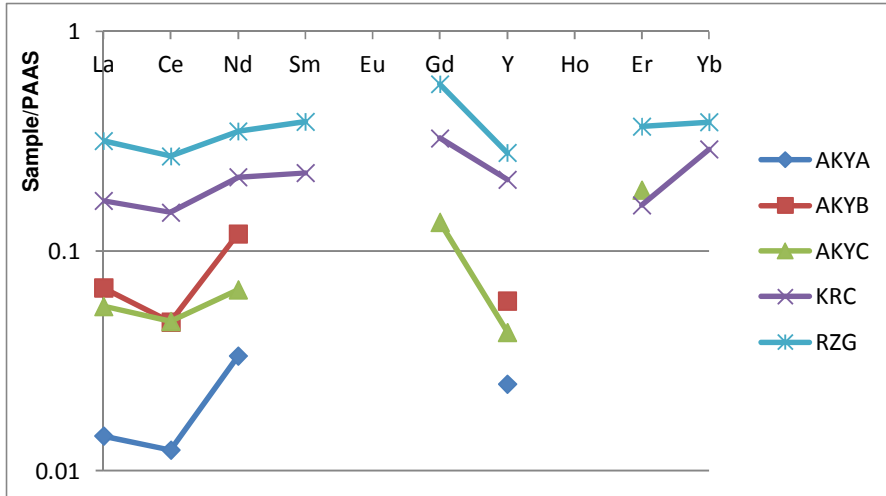


Figure 3.17. The REE patterns of geological samples from Datça

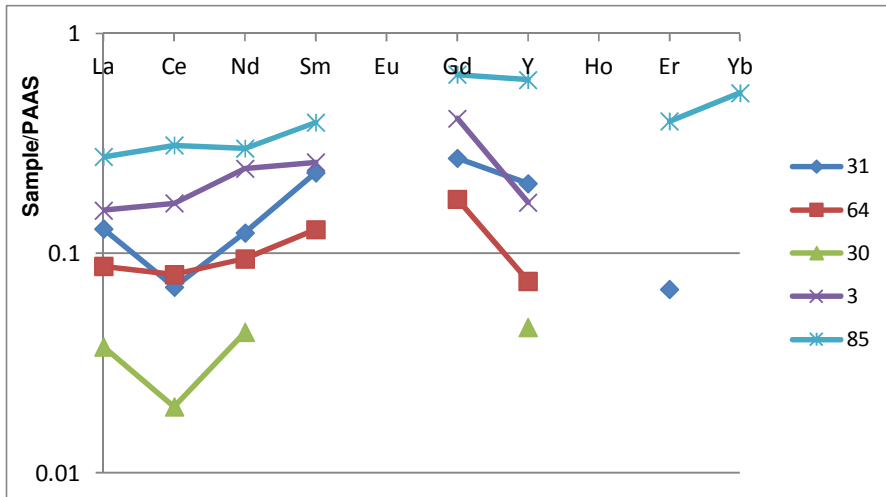


Figure 3.18. The REE patterns of the figurines that were made from local limestone

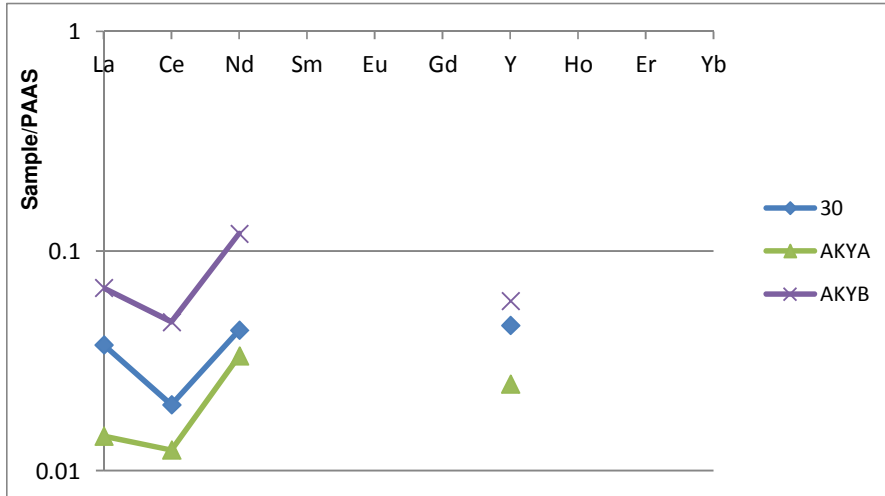


Figure 3.19. The REE patterns of ST.02.K9c.28B1 (30), AKYA, AKYB

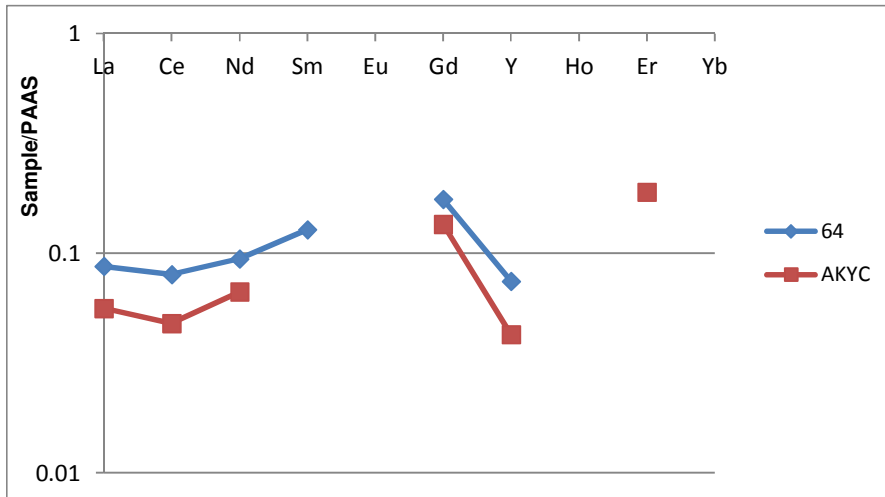
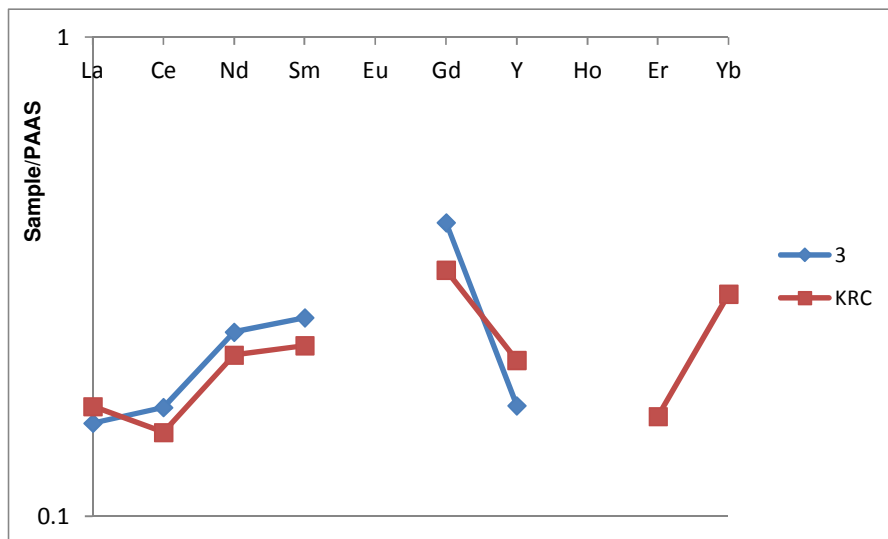
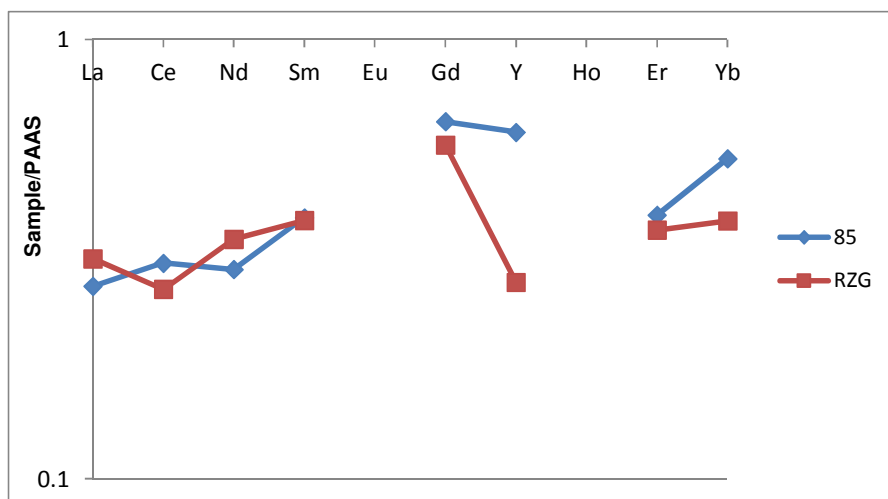


Figure 3.20. The REE patterns of ST.02.I8b.28A.2 (64), AKYC



**Figure 3.21.** The REE patterns of ST.06.I12.d8.21 (3), KRC



**Figure 3.22.** The REE patterns of ST.02.18b.19.A.12 (85), RZG

According to their PAAS normalized REE patterns, the four figurines, namely ST.06.I12.d8.21 (3), ST.02.K9c.28B1 (30), ST.02.I8b.28A.2 (64), ST.02.18b.19.A.12 (85) appear to be made from the local limestone from different locations in Datça as given in figures Figures 3.17.-3.22. When the REE enrichment, Ce anomaly and general behavior of REE patterns; the raw material of ST.06.I12.d8.21 could be match with the limestone from KRC, ST.02.K9c.28B1 with the limestone from either AKYA or AKYB, ST.02.I8b.28A.2 with the limestone from AKYC and ST.02.18b.19.A.12 with the limestone from RZG although there is a slight difference in their Ce anomaly.

The rest of the figurines then appear to form 4 different groups especially based on their degree of Ce anomalies. The figurines with REE patterns given in Figures 3.1.-3.3 could be defined as

*Group 1* with their extremely negative Ce anomalies. The figurines given in Figures 3.4.-3.15. could be defined as *Group 2* with their slightly to moderate Ce anomalies. Regarding the figurines in Figures 3.4-3.14 with the geological samples from K1 and K2 in Cyprus, although there are slight differences in REE enrichment, or general behavior from Gd to Y and from Er to Yb, it is reasonable to say the raw material of these figurines match with the limestone from K1. Then, the figurines with REE patterns given in Figure 3.15 are in accordance with the geological samples from K2, especially when REE enrichment is considered. Therefore, these figurines given in Figure 3.15. could be defined as *Group 3*.

*Group 4* is formed regarding to behavior of Nd-Sm in REE pattern given in Figure 3.16. *Group 4* is characterized by the peaks at Nd to Sm in their REE patterns. However, it is a result of foraminiferal tests in limestone.

The reason of difference at Y appearing in REE patterns of the figurines is mainly the influence by the incorporation of terrigenous materials into the limestone formation.

While Eu anomaly is another important parameter for determining different types of limestone, for many of the figurines and geological samples from Datça, Eu concentration was too low to be detected. For the figurines in which Eu could be determined as given in Figures 3.6, 3.9, 3.10, 3.11. 3.15, there is a positive anomaly just like the case for the limestone samples from K1 and K2. PAAS normalized positive Eu anomaly are found be affected by several processes including hydrothermal solutions, intense diagenesis, variations in plagioclase input or as a result of eolian input [82, 112, 113]. When the several figurines in which Eu concentration were determined are considered, it was observed that they exhibit positive Eu anomalies. It has been reported that hydrothermal activities occur in the deep sea regions, however, according to thin section analysis of the figurines and geological samples from Cyprus, the raw material of the figurines and the limestone samples from Cyprus were deposited under shallow sea environment. The positive Eu anomalies in archaeological and geological samples therefore may be due to the presence of plagioclase feldspar.

### 3.10 Multielement Diagrams of Figurines and Geological Samples

The process controlling the trace element composition of sedimentary rocks may be investigated using normalization diagrams similar to those called as spidergrams which are widely used in igneous rocks [111]. Although PAAS values of the elements are used in normalization of REE values for REE patterns, for multi-element diagrams C1 chondrite values of elements are used for normalization [106]. C1 was chosen in order to emphasize the differences in trace element chemistry between the carbonate rich limestone and meteoritic stone. C1 chondrite values of the elements are given in Table 3.13. The multi-element diagrams for the indicated samples are given in Figures 3.23 to 3.36.

**Table 3.13.** C1 values of the elements[114]

Element	mg/kg
Ba	2.41
Nb	0.246
La	0.237
Ce	0.612

Table 3.13. continued	
Sr	7.26
Nd	0.467
Sm	0.153
Hf	0.1066
Eu	0.058
Gd	0.2055
Y	1.57
Ho	0.0566
Er	0.1655
Yb	0.170

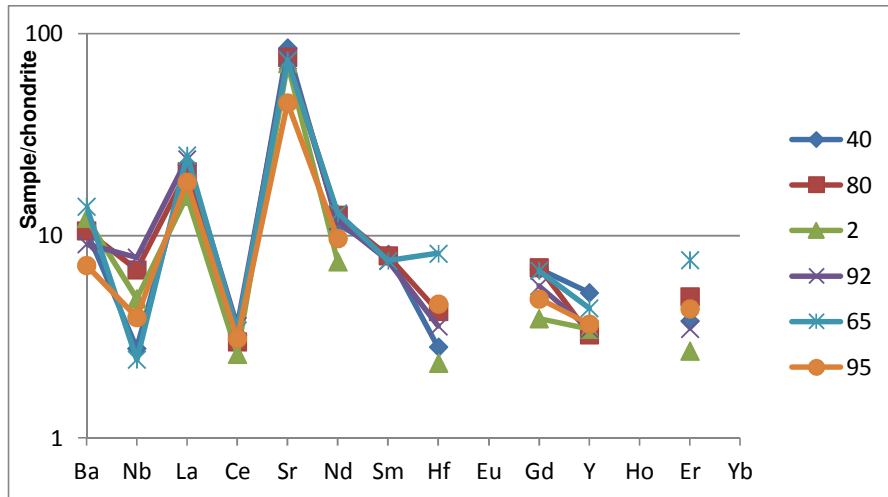


**Figure 3.23.** The multi-element diagrams of ST.06.I12.d5.c12 (2), ST.02.8B.19A.13 (40), ST.02.K9c.27b.1 (65), ST.02.I8b.23.9 (80), ST.02.I8b.28.B3 (92), ST.00.K8C.16.152 (95),

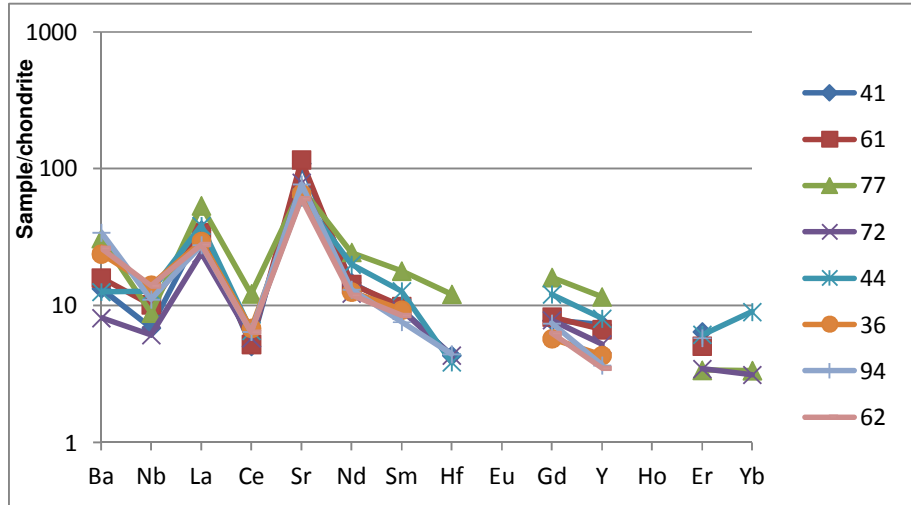


**Figure 3.24.** The multi-element diagrams of ST.02.I8b.28.A2 (36), ST.02.I8B.19.6 (41), ST.02.I8b.21.17 (44), ST.02.I8b.23.11 (61), ST.02.I8b.28A.2 (62), ST.02.I8b.15.17 (72), ST.02.K9c.27a.11 (77), ST.99.K8C.9.22 (94)

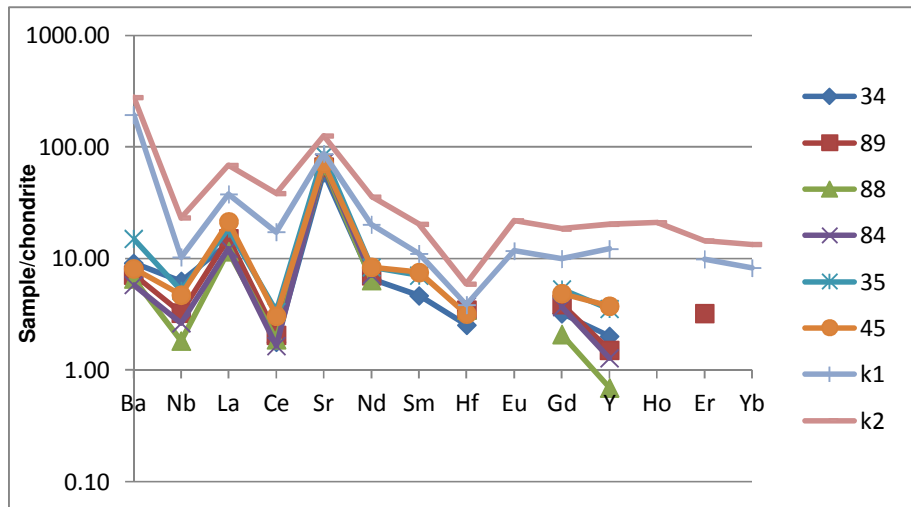


**Figure 3.25.** The multi-element diagrams of ST.02.I8B.19.b6 (34), ST.02.I8b.11.b9 (35), ST.02.I8b.25.12 (45), ST.02.I8b.19.A12 (84), ST.99.I9b.2.17 (88), ST.01.I8.B.10.26 (89)

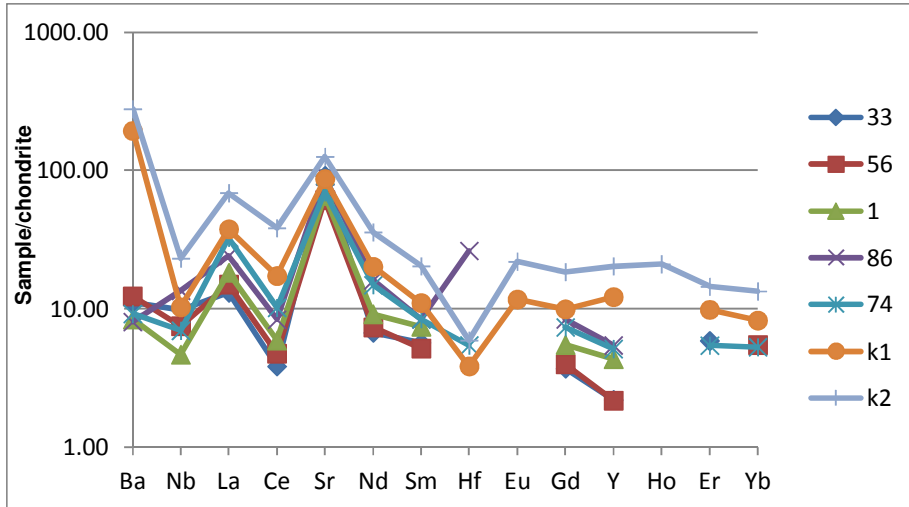


**Figure 3.26.** The multi-element diagrams of ST.02.I8b.16A.16 (33), ST.02.K9c.27A.13 (56), ST.02.I8b (74), ST.00.K8C.16.148 (86)

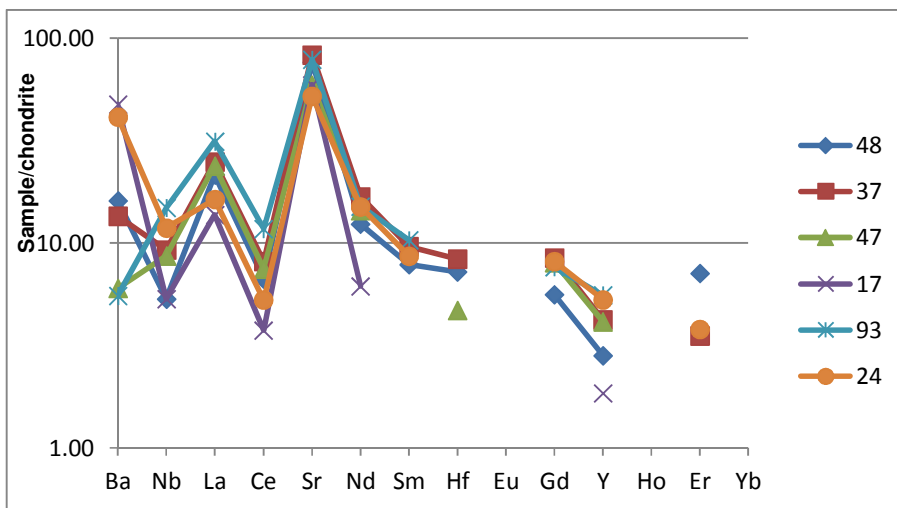


**Figure 3.27.** The multi-element diagrams of ST.06.I12.d3.9 (17), ST.02.I8b.16A.11 (24), ST.02.I8B.16.A.15 (37), ST.02.I8b.28.6.3 (47), ST.02.I8b.28.8 (48), ST.00.D8.A.5.25 (93)

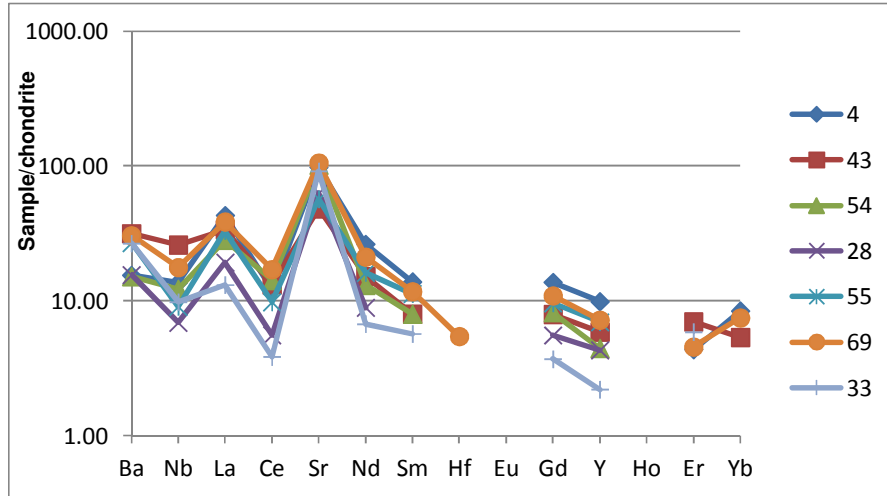


**Figure 3.28.** The multi-element diagrams of ST.06.H12.a3.16 (4), ST.02.I8b.11.c26 (28), ST.02.I8b.16A.16 (33), ST.02.I8b.28.A3 (43), ST.02.K9c.28.6 (54), ST.02.K9c.27.4 (55), ST.02.K9.c27.A12 (69)

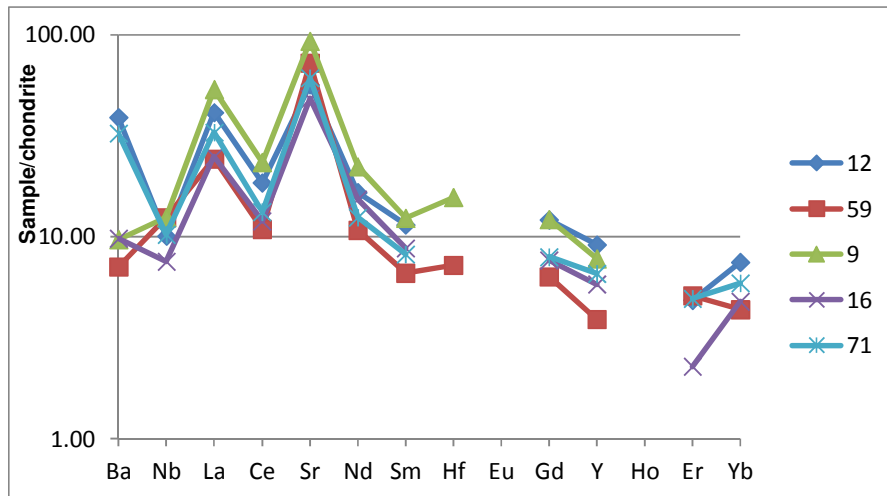


**Figure 3.29.** The multi-element diagrams of ST.06.H12.a2A.23 (9), ST.06.I12d.6A.11 (12), ST.06.I12.d5.B11 (16), ST.02.K9c.26.4 (59), ST.02.I8b.14.30 (71)

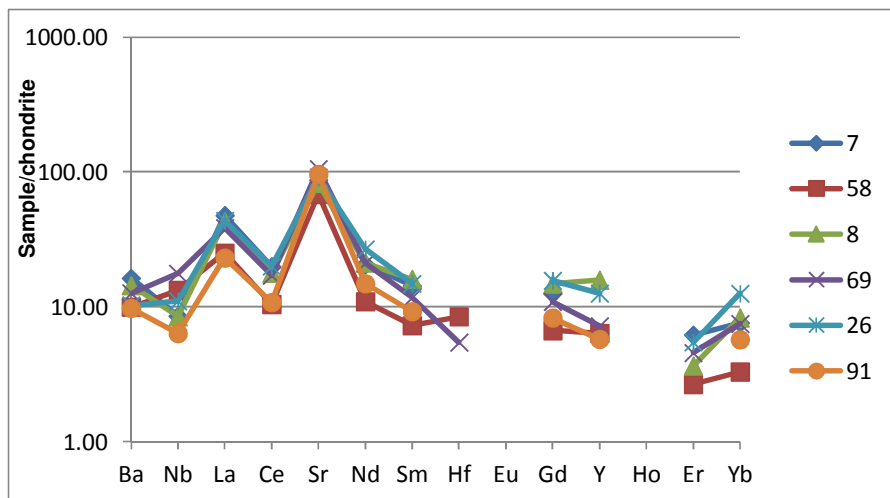


**Figure 3.30.** The multi-element diagrams of ST.06.I12.d7.43 (7), ST.06.I12.d5.A11 (8), ST.02.I8b.16A.11 (26), ST.02.I8b.14.20 (58), ST.02.K9.c27.A12 (69), ST.99.I9B.4 (91)

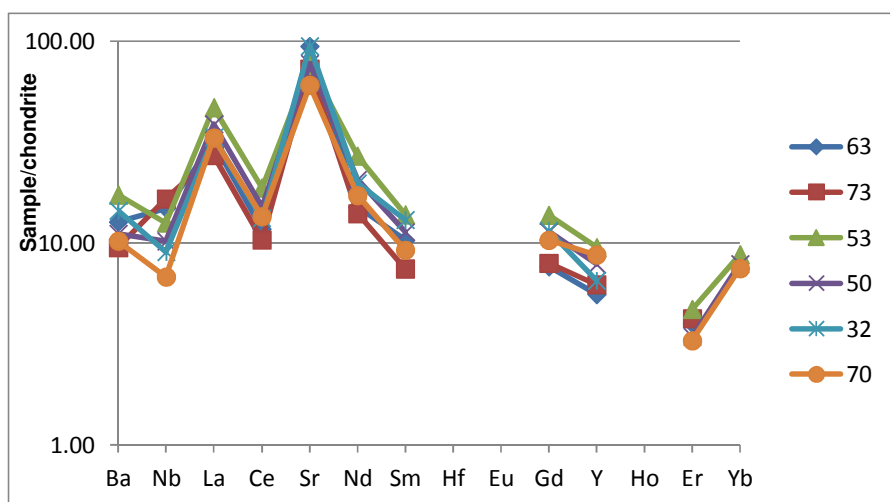


**Figure 3.31.** The multi-element diagrams of ST.02.I8b.28A.11 (32), ST.02.I8b.19.2 (50), ST.02.I8b.14.17 (53), ST.01.G11.D1 (63), ST.02.I8b.28.A9 (70), ST.02.I8b.16A.17 (73)

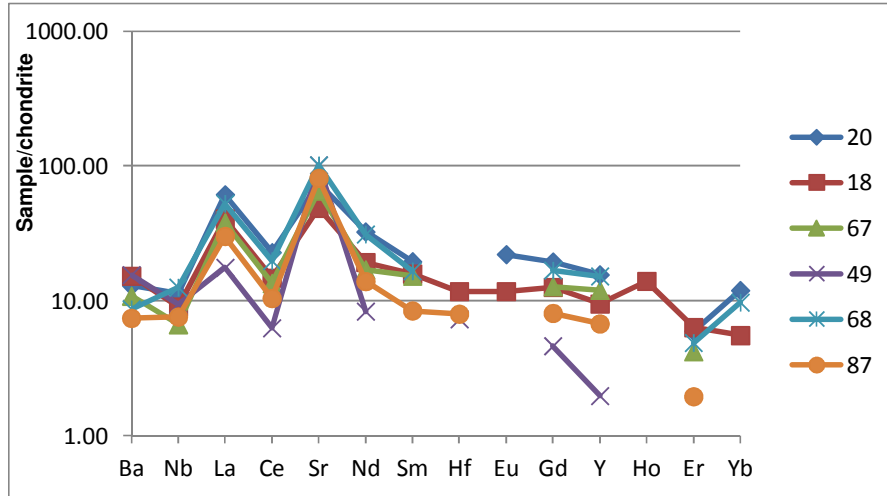


**Figure 3.32.** The multi-element diagrams of ST.06.I12.d5A.12 (18), ST.02.I8b.19.2 (49), ST.02.K9c.27A.3 (67), ST.02.K9.c28.14 (68), ST.99.I9b.4.65 (87)

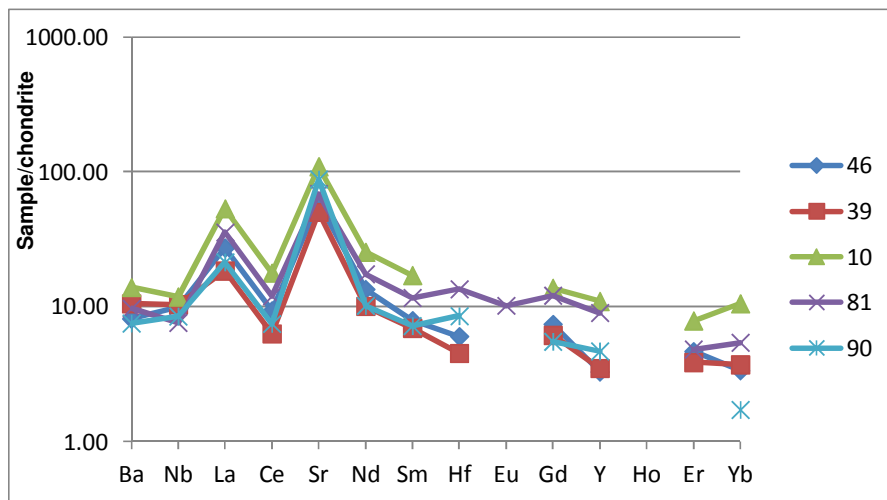


**Figure 3.33.** The multi-element diagrams of ST.06.I12.d6A.14 (10), ST.02.I8b.16.20 (39), ST.02.I8b.22.2 (46), ST.02.I8b.23.9 (81), ST.00.K8.C.16.151 (90)

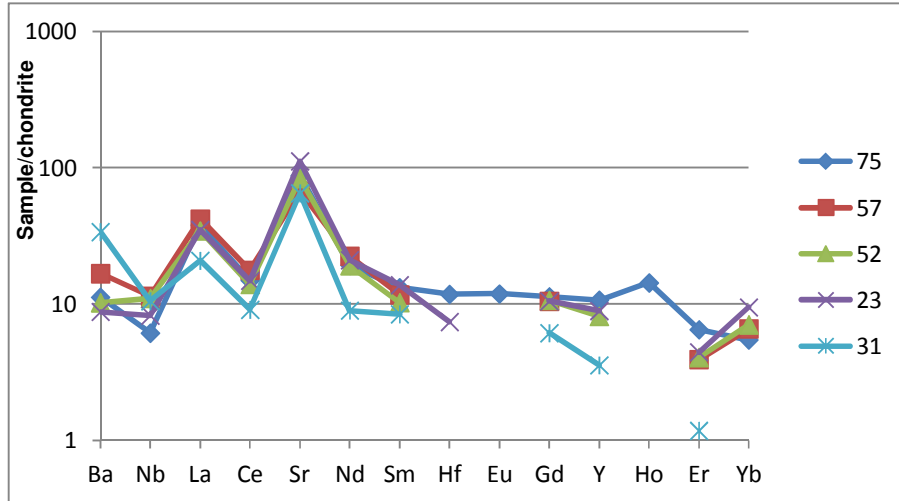


**Figure 3.34.** The multi-element diagrams of ST.02.I8b.16A.11 (23), ST.02.I8b.25.11 (31), ST.02.I8b.18.7 (52), ST.02.I8b.11b.10 (57), ST.02.I8b.28.3 (75)

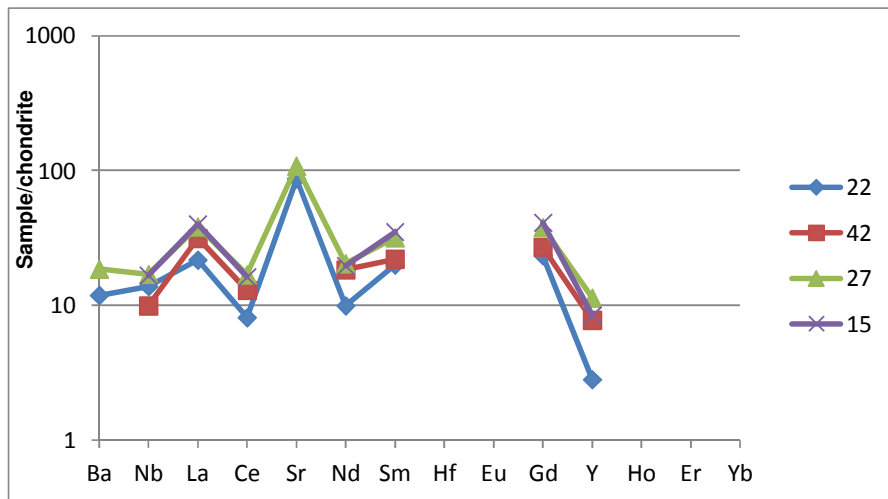


**Figure 3.35.** The multi-element diagrams of ST.06.I12.d7.45 (15), ST.02.I8b.18.3 (22), ST.02.I8b.16A.11 (27), ST.02.K9c.28.7.4 (42)

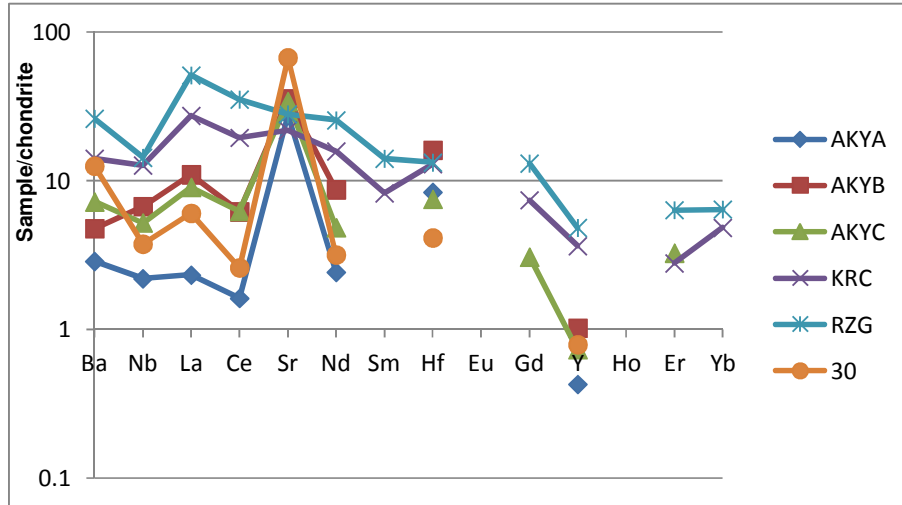


Figure 3.36. The multi-element diagrams of geological samples from Datça

### 3.11 Element Ratios for Figurines and Geological Samples

Besides REE patterns and multi-element diagrams of samples, fractionation of LREE, HREE, TREE and Eu anomaly or Ce anomaly could be discriminated for different types of limestone. LREE fractionation which is calculated as  $(La/Sm)_n$ , HREE fractionation which is calculated as  $(Gd/Yb)_n$ , and TREE which is calculated as  $(La/Yb)_n$  is given in Table 3.12. Ce anomalies of each sample along with total REE concentrations were also calculated and given in Table 3.14 and arranged according to the Ce anomalies.

Table 3.14. REE fractionations, Ce anomaly and  $\sum REE$  of samples

Samples	Ce/Ce*	La <sub>n</sub> /Yb <sub>n</sub>	La <sub>n</sub> /Sm <sub>n</sub>	Gd <sub>n</sub> /Yb <sub>n</sub>	Nd <sub>n</sub> /Sm <sub>n</sub>	$\sum REE$ (mg/kg)	Er/Nd
1	0.39		0.55		0.61	21.30	
2	0.20					15.46	0.13
3	0.91		0.60		0.93	35.54	
4	0.31	0.53	0.70	1.19	0.95	52.48	0.06
5	0.48	0.63	0.57	1.37	0.56	118.48	0.08
6	0.51	0.55	0.47	1.54	0.58	85.76	0.09
7	0.52	0.65	0.75	1.21	0.72	53.36	0.11
8	0.50	0.53	0.60	1.30	0.66	63.19	0.06
9	0.55		0.98		0.90	53.97	
10	0.41	0.52	0.70	0.95	0.74	61.04	0.11

**Table 3.14  
continued**

<b>Samples</b>	<b>Ce/Ce*</b>	<b>La<sub>n</sub>/Yb<sub>n</sub></b>	<b>La<sub>n</sub>/Sm<sub>n</sub></b>	<b>Gd<sub>n</sub>/Yb<sub>n</sub></b>	<b>Nd<sub>n</sub>/Sm<sub>n</sub></b>	<b>∑REE (mg/kg)</b>	<b>Er/Nd</b>
11	0.45	0.62	0.85	1.21	0.96	85.77	0.08
12	0.58	0.57	0.81	1.19	0.72	49.42	0.10
14	0.30	0.59	0.70	1.26	0.74	87.98	0.11
15	0.49		0.26		0.28	55.64	
16	0.53	0.54	0.64	1.17	0.87	33.57	0.05
17	0.34					11.31	
18	0.44	0.75	0.58	1.67	0.61	51.01	0.12
19	0.34		0.69		1.13	32.41	
20	0.44	0.53	0.71	1.19	0.83	79.50	0.06
22	0.46		0.25		0.25	27.03	
23	0.47	0.38	0.57	0.81	0.76	47.86	0.08
24	0.30		0.43		0.87	26.02	0.09
26	0.51	0.36	0.66	0.91	0.90	63.25	0.07
27	0.51		0.27		0.32	59.41	
28	0.36					20.03	
30	0.51					5.74	
31	0.55		0.56		0.53	23.04	0.05
32	0.45		0.58		0.76	39.81	
33	0.38		0.61		0.70	35.79	0.14
34	0.16		0.67		0.71	11.94	
35	0.22		0.59		0.59	18.09	
36	0.29		0.72		0.68	26.44	
37	0.35		0.58		0.88	29.14	0.07
38	0.33		0.84		1.23	11.54	
39	0.40	0.51	0.60	1.21	0.73	21.97	0.14
40	0.17		0.62		0.70	24.08	0.12

**Table 3.14  
continued**

<b>Samples</b>	<b>Ce/Ce*</b>	<b>La<sub>n</sub>/Yb<sub>n</sub></b>	<b>La<sub>n</sub>/Sm<sub>n</sub></b>	<b>Gd<sub>n</sub>/Yb<sub>n</sub></b>	<b>Nd<sub>n</sub>/Sm<sub>n</sub></b>	<b>∑REE (mg/kg)</b>	<b>Er/Nd</b>
41	0.18		0.85		0.78	33.95	0.16
42	0.46		0.32		0.42	37.28	
43	0.48	0.65	0.95	1.08		41.99	0.16
44	0.20	0.44	0.68	0.98	0.78	18.91	0.11
45	0.18		0.64		0.56	27.70	
46	0.41	0.84	0.78	1.61	0.85	25.05	0.12
48	0.35		0.62		0.79	22.92	
49	0.43					15.94	0.20
50	0.46	0.51	0.77	1.06	0.91	46.34	
52	0.47	0.50	0.76	1.10	0.93	44.10	0.06
53	0.45	0.55	0.76	1.15	0.98	57.28	0.07
54	0.62		0.80		0.82	31.32	0.06
55	0.36		0.66		0.72	35.94	
56	0.38	0.28	0.65	0.53	0.71	16.48	
57	0.49	0.66	0.81	1.17	0.96	52.36	0.18
58	0.52	0.78	0.78	1.48	0.75	30.90	0.06
59	0.56	0.57	0.83	1.06	0.82	27.44	0.09
60	0.58	0.58	0.77	1.15	0.75	51.26	0.17
61	0.19		0.78		0.73	32.55	0.11
62	0.29		0.74		0.70	24.20	0.13
63	0.45		0.68		0.73	34.16	
64	0.89		0.68		0.74	16.42	0.09
65	0.16		0.75		0.86	24.70	
66	0.47		0.77		0.91	49.68	0.21
67	0.44		0.56		0.56	71.43	0.08
68	0.42	0.56	0.71	1.27	0.94	46.81	

**Table 3.14  
continued**

<b>Samples</b>	<b>Ce/Ce*</b>	<b>La<sub>n</sub>/Yb<sub>n</sub></b>	<b>La<sub>n</sub>/Sm<sub>n</sub></b>	<b>Gd<sub>n</sub>/Yb<sub>n</sub></b>	<b>Nd<sub>n</sub>/Sm<sub>n</sub></b>	<b>∑REE (mg/kg)</b>	<b>Er/Nd</b>
<b>69</b>	0.51	0.53	0.74	1.07	0.90	43.19	0.06
<b>70</b>	0.48	0.46	0.81	1.01	0.93	36.71	0.08
<b>71</b>	0.53	0.57	0.90	0.99	0.76	27.26	0.07
<b>72</b>	0.28	0.79	0.59	1.84	0.67	32.55	0.14
<b>73</b>	0.45		0.82		0.94	33.58	0.10
<b>74</b>	0.39	0.64	0.87	1.02	0.88	51.83	0.11
<b>75</b>	0.47	0.72	0.65	1.52	0.73	57.00	0.13
<b>77</b>	0.28	1.65	0.67	3.50	0.68	21.23	0.12
<b>80</b>	0.16		0.59		0.79	44.56	0.05
<b>81</b>	0.40	0.68	0.69	1.63	0.75	10.02	0.14
<b>84</b>	0.15					69.75	0.10
<b>85</b>	1.10	0.51	0.70	1.21	0.76	29.96	
<b>86</b>	0.37		0.65		0.96	33.89	0.11
<b>87</b>	0.43		0.80		0.82	8.38	
<b>88</b>	0.19					11.82	0.05
<b>89</b>	0.17					24.21	
<b>90</b>	0.42		0.67		0.71	32.08	
<b>91</b>	0.51	0.42	0.56	1.06	0.80	21.70	0.06
<b>92</b>	0.18		0.72		0.79	13.68	
<b>93</b>	0.35		0.52		0.59	26.01	0.10
<b>94</b>	0.28		0.82		0.86	18.26	
<b>95</b>	0.20					21.30	0.16
<b>AKYA</b>	0.60					12.04	
<b>AKYB</b>	0.56					3.34	
<b>AKYC</b>	0.80					10.53	
<b>KRC</b>	0.81	0.58	0.75	1.12	0.96	35.49	

<b>Table 3.14 continued</b>							
<b>Samples</b>	<b>Ce/Ce*</b>	<b>La<sub>n</sub>/Yb<sub>n</sub></b>	<b>La<sub>n</sub>/Sm<sub>n</sub></b>	<b>Gd<sub>n</sub>/Yb<sub>n</sub></b>	<b>Nd<sub>n</sub>/Sm<sub>n</sub></b>	<b>∑REE (mg/kg)</b>	<b>Er/Nd</b>
<b>RZG</b>	0.82	0.82	0.82	1.49	0.91	60.03	
<b>K1</b>	0.54	0.47	0.77	0.88	0.91	55.55	0.17
<b>K2</b>	0.66	0.53	0.76	1.01	0.88	102.45	0.14
<b>K3-1</b>	0.60	0.66	0.77	1.27	0.93	45.28	0.14
<b>K3-2</b>	0.63	0.66	0.78	1.28	0.88	64.72	0.14
<b>K3-3</b>	0.50	0.66	0.81	1.20	0.98	37.98	0.17

(La/Yb)<sub>n</sub> ratios indicating TREE fractionation, vary between 0.28 and 1.65 for figurines in which this value could be calculated. The ratios between 0.9 and 1 are indicative of a moderate depletion of LREE [71]. (La/Yb)<sub>n</sub> ratio more than 1.3 suggested by Sholkovitz as an indicative for terrigenous particulate matter [115]. Lesser ratios imply that the signals of REEs were influenced by the LREE-depleted carbonate component. Therefore, by this definition except for figurine numbered ST.02.K9c.27a.11 (77), figurines exhibit generally depleted LREE characteristics.

(La/Yb)<sub>n</sub> ratios for geological samples from Datça could not be calculated due to the lack of Yb concentration that is generally found to be below detection limit. For other locations in Datça KRC and RZG show depletion of LREEs. Geological samples from 5 different location in Cyprus also have similar (La/Yb)<sub>n</sub> ratios indicating depletion of LREE.

(La/Sm)<sub>n</sub> ratio indicating LREE fractionation is between 0.59 and 0.98 for the figurines. In relation to MREEs and HREEs, a general enrichment of MREE, with concentration peaks at Nd to Sm, in fossil apatite has been reported [116]. The reason of this, as phosphates contain large concentrations of REEs, the presence of phosphatic phases in sediment may be important in controlling REE composition [66]. Therefore, the peaks at Nd to Sm in their REE pattern of ST.06.I12.d7.45 (15), ST.02.I8b.18.3 (22), ST.02.I8b.16A.11 (27), ST.02.K9c.28.7.4 (42) are a result of foraminiferal tests. It is also reported that (La/Sm)<sub>n</sub> ratio is significantly correlated with Y [66]. It is because, the substitution of Y and REE in the lattice of Ca-phosphate.

The effects of LREE/HREE fractionation in modern and ancient marine systems can be interpreted using Er/Nd (mg/kg) ratios [117]. The seawater has an Er/Nd ratio value of about 0.27 [66]. Er/Nd ratios for the figurines, are between 0.06 and 0.18 given in Table 3.12. There are few exceptions however, four of the figurines ST.06.I12.d5.B11 (16), ST.02.I8b.25.11 (31), ST.02.I8b.23.9 (80), ST.99.I9b.2.17 (88) have lower ratios, and two figurines ST.02.I8b.19.2 (49), ST.02.I8b.21.20 (66) have higher ratios of 0.20 and 0.21 given in Table 3.12. Studies show that the low Er/Nd ratios may be due to detrital materials which were transported during the sedimentary process and coatings on mineral phases to concentrate Nd with respect to Er. Er/Nd ratios for geological samples from Datça could not be calculated due to lack of Er values, because the concentrations were too low to be detected. However, it still means that geological samples from Datça were enriched in LREEs.

As it can be seen from the Table 3.12, figurines form three different groups according to their Ce anomalies. However, there is no direct relation with Ce anomalies and total REEs

concentrations. According to many studies on Ce anomaly, Ce can undergo oxidation in seawater from soluble Ce(III) to the highly insoluble Ce (IV), unlike other REEs [71, 115-117]. The subsequent fixation of Ce(IV) in particulate matter, including organic, is considered as the reason of distinctive depletion of Ce in oxygenated seawater. In interpreting REE distribution patterns of the limestones, we should evaluate the role of foraminifera tests in the marine geochemistry of the REE [115]. According to studies, foraminiferal calcite and Fe/Mn oxide coatings are perfect locations for the dissolved REEs to be clustered. The coatings host a large proportion of REE with Ce-depleted shale-normalized patterns similar to those of seawater.

Figurine samples in this study exhibit very extreme Ce anomaly ( $Ce/Ce^* \leq 0.30$ ), extreme to moderate Ce anomaly ( $Ce/Ce^*$  between= 0.30-0.70), and no Ce anomaly ( $Ce/Ce^*$  between 0.89 and 1.10). Meantime, the geological samples from Datça have moderate to slightly Ce anomalies between  $Ce/Ce^* = 0.56$  to 0.82. The geological samples from Cyprus have moderate Ce anomalies between 0.50 and 0.66.

### 3.12 Binary Diagrams of Figurines and Geological Samples

Binary diagrams, also sometimes called as variation or scattered diagrams are also helpful in appointing different types of stone. Among many others, it has been found that  $\Sigma REE$  vs Ce anomaly and  $(La/Sm)_n$  vs  $Sm_n$  diagrams are found to be best for discriminating groups of figurines according to their sources.  $\Sigma REE$  vs Ce anomaly and  $(La/Sm)_n$  vs  $Sm_n$  diagrams are given in Figure 3.37 and 3.38.

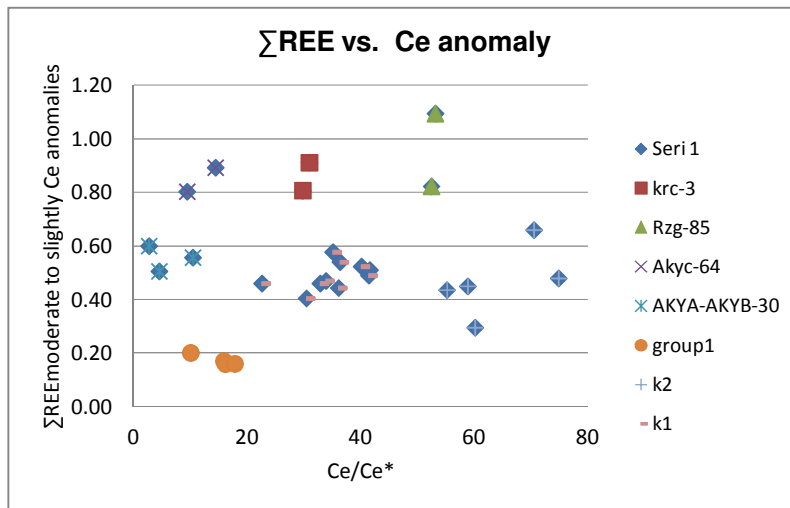


Figure 3.37.  $\Sigma REE$  ( $\mu g/kg$ ) vs Ce anomaly binary plot for all the samples

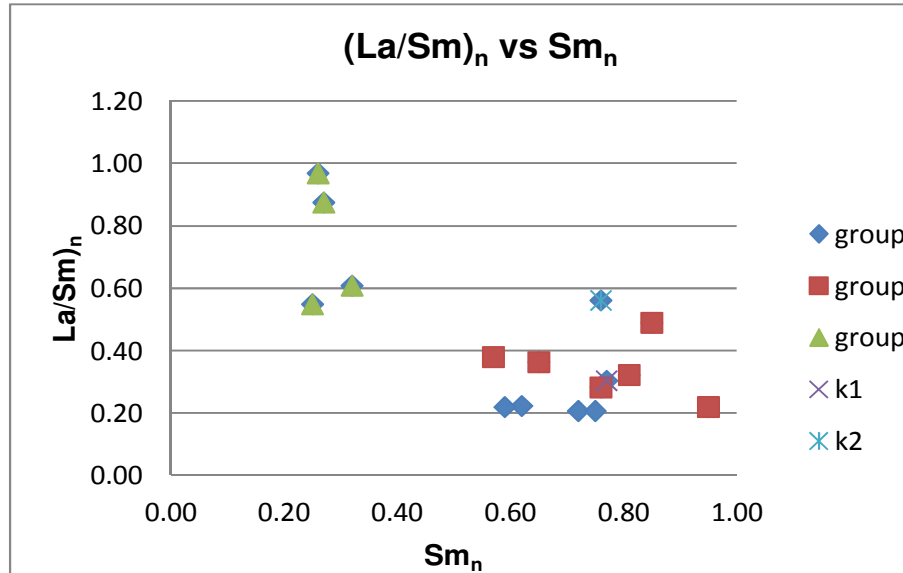


Figure 3.38.  $(La/Sm)_n$  vs  $Sm_n$  binary plot for all the samples

Ce anomaly for the figurines range between extremely negative anomaly to no anomaly which is  $Ce/Ce^* = 0.15 - 1.10$ . Ce anomaly for the geological samples from Datça is moderate to slightly Ce anomalies between  $Ce/Ce^* = 0.56-0.82$ . Geological samples from Cyprus also show moderate Ce anomaly which is  $Ce/Ce^* = 0.50-0.66$ . Meantime, total REE concentration for the figurines is between 5.74 and 118.5, for geological samples from Datça 12.1 and 60.0. Geological sample K1 in Cyprus have a total REE of 55.6 and the geological sample K2 in Cyprus have a total REE of 102.5 (Table 3.12). Although there is no direct correlation between total REE concentrations and Ce anomalies, the binary diagram of  $\sum REE$  vs Ce anomaly discriminates figurines that were probably made from local sources, figurines made from different sources in Cyprus, and a different group of figurines with undefined source.

$(La/Sm)_n$  vs  $Sm_n$  diagram of the samples which measures the degree of LREE fractionation is also helpful to specify two groups for the figurines. Here *Group 4* differs from the rest according to its LREE fractionation.

### 3.13 Statistical Evaluation of Chemical Analysis

For provenance investigation of limestone figurines, many elements were determined. In order to realize the similarities and correlations between various archaeological and geological samples, multivariate statistical methods were applied after initial evaluation of results using REE patterns and multi-element diagrams. Principal component analysis (PCA) and hierarchical cluster analysis with dendrogram representation were used in this study. PCA was employed to transform the original variables into a set of uncorrelated principal component scores. PCA has several advantages, which are: it employs all the useful element concentration data for every sample in the dataset; fewer combinations are plotted; the distinctions between groups are usually clear [119].

Hierarchical cluster analysis is then applied both groups to determine whether it results in a homogeneous cluster for geological samples and can be clearly discriminated from each other. It is also aimed to understand whether archaeological samples form different groups regarding their production based on chemical analysis and provide information on the source of raw

material of archaeological groups. Dendrograms are used to visualize the results which were obtained from cluster analysis.

### 3.13.1 Variable Selection for Hierarchical Cluster Analysis

Rather than using 19 elements and consequently element ratios which were determined through chemical analysis in this study in hierarchical cluster analysis, it is useful to analyze to correlations with each others. This process of reducing the number of variables to a smaller number of independent variables that control all the variables is called *dimensional scaling* [120]. By this process, the casual relationships would be more easily studied. Moreover in further studies, dimensional scaling would allow to determine only the reduced number of variables in chemical analysis which could be used as marker for provenance of limestone figurines.

One of the commonly used dimensional analysis methods is principal component analysis in archaeology [120]. Principal component analysis, PCA, is commonly used in provenance studies to examine graphically the grouping pattern of the samples in terms of their chemical compositions and assign these groups to a common origin of raw material. PCA involves a transformation of the dataset on the basis of eigenvector methods to determine the magnitude and the direction of maximum variance in the dataset distribution in hyperspace [121]. The PCA, before further evaluation of element concentrations of samples, provides a new basis for interpreting the entire data.

The PCA is related to identifying new dimensions that are called components [120]. The principal components method of extraction means finding a linear combination of that reflecting as much variables in original number of variables. Usually, a few components will substitute for most of the variation, and these components can be used to replace the original variables.

Using PCA, many elements that were determined could be reduced to obtain more reliable results for cluster analysis of the data. Doing so, PCA could also allow us to understand the possible fingerprints or markers for limestone figurines. Statistical analyses of the samples were performed by using the Statistics Package for Social Science (SPSS) [122]. 18 variables were chosen for multivariate analysis as follows: La, Ce, Nd, Y, Nb, Cr, Ce/Ce\*,  $\Sigma$ REE, Ba, Sr, Mn, Mg, Fe,  $\Sigma$ REE/(Ce/Ce\*), Sm, and ratios of Nd/Sm, Mn/Cr, and Fe/Mn. The selection of variables was made regarding to literature and primary evaluations of chemical analysis results through REE patterns, multi-element diagrams and binary plots.

The communalities indicating the amount of variance in each variable is given in Table 3.15. In first column Initial communalities are given and they are estimates of the variance in each variable accounted for by all components or factors. Extraction communalities in second column are estimates of the variance in each variable accounted for by the components. Higher values of extraction communalities mean extracted components represent the variables well.

**Table 3.15.** Communalities for PCA

Variables	Initial	Extraction
La	1.000	.948
Ce	1.000	.929
Nd	1.000	.950
Y	1.000	.919
Nb	1.000	.554
Cr	1.000	.877
Ce/Ce*	1.000	.882
ΣREE	1.000	.990
Ba	1.000	.389
Sr	1.000	.632
Mn	1.000	.887
Mg	1.000	.811
Fe	1.000	.911
ΣREE/ (Ce/Ce*)	1.000	.857
Sm	1.000	.908
Nd/Sm	1.000	.855
Mn/Cr	1.000	.660
Fe/Mn	1.000	.827

The initial eigenvalues of the PCA is given in Table 3.16. Eigenvalues given in first column are expected to be greater than 1 will be extracted, so the first five principal components form the extracted solution for this study.

**Table 3.16.** Initial Eigenvalues of the PCA

Component	Initial Eigenvalues		
	Total	% of Variance	Cumulative %
1	6.149	34.162	34.162
2	4.040	22.442	56.604
3	2.072	11.511	68.116
4	1.458	8.098	76.214
5	1.068	5.935	82.148
6	.759	4.218	86.366
7	.628	3.491	89.857

<b>Table 3.16. continued</b>			
8	.595	3.306	93.163
9	.525	2.917	96.080
10	.257	1.430	97.511
11	.112	.621	98.132
12	.106	.588	98.720
13	.080	.442	99.162
14	.061	.341	99.503
15	.043	.236	99.739
16	.029	.159	99.898
17	.017	.096	99.994
18	.001	.006	100.000

Extraction Sums of Squared Loadings and Rotation Sums of Squared Loadings of the PCA is given in Table 3.17. Cumulative % of the Extraction Sums of Squared Loadings indicates that approximately 82 % of the variability in the original 18 variables is explained by using 5 components. In other words, the complexity of the original data set can considerably be reduced by using these five components, with only an 18% loss of information. The rotation maintains the cumulative percentage of variation explained by the extracted components, but that variation given in the Totals is now spread more or less evenly over the components.

**Table 3.17.** Extraction Sums of Squared Loadings and Rotation Sums of Squared Loadings

Component	Extraction Sums of Squared Loadings			Rotation Sums of Squared Loadings		
	Total	% of Variance	Cumulative %	Total	% of Variance	Cumulative %
1	6.149	34.162	34.162	5.782	32.120	32.120
2	4.040	22.442	56.604	3.053	16.961	49.081
3	2.072	11.511	68.116	2.615	14.529	63.610
4	1.458	8.098	76.214	1.758	9.765	73.376
5	1.068	5.935	82.148	1.579	8.773	82.148

The rotated component matrix is given in Table 3.18. Rotation method here is *Varimax with Kaiser Normalization*. The rotated component matrix helps to determine how 18 of variables are weighted for each component and the correlation between the variables and components that were extracted. As it can be determined from the table, the first component is most highly correlated with  $\Sigma$ REE, La, Nd, and Y. However, Y is a better representative, because it is less correlated with the other four components. The second component is most highly correlated with Mn and Cr. The third component is most highly correlated with Fe/Mn. The fourth component is most highly correlated with Ce/Ce\* and fifth component with Mn/Cr.

**Table 3.18.** Rotated Component Matrix

	Component				
	1	2	3	4	5
La	.965	.066	.097	-.034	-.046
Ce	.762	.251	.332	.418	-.015
Nd	.953	.086	.121	-.042	-.138
Y	.947	-.139	.032	-.005	.038
Nb	.348	.059	.518	.395	-.068
Cr	.021	.896	.081	.185	-.181
Ce/Ce*	.187	.289	.411	.769	.054
$\Sigma$ REE	.981	.034	.133	.089	.014
Ba	.291	-.133	.517	.137	.029
Sr	.324	-.290	.177	-.638	.070
Mn	.099	.879	-.280	.058	.154
Mg	-.036	.794	.211	.359	-.077
Fe	.035	.728	.600	-.032	.140
$\Sigma$ REE/ (Ce/Ce*)	.774	-.072	-.166	-.472	-.051
Sm	.724	.059	.031	-.006	.616
Nd/Sm	.136	.007	.014	-.003	-.914
Mn/Cr	.012	-.128	-.628	-.086	.492
Fe/Mn	-.049	.090	.902	-.034	.024

Component Score Coefficient Matrix of PCA for this study is given in Table 3.19. This matrix is basically the set of weights used to calculate the component scores. Generally, Component Score Coefficient Matrix helps to understand the contribution of each variable to the component scores. In other words, strongly correlated variables that are highly correlated to the components are likely to have low weights in this table.

**Table 3.19.** Component Score Coefficient Matrix

	Component				
	1	2	3	4	5
La	.172	.022	-.026	-.031	-.055
Ce	.127	-.011	.016	.232	-.007
Nd	.171	.033	-.021	-.047	-.113
Y	.174	-.067	-.045	.049	-.003
Nb	.039	-.091	.146	.212	-.012
Cr	.002	.328	-.053	-.072	-.118
Ce/Ce*	.022	-.074	.038	.467	.066
ΣREE	.174	-.021	-.026	.066	-.012
Ba	.019	-.113	.213	.053	.053
Sr	.028	.010	.194	-.453	.046
Mn	.029	.364	-.183	-.097	.068
Mg	-.016	.241	-.004	.063	-.036
Fe	-.050	.279	.269	-.292	.131
ΣREE/ (Ce/Ce*)	.145	.078	-.055	-.300	-.076
Sm	.111	.013	.007	.003	.379
Nd/Sm	.055	.009	-.075	-.010	-.599
Mn/Cr	.032	-.008	-.244	.078	.271
Fe/Mn	-.080	.002	.444	-.208	.088

The scatter plots of the five principal components of figurine samples and geological samples are given in Figure 3.39. The first plot in the first row shows the first component on the vertical axis versus the second component on the horizontal axis, and the order of the remaining plots follows likewise. The scatterplot matrix shows that pc 1 vs. pc 2, pc 3 and pc 5 has a skewed distribution, which is because the first component Y concentration is skewed. Then, the two largest principal components, which contribute most of the total variance in the elemental variable, usually is the best method for the separation groups of samples [119, 123]. However, the case in this study is different, since five components which were determined by PCA are linearly correlated to each others. Therefore, as shown in Figure 3.39 either figurines or possible geological sources for their raw material could not be separated well enough.

Since the PCA does not reveal clear and homogeneous group, none of five components which were determined through the PCA could be used as variables in cluster analysis. Instead, using the information obtained from *Component Score Coefficient Matrix* given in Table 3.17, five variables are identified as the variables which would be used instead of original variables in hierarchical cluster analysis and are useful for discriminating geological sources and corresponding archaeological samples. These variables are: La, Mg, ΣREE concentration Ce/Ce\* and Mn/Cr ratio. The reason for identification, for instance La and ΣREE concentrations have higher weights for component 1, meantime less weights for other components. Instead of select Mn or Cr of which have higher weights for component 2, Mn/Cr ratio is chosen as another new variable along with La and ΣREE concentration. Mg and Ce/Ce\* are selected instead of using pc 2 and pc 4 which were determined by PCA.

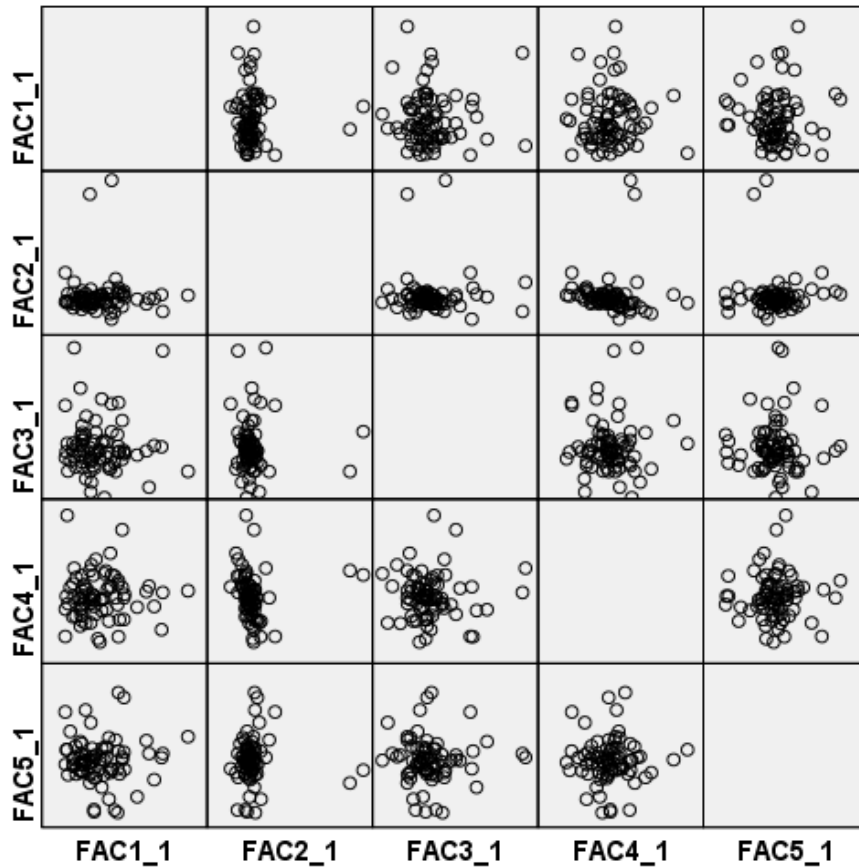


**Figure 3.39.** Scatter plots of five principal components scores

### 3.13.2 Hierarchical Cluster Analysis

Cluster analysis is considered as an excellent tool to identify quarried and raw materials used either in ancient monuments or statues [62, 124,125].

The main idea for cluster analysis is to create homogeneous groups of variables called clusters [126]. Clustering, creation of classification is probably one of the most fundamental methods of dealing with complex and complicated data [127]. Regarding to archaeology, hierarchical cluster analysis could be defined as artifact typology. The artifacts found at an excavation site for instance are grouped first according to broad classes such as their raw materials stone, ceramic, metal etc, then after several steps into more specific groups. The first step of a hierarchical cluster analysis in multivariate statistics is then measuring the similarities or dissimilarities or distances between each pair of cases in a dataset [127]. Once the computation of the distance between the cases is done, the cluster analysis method to create groups would be chosen [126].

Selection of samples or cases to be combined in clustering is the first basics of cluster analysis [126]. Then, the definition of variables on which to measure distance in samples is very critical in order to obtain a meaningful result.

Hierarchical cluster analysis begins with the idea that each case in the dataset is a separate entity [127].the first step is to combination of two cases into one cluster. At the next step of cluster analysis, either two other cases are combined into another cluster or a third case is

combined to the first existing cluster. This process continues to more and more inclusive clusters, and then finally almost all cases are combined into one big cluster.

The distance, then, is calculated by using Euclidean distance formula in this study. A data set with (n) objects, each of which is described by (d) attributes, is denoted by  $D=\{x_1, x_2, \dots, x_n\}$ , where  $x_i=(x_{i1}, x_{i2}, \dots, x_{id})^T$  is a vector denoting the i th object and  $x_{ij}$  is a scalar denoting the j th component or attribute of  $x_i$  [128]. The number of attributes (d) is also called the dimensionality of the data set. Consider the two data points  $x=(x_1, x_2, \dots, x_d)^T$  and  $y=(y_1, y_2, \dots, y_d)^T$ . In calculating Euclidean distance following formula is used;

$$d(x, y) = \left[ \sum_{j=1}^d (x_j - y_j)^2 \right]^{1/2}$$

Except Euclidean distance, there are some other distance measures and given below:

- Manhattan distance

$$d_{man}(x, y) = \sum_{j=1}^d |x_j - y_j|$$

- Maximum distance

$$d_{max}(x, y) = \max_{1 \leq k \leq d} |x_k - y_k|$$

- Minkowski distance

$$d_{mink}(x, y) = \left[ \sum_{j=1}^d |x_j - y_j|^r \right]^{1/r}, r \geq 1$$

r, here, is the order of the Minkowski distance

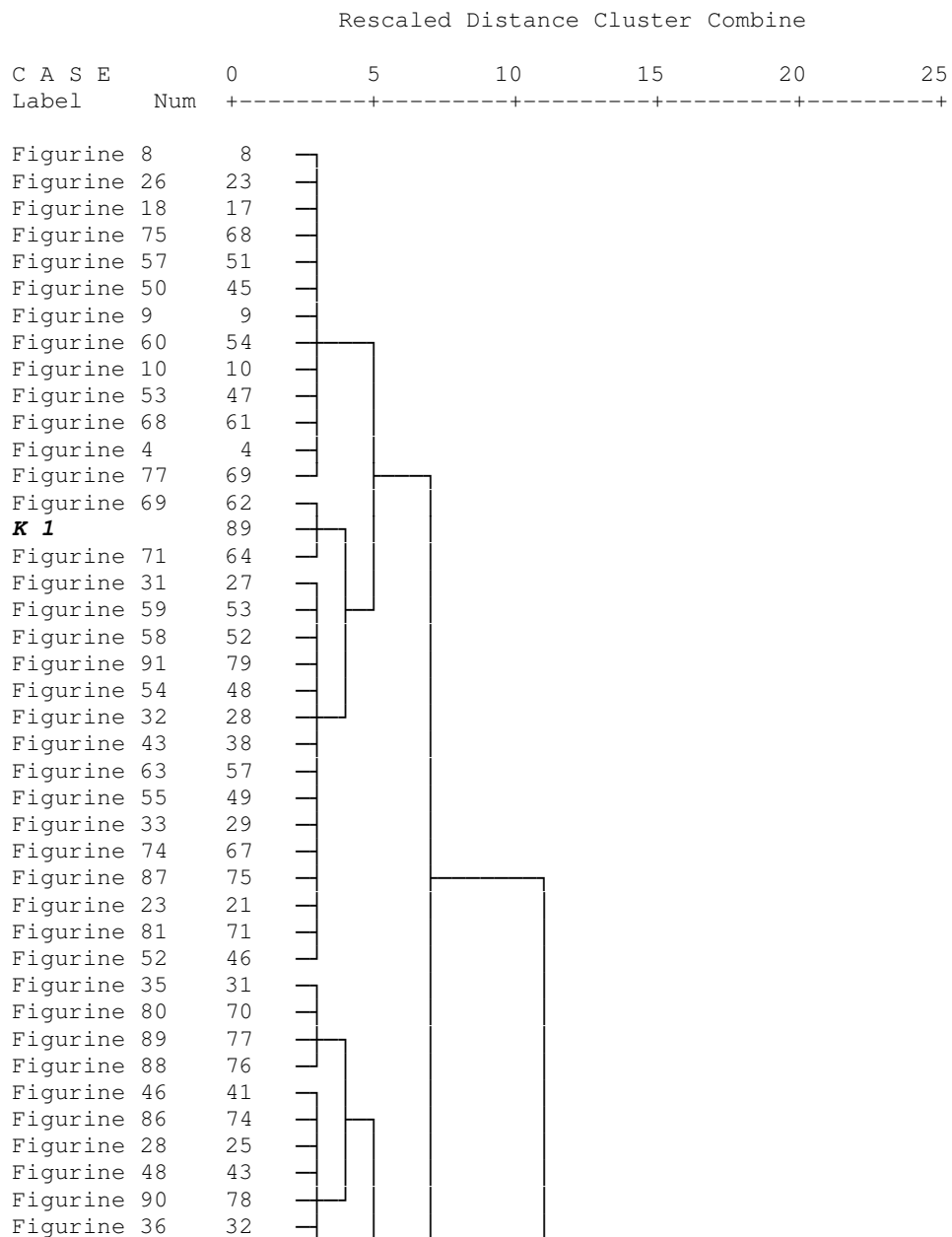
- Mahalanobis distance

$$d_{mah}(x, y) = (x - y)\Sigma^{-1}(x - y)^T$$

The groups in cluster analysis are constructed mainly based on individual element contents. This method does not take into account that the compositional nature of the element data, like the method based on element ratios. However, before hierarchical cluster analysis, dimensional analysis methods, PCA, were applied to this data in order to reduce the variables and realize the possible connection between variables. Moreover, some element ratios were also used as

variables in PCA. The element ratios used in PCA were chosen after the results of the preliminary evaluation of chemical analysis.

However, the PCA does not reveal clear different groups for this study. Therefore, none of five components which were determined through the PCA were used as variables in cluster analysis. Instead, using the information obtained by *Component Score Coefficient Matrix* five variables are identified as the variables which would be used in hierarchical cluster analysis. These variables are: La, Mg,  $\Sigma$ REE concentration, Ce/Ce\* and Mn/Cr ratio. The dendrogram of the samples indicating the groups among the figurines and raw materials sources of these groups are given in Figure 3.40. A good clustering for the figurines and geological samples are presented in the dendrogram.



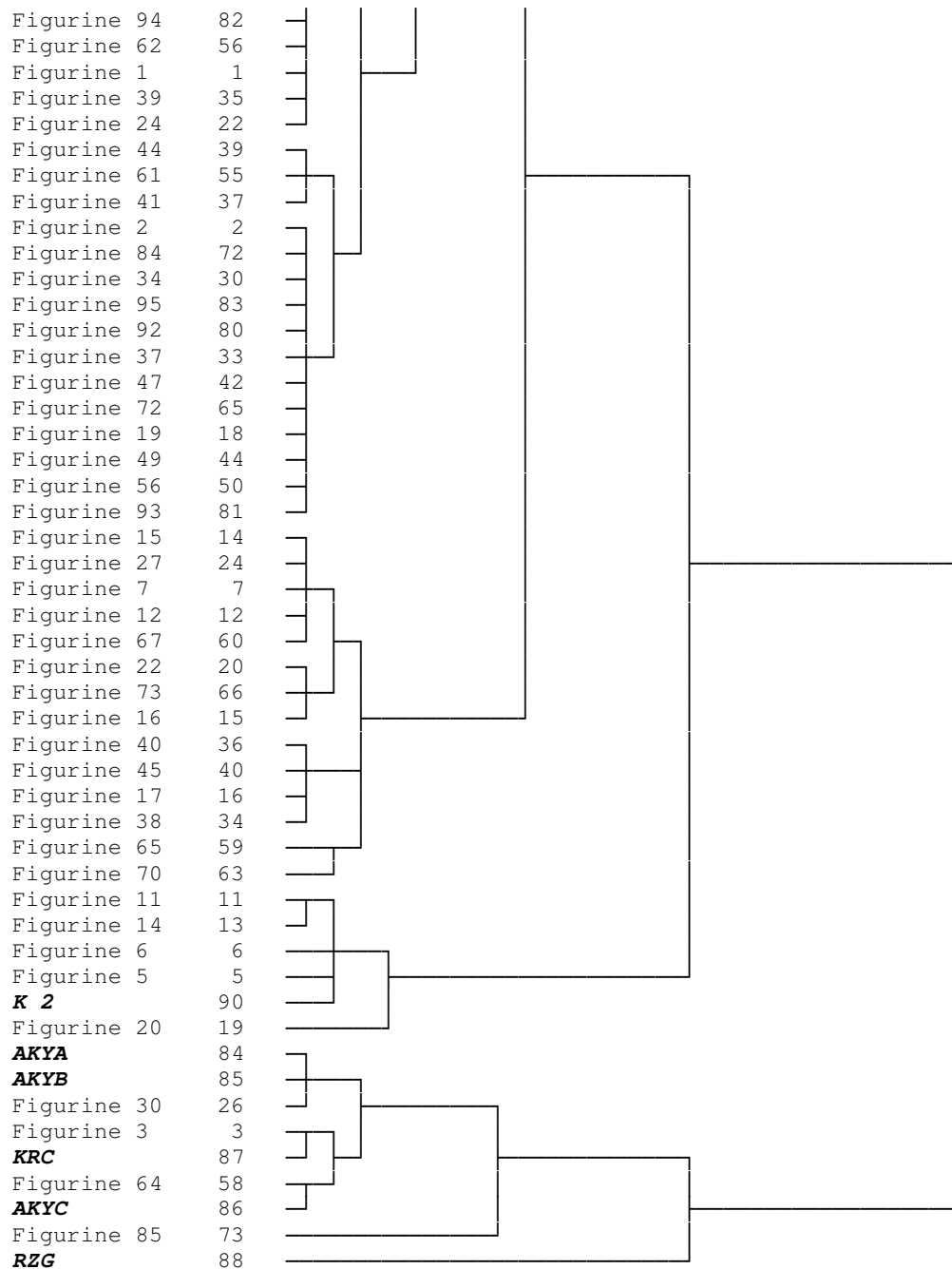


**Figure 3.40.** Dendrogram of archaeological and geological samples by Euclidean distance

Dendrogram is a tree diagram showing visually the relationship between the cases and the groups which were formed in cluster analysis [129]. In a dendrogram similar cases are represented on close branches of the tree as we can described and the cases that are not similar appear on widely separated branches [130].

There are different methods in construction of a dendrogram. One of them is *Furthest Neighbour* or *Complete Linkage Analysis* is used in this study. The criterion in this method for forming the branches is that in order to join a group, a specific case must have a specified degree of similarity member of the group from which it is most dissimilar [129]. Likewise, two groups combine to each other according to the specified degree of the similarity of the most dissimilar members of each group. In other words, the distance in this method is defined on the basis of furthest rather than nearest neighbours.

This method prevents the combination of dissimilar cases or clusters into another cluster [127]. In other words, complete linkage ensures that two clusters will not be joined together unless even the weakest similarity between any two cases is stronger than any other unused similarity score in the matrix.

In order to analyze the groups that formed in a dendrogram, it is better to start from right on horizontal axis where only two groups appear [130] Starting from the right there is a gap between 20 and 25 as seen in the dendrogram given in Figure 3.40 that splits all the samples into two clusters. This result with two big clusters is very reasonable since the geological samples incorporated into figurine samples in this analysis as possible raw material sources are from two different geological locations, Datça and Cyprus. According to their petrographic examinations, the samples from these locations represent two different types of limestone. So, according to this result, it is possible to detect local productions and figurines made of limestone from Cyprus.

Regardingly, there is another gap between 15 and 20. Here there are four groups that differ in limestones within the same location. This means namely K 1, Erdemli, and K 2, Değirmenlik, have dissimilarities even though they are within the same geological formation called Pachna. This difference also appears in micropaleontological examinations of thin sections of samples and REE patterns through chemical analysis.

For Datça, limestone from RZG location is also different from other limestones. In the gap from approximately 5 to 10, there are six groups. Here, number 85, the architectural fragment also differs and the big group of figurines of which their raw materials from Erdemli splits into two groups. In other words, when start from the left, it is clear that the limestone of Figurine 30 is either from AKYA or AKYB, the limestone of Figurine 3 is from KRC, the limestone of Figurine 64 is from AKYC. Architectural fragment 85 and then limestone from RZG are also connected to these groups as local.

For Cypriote production, although there are minor sub-groups, majority of figurines belong to the group which can be identified as K 1 since it is the geological source. The other group which can be identified as K 2 is smaller one, and Figurines 5, 6, 11, 14, and 20 belong to this group.

Based on the results through hierarchical cluster analysis, the variables La, Mg,  $\sum$ REE concentration, Ce/Ce\* and Mn/Cr ratio which were used to define the similarities or distances between each archaeological and geological sample and groups among them gave meaningful discrimination. Therefore, in further studies these five variables could be used to define the chemical characterization of limestone figurines and their provenance in hierarchical cluster analysis.



## CHAPTER 4

### CONCLUSION

In this study, the material characteristics of limestone figurines that were found at Emecik were investigated. The origin of raw material of these figurines and possibility of local production were also researched. For the characterization purpose, 85 limestone figurines from Emecik were sampled. Figurines that were sampled were covering all trenches in excavation site that the figurines had been found. According to the stratigraphic analysis and the stylistic evaluations of figurines, they are dated, from late 7<sup>th</sup> century to middle of 6<sup>th</sup> century B.C.

Sampled figurines include body or leg fragments, priest body fragments, lion fragments and more complete lion figurines, bird fragments, goat carrying male figurines, kouros feet and base fragments, miniature female figurine, drapery fragment, kouros head and body fragment, ornamented stone fragment, carbonate stone fragment and architectural fragment. Architectural fragment was also sampled in order to compare the results, since it is reasonable to assume that a limestone architectural element has been made out of a local limestone.

In order to investigate the origin of raw material, geological samples from different locations in Datça were collected. Five locations labeled as AKYA, AKYB, AKYC, RZG and KRC were pointed on the map using GPS during sampling. In order to homogenize these geological formations at least five samples were collected from each location. In the light of previous studies, the geological sampling was concentrated on the later deposits in the peninsula, marine sediments of which are also called as Yıldırımli formation from late Pliocene. Samples from Karaköy, Körmen Bay were also collected. However, according to XRD results, these samples appeared to be marly-claystone alternation with tuff intercalation. Therefore, the chemical results were not included in here.

Meantime, in order to research the Cypriote origin of the figurines, geological samples from five different locations labeled as K1, K2, K3-1, K3-2, and K3-3 in Cyprus were collected. K1 and K2 together represent *Lympia-Kossi chalk* within Pachna formation which is generally accepted as the original source for all of the figurines found elsewhere in Mediterranean. K3-1, K3-2, K3-3 are located at Karpaz peninsula in Cyprus where is suggested as another possible source for limestone statuettes. Geological sampling locations were pointed on the map using GPS during sampling. However, the micropaleontologic study of the geological samples from Karpaz indicates that their fossiliferous contents do not include foraminifera. Therefore, the chemical results of samples from Karpaz were not included in here.

Characterization and provenance studies in this work were investigated using mineralogical and chemical examinations of all the samples. Mineralogical investigation was performed through thin-section analysis, micropaleontologic study and XRD analysis. Thin-section examination of nine figurine samples revealed that figurines were made of limestone that is rich in planktonic foraminifera. According to micropaleontologic study, archaeological samples contain abundant and well preserved planktonic foraminifera (*Globoquadrina* spp., *Globigerina* spp., *Globigerinoides* spp., *Praeorbulina* spp.) and are characterized by a very fine grained, homogeneous texture. K1, Erdemli and K2, Değirmenlik samples from Cyprus include almost the same planktonic foraminiferal assemblages as well. Identified planktonic foraminiferal assemblages in archaeological and geological samples represent an interval within the Miocene time. A rich planktonic foraminiferal content and very fine grained homogeneous texture of the

examined samples are consistent with chalk lithology, a type of limestone which constitutes widely distributed Pachna formations represented by a thick chalk succession in Southern Cyprus. So the investigated figurines through thin sections were assigned to the Pachna formations by analyzing planktonic foraminifera. Almost the same fauna except for *Paragloborotalia* sp. and *Orbulina?* sp. is included in K2. In addition, Datça geological samples are not fossiliferous except for the sample KRC. This sample contains only rare bivalve and ostracoda shells but it is barren of planktonic or benthic foraminifera.

The other three figurines were sampled for thin section analysis after chemical analysis since they represent a different group according to their REE composition. It was then revealed that these three figurines, ST.06.I12.d8.21, fragment of a miniature female figurine, ST.02.K9c.28B1, ornamented fragment and ST.02.I8b.19.A12, architectural fragment are completely different from others and are not fossiliferous.

In XRD analysis of the figurine samples, Mg-calcite appeared to be the major mineral in most of the figurines. Meantime, calcite appeared to be the major mineral in the rest of the figurines. Trace quantities of dolomite is also present in some of the figurines. XRD results are then in accordance with the micropaleontologic evaluation. As it has been understood through thin-sections of the figurines majority of the figurines were made using foraminiferal limestone. Since foraminifera are composed of low or high Mg-calcite, it is expected to obtain such a mineral composition. However, in XRD analysis the same archaeological sample ST.02.K9c.28B1, ornamented fragment as in thin-section analysis and also ST.02.I8b.28A.2, small fragments are discriminated based on their mineralogical characteristics. In these archaeological samples dolomite appeared to be the major mineral.

Accordingly, evaluation of chemical results through their PAAS normalized REE patterns 4 figurines; ST.06.I12.d8.21 (3), ST.02.K9c.28B1 (30), ST.02.I8b.28A.2 (64), ST.02.I8b.19.A.12 (85) appear to be made from the local limestone from different locations in Datça. Moreover, when the REE enrichment, Ce anomaly and general behavior of REE patterns are considered; the raw material of ST.06.I12.d8.21 matches with the limestone from KRC, ST.02.K9c.28B1 with the limestone from either AKYA or AKYB, ST.02.I8b.28A.2 with the limestone from AKYC and ST.02.I8b.19.A.12 with the limestone from RZG although there is a slight difference in their Ce anomaly.

The rest of the figurines appear to form 4 different groups especially based on their degree of Ce anomalies. Group 1 is characterized with their extremely negative Ce anomalies. Group 2 and Group 3 are defined for their slight to moderate Ce anomalies. When Group 2 is compared with the geological samples from K1, Erdemli and K2, Değirmenlik in Cyprus, although there are slight differences in REE enrichment, or general behavior from Gd to Y and from Er to Yb, it is reasonable to say that the raw material of these figurines match with the limestone from K1. The reason of difference for Y is mainly the influence by the incorporation of terrigenous materials into the limestone formation.

Group 3 which is composed of ST.06.I12.d6.B (leg fragment), ST.06.H12.d5.15 (fragment), ST.06.H12.a5.22 (body fragment), ST.06.H12.a3.17 (leg fragment), and ST.06.I12.d7.44 (drapery fragment) is in accordance with the geological samples from K2, especially when REE enrichment is considered.

Group 4 is formed regarding to behavior of Nd-Sm in REE pattern. Group 4 is characterized by the peaks at Nd to Sm in their REE patterns as a result of foraminiferal tests in limestone.

While Eu anomaly is another important parameter for determining different types of limestone, for many of the figurines and geological samples from Datça, Eu concentration is found to be below the detection limits. For the figurines of which Eu could be determined, there is a positive

anomaly just like the case for the limestone samples from K1 and K2. The positive Eu anomalies in archaeological and geological samples therefore may be due to the presence of plagioclase feldspar.

For establishing multielement diagrams of figurines and geological samples, C1 meteorite values were chosen to normalize trace elements in order to emphasize the differences in trace element chemistry between the carbonate rich limestone and meteoritic stone. Although many aspects of geochemistry help to identify different groups for archaeological objects regarding their raw materials, here for instance limestone figurines, yet there is still a difference for provenance studies in geology and archaeology. Geological studies cover rather very long time period when compared to archaeological provenance studies. In archaeological studies, the main focus is the comparison with possible sources without taking into account the aspects of formation or diagenesis of those sources. This comparison then starts from the time when raw material was taken from that specific source. In other words, we are comparing figurines and raw material sources by keeping in mind that this possibility; the burials conditions of figurines or the diagenesis of geological source after the raw material had been taken could affect overall results. Therefore, using C1 values for multielement diagrams could give better results for understanding the differences and similarities between figurines and possible sources from Cyprus. The main difference appears at Ba enrichment. Geological samples from K1 and K2 gave much higher Ba values as compared to figurines. Another difference is Hf enrichment. For instance, for ST.00.K8C.16.148 (86) ST.02.K9c.27b.1 (65) and ST.06.H12.a2A.23 (9) Hf is more enhanced regarding to the geological samples. Both Ba and Hf are associated with terrigenous inclusion of the rock. Therefore, the differences for these elements could result from the burial conditions of figurines.

Figurines samples in this study exhibit very extreme Ce anomaly ( $Ce/Ce^* \leq 0.30$ ), extreme to moderate Ce anomaly ( $Ce/Ce^*$  between= 0.30-0.70), and no Ce anomaly ( $Ce/Ce^*$  between 0.89 and 1.10). Meantime, the geological samples from Datça have moderate to slightly Ce anomalies between  $Ce/Ce^* = 0.56$  to 0.82. The geological samples from Cyprus have moderate Ce anomalies between 0.50 and 0.66.

Geological samples from Cyprus and most of the figurines exhibit generally depleted LREE characteristics according to their TREE fractionation.  $(La/Yb)_n$  ratios for geological samples from Datça could not be calculated due to lack of Yb concentration that is generally found to be below detection limit.

For other locations in Datça KRC and RZG show depletion of LREEs. The effects of LREE/HREE fractionation can be also interpreted using Er/Nd (mg/kg) ratios. Er/Nd ratios for the figurines are between 0.6 and 0.18. There are few exceptions however, four of the figurines have lower ratios, and one figurine has higher ratio of 0.20. The low Er/Nd ratios may be due to detrital materials which were transported during the sedimentary process and coatings on mineral phases to concentrate Nd with respect to Er. Er/Nd ratios for geological samples from Datça could not be calculated due to lack of Er values, because they were found to be below detection limit. However, it still means that the geological samples from Datça were enriched in LREEs.

Some of the binary diagrams were also found useful in discriminating different groups for figurines and associating these groups to the geological sources. Although, there is no direct correlation between total REE concentrations and Ce anomalies, the binary diagram of  $\Sigma REE$  vs. Ce anomaly discriminates figurines that were probably made from local sources, figurines made from different sources in Cyprus, and a different group of figurines with undefined source.  $(La/Sm)_n$  vs.  $Sm_n$  diagram of the samples helps to differentiate Group 3 from the rest.

The four groups and local production that have been revealed by using the results of chemical and mineralogical analysis have also been confirmed by a multivariate statistics analysis. Hierarchical cluster analysis was considered to be the most appropriate for this research to identify different groups and their raw material sources. However, before doing so, the number of variables was reduced in order to obtain a clear result and good clustering for possible groups. This approach that is also called dimensional scaling was carried out by PCA. However, PCA does not reveal clear groups in this study; even it was not useful to discriminate different geological locations. Therefore, none of the five components which were determined through the PCA were used as new variables in cluster analysis. Instead, Component Score Coefficient Matrix *was used to define new variables* which would be used in hierarchical cluster analysis. These variables are: La, Mg,  $\Sigma$ REE concentration Ce/Ce\*, and Mn/Cr ratio.

The dendrogram that has been constructed in hierarchical cluster analysis discloses two main clusters for all geological and archaeological samples. These two clusters represent generally two distinct geological sampling locations, Datça and Cyprus. In other words, the different types of limestone formation from Datça and Cyprus are also detectable in the dendrogram. Accordingly, there are minor differences in limestone of K 1, Erdemli, and K 2, Değirmenlik, although they are within the same formation. Based on the dendrograms, four archaeological samples appear as the local productions. The rest of the figurines then were made from limestone from Cyprus.

When all the data above through various analyses are considered, it is obvious that 4 figurines; ST.06.112.d8.21 (3), ST.02.K9c.28B1 (30), ST.02.l8b.28A.2 (64), ST.02.18b.19.A.12 (85) were made from the local limestone in Datça. It is even safe to assume that the artists in Datça tried different sources from different locations in Datça peninsula in order to improve the quality of figurines. Even though 4 figurines among 85 figurines that were sampled seem to be small number for indicating a local workshop, these figurines are just the representative samples from large groups which were found in the same contexts.

The rest of the figurines were made of a limestone from the same formation in Cyprus which is called as Lympia-Kossi chalk of Pachna formation. This formation was also suggested by various searches as the source of limestone figurines of either Cypriote type or of mixed style.

According to the overall results of this study, the majority of figurines found at Emecik were made from limestone obtained from Pachna formation which is characterized by Miocene planktonic foraminiferal assemblages. However, here again as in Datça, artists used different limestone sources from different locations. Although figurines are all similar in their foraminiferal contents, we can assign two different locations as the source of figurines within Pachna formation. One group of figurines seems to be produced from limestone obtained around Erdemli. In the production of other group of figurines, limestone from Değirmenlik was used according to their foraminiferal contents and REE patterns.

The differences in Ce anomalies and in the behavior from Nd to Sm on the REE patterns of the larger group probably indicate different quarries of the same Pachna formation. Therefore, it is reasonable to say that there are actually at least 4 different quarries in Pachna formation in Cyprus for the production of limestone figurines just for the figurines found at Emecik.

In summary, Emecik limestone figurines form the following groups given in Table 4.1.

**Table 4.1.** The groups for Emecik limestone figurines

<b>Groups</b>	<b>Figurines</b>
<b>1, Pachna formation</b>	ST.06.I12.d5.c12 (2), ST.02.8B.19A.13 (40), ST.02.K9c.27b.1 (65), ST.02.I8b.23.9 (80), ST.02.I8b.28.B3 (92), ST.00.K8C.16.152 (95), ST.02.I8B.19.b6 (34), ST.02.I8b.11.b9 (35), ST.02.I8b.25.12 (45), ST.02.I8b.19.A12 (84), ST.99.I9b.2.17 (88), ST.01.I8.B.10.26 (89) ST.02.I8b.28.A2 (36), ST.02.I8B.19.6 (41), ST.02.I8b.21.17 (44), ST.02.I8b.23.11 (61), ST.02.I8b.28A.2 (62), ST.02.I8b.15.17 (72), ST.02.K9c.27a.11 (77), ST.99.K8C.9.22 (94)
<b>2, K1 Erdemli</b>	ST.02.I8b.16A.16 (33), ST.02.K9c.27A.13 (56), ST.02.I8b (74), ST.00.K8C.16.148 (86), ST.06.I12.d3.9 (17), ST.02.I8b.16A.11 (24), ST.02.I8B.16.A.15 (37), ST.02.I8b.28.6.3 (47), ST.02.I8b.28.8 (48), ST.00.D8.A.5.25 (93), ST.06.I12.d7.43 (7), ST.06.I12.d5.A11 (8), ST.02.I8b.16A.11 (26), ST.02.I8b.14.20 (58), ST.02.K9.c27.A12 (69), ST.99.I9B.4 (91), ST.02.I8b.28A.11 (32), ST.02.I8b.19.2 (50), ST.02.I8b.14.17 (53), ST.01.G11.D1 (63), ST.02.I8b.16A.17 (73), ST.06.I12.d5A.12 (18), ST.02.I8b.19.2 (49), ST.02.K9c.27A.3 (67), ST.02.K9.c28.14 (68), ST.99.I9b.4.65 (87), ST.06.I12.d6A.14 (10), ST.02.I8b.16.20 (39), ST.02.I8b.22.2 (46), ST.02.I8b.23.9 (81), ST.00.K8.C.16.151 (90), ST.02.I8b.16A.11 (23), ST.02.I8b.25.11 (31), ST.02.I8b.18.7 (52), ST.02.I8b.11b.10 (57), ST.02.I8b.28.3 (75), ST.06.I12.d8.19 (1), ST.02.I8b.16A.11 (24), ST.02.I8B.16.A.15 (37), ST.02.I8b.28.6.3 (47), ST.02.I8b.28.8 (48), ST.00.K8C.16.148 (86), of ST.06.I12.d3.9 (17), ST.06.I12.d5.17 (19), ST.02.I8B.11c.29 (38), ST.02.K9c.27A.13 (56), ST.02.I8b.28.A9 (70), ST.00.D8.A.5.25 (93),
<b>3, K2 Değirmenlik</b>	ST.06.I12.d6.B (5), ST.06.H12.d5.15 (6), ST.06.H12.a5.22 (11), ST.06.H12.a3.17 (14), ST.06.I12.d7.44 (20)
<b>4, Pachna formation</b>	ST.06.I12.d7.45 (15), ST.02.I8b.18.3 (22), ST.02.I8b.16A.11 (27), ST.02.K9c.28.7.4 (42)
<b>Local production</b>	ST.06.I12.d8.21 (3), ST.02.K9c.28B1 (30), ST.02.I8b.28A.2 (64), ST.02.I8b.19.A.12 (85)

Therefore, the case for these limestone figurines was like Greek pottery during Geometric or Archaic periods that were also found all over the Mediterranean and inspired the artists outside Greece. In that case, there were many local productions other than Attica imitating Attic vases that is because Attic vases were in modern worlds very trendy.

The theory of traveling artists from Cyprus to other site to produce figurines for the taste of Aegean market has been suggested by various researches such as Jenkins [2]. Likewise, the traveling artists brought their raw material along them has been repeatedly argued [25-27, 32]. This theory tries to explain the reason of various styles, while provenance of all figurines is from

Cyprus as generally accepted. In this research, an evidence for this theory is also been found. The archaeological sample ST.99.19B.4, carbonate stone provides an interesting conclusion. This untreated limestone is also from Cyprus, and supports the idea of trade of the raw material of the figurines as far as Emecik. In addition, the reason of bringing Cypriote limestone to Emecik and to other sites is most probably the compositions of limestone in Pachna formation. As it is understood through thin-section analysis of samples they are foraminiferal limestone. Therefore they could be preferred.

This research has proven that there was a local workshop in Emecik using local limestone. The artists in Emecik could also work with limestone from Cyprus to produces the figurines. The provenance of majority of other figurines is Cypriote. They were either made in Cyprus or import from Cyprus. However, stylistical evaluation and comparison is not possible for now. Further studies should involve other figurines from Emecik now kept in museum in order to make stylistical interpretations between figurines made from Cypriote limestone and figurines made from Datça limestone. Moreover, figurines found at other sites in especially Aegean region should be studied considering the existence of Emecik workshop other then Cyprus. In this study, La, Mg,  $\Sigma$ REE concentration Ce/Ce\*, and Mn/Cr ratio were found to be discriminated between Emecik and Cyprus limestones. So, these variables could be used in further studies for fingerprinting limestone figurines.

## REFERENCES

1. Tykot R.H., "Scientific Methods and Applications to Archaeological Provenance Studies", M. Martini, M. Milazzo and M. Piacentini (Eds.), Proceedings of the International School of Physics "Enrico Fermi" Course CLIV, IOS Press, Amsterdam 2004, 407-432.
2. Jenkins, I., "Cypriote Limestone Sculpture from Cnidus," in G. R. Tsetskhladze, et al. eds., *Periplus: Papers on Classical Art and Archaeology Presented to Sir John Boardman*, London (2000).
3. Tuna N., "Datça/Emecik/Sarılıman Mevkii Arkaik Tapınak 2002 Yılı Çalışmaları", *Kazi Sonuçları Toplantısı*, 2004, 25(2), 41-48.
4. Cornelius S., Hurlbut, Jr., Cornelis K., *Dana's Manual of Mineralogy*, Wiley, New York (1977).
5. Tucker M.E., *Sedimentary Petrology: An Introduction to the Origin of Sedimentary Rocks*, Blackwell Scientific Publishing, Malden (2001).
6. Konrad B., Krauskopf, D.K.B., *Introduction to Geochemistry*, McGraw-Hill International Editions, Singapore (1995).
7. Flügel E., *Microfacies of Carbonate Rocks*, Springer, Berlin (2004).
8. Blatt H., Middleton G., Murray R., *Origin of Sedimentary Rocks*, Prentice-Hall, New Jersey (1972).
9. Blatt H., *Sedimentary Petrology*, W.H. Freeman and Company, New York (1992).
10. Oates J.A.H., *Lime and Limestone*, Wiley-VCH, New York (1998).
11. Tucker M.E., *Sedimentary Petrology, An Introduction to the Origin of Sedimentary Rocks*, Blackwell Scientific Publications, London (1991).
12. Voegelin A.R., Nagler T.F., Samankassou E., Villav I.M., "Molybdenum Isotopic Composition of Modern and Carboniferous Carbonates", *Chemical Geology*, 2009, 265, 488-498.
13. Moissette P., Cornee J.J., Tayech B.M., Rahbi M., Andre J.P., Koskeridou E., Meon H., "The Western Edge of Mediterranean Pelagian Platform: A Messinian Mixed Siliciclastic-Carbonate Ramp in Northern Tunisia", *Palaeogeography, Palaeoclimatology, Palaeoecology*, 2010, 285, 85-103.
14. Titschack J., Bromley R.G., Freiwald A., "Plio-Pleistocene Cliff-bond, Wedge-shaped, Warm-temperate Carbonate Deposits from Rhodes (Greece)", *Sedimentary Geology*, 2005, 29-56.
15. Lubeseder S., "Palaeozoic Low-oxygen, High-latitude Carbonates: Silurian and Lower Devonian Nautiloid and Scyphocrinoid Limestones of the Anti-Atlas (Morocco)", *Palaeogeography, Palaeoclimatology, Palaeoecology*, 2008, 264, 195-209.

16. BouDagher-Fadel, "Biology and Evolutionary History of Larger Benthic Foraminifera", *Developments in Palaeontology and Stratigraphy*, 2008, 21, 1-37.
17. Schmidt D.N., Thierstein H.R., Bollman J., "The Evolutionary History of Size Variation of Planktic Foraminiferal Assemblages in Cenozoic", *Palaeogeography, Palaeoclimatology, Palaeoecology*, 2004, 212, 159-180.
18. Petrizzo M.P., "Palaeoceanographic and Palaeoclimatic Inferences from Late Cretaceous Planktonic Foraminiferal Assemblages from Exmouth Plateau", *Marine Micropaleontology*, 2002, 45, 117-150.
19. Boynton, R.S., *Chemistry and Technology of Lime and Limestone*, John Wiley & Sons, New York (1966).
20. Tucker M.E., Wright P.V., *Carbonate Sedimentology*, Blackwell Scientific Publishing, Oxford (1990).
21. Dunham R.J., "Classification of Carbonate Rocks According to Depositional Texture". In Ham, W.E. *Classification of Carbonate Rocks*, American Association of Petroleum Geologists Memoir, 1962, 117, 108-121.
22. CRC Handbook of Chemistry and Physics, Chemical Rubber Co., Cleveland (1971).
23. Polikreti K., Maniatis Y., Bassiakos Y., Kourou N., Karageorghis V., "Provenance of Archaeological Limestone with EPR Spectroscopy" *Journal of Archaeological Sciences*, 2004, 31(7), 1015-1028.
24. Richter G., *Archaic Greek Youths*, Phaidon Press, London (1960).
25. Kourou N., Karageorghis V., Maniatis Y., Polikreti K., Bassiakos, Y., *Limestone Statuettes of Cypriote Type Found in the Aegean: Provenance Studies*, A.G. Leventis Foundation, Nicosia (2002).
26. Sørensen, L.W., "Early Archaic Limestone Statuettes in Cypriote Style: A Review of their Chronology and Place of Manufacture", *RDAC*, 111-121, 1978.
27. Berges D., *Knidos, Beiträge zur Geschichte der archaischen Stadt*, Verlag Philipp von Zabern, Mainz am Rhein (2006).
28. Jenkins I., "Archaic Kouroi in Naucratis: The Case for Cypriot Origin", *American Journal of Archaeology*, 2001, 105 (2), 163-179.
29. Pryce F.N., *Catalogue of Sculpture in the Department of Greek and Roman Antiquities of British Museum I.1: Prehellenic and Early Greek*, London (1928).
30. Boardman J., *The Greeks Overseas*, London (1980).
31. Hermary A., "Sculptures Chyprio-ioniennes du Musée de l'Hermitage à Leningrad", *RDAC*, 173-178, 1991.
32. Senff R., "Zyprische u. Ostgriechische Statuetten aus Milet", in R. Laffineur and F. Vandennebeele, eds., *Cypriote Stone Sculpture*, Brussels-Liege (1994),
33. N. Tuna, N. Atıcı, Ü. Muşkara, İ. Sakarya, "Some Remarks on the Limestone Figurines Recently Found at the Archaic Sanctuary of Apollo in the Territory of Knidos", *Cyprus and The East Aegean*, 229-243, 2009.

34. Tuna N., Berges D., "Datça/Emecik/Sarıliman Mevkii Arkaik Kutsal Alan 1999 Yılı Çalışmaları", Kazı Sonuçları Toplantısı, 2001, 22(2), 127-136.
35. [http://www.tacdam.metu.edu.tr/index.php?option=com\\_content&task=view&id=21&Itemid=61](http://www.tacdam.metu.edu.tr/index.php?option=com_content&task=view&id=21&Itemid=61) last accessed 14.05.2012.
36. Tuna N., "Datça/Emecik/Sarı Liman Mevkii Arkaik Tapınak 2000 yılı Çalışmaları", Kazı Sonuçları Toplantısı, 2002, 23(2), 89-100.
37. Berges, D., "Knidos und das Bundesheiligtum der dorischen Hexapolis", Nürnberger Blätter zur Archäologie, 1995/96, 12, 103-120.
38. Rollinson R.H., Using Geochemical Data: Evaluation, Presentation, Interpretation, Edinburgh, Longman (1993).
39. Housecroft C.E., Sharpe A.G., Inorganic Chemistry, Edinburgh, Pearson Education (2001).
40. Topp N.E., The Chemistry of the Rare-Earth Elements, Amsterdam, Elsevier (1965).
41. Spedding F.H., Daane A.H., The Rare Earths, London, John Wiley (1961).
42. Petrucci R.H., Harwood W.S., Herring F.G. General Chemistry, New Jersey, Prentice Hall (2002).
43. Lipin, B.R., McKay, G.A. (eds), Geochemistry and Mineralogy of Rare Earth Elements, Washington, 1989.
44. Date A.R., Hutchison D., "Determination of Rare Earth Elements in Geological Samples by Inductively Coupled Plasma Source Mass Spectrometry", Journal of Analytical Atomic Spectrometry, 1987,
45. Halicz L., Segal I., Yoffe O., "Direct REE Determination in Fresh Waters Using Ultrasonic Nebulization ICP-MS", Geological Survey of Israel, 1999, 14, 1579-1581.
46. Mazumdar A., Tanaka K., Takahashi T., Kawabe I., "Characteristics of Rare Earth Element Abundances in Shallow Marine Continental Platform Carbonates of Late Neoproterozoic Successions from India", Geochemical Journal, 2003, 37, 277-289.
47. Madhavaraju J., González-León C.M., Yong II, Armstrong-Altrin J.S., Reyes-Campero L.M., "Geochemistry of the Mural Formation (Aptian-Albian) of the Bisbee Group, Northern Sonora, Mexico", Cretaceous Research, 2010, 31, 400-414.
48. Wilde P., Quinby-Hunt M.S., Erdtmann B.D., "The Whole-Rock Cerium Anomaly: A Potential Indicator of Eustatic Sea-Level Changes In Shales of The Anoxic Facies", Sedimentary Geology, 1996, 101, 43-53.
49. Wenner D.B., Herz N., "Provenance Signatures for Classical Limestone", in Waelkens M., Herz N., Moens L.(eds.), 1992, Ancient Stones: Quarrying, Trade and Provenance – Interdisciplinary Studies on Stones and Stone Technology in Europe and Near East from the Prehistoric to the Early Christian Period, Leuven University Press, Leuven (1992).
50. Holmes L.L., Harbottle G., "In the Steps of William the Conqueror: Neutron Activation Analysis of Caen Stone", Archaeometry 45 , 2 (2003) 199-220.

51. Shackley M.S., "Archaeological Petrology and The Archaeometry of Lithic Materials", *Archaeometry* 50.2, 2008, 194–215.
52. Riis P.J., Moltesen M., Guldager P., The National Museum of Denmark, Department of Near Eastern and Classical Antiquities. *Scultures I. Aegean, Cypriote and Graeco-Phoenician*, Copenhagen, 1989.
53. Holmes, L.L., Harbottle, G., "Compositional Characterization of French Limestone: A New Tool for Art Historians", *Archaeometry*, 1994, 36 (1), 25-39.
54. Holmes L.L., Harbottle G., "Compositional Fingerprinting: New Directions in the Study of Provenance of Limestone", *Gesta*, 1994, 33 (1), 10-18.
55. <http://www.limestonesculptureanalysis.com/default.asp> (last accessed on 02.02.2013)
56. Holmes L.L., Harbottle G., "The History of The Brookhaven National Laboratory Project in Archaeological Chemistry, and Applying Nuclear Methods To The Fine Arts", *Archaeometry* 49 , 2 (2007) 185–199.
57. Holmes L.L., Harbottle G., "The Romanesque Arch at the Cloisters Museum: Stone Analysis", *Gesta*, 2000, 39 (1), 24-27.
58. Holmes L.L., Little C.T., Sayre E.V., "Elemental Characterization of Medieval Limestone Sculpture from Parisian and Burgundian Sources", *Journal of Field Archaeology*, 1986, 13 (4), 419-438.
59. Pizarro C., Gonzalez-Saiz J.M., Esteban-Diez I., Saenz-Gonzalez C., Perez-Del-Notario N., Rodriguez-Tecedor S., "A Provenance Study of French Limestone based on Variable Selection from Compositional Profiles", *Archaeometry* 53, 6 (2011) 1099-1118.
60. Vito C.d, Ferrini V., Mignardi S., Piccardi L., Rosanna T., "Mineralogical-Petrographic and Geochemical Study to Identify The Provenance of Limestone from Two Archaeological Sites in The Sulmona Area (L'Aquila, Italy)", *Journal of Archaeological Science*, 2004, 31(10), 1391-1393.
61. Marinoni N., Pavese A., Bugini R., Silvestro G.d, "Black Limestone used in Lombard Architecture", *Journal of Cultural Heritage*, 2003, 3(4), 241-249.
62. Bello M.A., Martin A., "Microchemical Characterization of Building Stone from Seville Cathedral, Spain", *Archaeometry*, 1992, 34.1, 21-29.
63. Harrell J.A., "Ancient Egyptian Limestone Quarries: A Petrological Survey", *Archaeometry*, 1992, 34.1, 195-211.
64. Sanjurjo-Sánchez J., Trindade M.J., Blanco-Rotea R., Benavides Garcia R., Fernández Mosquera D., Burbidge C., Prudêncio M.I., Dias M.I. "Chemical and Mineralogical Characterization of Historic Mortars from the Santa Eulalia de Bóveda Temple, NW Spain", *Journal of Archaeological Science*, 2010, 37, 2346-2351.
65. Ortega L.A., Zuluaga M.C., Alonso-Olazabal A., "Geochemical Characterization of Archaeological Lime Mortars: Provenance Inputs", *Archaeometry*, 2008, 50.3, 387–408.
66. Jarvis K.E., "Determination of Rare Earth Elements in Geological Samples by Inductively Coupled Plasma Mass Spectrometry", *Journal of Analytical Atomic Spectrometry*, 1989, 4.

67. Armstrong-Altrin J.S., Surendra P., Verma P., "Geochemistry of Upper Miocene Kudankulam Limestones, Southern India", *International Geology Review*, 2003, 45, 16–26.
68. Tsolakidou A., Garrigos J.B., Kilikoglou V., "An Assessment of Dissolution Techniques for the Analysis of Ceramic Samples by Plasma Spectrometry", *Analytica Chimica Acta*, 2002, 474, 177-188.
69. Cullers, R., "Implications of Elemental Concentrations for Provenance, Redox Conditions, and Metamorphic Studies of Shales and Limestones Near Pueblo, CO, USA", *Chemical Geology*, 2002, 191, 305-327.
70. Roy P.D., Smyktaz-Kloss W., "REE Geochemistry of The Recent Playa Sediments From The Thar Desert, India: An Implication To Playa Sediment Provenance", *Chmie der Erde*, 2007, 67(1), 55-68.
71. Bellanca A., Masetti D., Neri R., "Rare Earth Elements in Limestone/Marlstone Couplets from The Albian-Cenomanian Cismon Section (Venetian Region, Northern Italy)" Assessing Ree Sensitivity To Environmental Changes", *Chemical Geology*, 1997, 141, 141-152.
72. Bolhar R., Kamber B.S., Moorbath S., Whitehouse M.J., Collerson K.D., "Chemical Characterization of Earth's Most Ancient Clastic Metasediments from The Isua Greenstone Belt, southern West Greenland", *Geochimica et Cosmochimica Acta*, 2005, 69(6), 1555-1573.
73. Igarashi, K., Akagi, T., Fu, F., Yabuki, S., "Determination of Rare-Earth Elements in a Limestone Geological Standard Reference Material by ICP-MS Following Solvent Extraction", *Analytical Sciences*, 2003, 35, 441-445.
74. Ionov D., Harmer R., "Trace Element Distribution in Calcite-Dolomite Carbonatites from Spitskop: Inferences for Differentiation of Carbonatite Magmas and The Origin of Carbonates in Mantle Xenoliths", *Earth and Planetary Science Letters*, 2002, 198(3-4), 495-510.
75. Müller G., Friedman G. (eds), *Recent Developments in Carbonate Sedimentology in Central Europe*, Berlin, Springer-Verlag (1968).
76. Ayhan İ.A., *Provenance Studies in Obsidian Samples from Çatalhöyük Excavations*, M.Sc. Thesis, METU (2002).
77. Öztürk S., *Use of Solid Phase Extraction for Preconcentration of Rare Earth Elements: Provenance Studies In Çatalhöyük Obsidians*, M.Sc. Thesis, METU (2003).
78. Bağcı M., Kibici Y., Yıldız A., Akıncı Ö.T., "Petrographical and Geochemical Investigation of Triassic Marbles Associated with Menderes Massif Metamorphics, Kavaklıdere, Muğla, SW Turkey", *Journal of Geochemical Exploration*, 2010, 107, 39-55.
79. Ebert A., Gnos E., Ramseyer K., Spandler C., Fleitmann D., Bitzios D., Decrouez D., "Provenance of Marbles from Naxos based on Microstructural and Geochemical Characterization", *Archaeometry*, 2010, 52 (2), 209-228.
80. Visco G., Gregori E., Tomassetti M., Campanella L., "Probably Counterfeit in Roman Imperial Age: Pattern Recognition Helps Diagnostic Performed with Inductive Coupled

Plasma Spectrometry and Thermogravimetry Analysis of a Torso and a Head of Roman Marble Statue”, *Microchemical Journal*, 2008, 88 (2), 210-217.

81. Jones, A.P., F. Wall, Williams, C.T. (eds) *Rare Earth Minerals: Chemistry, Origin and Ore Deposits*, New York (1996).
82. Madhavaraju J., Yong I.L., “Geochemistry of the Dalmiapuram Formation of the Uttatur Group (Early Cretaceous), Cauvery Basin, Southeastern India: Implications on Provenance and Paleo-Redox Conditions”, *Revista Mexicana de Ciencias Geológicas*, 2009, 26.2, 380-394.
83. Raut N.M., Huang Ls., Lin Kc., Aggarwal S.K., “Uncertainty Propagation Through Correction Methodology for The Determination Of Rare Earth Elements by Quadrupole Based Inductively Coupled Plasma Mass Spectrometry”, *Analytica Chimica Acta*, 2005, 530, 91-103.
84. Chang Q., Shinotsuka K., Shibata T., Yoshikawa M., Tatsumi Y., “Precise Determination of Rare Earth Elements and Yttrium For Jp-1 (Peridotite) by Microconcentric Desolvating Nebulisation Icp-Ms”, *Frontier Research on Earth Evolution*, 2004, 2, 1-4.
85. Elliott S., *Varian’s ICP-MS at work*, 1997.
86. Tuna N., *Archaeological Investigations at the Knidian Territorium*, METU, Ankara, 2012.
87. Phillipson A., *Reisen und forschungen im westlichen Kleinasien, 5: Karien südlichdes Maander und das Westliche Lykien: Erg. Heft. 183, zu Petermanns Mitteilungen*, (Gotha) 1915.
88. Ercan T., Günay E., Baş H., Can B., “Datça Yarımadasındaki Kuvaterner Yaşlı Volkanik Kayaçların Petrolojisi ve Kökensel Yorumu”, *Maden Tetkik ve Arama Dergisi*, 97-98, 46-57, 1981-1982.
89. Ersoy Ş., “Datça (Muğla) Yarımadasının Stratigrafisi ve Tektoniği”, *Türkiye Jeoloji Bülteni*, 34, 1-14, 1991.
90. Dirican M., *Geoarchaeometrical Study of Burgaz Area, Datça Peninsula, Turkey M.Sc. Thesis*, METU (2002).
91. Kayan İ., *Ankara Üniversitesi Dil ve Tarih-Cografya Fakültesi Dergisi*, Ankara, Ankara Üniversitesi, 1988, 11 (11), 51-70.
92. Dirik K., Türkmenoğlu A., Tuna N., Dirican M., *Datça Yarımada’sının Neotektoniği, Jeomorfolojisi ve Bunların Eski Medeniyetlerin Yerleşimi Üzerindeki Etkisi*, ODTÜ AFP-00-07-03-13 Kod Nolu Proje, Aralık 2003.
93. Yeşilyurt K.S., Taner G., “Datça Yarımadası’nın Geç Pliyosen Pelecypoda ve Gastropoda Faunası ve Stratigrafisi (Muğla-Güneybatı Anadolu)”, *Maden Tetkik ve Arama Dergisi* 125, 89-120, 2002.
94. Konstantinou G., *Geological Map of Cyprus 1:250000*, Ministry of Agriculture Natural Resources and Environment, Geological Survey Department, 1995.
95. [http://www.cyprusgeology.org/english/images/2\\_F1.htm](http://www.cyprusgeology.org/english/images/2_F1.htm) (last accessed on 02.02.2013)

96. Robertson A.H.F., Woodcock, N.H.. The Role of the Kyrenia Range Lineament, Cyprus, in the Geological Evolution of the Eastern Mediterranean Area. Phil. Trans. R.Soc. London, A 317; 141-177, 1986.
97. Robertson, A.H.F., Xenophontos, C. Development of Concepts Concerning the Troodos Ophiolite and Adjacent unit in Cyprus. In: Prichard, H.M., Alabaster, T., Harris, N.B.W. and Neary, C.R. (eds.), Magmatic Processes and Plate Tectonics. Geological Society Spec. Publ., No.76; 85-119, 1993.
98. Ducloz C., "Notes on the Geology of the Kyrenia Range. Cyprus Geological Survey Dept., Annual Report, 1963, 57-67. 1964.
99. Ducloz, C., "The Geology of the Bellapais-Kythrea Area of the Central Kyrenia Range", Cyprus Geol. Survey Dept. Bulletin, 6, 1-75, 1972.
100. [http://www.cyprusgeology.org/english/EN/2\\_2\\_geology\\_en.htm](http://www.cyprusgeology.org/english/EN/2_2_geology_en.htm) (last accessed on 02.02.2013)
101. [http://www.moa.gov.cy/moa/gsd/gsd.nsf/dmlPentadakylos\\_en/dmlPentadakylos\\_en?OpenDocument](http://www.moa.gov.cy/moa/gsd/gsd.nsf/dmlPentadakylos_en/dmlPentadakylos_en?OpenDocument) (last accessed on 02.02.2013)
102. <http://www.britannica.com/EBchecked/topic/588887/Tethys-Sea> (last accessed on 02.02.2013)
103. Robertson A.H.F.. "The Origin and Diagenesis of Cherts from Cyprus", Sedimentology, 24, 11-30, 1977.
104. Robertson A.H.F., Hudson J.D., "Pelagic Sediments in the Cretaceous and Tertiary History of the Troodos Massif, Cyprus". In: Hsü, K.J. and Jenkyns, C.H. (eds.), Pelagic Sediments on the Land and Under the Sea. International Association of Sedimentologists, Special Publication, 1, 403-436, 1974.
105. Housecroft C.E., Sharpe A.G., Inorganic Chemistry, Edinburgh, Pearson Education (2001).
106. Zambetakis-Lekkas A.I., Elefanti P., "Micropaleontology and Biostratigraphy Efficient Tools in Archaeological Research: Raw Material Provenance in the Upper Palaeolithic Kastritsa Cave, Ioannina Region (Greece)", Bulletin of the Geological Society of Greece 40, Proceedings of the 11th International Congress, Athens, May 2007.
107. Iaccarino S.M., Premoli Silva I., Biolzi M., Foresi I.M., Lirer F., Turco, E., Petrizzo M.R. *Practical Manual of Neogene Planktonic Foraminifera*. International School on Planktonic Foraminifera 6<sup>th</sup> Course (2007) Università di Perugia Press, Perugia, 181 pp.
108. Hakyemez A., Toker V. "Planktonic Foraminiferal Biostratigraphy From The Sedimentary Cover of Troodos Massif, Northern Cyprus: Remarks on Aquitanian-Langhian Biozonation", Stratigraphy, 7, 33-59, 2010.
109. Dr. Aynur HAKYEMEZ, MTA.
110. Deer W.A., Howie R.A., Zussman J., An Introduction to the Rock Forming Minerals, Prentice Hall, New York, 1992.
111. McLennan, S. M., "Rare Earth Elements in Sedimentary Rocks: Influence of Provenance and Sedimentary Processes", Geochemistry and Mineralogy of Rare Earth Elements (Lipin, B. R. and McKay, G. A., eds.), Rev. Mineral. 21, 169–200, 1989.

112. Kurian S., Nath, B.N., Ramaswamy V., Naman D., Gnaneshwar Rao. Kamesh, Raju K.A., Selvaraj. K., Chen C.T.A., "Possible, Detrital, Diagenetic and Hydrothermal Sources for Holocene Sediments of the Andaman Backarc Basin", *Marine Geology* (2008) 247, 178-193.
113. Nath B.N., Roelandts I., Sudhakar M., Plueger W.L., "Rare Earth Element Patterns of the Central Indian Basin Sediments Related to Their Lithology", *Geophysical Research Letters*, 1992, 19, 1197-1200.
114. Sun, Shen-su, McDonough, W. F., " Chemical and Isotopic Systematics of oceanic basalts: implications for Mantle Composition and Processes", In A.D. Saunders and M.J. Norry (eds.) *Magmatism in the Ocean Basins* , Spec. Publ. Vol. Geol. Soc. Lond. , 1989, 42, 313-345.
115. Sholkovitz E.R., "Rare Earth Elements in Marine Sediments and Geochemical Standards", *Chem. Geol.*, 1990, 88, 333-347.
116. Liu Y.G., Miah M.R.U., Schmitt R.A., "Cerium: A Chemical Tracer for Paleo-oceanic Redox Conditions", *Geochim. Cosmochim. Acta* 52, 1988, 1361-1371.
117. Elderfield H., German C.R., "Rare Earth Elements in Saanich Inlet, British Columbia, a Seasonally Anoxic Basin", *Geochim. Cosmochim. Acta* 53, 1989, 2561-2571.
118. Palmer M.R., "Rare Earth Elements in Foraminifera Tests", *Earth Planet Sci.Lett.* 73, 1985, 285-298.
119. Zhu J., Shan J., Qiu P., Qin Y., Wang C., He D., Sun B., Tong P., Wu S., "The Multivariate Statistical Analysis and XRD Analysis of Pottery at Xigongqiao Site", *Journal of Archaeological Science* (2004) 31, 1685–1691.
120. VanPool Todd L., Leonard Robert D., *Quantitative Analysis in Archaeology*, Wiley, Malaysia, 2011.
121. Glascock M., Neff H., "Neutron Activation Analysis and Provenance Research in Archaeology", *Meas. Sci. Technol.* (2003) 14, 1516–1526.
122. SPSS 16.0 (Statistical Package for the Social Sciences) for Windows Release 16.0.0 Standard License, Copyright© SPCC Inc., 1989–2010.
123. Agha-Aligol D., Oliyai P., Mohsenian M., Lamehi-Rachti M., Shokouhi F., "Provenance study of Ancient Iranian Luster Pottery using PIXE, Multivariate Statistical Analysis", *Journal of Cultural Heritage* (2009) 10, 487–492.
124. Mello. E., Monna D., Oddone M., "Discriminating Sources of Mediterranean Marbles: a Pattern Recognition Approach", *Archaeometry* (1988) 30, 102-108.
125. Moens L., Roos P., De Rudder J., De Paepe P., Waelkens M., "Identification of Archaeologically Interesting White Marbles by Instrumental Neutron Activation Analysis and Petrography: Comparison Between Samples from Afyon and Usak (Turkey)", *J. of Trace and Microprobe Techniques* (1987) 5, 101-114.
126. Aldenderfer Mark S., Blashfield Roger K., *Cluster Analysis*, Sage Publications, Beverly Hills, 1984.
127. Drennan Robert D., *Statistics for Archaeologists: A Commonsense Approach*, Springer, New York, 2009.

128. Tansel İ., Differentiation and Classification of Counterfeit and Real Coins by Applying Statistical Methods, M.Sc. Thesis, METU (2012).
129. Shennah S., Quantifying Archaeology, Edinburgh University Press, Edinburgh, 2004.
130. Orton C., Mathematics in Archaeology, Cambridge University Press, Cambridge, 1982.



## APPENDIX A

### ANALYTICAL FIGURES OF MERIT

**Table A.1.** Analytical Figures of merit for Y, Nb, Ce, Nd, Sm, Eu

	Y	Nb	La	Ce	Nd	Sm	Eu
<b>LOD (<math>\mu\text{g/kg}</math>)</b>	0.31	1.24	0.28	0.53	0.34	0.30	0.12
<b>LOQ (<math>\mu\text{g/kg}</math>)</b>	1.02	4.13	0.94	1.76	1.15	0.99	0.41
<b>Y=mx+n Calibration Plot Equation</b>	y = 48742x + 81919	y = 21775x + 71928	y = 48662x + 166317	y = 49162x + 155331	y = 20623x + 41764	y = 12704x - 51324	y = 46093x - 207059
<b>R<sup>2</sup></b>	0.9998	0.9995	0.9998	0.9998	1.000	0.9992	0.9992

**Table A.2.** Analytical Figures of merit for Gd, Ho, Er, Yb, Lu, Hf, Cr

	Gd	Ho	Er	Yb	Lu	Hf	Cr
<b>LOD (<math>\mu\text{g/kg}</math>)</b>	0.14	0.06	0.35	0.09	0.09	0.67	0.99
<b>LOQ (<math>\mu\text{g/kg}</math>)</b>	0.47	0.19	1.16	0.30	0.30	2.23	3.32
<b>Y=mx+n Calibration Plot Equation</b>	y = 12626x - 61075	y = 88117x - 195467	y = 29739x - 14303	y = 28670x - 152784	y = 28670x - 152784	y = 17961x - 58192	y = 178.4x + 1458.3
<b>R<sup>2</sup></b>	0.9992	0.9998	0.9994	0.9991	0.9991	0.9994	0.9995



## APPENDIX B

### RESULTS OF GEOLOGICAL AND ARCHAEOLOGICAL SAMPLES USING ICP-OES

**Table B.** Mg, Fe by standard additions and Mn, Sr, Ba by external calibration

<b>Constituent</b>					
<b>Samples</b>	<b>MgO %</b>	<b>Fe<sub>2</sub>O<sub>3</sub> %</b>	<b>Mn mg/kg</b>	<b>Sr mg/kg</b>	<b>Ba mg/kg</b>
<b>26</b>	0.59±0.03	0.61±0.02	245±4.90	662±19.9	24.8±1.49
<b>27</b>	0.40±0.03	1.03±0.06	374±11.2	786±55.1	44.9±1.71
<b>28</b>	0.48±0.03	0.39±0.03	228±6.85	458±32.1	37.5±1.43
<b>31</b>	0.46±0.02	0.61±0.04	192±9.62	473±32.9	72.3±4.34
<b>32</b>	0.50±0.02	1.15±0.05	161±3.23	686±48.1	34.8±2.78
<b>33</b>	0.56±0.03	0.53±0.03	233±6.99	666±46.6	26.7±1.01
<b>34</b>	0.41±0.02	0.47±0.03	161±8.07	429±30.1	21.9±1.32
<b>35</b>	0.45±0.02	0.37±0.03	142±7.08	616±43.1	36.3±2.18
<b>36</b>	0.84±0.04	0.89±0.05	149±4.46	478±33.5	57.5±2.19
<b>37</b>	0.26±0.01	0.49±0.03	274±5.47	601±12.0	32.6±2.61
<b>38</b>	0.52±0.02	0.60±0.03	310±15.5	579±40.6	62.5±3.75
<b>39</b>	0.50±0.02	0.49±0.03	118±2.36	365±7.30	25.3±2.03
<b>40</b>	0.56±0.03	0.23±0.02	188±5.63	617±43.2	25.5±0.97
<b>41</b>	0.51±0.03	0.55±0.04	212±6.36	796±55.7	32.1±1.22
<b>42</b>	0.48±0.03	0.63±0.04	167±2.12	578±13.5	47.5±1.82
<b>43</b>	0.56±0.03	0.62±0.02	163±3.26	349±6.98	76.1±6.08
<b>44</b>	0.66±0.04	0.78±0.05	298±6.47	448±33.1	30.3±1.15

**Table B. continued**

<b>Samples</b>	<b>MgO %</b>	<b>Fe<sub>2</sub>O<sub>3</sub> %</b>	<b>Mn mg/kg</b>	<b>Sr mg/kg</b>	<b>Ba mg/kg</b>
45	0.56±0.03	0.50±0.02	205±4.11	520±15.1	19.5±1.17
46	0.45±0.03	1.27±0.07	172±5.17	431±30.2	19.6±0.74
47	0.52±0.03	0.45±0.02	245±4.89	428±8.57	14.5±1.16
48	0.47±0.03	0.40 ±0.03	172±5.17	554±38.8	38.8±1.47
49	0.49±0.03	2.76±0.16	349±10.5	737±51.6	37.4±1.42
50	0.39±0.03	0.87±0.05	184±5.53	562±39.3	26.8±1.02
52	0.48±0.03	1.02±0.06	235±7.06	608±42.6	24.7±0.94
53	0.57±0.03	1.26±0.07	204±6.12	553±38.7	41.7±1.59
54	0.58±0.03	1.60±0.06	148±2.96	738±51.7	36.5±2.92
55	0.56±0.03	0.59±0.03	145±2.90	413±28.9	26.9±2.15
56	0.36±0.02	0.43±0.03	227±11.3	444±31.2	29.7±1.78
57	0.43±0.03	0.22±0.02	114±2.28	489±14.7	40.4±2.43
58	0.43±0.02	0.94±0.04	224±4.47	497±34.8	23.9±1.92
59	0.59±0.03	0.45±0.02	136±2.71	527±15.8	17.1±1.03
60	0.32±0.02	0.16±0.01	161±3.23	326±9.78	85.7±5.14
61	0.47±0.02	0.50±0.03	229±4.59	845±59.2	38.4±3.07
62	0.59±0.03	0.78±0.04	180±3.60	441±30.8	63.5±5.08
63	0.67±0.02	0.64±0.05	173±8.64	684±47.8	30.7±1.84
64	3.86±0.19	0.41±0.02	159±3.19	59±2	80.9±4.86
65	0.57±0.02	0.49±0.03	321±9.64	535±37.5	33.6±1.28
66	0.47±0.03	0.80±0.05	128±2.24	421±28.9	32.9±2.19
67	0.31±0.02	0.41±0.02	167±3.34	474±33.2	26.1±2.09

<b>Table B. continued</b>					
<b>68</b>	0.70±0.03	0.56±0.03	205±4.10	735±14.7	20.9±1.67
<b>69</b>	0.71±0.03	1.15±0.05	124±2.48	766±15.3	30.5±2.44
<b>70</b>	0.37±0.02	0.22±0.02	268±5.36	440±8.79	24.6±1.97
<b>71</b>	0.37±0.03	0.96±0.06	131±3.94	443±31.1	78.3±2.97
<b>72</b>	0.54±0.03	0.69±0.03	135±2.70	574±40.2	19.6±1.56
<b>73</b>	0.73±0.03	0.32±0.02	249±4.98	529±10.6	22.9±1.83
<b>74</b>	0.57±0.03	0.43±0.02	197±3.94	507±10.1	22.1±1.77
<b>75</b>	0.47±0.03	0.75±0.05	178±5.35	637±44.9	27.1±1.03
<b>77</b>	0.73±0.04	0.84±0.04	207±4.13	525±15.8	74.4±4.47
<b>80</b>	0.61±0.02	0.55±0.03	171±8.54	555±38.9	29.4±1.76
<b>81</b>	0.53±0.03	0.74±0.03	178±3.55	500±34.9	23.3±1.87
<b>84</b>	0.48±0.02	0.23±0.01	132±2.64	527±10.5	13.9±1.12
<b>85</b>	3.51±0.19	1.02±0.04	194±3.89	521±15.6	93.1±5.59
<b>86</b>	0.72±0.04	1.02±0.04	176±3.51	660±47.2	19.4±1.67
<b>87</b>	0.52±0.03	0.46±0.02	230±4.59	590±43.3	17.91.56±
<b>88</b>	0.68±0.04	0.64±0.03	234±4.68	500±34.9	15.9±1.48
<b>89</b>	1.14±0.05	0.29±0.01	238±4.77	480±33.7	17.2±1.55
<b>90</b>	0.75±0.04	0.34±0.02	243±4.86	640±43.6	18.1±1.64
<b>91</b>	0.89±0.04	0.56±0.03	141±2.81	700±51.3	23.5±1.78
<b>92</b>	1.20±0.05	0.70±0.03	254±5.09	560±38.2	21.9±1.75
<b>93</b>	1.17±0.05	0.63±0.03	191±3.82	570±39.0	13.3±1.09
<b>94</b>	0.97±0.04	0.56±0.03	124±2.47	560±38.2	82.3±3.05
<b>95</b>	0.57±0.03	0.60±0.03	151±3.02	580±42.9	17.2±1.55



## APPENDIX C

### RESULTS OF GEOLOGICAL AND ARCHAEOLOGICAL SAMPLES USING ICP-MS

**Table C.1.** Results of geological and archaeological samples using ICP-MS and external calibration for Cr, Y, Nb, La, Ce, Nd and Sm.

Samples	Constituent (mg/kg)						
	Cr	Y	Nb	La	Ce	Nd	Sm
<b>AKYA (n=6)</b>	80.1±5.92	0.24±0.05	0.36±0.06	0.26±0.03	0.43±0.07	0.49±0.09	n.d.
<b>AKYB (n=7)</b>	40.3±7.41	0.57±0.12	1.10±0.21	1.24±0.14	1.64±0.25	1.77±0.32	n.d.
<b>AKYC (n=8)</b>	32.6±4.93	0.41±0.04	0.85±0.13	1.02±0.18	1.66±0.17	0.98±0.19	n.d.
<b>KRC (n=6)</b>	182±17	2.04±0.23	2.08±0.24	3.08±0.36	5.17±0.34	3.20±0.33	0.63±0.09
<b>RZG (n=4)</b>	138±4	2.70±0.25	2.34±0.20	5.74±0.21	9.36±0.25	5.17±0.21	1.08±0.02
<b>K1 (n=3)</b>	10.6±0.60	6.82±0.49	1.69±0.11	4.25±0.05	4.61±0.08	4.10±0.33	0.85±0.07
<b>K2 (n=3)</b>	21.7±1.24	11.39±0.8 2	3.80±0.25	7.76±0.09	10.2±0.17	7.26±0.58	1.56±0.12
<b>K3-1 (n=2)</b>	6.16±0.35	5.18±0.37	0.57±0.04	3.57±0.04	4.39±0.07	3.48±0.28	0.71±0.06
<b>K3-2 (n=2)</b>	10.1±0.58	7.46±0.54	0.69±0.04	4.95±0.06	6.26±0.10	4.57±0.37	0.98±0.08
<b>K3-3 (n=2)</b>	3.63±0.21	4.68±0.34	0.36±0.02	3.04±0.03	3.12±0.05	2.99±0.24	0.58±0.07
<b>1</b>	32.9±3.61	2.43±0.13	0.76±0.01	2.06±0.08	1.57±0.18	1.86±0.11	0.57±0.03
<b>2</b>	6.70±0.73	1.94±0.04	0.80±0.06	1.78±0.13	0.69±0.01	1.51±0.09	n.d.
<b>3</b>	20.5±1.17	1.64±0.12	2.66±0.17	2.85±0.03	5.83±0.10	3.57±0.29	0.72±0.06
<b>4</b>	13.3±0.76	5.55±0.40	2.24±0.15	4.86±0.06	3.22±0.05	5.34±0.43	1.06±0.08
<b>5</b>	9.68±1.22	15.58±1.2 6	1.94±0.10	9.60±0.44	8.71±0.71	7.65±0.54	2.56±0.20
<b>6</b>	6.21±0.78	12.50±1.0 1	1.70±0.09	5.84±0.27	6.17±0.50	5.88±0.41	1.90±0.15
<b>7</b>	8.75±0.96	4.73±0.10	1.40±0.10	5.38±0.39	5.28±0.03	4.17±0.25	1.09±0.11

**Table C.1.  
continued**

<b>Samples</b>	<b>Cr</b>	<b>Y</b>	<b>Nb</b>	<b>La</b>	<b>Ce</b>	<b>Nd</b>	<b>Sm</b>
<b>8</b>	8.56±1.08	8.87±0.72	1.39±0.07	4.83±0.22	4.73±0.38	4.30±0.30	1.22±0.10
<b>9</b>	817±46.6	4.36±0.31	2.04±0.13	6.06±0.07	6.21±0.10	4.51±0.36	0.95±0.08
<b>10</b>	11.9±1.31	6.13±0.13	1.94±0.14	6.01±0.44	4.73±0.02	5.15±0.30	1.30±0.13
<b>11</b>	95.3±5.43	9.63±0.69	2.82±0.18	7.56±0.09	6.72±0.11	6.92±0.55	1.36±0.11
<b>12</b>	4.40±0.48	5.10±0.10	1.65±0.12	4.65±0.34	4.92±0.03	3.36±0.20	0.87±0.09
<b>14</b>	7.63±0.84	9.92±0.51	2.07±0.02	8.57±0.33	4.91±0.56	7.38±0.44	1.88±0.09
<b>15</b>	5.49±0.31	4.71±0.34	2.74±0.18	4.51±0.05	4.33±0.07	4.00±0.32	2.69±0.22
<b>16</b>	3.20±0.18	3.26±0.23	1.24±0.08	2.82±0.03	3.17±0.05	3.10±0.25	0.67±0.05
<b>17</b>	5.03±0.64	1.04±0.08	0.87±0.04	1.55±0.07	1.00±0.08	1.25±0.09	n.d.
<b>18</b>	10.1±1.27	5.31±0.43	1.48±0.07	4.56±0.21	3.93±0.32	3.92±0.27	1.21±0.10
<b>19</b>	5.22±0.30	1.68±0.12	0.99±0.06	3.32±0.04	2.58±0.04	4.40±0.35	0.73±0.06
<b>20</b>	5.01±0.29	8.75±0.63	1.86±0.12	6.93±0.08	6.08±0.10	6.60±0.53	1.49±0.12
<b>22</b>	7.07±0.40	1.58±0.11	2.27±0.15	2.45±0.03	2.16±0.04	2.02±0.16	1.53±0.12
<b>23</b>	6.52±0.37	5.02±0.36	1.35±0.09	3.96±0.05	3.95±0.06	4.27±0.34	1.05±0.08
<b>24</b>	16.1±1.74	2.96±0.15	1.94±0.02	1.84±0.07	1.40±0.16	3.05±0.18	0.66±0.03
<b>26</b>	12.4±0.71	7.04±0.51	1.81±0.12	4.92±0.06	5.31±0.09	5.44±0.44	1.13±0.09
<b>27</b>	6.39±0.36	6.38±0.46	2.79±0.18	4.32±0.05	4.49±0.07	4.15±0.33	2.43±0.19
<b>28</b>	10.6±1.35	2.41±0.20	1.13±0.06	2.18±0.10	1.48±0.12	1.81±0.13	n.d.
<b>30</b>	7.83±0.86	0.44±0.02	0.61±0.01	0.68±0.03	0.69±0.08	0.64±0.04	n.d.
<b>31</b>	9.55±1.21	2.24±0.18	1.73±0.09	2.35±0.11	2.42±0.20	1.82±0.13	0.65±0.05
<b>32</b>	8.40±0.48	3.64±0.26	1.48±0.10	3.77±0.04	3.54±0.06	4.00±0.32	1.00±0.08
<b>33</b>	8.76±0.96	4.13±0.21	1.34±0.01	3.34±0.13	2.50±0.29	3.09±0.19	0.83±0.04

**Table C.1.  
continued**

<b>Samples</b>	<b>Cr</b>	<b>Y</b>	<b>Nb</b>	<b>La</b>	<b>Ce</b>	<b>Nd</b>	<b>Sm</b>
<b>34</b>	6.09±0.67	1.13±0.02	1.03±0.08	1.55±0.11	0.47±0.01	1.33±0.08	0.36±0.04
<b>35</b>	7.71±0.84	1.99±0.04	0.85±0.06	2.10±0.15	0.89±0.01	1.69±0.10	0.54±0.05
<b>36</b>	10.8±1.18	2.43±0.05	2.32±0.17	3.33±0.24	1.82±0.01	2.56±0.15	0.71±0.07
<b>37</b>	9.52±0.54	2.37±0.17	1.52±0.10	2.81±0.03	2.17±0.04	3.42±0.27	0.74±0.06
<b>38</b>	5.87±0.33	0.56±0.04	0.78±0.05	1.35±0.02	0.99±0.02	1.60±0.13	0.25±0.02
<b>39</b>	8.65±0.95	1.96±0.10	1.70±0.02	2.08±0.08	1.67±0.19	2.04±0.12	0.53±0.03
<b>40</b>	3.53±0.39	2.93±0.06	0.45±0.03	2.53±0.19	0.86±0.01	2.32±0.14	0.62±0.06
<b>41</b>	5.48±0.60	4.06±0.08	1.13±0.08	4.03±0.30	1.35±0.01	2.99±0.18	0.72±0.07
<b>42</b>	7.85±0.45	4.37±0.31	1.63±0.11	3.55±0.04	3.45±0.06	3.72±0.30	1.69±0.14
<b>43</b>	9.93±1.09	3.29±0.17	4.26±0.05	3.81±0.15	3.51±0.40	3.08±0.18	0.61±0.03
<b>44</b>	12.8±1.33	4.49±0.23	2.09±0.02	4.33±0.16	1.74±0.20	4.06±0.24	0.97±0.05
<b>45</b>	4.51±0.49	1.77±0.04	0.78±0.06	2.42±0.18	0.81±0.01	1.70±0.10	0.57±0.06
<b>46</b>	8.86±0.97	1.84±0.10	1.63±0.02	3.08±0.12	2.49±0.29	2.73±0.16	0.60±0.03
<b>47</b>	8.02±0.46	2.32±0.17	1.42±0.09	2.68±0.03	1.99±0.03	2.92±0.23	n.d.
<b>48</b>	7.00±0.77	1.58±0.08	0.87±0.01	2.42±0.09	1.78±0.20	2.51±0.15	0.60±0.03
<b>49</b>	7.97±1.01	1.11±0.09	1.55±0.08	1.99±0.09	1.67±0.14	1.69±0.12	n.d.
<b>50</b>	9.82±0.56	4.37±0.31	1.67±0.11	4.38±0.05	4.03±0.07	4.18±0.33	0.87±0.07
<b>52</b>	7.14±0.41	4.56±0.33	1.81±0.12	3.89±0.04	3.72±0.06	3.89±0.31	0.78±0.06
<b>53</b>	12.7±0.73	5.34±0.38	2.06±0.13	5.29±0.06	4.99±0.08	5.48±0.44	1.06±0.08
<b>54</b>	11.3±1.24	2.49±0.05	2.01±0.15	3.18±0.23	3.77±0.02	2.65±0.16	0.61±0.06
<b>55</b>	11.1±1.40	3.87±0.31	1.48±0.07	3.73±0.17	2.60±0.21	3.28±0.23	0.86±0.07
<b>56</b>	6.61±0.72	1.22±0.06	1.23±0.01	1.69±0.06	1.27±0.14	1.49±0.09	0.40±0.02

**Table C.1.  
continued**

<b>Samples</b>	<b>Cr</b>	<b>Y</b>	<b>Nb</b>	<b>La</b>	<b>Ce</b>	<b>Nd</b>	<b>Sm</b>
<b>57</b>	5.09±0.29	5.46±0.39	1.88±0.12	4.76±0.05	4.72±0.08	4.57±0.37	0.90±0.07
<b>58</b>	10.1±1.26	3.57±0.29	2.17±0.11	2.83±0.13	2.78±0.23	2.22±0.16	0.56±0.04
<b>59</b>	7.39±0.81	2.18±0.11	2.04±0.02	2.74±0.10	2.90±0.33	2.19±0.13	0.51±0.02
<b>60</b>	5.17±0.57	5.34±0.11	1.92±0.14	4.66±0.34	5.08±0.03	3.71±0.22	0.93±0.09
<b>61</b>	8.55±0.94	3.73±0.08	1.67±0.12	3.87±0.28	1.39±0.01	2.91±0.17	0.76±0.08
<b>62</b>	10.6±1.17	1.96±0.04	2.29±0.17	3.16±0.23	1.71±0.01	2.42±0.14	0.65±0.06
<b>63</b>	9.03±0.99	3.12±0.16	2.43±0.03	3.53±0.13	3.12±0.36	3.05±0.18	0.79±0.04
<b>64</b>	26.9±2.95	0.72±0.04	2.75±0.03	1.59±0.06	2.77±0.32	1.39±0.08	0.35±0.02
<b>65</b>	4.10±0.45	2.46±0.05	0.40±0.03	2.82±0.21	0.91±0.01	2.63±0.15	0.57±0.06
<b>66</b>	12.7±0.73	2.49±0.10	2.51±0.16	3.49±0.04	3.33±0.05	3.37±0.27	0.69±0.06
<b>67</b>	3.64±0.46	6.71±0.54	1.10±0.06	4.30±0.20	3.59±0.29	3.46±0.24	1.17±0.09
<b>68</b>	9.37±0.53	8.52±0.61	2.06±0.13	5.94±0.07	5.26±0.09	6.31±0.50	1.27±0.10
<b>69</b>	42.1±2.40	4.03±0.29	2.90±0.19	4.35±0.05	4.54±0.07	4.29±0.34	0.90±0.07
<b>70</b>	3.25±0.19	4.88±0.35	1.11±0.07	3.74±0.04	3.59±0.06	3.49±0.28	0.71±0.06
<b>71</b>	58.6±6.42	3.68±0.08	1.68±0.12	3.71±0.27	3.53±0.01	2.53±0.15	0.62±0.06
<b>72</b>	4.27±0.54	2.92±0.24	1.00±0.05	2.71±0.12	1.53±0.12	2.50±0.17	0.70±0.06
<b>73</b>	n.d.	3.49±0.18	2.71±0.03	3.07±0.12	2.76±0.032	2.84±0.17	0.57±0.03
<b>74</b>	6.74±0.74	2.88±0.15	1.14±0.01	3.69±0.14	2.71±0.31	3.01±0.18	0.64±0.03
<b>75</b>	6.95±0.88	5.99±0.48	1.00±0.05	4.29±0.19	3.98±0.32	3.91±0.27	1.01±0.08
<b>77</b>	6.22±0.79	6.50±0.53	1.45±0.07	6.05±0.27	3.25±0.26	4.97±0.35	1.37±0.11
<b>80</b>	10.2±1.13	1.82±0.04	1.11±0.08	2.35±0.17	0.79±0.01	2.57±0.15	0.61±0.06
<b>81</b>	6.72±0.85	5.02±0.41	1.24±0.06	4.02±0.18	3.18±0.26	3.53±0.25	0.89±0.07

<b>Table C.1. continued</b>							
<b>Samples</b>	<b>Cr</b>	<b>Y</b>	<b>Nb</b>	<b>La</b>	<b>Ce</b>	<b>Nd</b>	<b>Sm</b>
<b>84</b>	3.16±0.35	0.72±0.01	0.43±0.03	1.39±0.10	0.44±0.01	1.45±0.09	n.d.
<b>85</b>	23.7±2.60	5.91±0.31	2.56±0.03	4.99±0.19	10.72±1.23	4.42±0.27	1.09±0.05
<b>86</b>	7.70±0.44	3.05±0.22	2.22±0.14	2.73±0.03	2.23±0.04	3.27±0.26	0.64±0.05
<b>87</b>	6.78±0.86	3.79±0.31	1.25±0.06	3.40±0.15	2.78±0.23	2.83±0.20	0.65±0.05
<b>88</b>	89.7±9.83	0.39±0.01	0.30±0.02	1.31±0.10	0.50±0.01	1.29±0.08	n.d.
<b>89</b>	13.9±1.53	0.85±0.02	0.53±0.04	1.71±0.13	0.55±0.01	1.42±0.08	n.d.
<b>90</b>	8.64±1.09	2.61±0.21	1.39±0.07	2.41±0.11	1.98±0.16	2.06±0.14	0.55±0.04
<b>91</b>	6.89±0.39	3.22±0.23	1.04±0.07	2.60±0.03	2.87±0.05	3.01±0.24	0.70±0.06
<b>92</b>	7.54±0.83	1.94±0.04	1.28±0.09	2.70±0.20	0.95±0.01	2.41±0.14	0.57±0.06
<b>93</b>	5.05±0.55	1.23±0.06	1.60±0.02	1.48±0.06	1.02±0.12	1.37±0.08	0.44±0.02
<b>94</b>	8.23±0.90	2.05±0.11	1.82±0.02	3.13±0.12	1.71±0.20	2.66±0.16	0.58±0.03
<b>95</b>	4.79±0.52	2.05±0.04	0.64±0.05	2.08±0.15	0.83±0.01	1.97±0.12	n.d.

**Table C.2.** Results of geological and archaeological samples using ICP-MS and external calibration for Eu, Gd, Ho, Er, Yb, Lu, and Hf

<b>Samples</b>	<b>Constituent (mg/kg)</b>						
	<b>Eu</b>	<b>Gd</b>	<b>Ho</b>	<b>Er</b>	<b>Yb</b>	<b>Lu</b>	<b>Hf</b>
<b>AKYA (n=6)</b>	n.d.	n.d.	n.d.	n.d.	n.d.	n.d.	0.89±0.14
<b>AKYB (n=7)</b>	n.d.	n.d.	n.d.	n.d.	n.d.	n.d.	1.71±.16
<b>AKYC (n=8)</b>	n.d.	0.32±0.05	n.d.	0.27±0.03	n.d.	n.d.	0.80±0.13
<b>KRC (n=6)</b>	n.d.	0.76±0.09	n.d.	0.23±0.03	0.37±0.03	n.d.	1.38±0.14
<b>RZG(n=4)</b>	n.d.	1.34±0.11	n.d.	0.52±0.09	0.49±0.01	n.d.	1.41±0.17
<b>K1 (n=3)</b>	0.27±0.02	1.02±0.04	n.d.	0.82±0.09	0.64±0.02	n.d.	0.34±0.03

Table C.2 continued

Samples	Eu	Gd	Ho	Er	Yb	Lu	Hf
K2(n=3)	0.51±0.04	1.90±0.07	0.36±0.01	1.20±0.13	1.04±0.03	n.d.	0.53±0.04
K3-1(n=2)	n.d.	0.88±0.03	n.d.	0.58±0.08	0.38±0.01	n.d.	0.24±0.02
K3-2(n=2)	0.24±0.01	1.23±0.04	0.23±0.01	0.76±0.11	0.53±0.01	n.d.	n.d.
K3-3(n=2)	n.d.	0.72±0.02	n.d.	0.60±0.08	0.33±0.01	n.d.	0.32±0.03
1	n.d.	0.57±0.01	n.d.	n.d.	n.d.	n.d.	n.d.
2	n.d.	0.40±0.05	n.d.	0.22±0.03	n.d.	n.d.	0.21±0.03
3	n.d.	0.96±0.03	n.d.	n.d.	n.d.	n.d.	1.07±0.09
4	n.d.	1.41±0.05	n.d.	0.36±0.05	0.65±0.02	n.d.	n.d.
5	0.52±0.04	2.68±0.03	0.44±0.02	0.75±0.11	1.08±0.03	n.d.	0.40±0.03
6	n.d.	2.09±0.02	n.d.	0.58±0.08	0.74±0.02	n.d.	n.d.
7	n.d.	1.29±0.15	n.d.	0.51±0.07	0.59±0.02	n.d.	n.d.
8	n.d.	1.52±0.02	n.d.	0.30±0.04	0.64±0.02	n.d.	n.d.
9	n.d.	1.25±0.04	n.d.	n.d.	n.d.	n.d.	1.39±0.11
10	n.d.	1.41±0.17	n.d.	0.65±0.09	0.81±0.02	n.d.	n.d.
11	n.d.	1.88±0.06	0.60±0.02	0.64±0.09	0.85±0.02	n.d.	0.68±0.05
12	n.d.	1.25±0.15	n.d.	0.40±0.06	0.58±0.02	n.d.	2.36±0.28
14	0.55±0.04	2.34±0.03	0.57±0.02	0.94±0.14	1.02±0.03	n.d.	n.d.
15	n.d.	3.72±0.13	n.d.		n.d.	n.d.	n.d.
16	n.d.	0.79±0.03	n.d.	0.19±0.03	0.37±0.01	n.d.	n.d.
17	n.d.	n.d.	n.d.	n.d.	n.d.	n.d.	n.d.
18	0.27±0.02	1.29±0.01	0.24±0.01	0.53±0.08	0.43±0.01	n.d.	1.04±0.08
19	n.d.	1.62±0.06	n.d.		n.d.	n.d.	n.d.

**Table C.2 continued**

<b>Samples</b>	<b>Eu</b>	<b>Gd</b>	<b>Ho</b>	<b>Er</b>	<b>Yb</b>	<b>Lu</b>	<b>Hf</b>
20	0.60±0.05	2.00±0.07	n.d.	0.49±0.07	0.92±0.02	n.d.	n.d.
22	n.d.	2.40±0.08	n.d.		n.d.	n.d.	n.d.
23	n.d.	1.08±0.04	n.d.	0.37±0.05	0.73±0.02	n.d.	0.66±0.05
24	n.d.	0.83±0.01	n.d.	0.31±0.05	n.d.	n.d.	n.d.
26	n.d.	1.60±0.06	n.d.	0.45±0.07	0.97±0.03	n.d.	n.d.
27	n.d.	3.89±0.13	n.d.		n.d.	n.d.	n.d.
28	n.d.	0.57±0.01	n.d.	n.d.	n.d.	n.d.	n.d.
30	n.d.	n.d.	n.d.	n.d.	n.d.	n.d.	0.37±0.04
31	n.d.	0.63±0.01	n.d.	0.10±0.01	n.d.	n.d.	0.31±0.03
32	n.d.	1.18±0.04	n.d.	n.d.	n.d.	n.d.	n.d.
33	n.d.	0.84±0.01	n.d.	0.49±0.07	n.d.	n.d.	0.60±0.07
34	n.d.	0.33±0.04	n.d.	n.d.	n.d.	n.d.	0.22±0.03
35	n.d.	0.55±0.07	n.d.	n.d.	n.d.	n.d.	n.d.
36	n.d.	0.59±0.07	n.d.	n.d.	n.d.	n.d.	n.d.
37	n.d.	0.87±0.03	n.d.	0.29±0.04	n.d.	n.d.	0.74±0.06
38	n.d.	0.34±0.01	n.d.		n.d.	n.d.	0.84±0.07
39	n.d.	0.63±0.01	n.d.	0.32±0.05	0.29±0.01	n.d.	0.40±0.05
40	n.d.	0.70±0.08	n.d.	0.31±0.05	n.d.	n.d.	0.25±0.03
41	n.d.	0.80±0.10	n.d.	0.53±0.08	n.d.	n.d.	0.38±0.05
42	n.d.	2.79±0.10	n.d.		n.d.	n.d.	n.d.
43	n.d.	0.81±0.01	n.d.	0.58±0.08	0.41±0.01	n.d.	1.20±0.14
44	n.d.	1.24±0.02	n.d.	0.51±0.07	n.d.	n.d.	0.34±0.04

Table C.2 continued

Samples	Eu	Gd	Ho	Er	Yb	Lu	Hf
45	n.d.	0.50±0.06	n.d.	n.d.	n.d.	n.d.	0.28±0.03
46	n.d.	0.76±0.01	n.d.	0.38±0.06	0.26±0.01	n.d.	0.53±0.06
47	n.d.	0.83±0.03	n.d.	n.d.	n.d.	n.d.	0.42±0.03
48	n.d.	0.58±0.01	n.d.	0.59±0.09	n.d.	n.d.	0.64±0.08
49	n.d.	0.48±0.01	n.d.	n.d.	n.d.	n.d.	0.65±0.05
50	n.d.	1.17±0.04	n.d.	0.28±0.04	0.61±0.02	n.d.	n.d.
52	n.d.	1.10±0.04	n.d.	0.34±0.05	0.55±0.01	n.d.	n.d.
53	n.d.	1.41±0.05	n.d.	0.39±0.06	0.68±0.02	n.d.	n.d.
54	n.d.	0.84±0.10	n.d.	n.d.	n.d.	n.d.	n.d.
55	n.d.	0.98±0.01	n.d.	n.d.	n.d.	n.d.	n.d.
56	n.d.	0.41±0.01	n.d.	0.32±0.05	0.42±0.01	n.d.	0.27±0.03
57	n.d.	1.08±0.04	n.d.	0.32±0.05	0.51±0.01	n.d.	n.d.
58	n.d.	0.69±0.01	n.d.	0.22±0.03	0.26±0.01	n.d.	0.75±0.06
59	n.d.	0.65±0.01	n.d.	0.42±0.06	0.34±0.01	n.d.	0.64±0.08
60	n.d.	1.18±0.14	n.d.	0.46±0.07	0.56±0.02	n.d.	0.32±0.04
61	n.d.	0.85±0.10	n.d.	0.42±0.06	n.d.	n.d.	n.d.
62	n.d.	0.64±0.08	n.d.	n.d.	n.d.	n.d.	n.d.
63	n.d.	0.79±0.01	n.d.	0.33±0.05	n.d.	n.d.	n.d.
64	n.d.	0.41±0.01	n.d.	n.d.	n.d.	n.d.	1.55±0.19
65	n.d.	0.69±0.08	n.d.	0.63±0.09	n.d.	n.d.	0.72±0.09
66	n.d.	0.79±0.03	n.d.	0.31±0.05	n.d.	n.d.	0.93±0.07
67	n.d.	1.31±0.01	n.d.	0.35±0.05	n.d.	n.d.	n.d.

**Table C.2**  
continued

<b>Samples</b>	<b>Eu</b>	<b>Gd</b>	<b>Ho</b>	<b>Er</b>	<b>Yb</b>	<b>Lu</b>	<b>Hf</b>
68	n.d.	1.73±0.06	n.d.	0.40±0.06	0.75±0.02	n.d.	n.d.
69	n.d.	1.12±0.04	n.d.	0.38±0.05	0.58±0.02	n.d.	0.49±0.04
70	n.d.	1.06±0.04	n.d.	0.27±0.04	0.58±0.02	n.d.	n.d.
71	n.d.	0.82±0.10	n.d.	0.41±0.06	0.46±0.01	n.d.	0.46±0.06
72	n.d.	0.81±0.01	n.d.	0.29±0.04	0.24±0.01	n.d.	0.39±0.03
73	n.d.	0.81±0.01	n.d.	0.35±0.05	0.34±0.01	n.d.	n.d.
74	n.d.	0.75±0.01	n.d.	0.45±0.07	0.41±0.01	n.d.	0.48±0.06
75	0.27±0.02	1.16±0.01	0.25±0.01	0.54±0.08	0.42±0.01	n.d.	1.05±0.08
77	n.d.	1.65±0.02	n.d.	0.28±0.04	0.26±0.01	n.d.	1.07±0.09
81	0.24±0.02	1.24±0.01	n.d.	0.40±0.06	0.42±0.01	n.d.	1.20±0.10
84	n.d.	0.38±0.05	n.d.	n.d.	n.d.	n.d.	0.33±0.04
85	n.d.	1.52±0.02	n.d.	0.57±0.08	0.69±0.02	n.d.	0.77±0.09
86	n.d.	0.87±0.03	n.d.	n.d.	n.d.	n.d.	2.33±0.19
87	n.d.	0.83±0.01	n.d.	0.16±0.02	n.d.	n.d.	0.71±0.06
88	n.d.	0.21±0.03	n.d.	n.d.	n.d.	n.d.	0.31±0.04
89	n.d.	0.40±0.05	n.d.	0.27±0.04	n.d.	n.d.	0.31±0.04
90	n.d.	0.56±0.01	n.d.	0.14±0.06	n.d.	n.d.	0.75±0.06
91	n.d.	0.85±0.03	n.d.	n.d.	0.44±0.01	n.d.	n.d.
92	n.d.	0.58±0.07	n.d.	0.29±0.04	n.d.	n.d.	0.32±0.04
93	n.d.	0.38±0.01	n.d.	n.d.	n.d.	n.d.	n.d.
94	n.d.	0.76±0.01	n.d.	0.48±0.07	n.d.	n.d.	0.40±0.05
95	n.d.	0.50±0.06	n.d.	0.36±0.05	n.d.	n.d.	0.41±0.05

**Table C.3.** Results of geological and archaeological samples using ICP-MS for Cr, Y, Nb, La, Ce, Nd and Sm. Results are corrected by matrix factor.

	Cr	Y	Nb	La	Ce	Nd	Sm
38	25.3±1.44	1.58±0.11	1.17±0.08	2.84±0.03	2.27±0.04	3.68±0.29	0.49±0.04
39	37.2±4.07	5.47±0.28	2.55±0.03	4.36±0.17	3.85±0.44	4.70±0.28	1.06±0.05
40	15.2±1.66	8.20±0.17	0.68±0.05	5.31±0.39	1.97±0.01	5.33±0.31	1.24±0.12
41	23.6±2.58	11.4±0.23	1.69±0.12	8.47±0.62	3.09±0.02	6.88±0.41	1.44±0.14
42	33.8±1.93	12.2±0.88	2.44±0.16	7.45±0.09	7.92±0.13	8.57±0.69	3.38±0.27
43	42.7±4.67	9.20±0.48	6.39±0.07	8.00±0.30	8.07±0.92	7.09±0.43	1.22±0.06
44	52.4±5.74	12.6±0.65	3.13±0.03	9.09±0.35	4.00±0.46	9.33±0.56	1.95±0.10
45	19.4±2.12	5.89±0.10	1.16±0.09	5.08±0.37	1.87±0.01	3.92±0.23	1.15±0.11
46	38.1±4.17	5.15±0.27	2.44±0.03	6.47±0.25	5.73±0.66	6.28±0.38	1.21±0.06
47	34.5±1.96	6.48±0.47	2.13±0.14	5.63±0.06	4.57±0.07	6.72±0.54	n.d.
48	30.1±3.29	4.43±0.23	1.31±0.01	5.09±0.19	4.09±0.47	5.78±0.35	1.20±0.06
49	34.3±4.32	3.09±0.25	2.32±0.12	4.18±0.19	3.83±0.31	3.89±0.27	n.d.
50	42.2±2.41	12.3±0.88	2.51±0.16	9.20±0.11	9.26±0.15	9.60±0.77	1.73±0.14
52	30.7±1.75	12.8±0.92	2.71±0.18	8.17±0.09	8.55±0.14	8.95±0.72	1.57±0.13
53	54.8±3.12	14.9±1.08	3.09±0.20	11.11±0.13	11.47±0.19	12.60±1.01	2.11±0.17
54	48.9±5.35	6.97±0.14	3.01±0.22	6.68±0.49	8.67±0.05	6.10±0.36	1.22±0.12
55	47.7±6.02	10.9±0.88	2.22±0.11	7.83±0.36	5.98±0.49	7.54±0.53	1.72±0.14
56	28.4±3.11	3.41±0.18	1.84±0.02	3.56±0.14	2.91±0.33	3.43±0.21	0.79±0.04
57	21.9±1.25	15.3±1.10	2.82±0.18	9.99±0.11	10.85±0.18	10.50±0.84	1.79±0.14
58	43.1±5.43	9.99±0.81	3.26±0.16	5.94±0.27	6.39±0.52	5.10±0.36	1.11±0.09
59	31.8±3.48	6.11±0.32	3.06±0.03	5.75±0.22	6.66±0.76	5.03±0.30	1.01±0.05
60	22.2±2.44	14.9±0.31	2.88±0.21	9.79±0.72	11.68±0.06	8.53±0.50	1.85±0.19

<b>Table C.3. continued</b>							
	<b>Cr</b>	<b>Y</b>	<b>Nb</b>	<b>La</b>	<b>Ce</b>	<b>Nd</b>	<b>Sm</b>
<b>61</b>	36.8±4.03	10.5±0.21	2.50±0.18	8.12±0.60	3.19±0.02	6.69±0.39	1.51±0.15
<b>62</b>	45.9±5.03	5.48±0.11	3.44±0.25	6.64±0.49	3.93±0.14	5.56±0.33	1.30±0.13
<b>63</b>	38.8±4.25	8.74±0.45	3.65±0.04	7.41±0.28	7.17±0.82	7.03±0.42	1.58±0.08
<b>64</b>	115±12	2.01±0.10	4.12±0.04	3.33±0.13	6.36±0.73	3.19±0.19	0.71±0.03
<b>65</b>	17.6±1.93	6.88±0.14	0.60±0.04	5.92±0.43	2.08±0.01	6.04±0.36	1.15±0.11
<b>66</b>	54.9±3.13	6.96±0.50	3.76±0.24	7.33±0.08	7.67±0.12	7.75±0.62	1.39±0.11
<b>67</b>	15.7±1.98	18.8±1.52	1.64±0.08	9.02±0.41	8.25±0.67	7.95±0.56	2.34±0.19
<b>68</b>	40.3±2.30	23.9±1.72	3.09±0.20	12.47±0.14	12.09±0.20	14.51±1.16	2.54±0.20
<b>69</b>	181±10	11.3±0.81	4.35±0.28	9.14±0.11	10.45±0.17	9.87±0.79	1.79±0.14
<b>70</b>	14.0±0.80	13.7±0.98	1.67±0.11	7.86±0.09	8.27±0.13	8.02±0.64	1.41±0.11
<b>71</b>	252±28	10.3±0.21	2.52±0.19	7.78±0.57	8.12±0.04	5.81±0.34	1.25±0.12
<b>72</b>	18.4±2.32	8.18±0.66	1.50±0.08	5.69±0.26	3.53±0.29	5.74±0.40	1.41±0.11
<b>73</b>	n.d.	9.76±0.50	4.07±0.04	6.45±0.25	6.34±0.73	6.53±0.39	1.14±0.06
<b>74</b>	28.9±3.17	8.06±0.42	1.71±0.02	7.75±0.30	6.24±0.71	6.93±0.42	1.29±0.06
<b>75</b>	29.9±3.77	16.8±1.36	1.51±0.08	9.01±0.41	9.16±0.74	9.00±0.63	2.02±0.16
<b>77</b>	26.8±3.38	18.2±1.47	2.17±0.11	12.72±0.58	7.47±0.61	11.44±0.80	2.74±0.22
<b>80</b>	44.3±4.85	5.09±0.10	1.67±0.12	4.93±0.36	1.83±0.01	5.90±0.35	1.22±0.12
<b>81</b>	28.9±3.65	14.1±1.14	1.87±0.09	8.44±0.38	7.32±0.59	8.13±0.57	1.78±0.14
<b>84</b>	13.6±1.49	2.01±0.04	0.65±0.05	2.91±0.21	1.01±0.01	3.33±0.20	n.d.
<b>85</b>	102±11	16.6±0.86	3.83±0.04	10.48±0.40	24.65±2.82	10.16±0.61	2.18±0.11
<b>86</b>	33.1±1.89	8.55±0.62	3.33±0.22	5.74±0.07	5.12±0.10	7.53±0.60	1.29±0.10
<b>87</b>	29.2±3.68	10.6±0.86	1.87±0.09	7.14±0.32	6.38±0.52	6.50±0.45	1.29±0.10

**Table C.3.**  
continued

	<b>Cr</b>	<b>Y</b>	<b>Nb</b>	<b>La</b>	<b>Ce</b>	<b>Nd</b>	<b>Sm</b>
<b>88</b>	385±42	1.09±0.02	0.45±0.03	2.74±0.20	1.15±0.01	2.97±0.18	n.d.
<b>89</b>	59.9±6.56	2.37±0.05	0.80±0.06	3.58±0.26	1.26±0.01	3.28±0.19	n.d.
<b>90</b>	37.2±4.69	7.32±0.59	2.08±0.10	5.07±0.23	4.56±0.37	4.75±0.33	1.10±0.09
<b>91</b>	29.6±1.69	9.02±0.65	1.56±0.10	5.46±0.06	6.59±0.11	6.93±0.55	1.41±0.11
<b>92</b>	32.4±3.55	5.43±0.11	1.92±0.14	5.67±0.42	2.19±0.01	5.53±0.33	1.15±0.11
<b>93</b>	21.7±2.38	3.45±0.18	2.41±0.03	3.11±0.12	2.35±0.27	3.14±0.19	0.87±0.04
<b>94</b>	35.4±3.88	5.75±0.30	2.73±0.03	6.57±0.25	3.94±0.45	6.11±0.37	1.16±0.06
<b>95</b>	20.6±2.25	5.74±0.12	0.97±0.07	4.37±0.32	1.90±0.01	4.53±0.27	n.d.

**Table C. 4.** Results of geological and archaeological samples using ICP-MS for Eu, Gd, Ho, Er, Yb, Lu and Hf. Results are corrected by matrix factor.

<b>Samples</b>	<b>Eu</b>	<b>Gd</b>	<b>Ho</b>	<b>Er</b>	<b>Yb</b>	<b>Lu</b>	<b>Hf</b>
<b>36</b>	n.d.	1.18±0.14	n.d.	n.d.	n.d.	n.d.	n.d.
<b>37</b>	n.d.	1.74±0.06	n.d.	0.58±0.09	n.d.	n.d.	0.89±0.07
<b>38</b>	n.d.	0.68±0.02	n.d.		n.d.	n.d.	1.01±0.08
<b>39</b>	n.d.	1.26±0.02	n.d.	0.64±0.09	0.63±0.02	n.d.	0.48±0.06
<b>40</b>	n.d.	1.40±0.17	n.d.	0.63±0.09	n.d.	n.d.	0.30±0.04
<b>41</b>	n.d.	1.60±0.19	n.d.	1.07±0.16	n.d.	n.d.	0.46±0.05
<b>42</b>	n.d.	5.57±0.19	n.d.		n.d.	n.d.	n.d.
<b>43</b>	n.d.	1.63±0.02	n.d.	1.16±0.17	0.91±0.02	n.d.	1.44±0.17
<b>44</b>	n.d.	2.48±0.03	n.d.	1.01±0.15	1.53±0.04	n.d.	0.41±0.05
<b>45</b>	n.d.	1.00±0.12	n.d.	n.d.	n.d.	n.d.	0.34±0.04
<b>46</b>	n.d.	1.52±0.02	n.d.	0.77±0.11	0.57±0.02	n.d.	0.64±0.08

**Table C.4.**  
continued

<b>Samples</b>	<b>Eu</b>	<b>Gd</b>	<b>Ho</b>	<b>Er</b>	<b>Yb</b>	<b>Lu</b>	<b>Hf</b>
47	n.d.	1.65±0.03	n.d.	n.d.	n.d.	n.d.	0.50±0.04
48	n.d.	1.15±0.02	n.d.	1.18±0.17	n.d.	n.d.	0.77±0.09
49	n.d.	0.95±0.01	n.d.	n.d.	n.d.	n.d.	0.78±0.06
50	n.d.	2.34±0.08	n.d.	0.57±0.08	1.34±0.04	n.d.	n.d.
52	n.d.	2.19±0.08	n.d.	0.67±0.10	1.20±0.03	n.d.	n.d.
53	n.d.	2.82±0.10	n.d.	0.78±0.11	1.49±0.04	n.d.	n.d.
54	n.d.	1.68±0.20	n.d.	n.d.	n.d.	n.d.	n.d.
55	n.d.	1.97±0.02	n.d.	n.d.	n.d.	n.d.	n.d.
56	n.d.	0.82±0.01	n.d.	0.63±0.09	0.93±0.02	n.d.	0.33±0.04
57	n.d.	2.16±0.07	n.d.	0.65±0.09	1.12±0.03	n.d.	n.d.
58	n.d.	1.37±0.01	n.d.	0.44±0.06	0.56±0.02	n.d.	0.90±0.07
59	n.d.	1.30±0.02	n.d.	0.84±0.12	0.74±0.02	n.d.	0.77±0.09
60	n.d.	2.36±0.28	n.d.	0.91±0.13	1.24±0.03	n.d.	0.38±0.05
61	n.d.	1.70±0.20	n.d.	0.84±0.12	n.d.	n.d.	n.d.
62	n.d.	1.29±0.15	n.d.	n.d.	n.d.	n.d.	n.d.
63	n.d.	1.57±0.02	n.d.	0.66±0.10	n.d.	n.d.	n.d.
64	n.d.	0.82±0.01	n.d.	n.d.	n.d.	n.d.	1.87±0.22
65	n.d.	1.38±0.17	n.d.	1.25±0.18	n.d.	n.d.	0.87±0.10
66	n.d.	1.58±0.05	n.d.	0.63±0.09	n.d.	n.d.	1.11±0.09
67	n.d.	2.62±0.03	n.d.	n.d.	n.d.	n.d.	n.d.
68	n.d.	3.46±0.12	n.d.	0.81±0.12	1.65±0.04	n.d.	n.d.
69	n.d.	2.24±0.08	n.d.	0.75±0.11	1.27±0.03	n.d.	0.58±0.05

**Table C.4.  
continued**

<b>Samples</b>	<b>Eu</b>	<b>Gd</b>	<b>Ho</b>	<b>Er</b>	<b>Yb</b>	<b>Lu</b>	<b>Hf</b>
70	n.d.	2.12±0.07	n.d.	0.54±0.08	1.27±0.03	n.d.	n.d.
71	n.d.	1.63±0.20	n.d.	0.82±0.12	1.00±0.03	n.d.	0.55±0.07
72	n.d.	1.61±0.02	n.d.	0.57±0.08	0.53±0.01	n.d.	0.46±0.04
73	n.d.	1.63±0.02	n.d.	0.70±0.10	0.74±0.02	n.d.	n.d.
74	n.d.	1.51±0.02	n.d.	0.90±0.13	0.90±0.02	n.d.	0.58±0.07
75	0.69±0.05	2.33±0.02	0.81±0.03	1.08±0.16	0.93±0.02	n.d.	1.26±0.10
77	n.d.	3.30±0.03	n.d.	0.56±0.08	0.57±0.02	n.d.	1.29±0.10
80	n.d.	1.43±0.17	n.d.	0.83±0.12	n.d.	n.d.	0.45±0.05
81	0.59±0.05	2.48±0.03	n.d.	0.80±0.12	0.92±0.02	n.d.	1.44±0.12
84	n.d.	0.76±0.09	n.d.	n.d.	n.d.	n.d.	0.40±0.05
85	n.d.	3.03±0.04	n.d.	1.14±0.17	1.51±0.04	n.d.	0.92±0.11
86	n.d.	1.73±0.06	n.d.	n.d.	n.d.	n.d.	2.80±0.22
87	n.d.	1.66±0.02	n.d.	0.32±0.05	n.d.	n.d.	0.85±0.07
88	n.d.	0.43±0.05	n.d.	n.d.	n.d.	n.d.	0.37±0.04
89	n.d.	0.80±0.10	n.d.	n.d.	n.d.	n.d.	0.37±0.04
90	n.d.	1.13±0.01	n.d.	0.28±0.04	n.d.	n.d.	0.91±0.07
91	n.d.	1.70±0.06	n.d.	n.d.	0.97±0.03	n.d.	n.d.
92	n.d.	1.16±0.14	n.d.	0.57±0.08	n.d.	n.d.	0.38±
93	n.d.	0.76±0.01	n.d.	n.d.	n.d.	n.d.	n.d.
94	n.d.	1.52±0.02	n.d.	0.96±0.14	n.d.	n.d.	0.47±0.06
95	n.d.	1.00±0.12	n.d.	0.72±0.11	n.d.	n.d.	0.49±0.06

## VITA

### PERSONAL INFORMATION

**Surname, Name:** Muşkara, Üftade

**Nationality:** Turkish

**Date and Place of Birth:** October 1, 1975 – Antalya, Turkey

**Marital Status:** Bachelor with one son

**e-mail:** [uftadem@gmail.com](mailto:uftadem@gmail.com)

### Education

- [2004-2007] M.S., METU – Archaeometry, Ankara  
[1998-2000] M.A., Akdeniz University- Classical Archaeology, Antalya  
[1993- 1997] B.A., Ege University-Classical Archaeology, İzmir  
[1992- 1993] Jacksonville University – ISE program - Florida, USA  
[1992-1988] Antalya High School, Antalya

MS. Thesis “Provenance Studies on Limestone Archaeological Artifacts Using Trace Element Analysis”, May 2007.

MA. Thesis “Güney Batı Anadolu’da Black on Red Tekniğinde Üç Arkaik Krater- Dinos”, June 2000.

### Excavation Experiences

- [1997] in “Perge Excavation- Antalya” by Prof.Dr. Haluk Abbasoğlu (İstanbul University- Classical Archaeology Department)  
[1996] in “Alexandria Troas Surveys - Çanakkale” by Prof.Dr. Coşkun Özgünel ( Ankara University-Classical Archaeology Department)  
[1995- 1993] “Klazomenai Excavation- İzmir” by Prof.Dr. Güven Bakır (Ege University – Classical Archaeology Department)

### Grants

- [2006-2008] TÜBİTAK, 106T089, “Elektrokimyasal Hidrür Oluşturmalı Atomik Absorpsiyon Spektrometri ile Bizmut Tayini için Duyarlı Yöntem Geliştirilmesi”.  
[2008] METU, Graduate School of Natural and Applied Science, 2006-2007, Archaeometry Graduate Program Best Thesis Award.

### Publications

#### International Congress

Muşkara Ü., Ataman O.Y., Tuna N., Bakırdere S., “Characterization of Limestone Figurines from Datça-Emecik by Using Rare Earth Elements”, 8th Aegean Analytical Chemistry Days, İzmir, 16-20 September 2012.

N. Tuna, N. Atıcı, Ü. Muşkara, İ. Sakarya, “Some Remarks on the Limestone Figurines Recently Found at the Archaic Sanctuary of Apollo in the Territory of Knidos”, Cyprus and The East Aegean, 229-243, 2009.

Muřkara Ü., Ataman O.Y., Demirci ř., Bakırdere S., "Hammadde Kaynađının Belirlenmesine Yönelik Emecik Figürinlerinin Arkeometrik İncelemesi", 24. Arkeometri Sonuđları Toplantısı, 2008.

Muřkara Ü., Bakırdere S., Demirci ř., Tuna N., Ataman O.Y., "Matrix Element Compositions and REE Patterns Of A Group Of Limestone Figurines Obtained From Emecik / Datça", 37th International Symposium on Archaeometry , Siena, May 12th – 16th, 2008.

Üftade Muřkara, O. Yavuz Ataman, řahinde Demirci, Sezgin Bakırdere, "Datça/Emecik/Sarı Liman Mevkii Arkaik Kutsal Alanından Çıkan Bazı Kireçtaşı Heykelciklerin Arkeometrik Yönden İncelenmesi", 28. Uluslararası Kazı, Arařtırma ve Arkeometri Sempozyumu, 29 Mayıs-2 Haziran 2006, Çanakkale, 42-58.

Fırat Aydın, Sezgin Bakırdere, Üftade Muřkara, O. Yavuz Ataman, "Türkiye'de Yetiřen Baharat ve řifalı Otlarda Atomik Spektrometriyle Gerekli ve Zehirli Elementlerin Tayini", XIX. Ulusal Kimya Kongresi, 30 Eylül-4 Ekim 2005, Kuşadası.